

Soprintendenza speciale per i
Beni Archeologici di Roma



Università degli Studi di L'Aquila
Dipartimento di Ingegneria Civile,
Edile-Architettura e Ambientale



ENEA

Italian National Agency for New Technologies,
Energy and Sustainable Economic Development

**ROMA
TRE**
UNIVERSITÀ DEGLI STUDI



ISSN 2612-4009

DYNAMIC INTERACTION OF SOIL AND STRUCTURE (DISS_13)

PROCEEDINGS OF THE 3rd INTERNATIONAL WORKSHOP
Dynamic Interaction between Soil, Monuments and Built Environment
ROME, 12-13 DECEMBER 2013

Edited by
Carlo Baggio
Paolo Clemente
Yutaka Nakamura
Luciana Orlando
Antonio Rovelli
Gianfranco Valente

Proceedings of the 3rd International
Workshop on
“Dynamic Interaction of
Soil and Structure (DISS_13)”

*Dynamic Interaction between Soil,
Monuments and Built Environment*

Rome, 12-13 December 2013

Organization

Scientific Committee:

Arrigo Caserta
Giuliano Milana

Organizing Committee:

Paolo Clemente
Gino D'Ovidio
Dante Galeota
Antonio Rovelli
Marco Tallini
Gianfranco Valente

The Workshop received supports by:

University of L'Aquila and its Dpt. ICEAA, Department of Achitecture of the University Roma Tre, University Roma Tre, Società Roma Metropolitane s.r.l., Istituto Nazionale Geofisica, ENEA, Cassa di Risparmio di L'Aquila, Fondazione Cassa di Risparmio di L'Aquila, ANCE L'Aquila

DYNAMIC INTERACTION OF SOIL AND STRUCTURE (DISS_13)

PROCEEDINGS OF THE 3rd INTERNATIONAL WORKSHOP
Dynamic Interaction between Soil, Monuments and Built Environment
ROME, 12-13 DECEMBER 2013

Edited by
Carlo Baggio
Paolo Clemente
Yutaka Nakamura
Luciana Orlando
Antonio Rovelli
Gianfranco Valente

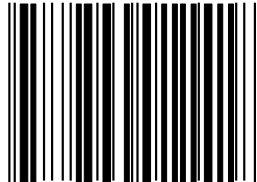
DISS_Edition c/o DICEAA - L'Aquila University - via Giovanni Gronchi, 18
67040 L'Aquila - +39.0862.434552

*This book has an internal distribution between Authors, Researchers and public
scientific Libraries, without any commercial interest*

1st edition: April 2015

ISSN 2612-4009

ISEN 978-88-940114-1-8



9 788894 011418

In the same collection, Proceedings of the International Workshops
“*Dynamic Interaction of Soil and Structure*”:

1st DISS_10, L'Aquila 19 March 2010, D'Ovidio G., Nakamura Y., Rovelli A.,
Valente G., Aracne, ISBN 978-88-548-3693-8.

2nd DISS_12, L'Aquila 29-30 March 2012, Clemente P., D'Ovidio G., Nakamura
Y., Rovelli A., Tallini M., Totani G., Valente G., *DISS_Edition*,
ISBN 978-88-94011-0-1.

INDEX

- 7 Preface
9 Opening address
- SESSION I**
- 11 REPAIRING CONNECTIONS BETWEEN STATUES AND THE BODY OF CONSTANTINE'S ARCH
Carlo Baggio, Cinzia Conti
- 21 SEISMIC HAZARD AND LOCAL RESPONSE IN THE PRESERVATION OF CULTURAL HERITAGE
Antonio Rovelli, Cinzia Conti
- 33 VIBRATION ANALYSIS AND INNOVATIVE TECHNOLOGIES IN THE PRESERVATION OF CULTURAL HERITAGE
Paolo Clemente, Cinzia Conti, Alessandro De Stefano
- 47 A METHODOLOGY TO ANALYZE AMBIENT VIBRATIONS IN THE COLOSSEUM
Arrigo Caserta, Paolo Clemente, Cinzia Conti, Gino D'Ovidio, Yutaka Nakamura, Rossella Rea, Antonio Rovelli, Gianfranco Valente
- SESSION II**
- 79 THE IMPORTANCE OF DEFINING THE GEOMETRY OF FOUNDATIONS AND SOIL LAYERS FOR DYNAMIC ANALYSIS OF COLOSSEUM
Heinz-Jürgen Beste, Paolo Clemente, Cinzia Conti, Gino D'Ovidio, Yutaka Nakamura, Luciana Orlando, Rossella Rea, Antonio Rovelli, Gianfranco Valente
- 111 SHM EXPERIENCES OF MONUMENTS IN DIFFERENT STRUCTURAL, USE AND ENVIRONMENTAL CONDITIONS
Claudio Modena
- 153 DYNAMIC CHARACTERISTICS OF GREAT BRONZE BUDDHA OF KAMAKURA USING MICROTREMOR
Yutaka Nakamura, Jun Saita, Mitsuhiro Tachibana and Tsutomu Sato
- SESSION III**
- 183 CRACKING PATTERN AND SEISMIC PERFORMANCE ASSESSMENT OF THE ORVIETO CATHEDRAL
Gerardo De Canio
- 217 EFFECTS OF AMBIENT VIBRATIONS ON HERITAGE BUILDINGS: OVERVIEW AND WIRELESS DYNAMIC MONITORING APPLICATIONS
Giorgio Monti, Fabio Fumagalli, Giuseppe Carlo Marano, Giuseppe Quaranta, Rossella Rea, Barbara Nazzaro
- 231 THE APRIL 2009 L'AQUILA EARTHQUAKES: RECORDINGS IN THE COLOSSEUM AREA
Arrigo Caserta, F. Marra, A. Govoni, A. Rovelli
- 243 EVALUATION OF THE STRUCTURAL HEALTH STATUS OF THE COVERINGS OF VILLA OF THE MYSTERIES IN POMPEII

Bruno Carpani

SESSION IV

- 263 DYNAMIC CHARACTERISTICS OF THE MEMORIAL COLUMNS OF
TRAJAN AND MARCUS AURELIUS USING MICROTREMOR
Yutaka Nakamura, Jun Saita and Tsutomu Sato
- 281 THE COCLID COLUMNS IN ROME: AMBIENT VIBRATION SRVEY
AND COMPARISON WITH PREVIOUS RESULTS
*Giovanni Bongiovanni, Giacomo Buffarini, Paolo Clemente, Cinzia Conti,
Francesco Del Monaco, Federica Durante, Antonio Rovelli, Fernando
Saitta, Sandro Serafini, Marco Tallini, Gianfranco Valente*
- 295 EXPERIMENTAL ANALYSIS AND NUMERICAL MODELLING OF
SANTA MARIA IN COLLEMAGGIO BASILICA IN L'AQUILA
Sara Amoroso, Iolanda Gaudiosi, Giuliano Milana, Marco Tallini
- 311 Authors index

Introduction

It is a great pleasure for me to open this international workshop on 2013; it is the third edition following the first on 2010, and the second on 2012. At the time of L'Aquila earthquake on 6 April 2009, a spontaneous group grown up about researches on Dynamic interaction of Soil and Structure (DISS), between University of L'Aquila, ENEA, INGV, the Society of Roma Metropolitane s.r.l. and others.

Japan country lives since long time with strong and frequent earthquakes, and it would seem the natural location for advanced seismic studies.

Professor Nakamura is one of the world's leading scientists in engineering seismology. He is President of the System and Data Research Company and a visiting professor at the Tokyo Institute of Technology. Our special thanks go to the Organizing Committee who made this important event possible.

One of the most important causes of damage to structures is inaccuracy in estimating earthquake excitation characteristics during the design phase.

It is well known that many of the buildings in L'Aquila were built well over a hundred years ago. Hence the earthquake acted upon a variety of structures, some only designed for structural loads whilst others with no structural design at all. It is therefore reasonable to expect that the majority of structures experienced some damage.

The soil conditions of the area and the geological formation had a significant effect on the distribution of the structural damage.

The information that can be gathered from studies, symposia and workshops on microzonation and dynamic soil-structure interaction will contribute to more accurate estimations of expected ground motion caused by earthquakes and clarify governing principles for the structural rehabilitation of damaged buildings.

This is the main focus of these important workshops.

In concluding my speech, I would like to wish you all a fruitful and pleasant stay in our University.

*Director of Dept. ICEAA, University of L'Aquila, Dante Galeota
L'Aquila, 12 December 2013.*

Greetings from the Director of the “Dipartimento di Architettura”, Roma Tre University

We welcome you to the Third International Workshop “Dynamic Interaction of Soil and Structure”.

Dynamic interaction of soil and structure, goal of the DISS workshops, is a highly specialized topic, but this edition is devoted mainly to protection of cultural heritage, from imperial columns in Rome to villas in Pompeii, from Coliseum and Constantine’s Arch to Orvieto and L’Aquila monuments.

In our Department many members of the staff are deeply involved in research concerning protection of cultural heritage by different point of views; in many cases fruitful cooperation exists with Superintendencies for cultural heritage.

So we are honoured to host in our campus this special 2013 edition of the event.

First of all we would like to welcome Professor Yutaka Nakamura, one of the world leading experts in Engineering Seismology.

Special thanks for patronage or sponsorship go to Roma Tre University, ENEA, Soprintendenza Speciale per i Beni Archeologici di Roma (SSBAR), INGV, Università degli Studi di L’Aquila.

So, too, we are delighted to welcome staff from superintendencies and in particular to members of SSBAR.

And finally our special thanks to the Organizing Committee.

The papers submitted and accepted for presentation will be included in the workshop proceedings.

A hearty welcome to all of you. We look forward to see you again in our campus.

May the workshop proceed.

Elisabetta Pallottino

Director, Dipartimento di Architettura; Professor of Architectural Conservation

L’Aquila, 12 December 2013.

Repairing of connections between statues and the body of Constantine's arch

Carlo Baggio¹, Cinzia Conti²

Abstract

This paper presents and illustrates recent local restoration of Dacians in the upper part of the Constantine's Arch in Rome. The eight statues standing on entablature of columns sixteen meters above ground level are fastened to the main body of the arch by round iron bars driven inside the statue and the arch wall section.

During summer 2013 observation from a telescopic truck crane revealed deterioration of connections which appeared rusted and broken. The paper deals with methodology of interventions as well as numerical analysis carried out to establish efficiency of connectors against earthquakes. Results obtained by simple rigid body behaviour and by finite element analysis are presented and discussed.

1 'Roma Tre' University, Rome, Italy.

2 Soprintendenza Speciale per i Beni Archeologici di Roma.

1. Introduction

Honorary arches are outstandingly significant examples of roman architecture; Constantine's Arch rises near the Coliseum and is, owing to its size, the most impressive honorary arch of the roman age (26 meters length, 10 m width, 21 m height). The monument experienced a number of restoration works during its life; in the modern age in 1720, in 1955 e in the nineties. During the restoration in 1955 steel bars were bored vertically inside the four columns in the corners and tied in pairs at the top. On each façade there are four marble columns connected at the top by an entablature from which an attic rises. The attic is enveloped by eight marble Trajan statues, the Dacians, standing on marble bases or plinths supported by the cornice of the entablature. During summer 2013, from a telescopic truck crane, damage was observed in relation to the metal rods connecting the statues to the main body of the arch; a complete scaffolding was erected around the arch to examine closely all the connectors of the eight Dacians. (See figures 1-6).

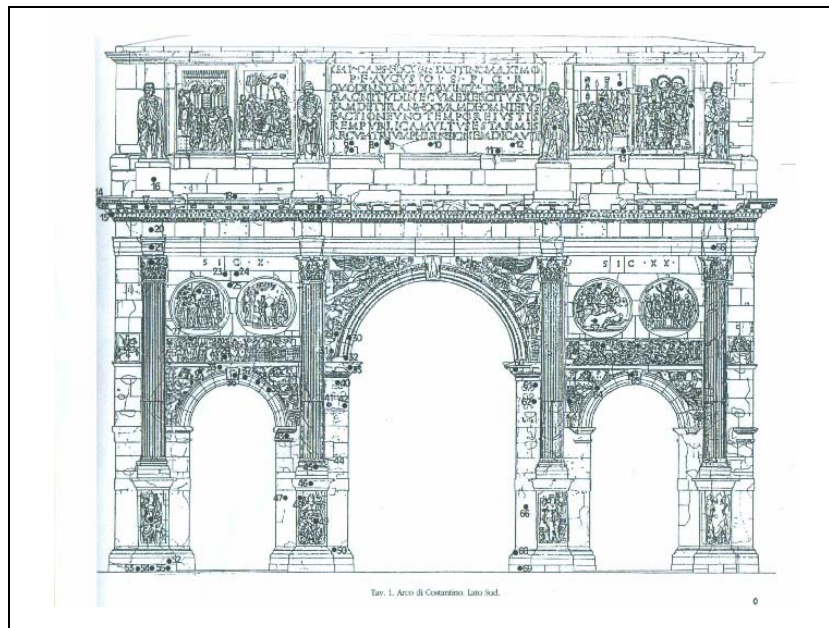
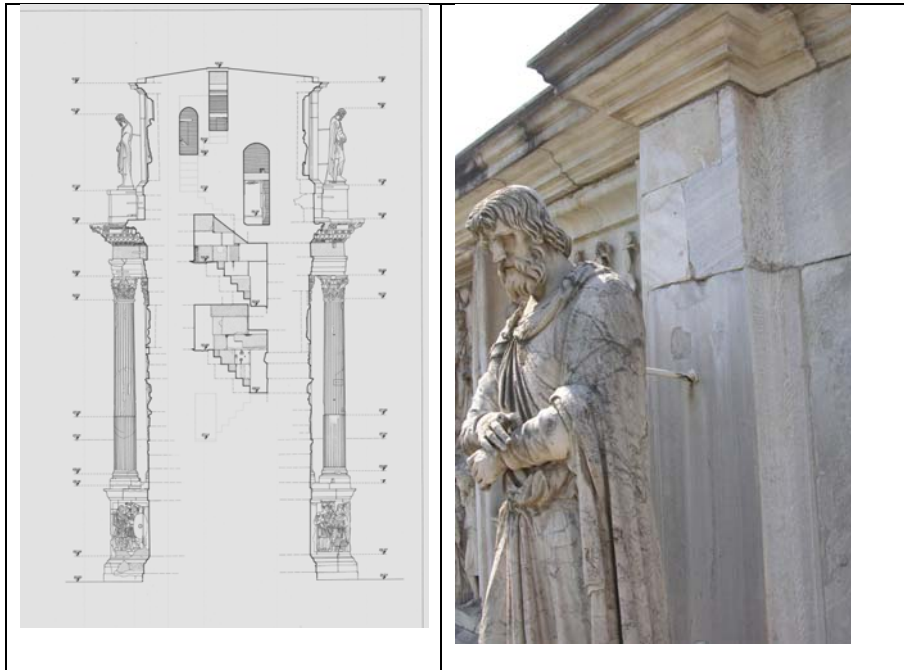


Figure 1. Front

The rod fastening the statue at the South-East corner of the arch came out to be completely fractured, separated into two pieces (see figure 7), i.e. that specific Dacian was unfastened and free to overturn under a minor seismic event: in fact the base of this statue is broken into two pieces and a collapse mechanism involving uplifting and rotation about an axis parallel to the arch front could be activated easily (see figure 9)

The work team decided to remove the eight bars from inside the statues and the body of the arch and to substitute them all with stainless steel bars. Some of the removed bars shown heavy damage, ageing, oxidation with deep brittle coating around the nucleus of the metal, chemical attack by moist air and contaminated environment.



Figures 2-3. Section- Statue

A laser scanning survey of one of the most damaged statues was carried out (figure 10); damage is related to fractures and lacking of material in the marble of the feet and large holes in the tunic of the Dacian (figure 8). From the 3D solid model obtained by the survey,

volume and center of mass, G , of the statue can be drawn: volume is equal to 0.884 mc, that's to say each Dacian has a weight of about 23.9 kN; the position of G is plotted in figure 11.



Figure 4-5 Rusted bar inside the broken cover.

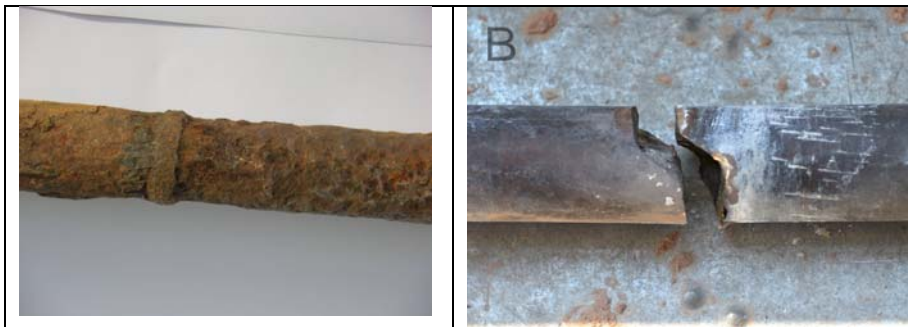


Figure 6 - 7. damaged bars



Figure 8 - 9. Material damages

2. Seismic hazard and vulnerability

Following Italian Code, free-field peak ground acceleration relative to the Coliseum site is $S \times 0.118g$, assuming the return period equal to 475 years and $S=1.5$ for soil of class C. The maximum amplification factor results 2.625.



Figure 10 - 11. Statue model and center of mass

The modal analysis of the arch has been taken from literature [2]; the arch was analyzed by a finite element code (ADINA) with homogeneous, elastic, isotropic material. The fundamental shape corresponds to a transversal vibration with a frequency $n_1=4.1$ Hz; the second mode is longitudinal with a frequency $n_2=6.1$ Hz (see figure 12).

3. Analysis of the Dacian as an oscillating rigid body

Dynamic analysis of the statue (without connections with the arch) can be achieved modelling it as a rigid body oscillating on its support

(inverted pendulum) on the basis of [1] taking into account only 2D motion; for the transversal motion about an axis parallel to the major side of the basement, the generalized displacement vector of the center of mass \mathbf{S} results:

$$\mathbf{S} = \begin{Bmatrix} s_{Gx} \\ s_{Gy} \\ \theta = 1 \end{Bmatrix} = \begin{Bmatrix} 1.296 \\ 0.406 \\ 1 \end{Bmatrix}$$

The mass matrix \mathbf{M} is:

$$\mathbf{M} = \begin{bmatrix} m & & \\ & m & \\ & & J_G \end{bmatrix} = \begin{bmatrix} 0.88 & & \\ & 0.88 & \\ & & 0.62 \end{bmatrix}$$

The generalized mass becomes:

$$M = \mathbf{S}^T \mathbf{M} \mathbf{S} = 1.997$$

The generalized dragging force $T = \mathbf{S}^T \mathbf{M} \mathbf{T}$ (vector \mathbf{T} transforms mass in translational mass) is:

$$\mathbf{T} = \begin{Bmatrix} 1 \\ 0 \\ 0 \end{Bmatrix}; \quad T = 1.14$$

The maximum resisting force (generalized) is equal to $F_0 = S \cdot g$, with g gravity acceleration and $S = \mathbf{S}^T \mathbf{M} \mathbf{G}$ (vector \mathbf{G} transforms mass in gravity mass):

$$\mathbf{G} = \begin{Bmatrix} 0 \\ -1 \\ 0 \end{Bmatrix}; \quad S = -0.357$$

In figure 13, reported by [1], the maximum displacement of an s.d.o.f. oscillating body under a number of accelerograms is plotted in terms of two parameters β and γ : $\beta = \frac{S \cdot g}{M \cdot q_u} = 5.6$; $\gamma = \frac{T \cdot A}{M \cdot q_u} = 8.3$;

the statue, without connection bars, under expected seismic action (Peak acceleration $A = 0.118g \times 1.5 \times 2.625 = 0.464g$) would oscillate on its base but the maximum displacement would be nearly one-

fourth of the ultimate one. In case of longitudinal rocking, due to longer side of the basement, the motion wouldn't be triggered. Apparently reassuring this result doesn't take into account a number of other events such as 3D rocking motion about a vertex of the base, i.e. torsional motion of the statue [6] or fracturing of the base itself (see figure 9).

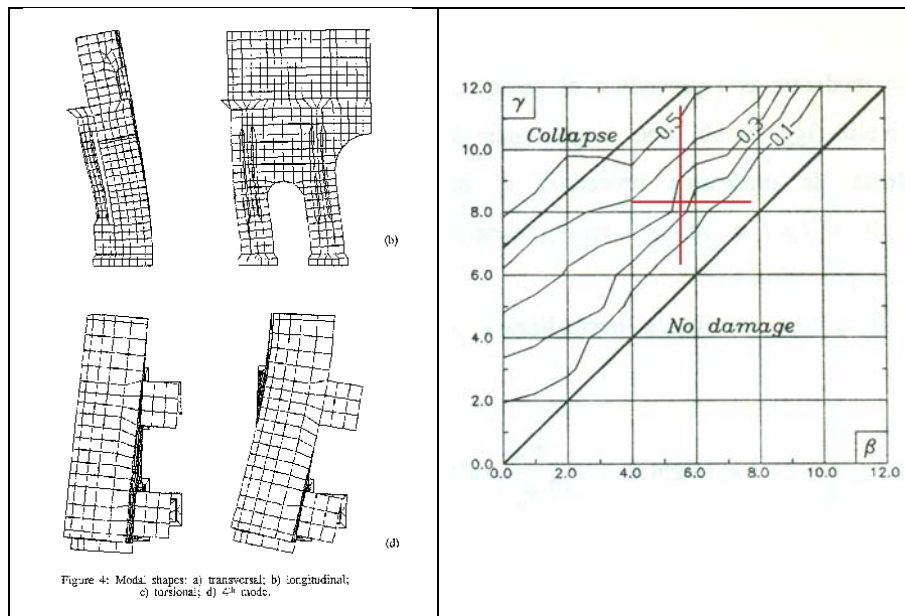


Figure 12 - 13. Gambarotta & Lagomarsino (1993). Baggio (1990).

From the point of view of good engineering practice and for the sake of safety of the monuments and of the visitors there is no doubt that the Dacians must be connected with the arch walls.

A finite element analysis has been carried out, modelling the statue with sufficient accuracy by nearly 4000 brick elements (see figure 14). Element material has been considered homogeneous, elastic and isotropic.

The analysis aims to compare the stress state of marble of the statue fastened or unfastened to the arch body. In figures 16-17 are plotted the results in terms of stress when a static horizontal mass load is applied, in the longitudinal direction, equal to 40% of the self-weight of the statue. Owing to modelling of base supports as no-tension vertical

springs, tensile stresses are negligible and the comparison regards compression stresses, the higher values of which can be detected around the fractured zone of the marble tunic. So the maximum values of compression stresses vary from 1.1 MPa in the fastened statue to 2.0 MPa in the unfastened one.

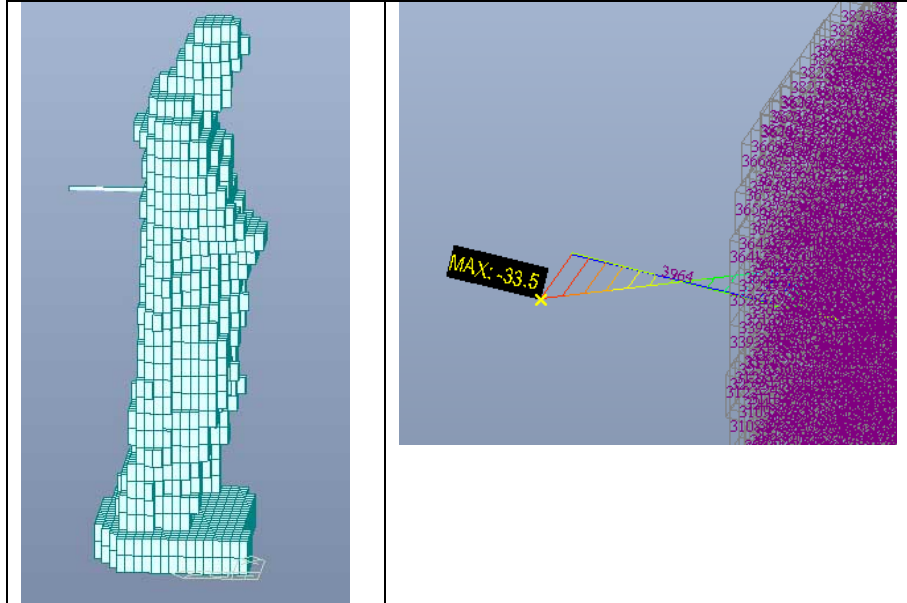


Figure 14 -15. Finite element model and bending moments in the bar

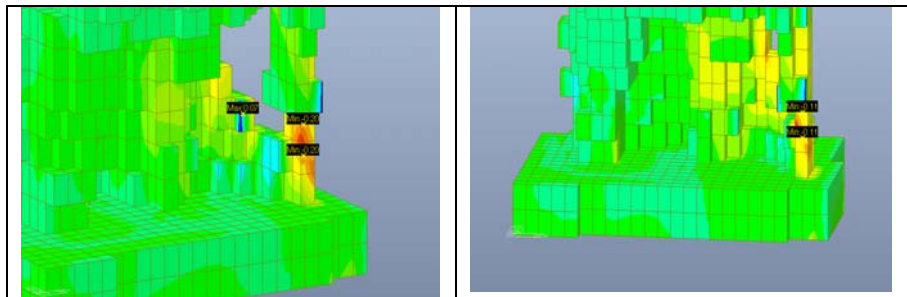


Figure 16 - 17. Stresses in the unfastened model (left) and the fastened one (right)

Conclusions

This paper takes origin from a cooperation with archeologists and architects of Soprintendenza Archeologica di Roma.

Cooperation provided expert judgment in a very specific situation; so a decision had to be taken with promptness and firmness, in view of safety of the monument and with good engineering professional practice; all the same, approaches assumed from literature and accurate finite element model were useful in decision making.

Future works

Even though a great amount of measurements were carried out in recent years around the Coliseum and Constantine's arch [4] to estimate local site effect like predominant frequency and amplification factor, the H/V technique could be useful also on buildings.

Once the measurement of the dynamic response of the arch to environmental actions such as the vibrations induced by traffic will be available, it would be possible the dynamic identification of the arch and the refinement of a finite element model with tuned parameters, so to perform a fully dynamic analysis of the statues.

References

[1] Baggio, C., (1990), *Sullo studio del comportamento sismico delle strutture murarie. Risposta sismica di catene cinematiche di corpi rigidi*, in Studi e Ricerche sulla sicurezza sismica dei monumenti, 11, Dipartimento di Ingegneria Strutturale e Geotecnica, Università La Sapienza.

[2] Gambarotta e Lagomarsino (1993), *Structural analysis of Roman honorary arches: Constantine's Arch*, Structural Repair and Maintenance of Historical Buildings III, a cura di C.A. Brebbia e R.J.B. Frewer.

[3] Funicello R, Giordano G., (2008), *La nuova carta geologica di Roma: litostratigrafia e organizzazione stratigrafica*, in Mem. Descr. Carta geol. It. LXXX.

[4] Nakamura, Y., (2010), *The H/V Technique and Example of its Application for L'Aquila and Rome Areas*, Proc. of Workshop DISS_10, a cura di G. D'Ovidio, Y. Nakamura, A. Rovelli, G. Valente.

[5] Software MIDAS Gen 2012.

[6] Di Egidio, A., Zulli, D., Contento, A., (2012), *Seismic response of three-dimensional rocking rigid blocks with a rectangular base*, Proc. Workshop DISS_12, a cura di P. Clemente, G. D'Ovidio, A. Rovelli, M. Tallini, G. Totani, G. Valente.

Seismic Hazard and Local Response in the Preservation of Cultural Heritage

Antonio Rovelli¹, Cinzia Conti²

Abstract

This paper presents a review of investigations aimed at assessing potential earthquake-induced ground motions in the city of Rome. The diffuse historical heritage and the presence of invaluable monuments to preserve required accurate studies of local geological conditions. This information is important to reach a more refined, site-dependent seismic input estimate where also the individual monument structure and its intrinsic vulnerability are properly taken into account. Many of the investigations dated back to the last decade of the past century when instrumental data from significant earthquakes were not yet available for the city of Rome. In those times, analysis methods were mostly based on geological inferences to reconstruct the local near-surface structure and develop site response theoretical computations. The 6 April 2009, Mw 6.3 L'Aquila earthquake has provided several important records of ground motion in the city for moderate magnitude earthquakes occurring in central Apennines where the largest magnitude earthquakes of interest for Rome are expected. These data are fundamental for a comparison of past ground motion predictions with real observations in Rome, and confirm the validity of the methodologies used before the 2009 L'Aquila earthquake. The assessment of future destructive ground motions in Rome is now more feasible because it can be based on the scaling of the really experienced monument shaking at moderate magnitudes.

1 Istituto Nazionale di Geofisica e Vulcanologia, Roma, Italy.

2 Soprintendenza Speciale per i Beni Archeologici di Roma, Italy.

The relation between local geology and historical monuments in the city of Rome

In the last decades of the past century, geologists and geophysicists of Roman universities and scientific institutions focused their attention on the not negligible role that local geology plays on the every-day life of the city. The awareness that geological factors influenced the origin and the history of Rome led an eminent geologist, Renato Funiello, to promote systematic studies of the geological evolution of the region and the relationship between the growth of the city and its geology (see papers of volume [1] and references therein).

In the plethora of those issues of research, monuments of Rome were primary targets of study in the nineties. Giangiacomo Martines was in charge of maintenance of columns of Trajan and Marcus Aurelius in those years. Since 1979 until 2002, as executive chief he promoted the first instrumental investigations on these famous monuments, with interventions of scientific institutions thanks to a cooperative effort with Antonino Giuffrè and Enzo Boschi, from university and ING, respectively and Maurizio Diana and Mauro Basili from ENEA. Rossella Rea, in charge of maintenance of Colosseum since 2003, coordinated several studies of historical earthquakes that were experienced by the monument and promoted dynamic investigations to test the monument behavior in relation with the Metro C excavations.

The results of these researches showed the strict dependence of the history of monuments on the peculiarities of sites where monuments were erected. In the following, we illustrate some of the most representative steps of activities begun several decades ago. Many other relevant papers are listed in references.

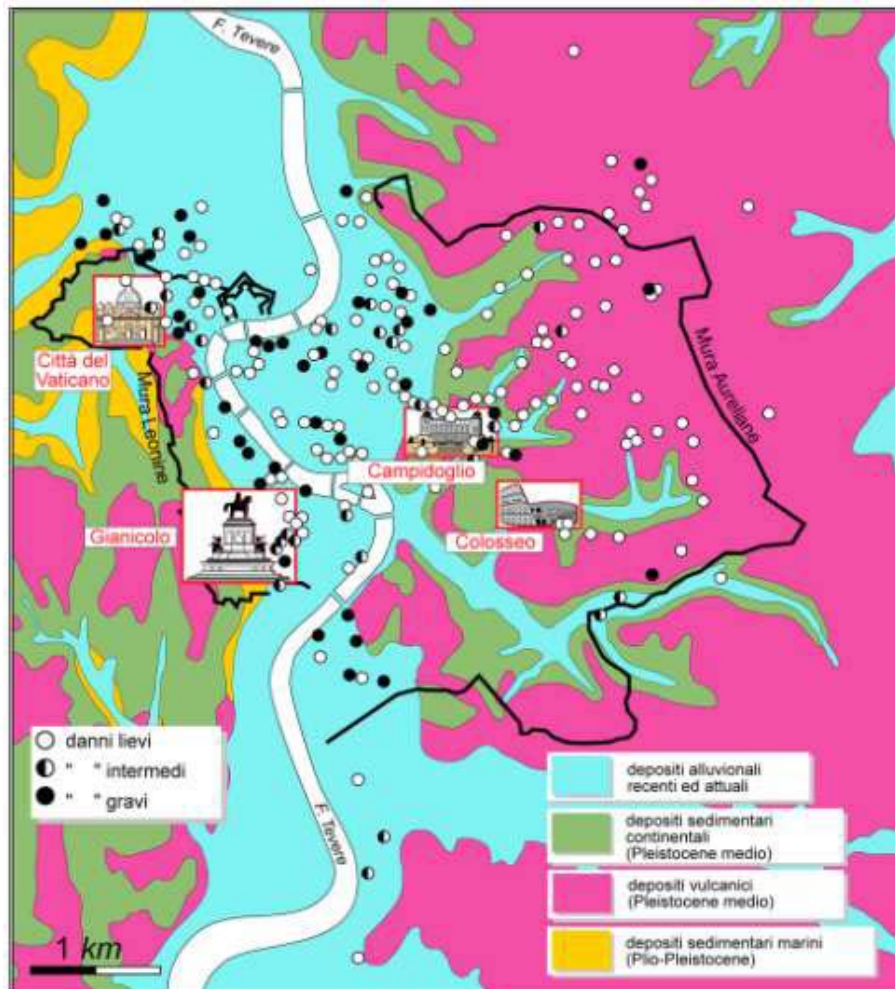


Figure 1. Damage distribution following the 1915 Fucino earthquake (redrawn from [2]). This damage evaluation first remarked the occurrence of a significant amplification effect on the alluvial sediments of the Tiber river in downtown Rome. The largest part of the monumental patrimony of Rome is located in this study area.

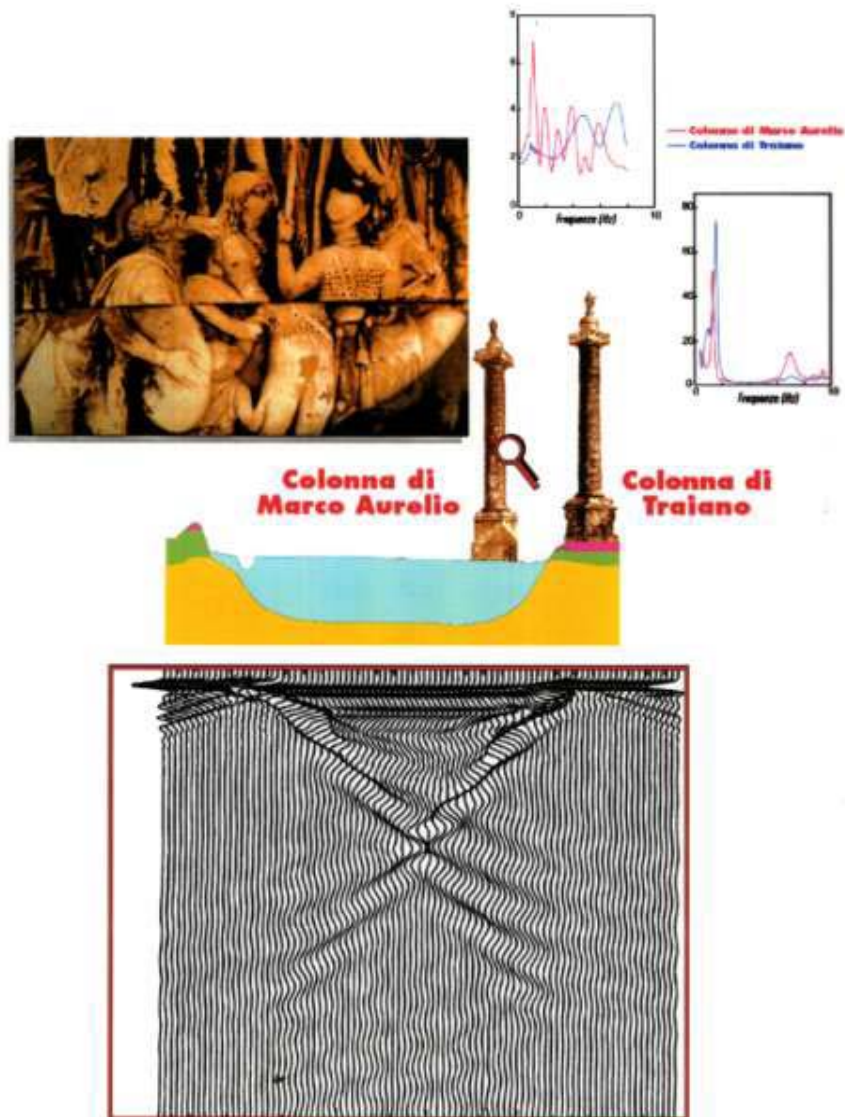


Figure 2. The different damage of the Coclid columns in Rome is consistent with a different shaking level of their sites during historical earthquakes [3]. The fundamental vibration mode of the Marcus Aurelius column corresponds to a frequency band that is significantly amplified locally because of the soft upper layers of the Tiber river valley. Numerical simulations by Boschi et al. (1995) indicated a factor of 4 to 6 amplification at the base of the Marcus Aurelius column .

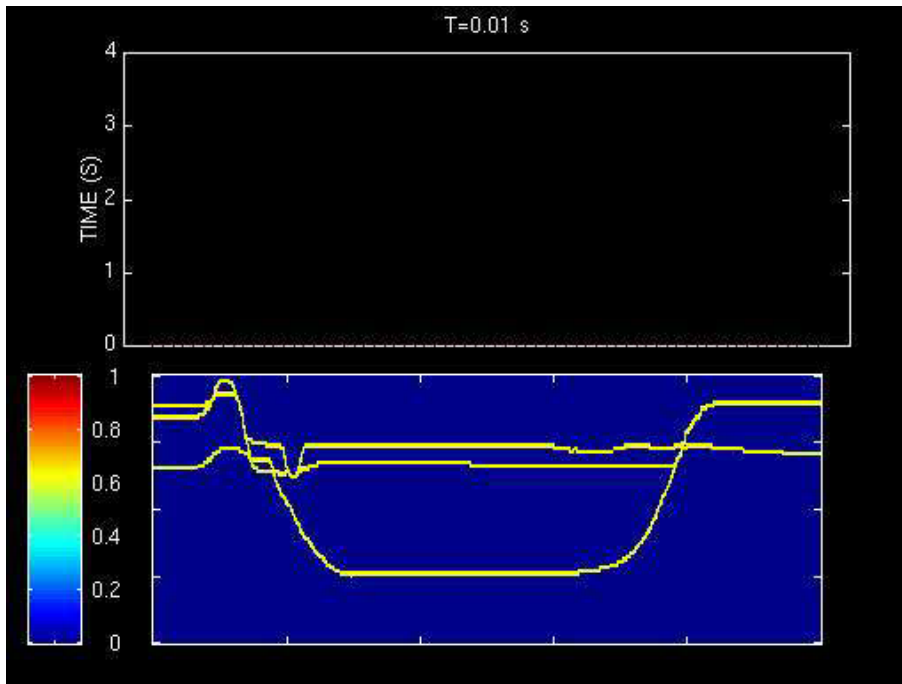


Figure 3. 2-D modeling of the transient response of the Tiber river valley when excited by a delta-like input (courtesy by Arrigo Caserta, the movie that describes the numerical simulation is available on request). Details are illustrated in [4].

Ground Motions Recorded in Rome during the April 2009 L'Aquila Seismic Sequence

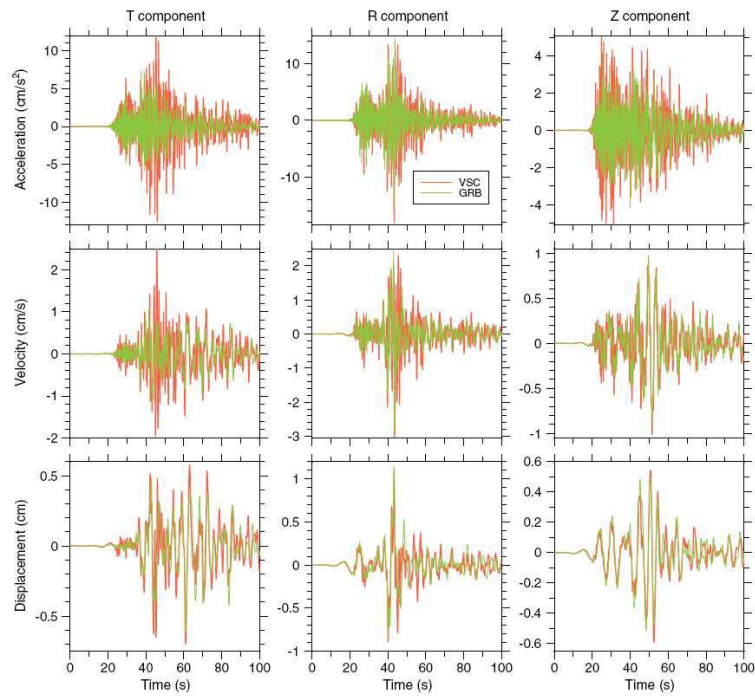


Figure 4. Observations of ground motion in downtown Rome during the April 2009 L'Aquila earthquake (redrawn from [5]). VSC and GRB, few hundreds of meters away, are two seismological stations installed on Holocene alluvial sediments and Pleistocene volcanites, respectively. This figure confirms the high-frequency amplification effect on the Tiber river sedimentary deposits: accelerations at VSC are significantly larger than those of GRB, although displacements do not change between the two sites.

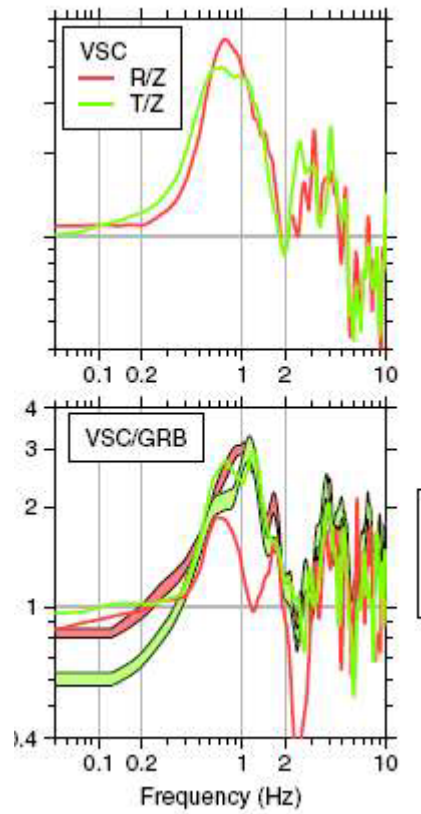


Figure 4. Variations of ground motion in downtown Rome during the April 2009 L'Aquila earthquake (from Caserta et al., 2013). The relative amplification at VSC around 1 Hz is estimated in a factor of 3 compared to GRB. However, absolute amplification of VSC is likely larger since also GRB is amplified around 1 Hz (see Fig.5).

Ground Motions Recorded in Rome during the April 2009 L'Aquila Seismic Sequence

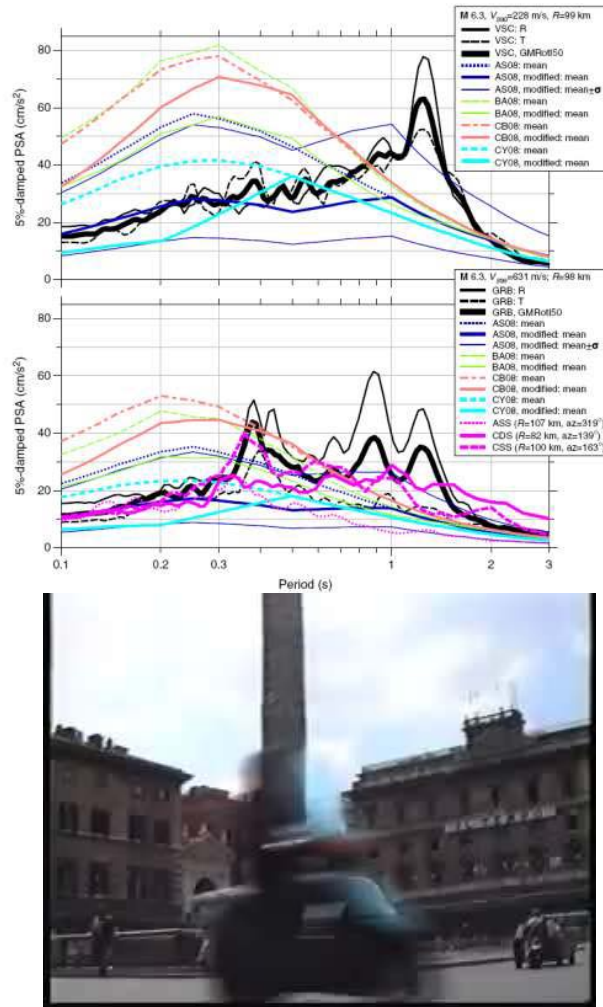


Figure 5. Response spectra(5% damping) at stations in downtown Rome during the 6 April 2009 L'Aquila earthquake (from Caserta et al., 2013). A large (by a factor of 4) deviation from expectations is found at periods around 1 sec. A shaking table experiment was realized at the Institute of Earthquake Engineering and Engineering Seismology of Skopje (November 1995) using a similar value of the site ground motion amplification. In that experiment, a column model (1:3 scale) was excited by a realistic seismic input (the movie is available on request). The result of the shaking table experiment was the generation of cracks in the column body for severe inputs as well as a sliding effect between column blocks in the central part of the column model.

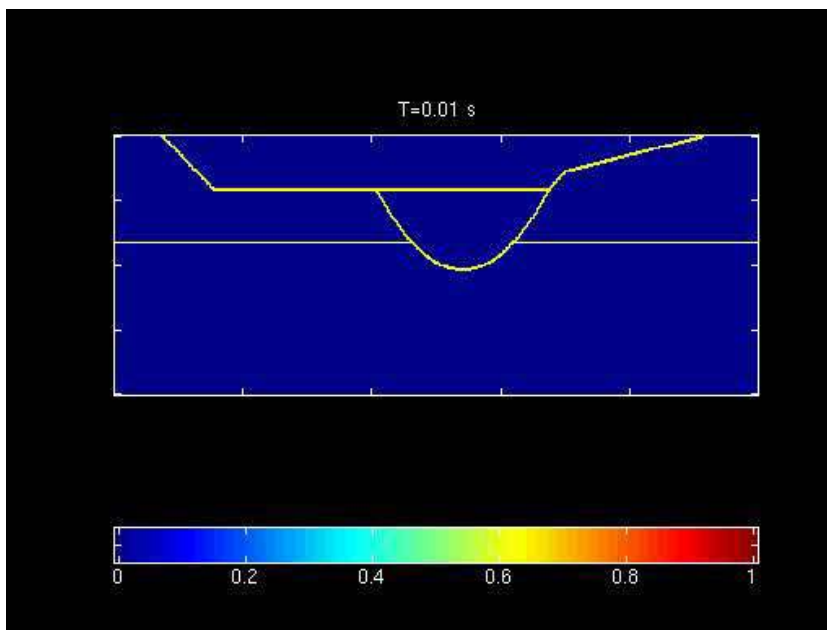
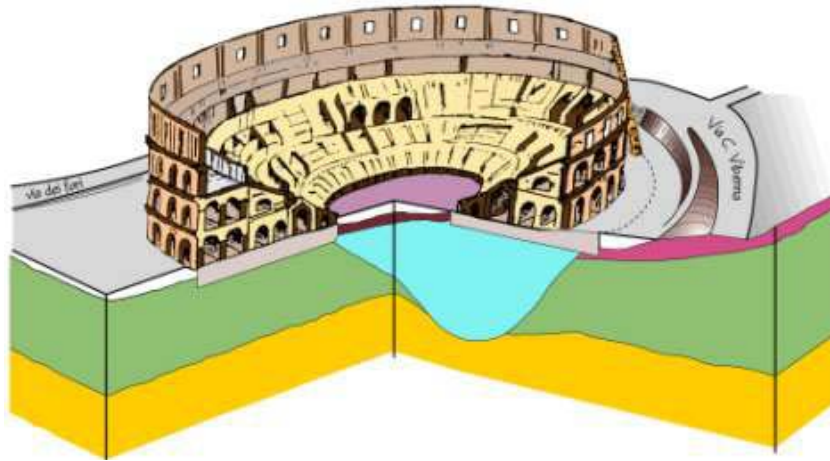


Figure 6. Sketch of the geological structure beneath the Colosseum (redrawn from [6] and [7]) and expected variations of ground motion during earthquakes (courtesy by Arrigo Caserta, the animation that illustrated the numerical simulation is available on request).

References

[1] Funiciello, R. et alii (1995). La Geologia di Roma, *Memorie Descrittive della Carta Geologica d'Italia*, Volume L, p. 550, Istituto Poligrafico e Zecca dello Stato, Roma.

[2] Ambrosini, S., S. Castenetto, F. Cevolani, E. Di Loreto, R. Funiciello, L. Liperi, and D. Molin (1986). Risposta sismica dell'area urbana di Roma in occasione del terremoto del Fucino del 13-1-1915, *Mem. Soc. Geol. It.*, 35, 445–452.

[3] Boschi, E., A. Caserta, C. Conti, M. Di Bona, R. Funiciello, L. Malagnini, F. Marra, G. Martines, A. Rovelli, and S. Salvi (1995). Resonance of subsurface sediments – An unforeseen complication for designers of Roman columns, *Bull. Seism. Soc. Am.*, 85, 320-324.

[4] Rovelli A., Caserta A., Malagnini L., Marra F (1994). Assessment of potential strong ground motions in the city of Rome, *Annali di Geofisica*, 37, 1745-1769.

[5] Caserta, A., D. M. Boore, A. Rovelli, A. Govoni, F. Marra, G. Della Monica, and E. Boschi (2013). Ground motions recorded in Rome during the April 2009 L'Aquila seismic sequence: Site response and comparison with ground-motion predictions based on a global dataset, *Bull. Seism. Soc. Am.*, 3, 1860–1874, doi: 10.1785/0120120153.

[6] Funiciello, R., L. Lombardi, F. Marra, and M. Parotto (1995). Seismic damage and geological heterogeneity in Rome's Colosseum area: are they related?, *Annali di Geofisica*, 37, 927-937.

[7] Moczo, P., A. Rovelli, P. Labák, and L. Malagnini (1995). Seismic response of the geologic structure underlying the Roman Colosseum and a 2-D resonance of a sediment valley, *Annali di Geofisica*, 37, 939-956.

[8] Bozzano, F., Funiciello, R., Marra, F., Rovelli, A., Valentini, G. (1995) “*Il sottosuolo dell'area dell'anfiteatro Flavio in Roma*”, 405÷422.

[9] Nakamura, Y. (1996). “Seismic response of roman Colosseum and its foundation by using micro-tremor measurements”, *The 10th Japan Earthquake Engineering Symposium*, pp. 2625-2630, 1998.

[10] Coarelli F., Gregori G.L., Lombardi L., Orlandi S., Rea R., Vismara C., “*Il Colosseo*”, Electa, Milano, 1999.

[11] Nakamura, Y., Gurler, E.D., Saita, J., Rovelli, A., Donati, S., (2000). Vulnerability investigation of roman Colisseum using ambient vibration, *12WCEE2000*, paper 2660.

[12] Jappelli R., Rea R., Schingo G., “Artificial openings in the foundation of the Colosseum”, *AITES-ITA 2001 World Tunnel Congress, Milano*, June 2001.

[13] Orlando L., Bernabini M. (2002), “La geofisica nella caratterizzazione delle fondazioni dell’anfiteatro Flavio”, *21° Convegno nazionale, Gruppo nazionale di geofisica della terra solida*.

[14] Akinci A., Olsen K. B., Rovelli A., Marra F., Malagnini L. (2002) “Simulazioni 3-D e produzione di scenari di scuotimento nella città di Roma”, *21° Convegno nazionale, Gruppo nazionale di geofisica della terra solida*.

[15] Olsen, K.B., A. Akinci, A. Rovelli, F. Marra, and L. Malagnini (2006). 3D ground-motion estimation in Rome, Italy, *Bull. Seism. Soc. Am.*, 96, 133-146.

[16] Cerone, M., A. Rovelli, and G. Valente (2004). “*Indagine preliminare per l’Identificazione Dinamica del Colosseo*”, ANIDIS.

[17] Caserta, A., M. Cerone, F. Crisi, A. Delladio, G. D’Ovidio, A. Govoni, F. Marra, Y. Nakamura, A. Rovelli, and G. Valente (2010). “*Dynamic interaction of soil and structure by rail traffic*”, Proceedings of Workshop DISS_10, L’Aquila, 19 March 2010, Aracne, ISBN 978-88-548-3693-x.

[18] Caserta, A. P. Clemente, Y. Nakamura, A. Rovelli, and G. Valente (2012). “*Identification of the mean elasticity modules for soil Colosseum interaction*”, DISS_12, L’Aquila, March 2012, in print, Aracne, ISBN 978-88-548-xxxx-x.

[19] Donati, S. R., Funicello and A. Rovelli (1999). Seismic response in archaeological areas: the case-histories of Rome, *Jou. Applied Geophys.*, 41 (2-3), 229-239.

[20] F. Bozzano, A. Caserta, A. Govoni, F. Marra, and S. Martino (2008). Static and dynamic characterization of alluvial deposits in the Tiber River Valley: New data for assessing potential ground motion in the City of Rome, *Jou. Geophys. Res.*, 113, B01303, doi: 10.1029/2006JB004873.

Vibration analysis and innovative technologies in the seismic preservation of cultural heritage

Paolo Clemente¹, Cinzia Conti², Alessandro De Stefano³

Abstract

In order to preserve historical buildings and monuments against the effects of earthquakes a detailed analysis is needed to evaluate the characteristics of the seismic input and the dynamic behaviour of structures under seismic actions and to choose the most suitable seismic rehabilitation technique. In this paper the experimental analyses carried out on the Colosseum and the Lateran Obelisk are first shown. Then the application of seismic isolation in historical buildings is discussed and a new structure for the seismic isolation of existing building is presented.

1 ENEA C.R. Casaccia, Rome, Italy.

2 SSBA, Rome, Italy.

3 Politecnico di Torino, Turin, Italy.

1. Introduction

Italians are best known in the world as experts and lovers of arts. Actually, our country has given birth to several artists as well as to famous engineers and architects that realized impressive structures and most of the worldwide cultural heritage is in Italy, giving us the duty to preserve it. The safeguard of cultural heritage must be ensured for future generations not only in reason of the cultural identity of the population it represents, but also because cultural heritage could be a driving force for the economy (Clemente et al., 2012).

In the past, but also recently, earthquakes caused relevant damages to historical buildings and monuments. The earthquakes that struck Umbria and Marche in 1997, Molise in 2002, Abruzzo in 2009 and Emilia in 2012, are only few well-known examples in Italy. In order to guarantee the conservation of the cultural heritage arrived up to our age for the future generations, it is important a suitable prevention politics that requires a big effort. For each selected areas and buildings a detailed analysis is needed to understand:

- the characteristics of the seismic input, by means of basic hazard analysis and local seismic response; this can be done only on the basis of a suitable monitoring of the area (Bongiovanni et al. 2012; Bergamasco et al., 2012);
- the seismic performance of buildings; the knowledge of the dynamic behaviour under seismic actions of structures of interest should also be performed by means of the seismic monitoring (Clemente & Buffarini, 2009; De Stefano & Clemente, 2009).

In the last decades new technologies have been developed in order to improve the seismic resistance of structures. These are mainly seismic isolation systems and energy dissipation systems consisting of various types of passive devices (elastic-plastic, viscous, viscous-elastic and electro-inductive dampers). The practical application of such new technologies is quite different for cultural heritage structures with reference to civil buildings (Clemente et al., 2012).

In this paper some relevant experiences carried out on the experimental dynamic analysis of monuments and some interesting applications of seismic isolation are presented.

2. Experimental vibration analysis of monuments

The first step in a preservation effort is the investigation of the health status of the structure. This should always include the analysis of dynamic behavior, especially if earthquake and traffic induced vibrations could affect the structure. The results of two relevant some experimental studies carried out by ENEA are shown in the following.

2.1 *The Colosseum*

In the framework of a large project organized by ENEA in collaboration with the *Soprintendenza Speciale per i Beni Archeologici (SSBA) di Roma* and ISMES, the effects of the traffic-induced vibrations on several monuments in Rome were investigated (Clemente et al., 1988; Bongiovanni et al., 1990; Clemente et al., 1994; Clemente, 1995; Clemente, 2002). The Colosseum was one of these. It was not very healthy due to many reasons, and also to the vibrations induced by the very chaotic traffic of Rome. The structure was instrumented to study the effects of the traffic-induced vibrations, as well as the vibrations from the near underground, and to have a first glance at its dynamic characteristics (Clemente & Bongiovanni, 1993).

Eighteen seismometers were used, deployed in four different configurations (Figure 1). Data processing consisted in the statistic analysis, which allows to determine the maximum and effective values of the velocity, and spectral analysis, which resulted in the characterization of the structural resonances and the associated modal shapes. Recordings at different hours of the two days were performed, each of them lasting 30 minutes. Some interesting features were found:

- the velocity effective values over successive time intervals lasting 1.28 sec were always lower than 0.12 *mm/sec* and the peak values lower than 0.32 *mm/sec*;
- the records obtained during the transit of the train showed that this is apparent only at the basement, while there is amplification

- over the whole time range going from the basement to the top of the wall;
- the cross spectral analysis individuates the frequencies ($f_1=1.46$, $f_2=1.70$, $f_3=2.75$ Hz) that can be considered structural resonances and the corresponding peak amplitudes of the power spectral density give an idea of the associated modal shapes.

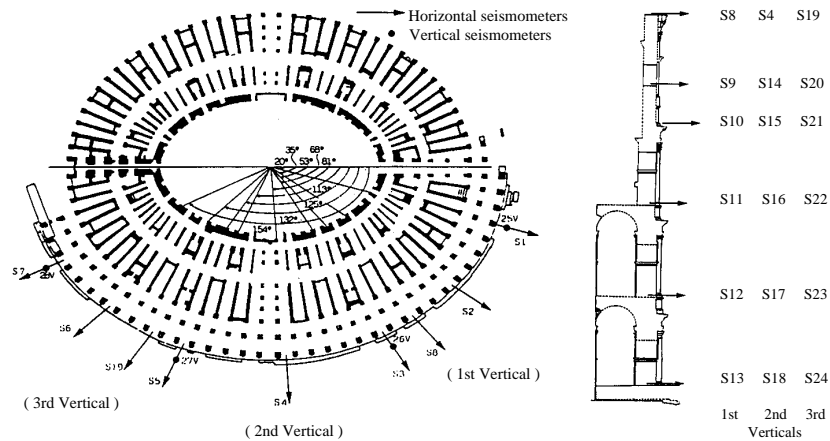


Figure 1. Plan view and sections of the seismometer locations

The seismograms obtained from the vertical sensors showed as the train transit fade rapidly. A lack of structural continuity of the top portion of the basement could explain this behavior. Also the heterogeneity of the soil underlying the monument could play an important role (Clemente & Bongiovanni, 1993).

2.2 The Lateran Obelisk

The Lateran Obelisk is made of three monolithic tapered red granite blocks, which exhibit various cracks, visible particularly near the contact surfaces between the blocks. Metallic links and small pieces of granite added during past restorations connect the blocks to each other. The Obelisk rests on a rectangular prismatic pedestal, which is positioned in turn on a wide stone base, whose depth is not known as well as the foundation conditions. The Obelisk itself is 32.18 m tall, the pedestal is about 10 m tall.

The experimental analysis was carried out by using 15 seismometers (Figure 2). The choice of the sensor locations was influenced by their accessibility and the presence of a plane surface (Buffarini et al., 2008). Several measurements lasting about 300 s were carried out during the day, when traffic induced vibrations of various intensities have been recorded, but also during the night in presence of ambient noise only. Peak values of the velocity are low on the basement while become important at the top.

Records of ambient noise were also obtained in two triaxially stations located about 10 m S (St1) and 30 m SW (St2) of the Obelisk, respectively. In a successive velocimetric survey, ambient noise records were obtained along a superficial array (C1, C2, C3, D1, D2 and D3) as well as in 2 stations located underground (A and B), on the basement of the S. Giovanni Church.

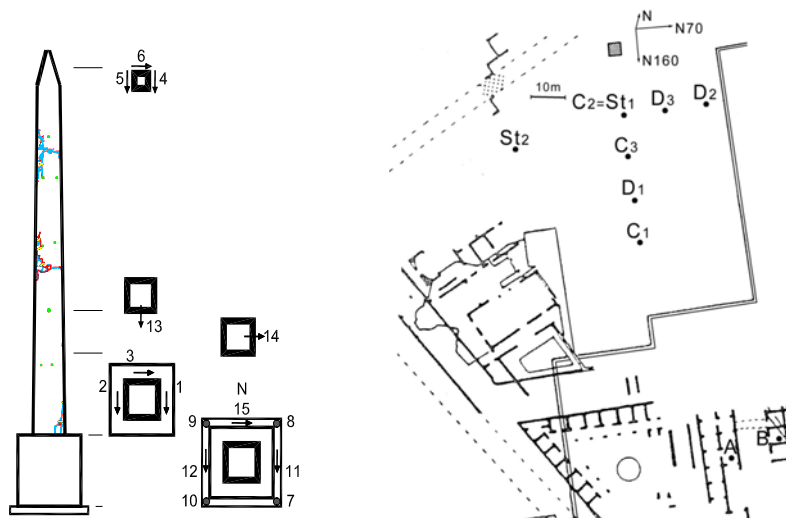


Figure 2 Sensor location on the Obelisk and on the soil and in the underground

A detailed numerical analysis was carried out (Buffarini et al. 2009). The Obelisk model was first performed by matching the numerical frequencies and modal shapes with the experimental ones. The first two modal shapes in the NS plotted in figure 3. Then the finite element model was used for the non-linear static analysis of the Obelisk, in which gap elements having no tensile resistance but infinite

compression strength were introduced at the sections between the Obelisk and the pedestal, and under the pedestal.

The results can be summarized as follows:

- spectral analysis showed a first mode corresponding at 1.27 Hz in the NS direction and a second mode, almost at the same frequency, in the WE direction; the third and the fourth modes, in the NS and WE direction are associated to frequencies of 6.15 Hz and 6.73 Hz , respectively; under vibrations of low amplitudes, such as ambient and traffic-induced vibrations, the Obelisk and its pedestal behave as a whole;
- no soil amplification of horizontal components has been found but significant amplifications of the vertical component are present at frequencies higher than 10 Hz , probably due to adjacent and/or buried structures; these amplifications are not apparent on the basement and therefore do not influence the input to the Obelisk;
- the seismic analysis, performed by means of non linear static analysis, confirmed the high vulnerability of such structures to seismic actions; in spite of that, the Obelisk did not suffer any significant effects during the Avezzano Earthquake of January 13th, 1915, which caused the collapse of a statue on the façade of the San Giovanni in Laterano Basilica.

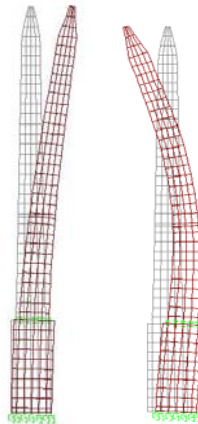


Figure 6 Modal shapes of the Obelisk in NS direction

3. Application of seismic isolation in cultural heritage buildings

The seismic rehabilitation of historical constructions is quite hard. They are often vulnerable even to moderate events, because were built without accounting for the seismic actions, are characterized by an irregular form and shallow foundations, which represent weak points in their structural capacity. It is worth reminding that the rehabilitation works must guarantee the preservation of the original monumental characteristics, identity and historical value. Furthermore, under earthquakes of high intensity, structures seismically improved by means of traditional techniques, can just guarantee against the collapse, but cannot avoid heavy damages to structural and non-structural elements. On the other hand, due to their historical importance and to the daily presence of tourists, the seismic rehabilitation of historical buildings must aim at the protection of both human life and cultural heritage.

In this context, traditional techniques, based on the increasing of strength and ductility, are not suitable for the seismic rehabilitation of cultural heritage buildings, as several past experiences demonstrated. As a matter of fact, buildings damaged by earthquakes and repaired by means of traditional techniques suffered the same damages after successive events. Therefore use of new technologies is advisable, such as seismic isolation.

3.1 Basic concepts and notable applications

As well known seismic isolation is based on a terrific reduction of the seismic actions, which affect the structure, instead of relying on its strength. This result is obtained by increasing the fundamental period of vibration of the building, so that it becomes less vulnerable to earthquakes. In fact, the superstructure will be loaded by low effects thanks to the filtering of the seismic isolation system. Obviously, the isolation system should be designed so as to reduce the seismic action in the structure to the value that the restored building will be able to support in the elastic range.

Seismic isolation have already been used for the retrofit of historical buildings. Two interesting cases are shown in the following.

The Saint Francisco city hall, built after the collapse of the previous structure during the 1906 earthquake, suffered heavy damages due to the 1989 Loma Prieta earthquake. The retrofit was done by means of the insertion of an isolation system and the realization of concrete shear walls. The foundations were first reinforced with new beams and a new deck was realized above the isolation interface. Then, the structural elements were shored up and the foundations were cut at their top. Hydraulic jacks were used as temporary supports for steel columns and brick walls to install the lead rubber bearings under each column. The isolation system was completed in 1998.

Another interesting intervention was designed by Melkumyan for a masonry school building in Vanadzor, Armenia, after the 1988 earthquake. The intervention was realized with the following construction phases (Figure 7): i) realization of windows in the masonry walls at the isolation device positions; the window should be high enough to contain a lower and an upper reinforced concrete beams and the isolator device; ii) construction of the portion of the lower reinforced concrete beam, with the overlap steel bar between the beam portion of the considered window and the next ones; iii) installation of the isolation device; iv) realization of the portion of the upper reinforced concrete beam, with the overlap steel bar between the adjacent windows; v) realization of the sandwich beams above and below the isolators; vi) cutting of masonry between the windows.

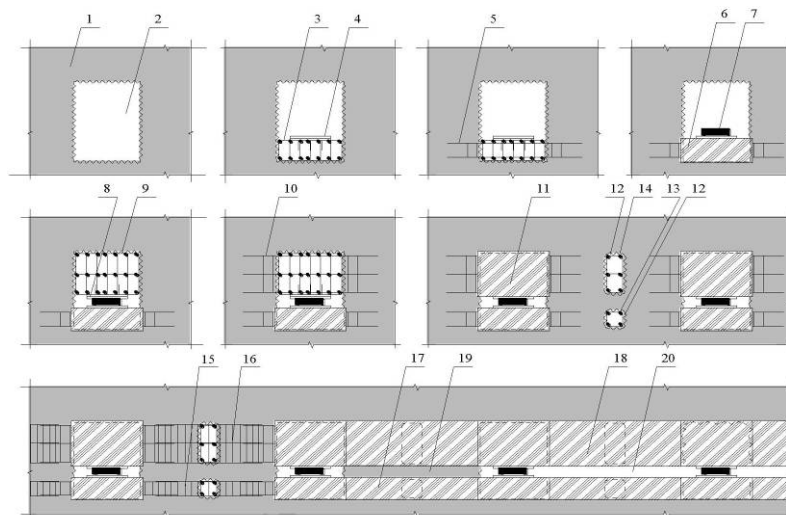


Figure 7. Construction phases of isolation system in the school in Vanadzor (courtesy by M. Melkumyan)

Among the proposals with this procedure, not realized at the moment, it is worth reminding the seismic retrofit of the Iran Bastan Museum in Tehran [Santini et al., 2007; Clemente et al., 2009) and the seismic retrofit of a residential building in Belluno, Italy.

3.2 A new seismic isolation structure for existing buildings

The new seismic isolation structure for existing buildings (SISEB) consists in the realization of an isolated platform under the foundations of the building, without touching the building itself (Figure 8). A discontinuity between the foundations and the soil is created by means of the insertion of horizontal pipes and the positioning of isolation devices at their horizontal diametric plane. In order to facilitate the successive operations, the pieces of pipe have a particular shape and are composed by two portions, the lower and the upper cylindrical sectors, respectively, which are connected by means of removable elements.

Then the building is separated from the surrounding soil in order to allow the horizontal displacements required by the isolation system. So the structure is seismically isolated but not interested by interventions that could modify its architectural characteristics, which is very important for historical buildings.

Even underground level are not modified but can be part of the seismically protected structure. The first step is the excavation of a trench at one side of the building and the successive insertion of pipes by means of auger boring or micro-tunneling technique; the diameter of pipes should be at least 2 m, in order to allow the inspection of the isolation system. The pipes have a particular shape and are composed by a lower and an upper cylindrical sectors, which are connected by means of removable elements. In the second step the connection elements placed in correspondence of the isolation devices are removed and each pipe is joined with the two adjacent ones, for example by means of a reinforced concrete elements. The isolation devices are positioned and the upper adjacent sectors are connected in correspondence of the isolators; successively also the other connection elements are removed, so the lower and upper cylindrical sectors are definitely separated. Finally vertical walls are built along the four sides of the building and a rigid connection, a concrete slab or other, is realized between the building and the isolation system. The stiffening of the soil should also be done at the beginning or at the end of the construction phases.

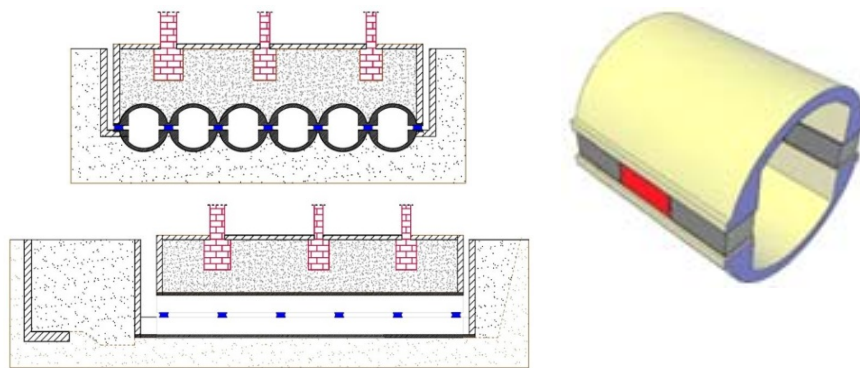


Figure 9. Isolation system for existing buildings: longitudinal and transversal cross-sections (left) and typical pipe element (right).

The system allows also the realization of a tunnel for pedestrian or vehicles. The size of the pipes must guarantee the accessibility and the possibility to substitute the devices. It is worth reminding that the solution presents the advantages that the building and its architectural

aspect are not changed and so are the underground levels; this is a very important requirement for historical and monumental structures (Buffarini et al., 2012).

Two problems can arise during the micro-tunnelling operations: the soil settlement and the vibrations induced at the surface level. The previous experiences suggest that minor threats should be expected from induced vibrations, but theoretical and experimental deeper studies are needed. More serious problems can arise by settlements (Clemente et al., 2011). So a specific analysis was carried out with reference to a case study for which the mechanical properties of the ground were known with sufficient accuracy. A FE 2-D model was set up and then exploited in *Diana 2* environment. The vertical edges of the model were kept far enough from the perturbed zone, in order to minimize their influence. The nodes belonging to those edges were restrained by means of spring and dampers able to cut-off the wave reflection. In the model the soil was described as a layered continuum indefinitely extended, supported by the bedrock at 17 m depth. The plane deformation condition was imposed and the boundary nodes respected the following restraining conditions: vertical displacements were inhibited at the nodes belonging to the lower horizontal edge; horizontal displacements were inhibited at the nodes belonging to both the lateral vertical edges. Different strategies were considered for the insertion of the pipes. In any case settlements lower than 10 mm were evaluated (Clemente & De Stefano, 2011).

The seismic isolation structure for existing buildings has been proposed for the seismic rehabilitation of historical buildings in L'Aquila, Italy, after the 2009 earthquake.

4. Conclusions

The preservation of historical buildings and monuments against earthquakes should consider the following steps:

- analysis of the characteristics of the seismic input at each site, by means of hazard analysis and seismic local response; this can be done only by means of a suitable monitoring of the area; the structural check should refer to the maximum expected event at each site;

- knowledge of the dynamic characteristics and the behaviour under seismic actions; also this should be performed by means of a suitable seismic monitoring;
- choice of the most suitable rehabilitation technique, which should obtain an equilibrium between the safety and the conservation requirements.

In fact, the seismic rehabilitation of historical constructions is a quite delicate issue, due to their historical importance and to the daily presence of tourists. They are often very vulnerable even to moderate events and traditional techniques are not suitable. Their rehabilitation must guarantee the preservation of the original monumental characteristics, identity and historical value. Therefore use of new technologies, such as seismic isolation, is advisable. These requirements are guaranteed by the new seismic isolation system for existing buildings presented in this paper.

REFERENCES

- Bergamasco I., Papaccio V., Carpani B., Clemente P., Saitta F., 2012. *Seismic preservation of the archeological site of Pompeii. Preliminary analyses*. In Knowledge, Diagnostics and Preservation of Cultural Heritage - Speciale Energia, Ambiente e Innovazione, 48-55, ENEA, Roma.
- Bongiovanni G., Buffarini G., Clemente P., Paciello A., Rinaldis D., Verrubbi V., Martini G., Zini A., Martino S., 2012. *Seismic Preservation of Cerreto di Spoleto Historical Centre*. In Knowledge, Diagnostics and Preservation of Cultural Heritage - Speciale Energia, Ambiente e Innovazione, 17-25, ENEA, Roma.
- Bongiovanni G., Celebi M., Clemente P., 1990. *The Flaminio Obelisk in Rome: vibrational characteristics as part of preservation efforts*. Int. J. of Earthquake Engineering and Structural Dynamics, 19: 107-118.
- Buffarini G., Clemente P., Serafini S., De Stefano A., Olivieri R., Salvatori A., 2012. *Experimental dynamic analysis and seismic rehabilitation of Palazzo Margherita in L'Aquila*. In Knowledge, Dia-

- gnostics and Preservation of Cultural Heritage - Speciale Energia, Ambiente e Innovazione, 63-68, ENEA, Roma.
- Buffarini G., Clemente P., Paciello A., Rinaldis D., 2008. *Vibration Analysis of the Lateran Obelisk*. In: 14th World Conference on Earthquake Engineering, Beijing, 12-17 October, S11-055.
- Buffarini G., Clemente P., Paciello A., Rinaldis D., 2009. *The Lateran Obelisk: Experimental analysis and modelling*. In: Protection of Historical Buildings, PROHITECH 09, F.M. Mazzolani (ed.), Rome, 21-24 June, 1: 841-848, London: Taylor & Francis Group.
- Clemente P., 1995. *Traffic-Induced Vibrations on Structures*. In: IABSE Report Extending the Lifespan of Structures, 73(2): 1111-1116.
- Clemente P., 2002. *L'analisi dinamica sperimentale nella salvaguardia dei beni culturali. Alcune esperienze dell'ENEA*. ENEA, Roma.
- Clemente P., 2002. *Vibrazioni indotte dal traffico: un'insidia per i monumenti*. In: Complessità e Sviluppo 2002, 148-156, Roma: ENEA.
- Clemente P., Bongiovanni G., 1993. *Ambient Vibration Effects on the Colosseum*. In: IABSE Report Structural Preservation of the Architectural Heritage, 70: 107-114.
- Clemente P., Bongiovanni G., Marzi C., 1988. *La colonna Antonina in Roma: valutazione degli effetti delle vibrazioni ambientali*. In: Conoscere per intervenire, 3rd ASS.I.R.C.CO. Conf., Catania, 10-12 November, 207-217.
- Clemente P., Buffarini G., 2009. *Dynamic response of buildings of the cultural heritage*. In Boller C., Chang F.K., Fujino Y. (eds), Encyclopedia of Structural Health Monitoring, John Wiley & Sons Ltd, Chichester, UK, 2243-2252.
- Clemente P., Di Lazzaro P., Giorgi R. (Eds), 2012. *Knowledge, Diagnostics and Preservation of Cultural Heritage*. Speciale Energia, Ambiente e Innovazione, ENEA, Roma.
- Clemente P., De Stefano A., 2011. *Application of seismic isolation in the retrofit of historical buildings*. In Brebbia C.A. & Maugeri M.

- (eds) Earthquake Resistant Engineering Structures VIII, 41-52, WIT Transactions on The Built Environment, Vol. 120.
- Clemente P., De Stefano A., Zago R., 2012. *Seismic retrofit of historical buildings with seismic isolation*. Proc. 8th Int. Conf. on Struct. Analysis of Historical Constr., SAHC, (Wroclaw, 15-17 Oct.), Paper No. 196.
- Clemente P., De Stefano A., Renna S., 2011. *Isolation system for existing buildings*. Proc., 12th World Conf. on Seismic Isolation, Energy Dissipation and Active Control of Structures - 12WCSI (Sept. 20-23, Sochi, Russia), ASSISi.
- Clemente P., Rinaldis D., Bongiovanni G., 1994. *Dynamic characterization of the Tempio della Minerva Medica*. In: 10th European Conference on Earthquake Engineering, Vienna, 28 Aug. - 2 Sept., 2: 981-986, Rotterdam: Balkema.
- Clemente P., Santini A., Ashtiany M. G., 2009. *The proposed isolation system for the Iran Bastan Museum*. In Mazzolani F.M. (ed), Protection of Historical Buildings, PROHITECH 09 (Proc., Int. Conf. on Protection of Historical Buildings, Rome, Italy, 21-24 June 2009), Vol. 1, 575-682, Taylor & Francis Group, London,
- De Stefano A., Clemente P., 2009. *Structural health monitoring of historic buildings*. In Karbhari V.M. and Ansari F. (Eds) Structural Health Monitoring of Civil Infrastructure Systems, Woodhead Publishing Ltd.
- Santini A., Clemente P., Ghafory-Ashtiany M., 2007. *Seismic rehabilitation of the Iran Bastan Museum*. Proc., Fifth International Conference on Seismology and Earthquake Engineering (SEE5, May 13-16 Tehran), IEES, Tehran.

A methodology to analyze ambient vibrations in the Colosseum

Arrigo Caserta², Paolo Clemente¹, Cinzia Conti⁵,
Gino D'Ovidio³, Yutaka Nakamura⁴,
Rossella Rea⁵, Antonio Rovelli², Gianfranco Valente³

Abstract

For the dynamic soil Colosseum interaction, subjected to ambient vibrations, we propose a methodology which collects three models used with success in the disciplines Geophysics, Structural and Transportation Engineering. The trains' transit produces the vibrations in our global model. Firstly, we use such vibrations to identify the map of elastic modules, in elevation by the modal analysis, in the foundations and soil by the diagrams H/V. Finally, this methodology solves the unique problem of the linear elastic behaviour of the monument subjected to different dynamic actions.

1. ENEA Rome, 2. INGV Rome. 3. L'Aquila University. 4. S.D.R. Tokyo.
5. Soprintendenza speciale per i Beni Archeologici di Roma.

1. Introduction

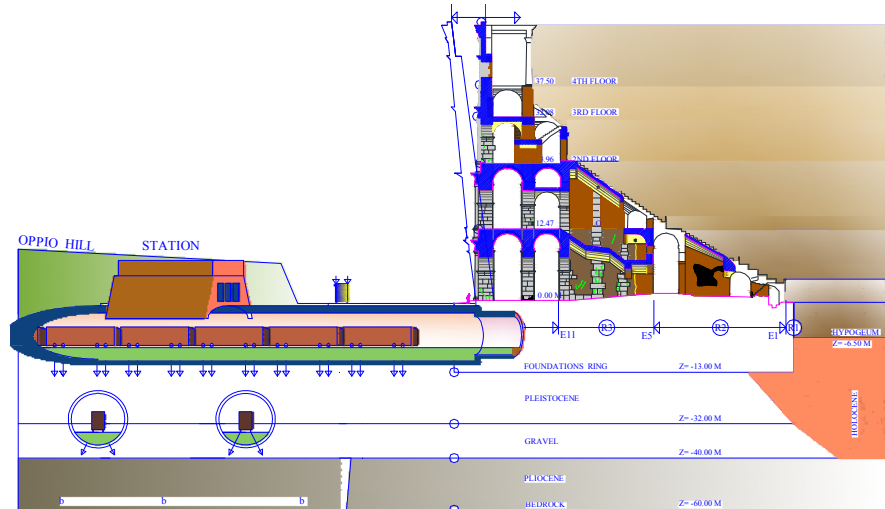


Figure 1. Section on R.A. XLVII. Vehicles' action and monument vibrations.

The ambient vibrations of Colosseum are due to external random dynamic actions as: a) trains' transit, b) ground traffic, c) the wind, d) the people on the steps of arena, especially 2000 years ago.

Since 2000 years, the ambient vibrations act on the walls, producing a linear elastic behaviour of the material, everytime. This research starts with the conclusion of "Il Restauro del Colosseo" (2000), when the power of new PC promised to analyze 500,000 requested d.o.f.

This paper collects the sense of all the work shown in detail in preceding papers about this argument, like in DISS_10 and DISS_12 [28, 31, 34, 36, 37, 38, 39, 40, 42,...,45].

We are interested on a 3D FE model for the dynamic interaction of soil and Colosseum with linear elastic behaviour, under the action of light dynamic actions.

2. The models

2.1. Limit Equilibrium Method (L.E.M.) by structural engineering

In the 18th century, De La Hire and Coulomb proposed the L.E.M. [50], as in Figure 2, with the following approximations:

1. static horizontal loads,
2. monotonic horizontal loads,
3. horizontal acceleration constant along the height;
4. nihil tensile strength,
5. structure fixed at the basis, as in Figure 4;
6. macro elements generation by cutting planes;
7. transformation of the problem from 3D to 2D;
8. the equilibrium conditions alone are imposed, in order to evaluate the collapse multiplier μ ;
9. introduction of plastic hinges.

Different cutting planes are considered, by the aid of existing damages too, different mechanisms and plastic hinges are obtained, the equilibrium conditions are imposed, different load multipliers are found, the adopted one is $\mu = \min[\mu_1, \mu_2]$

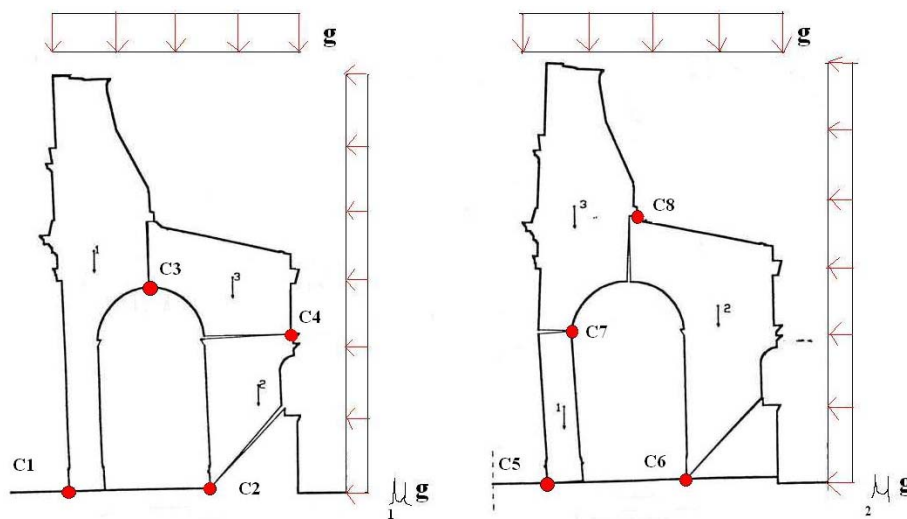


Figure 2. LEM, n. 2 mechanisms and plastic hinges C1..C8.

The approximations are too many, and their uncontrolled accuracies may lead to errors around 200% [30], which means that the model is metaphysic and useless; the problem is closed with the phrase: “*Qu’il n’emploiera plus soixante pages de calcul pour arriver à une conclusion qu’on peut établir par un raisonnement de dix lignes*” [47].

2.2 The model by structural engineering for identification

Usually, the structural engineers assume the hypothesis of elastic monument fixed at the basis as in Figure 3 [29, 33], which is unsatisfactory for our initial purpose.

It is equivalent to admit the presence of a rigid plate between monument and soil, the respective actions cannot be transmitted between them, and the dynamic actions are reflected by this plate.

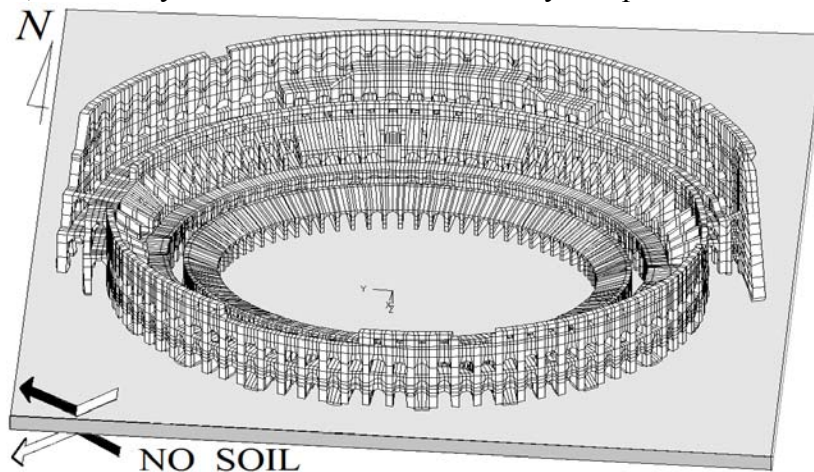


Figure 3. Model fixed at the basis, by Structural Engineers.

2.3 The model by transportation engineering

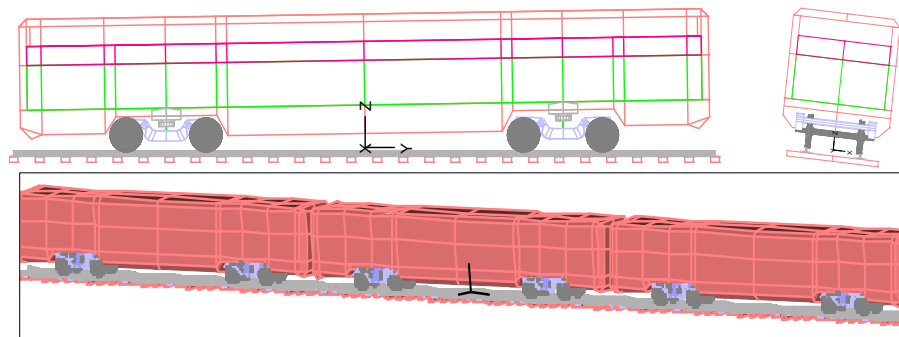


Figure 4. The model by Transportation Engineering: a) wagon, b) convoy.

We use a multibody system [34÷40, 42, 44, 45, 48, 49], and with respect the reality we reproduce the same: a) rails of Metro B and C, as sleepers, straight, transition, curve and rise between the two rails; b) wagon as dimensions, centre of gravity, mass, the three inertial moments for rolling, rocking and winding; d) convoy with six wagons; e) profiles for wheels and rails, with irregularities too; f) suspensions for springs and dampers.

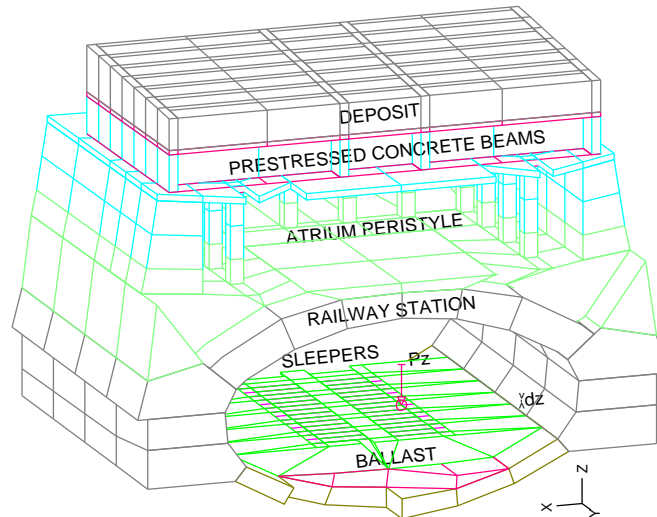


Figure 5. Section in the Colosseum station, load Pz and its displacement dz

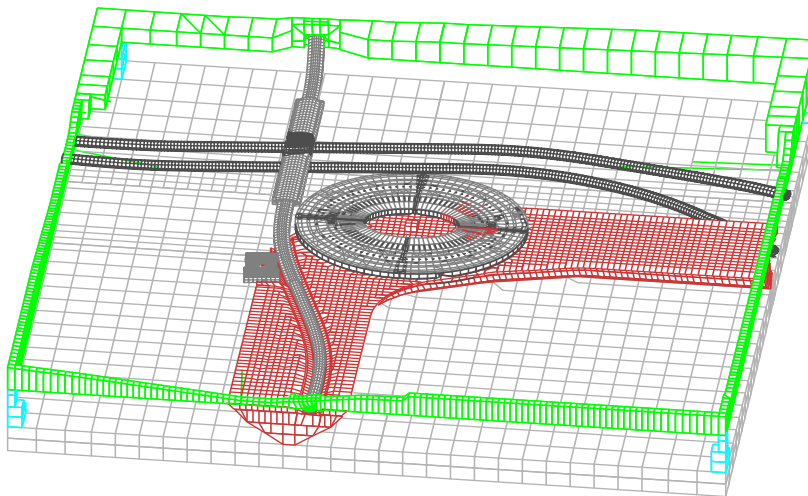


Figure 6. The soil volume 600 x 600 x 80 m.

2.4 The model by geophysics

The train model produces about n. 12,000 time histories of the loads at all the i-th crossings between rail and sleepers for the n. 4 trains, as ${}^iF_x(t)$, ${}^iF_y(t)$, ${}^iF_z(t)$; these forces are changed of versus, and they are applied to the model by Geophysics as in Figure 5 and 6.

The right size for dynamic analysis is defined by Geophysics Science [3, 10, 11, 12, 13, 18, 24, 25, 41], because the seismic waves may have a length around many centuries of meters, and a homogenization of the soil is necessary.

2.5 The proposed model

Since 1971 [51] a theoretical model was at disposal to discretize the analytical problem, and it was easy to foresee the power of PC which was attained in the actual third millennium.

We realized that:

- a) rich tests were at disposal, in over 200 points, never used for identification;
- b) n. 3 accurate independent models were developed by Geophysics, Transportation and Structural Engineering;

The operative tool of this methodology requests an interdisciplinary work very long and laborious, but arriving to a tool having an accuracy within few percent.

Firstly, we use such vibrations to identify the map of elastic modules E, in elevation by the modal analysis, in the foundation and soil by the diagrams H/V. Then, we arrive to the analytical knowledge, as in Figure 28, everywhere in this model, of:

- a) the gravity stress σ_G ,
- b) the small range of stresses due to ambient vibrations

$$\eta = |\Delta\sigma_G / \sigma_{G|MAX}| \cong 1/1000.$$

The proposed model of dynamic interaction between soil and structure (DISS) is represented in Figure 7. For a natural dynamic action, different points at bedrock have the same acceleration (± 0.03 g), but ascending along a vertical line the accelerations change for different inertial actions. The deformations due to vibrations are developed in 3D.

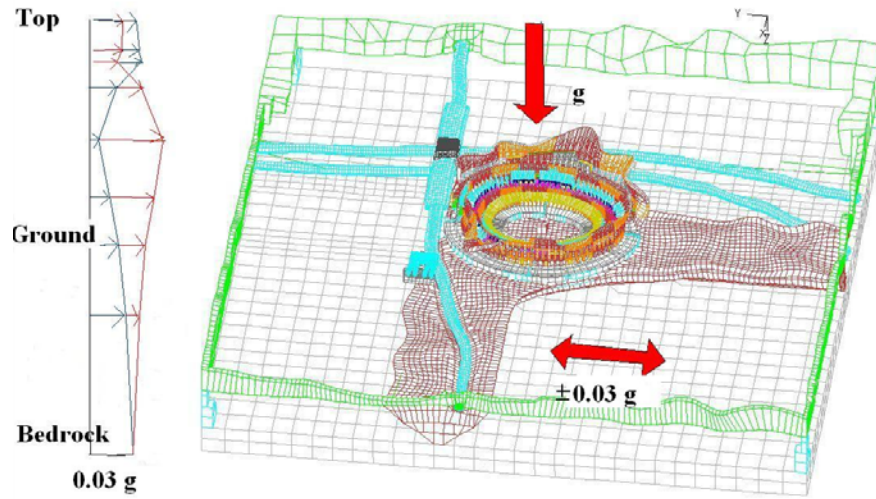
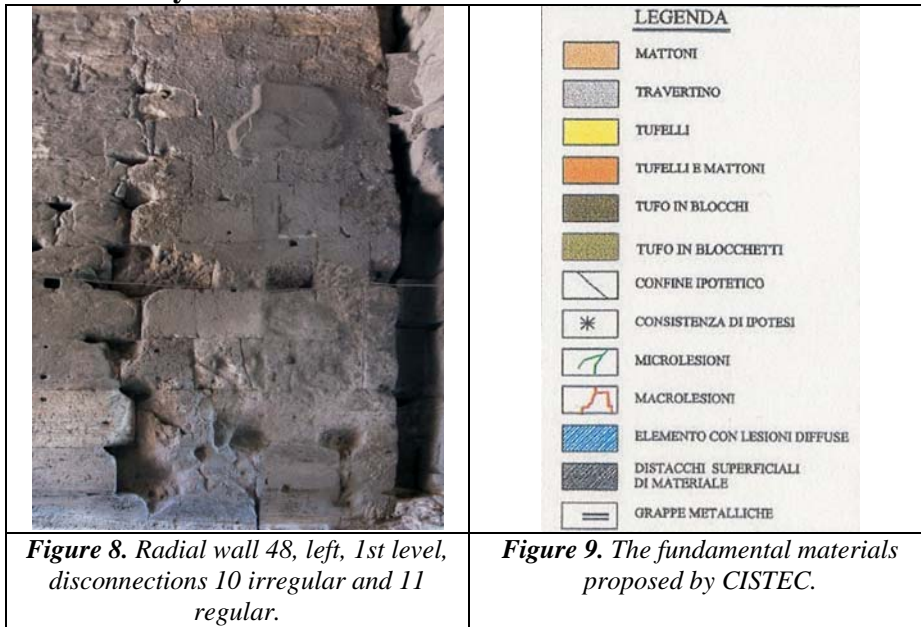


Figure 7. The proposed model of DISS for Colosseum..

3. Geometry



By CISTEC [46] for elevation; for cryptoportici and hypogea by Beste, Mertens, Schingo, Rea [8, 14, 17, 19, ..., 22].

We have the luck to know the geometry with accuracy, and all the densities are around 1.8÷2.2 t/mc.

3.1. Walls' disconnections

Table 1. Evident disconnections; Left/Right from outside; 1° and 2° levels.

| R | cylindrical vertical surfaces | | | | | | R | cylindrical vertical surfaces | | | | | |
|---|-------------------------------|----|---|---|---|---|----|-------------------------------|----|---|---|---|---|
| W | 11 | 10 | 9 | 8 | 7 | 6 | W | 11 | 10 | 9 | 8 | 7 | 6 |
| 2 | 2 | | 2 | | | | 41 | 2 | | | | | |
| 3 | 1L/2 | | | | | | 42 | 2 | | | | | |

Were performed about 70 disconnections between walls, by CISTEC drawings [43], and the help by Maurizio Cerone, Figg. 8, 9, 10.

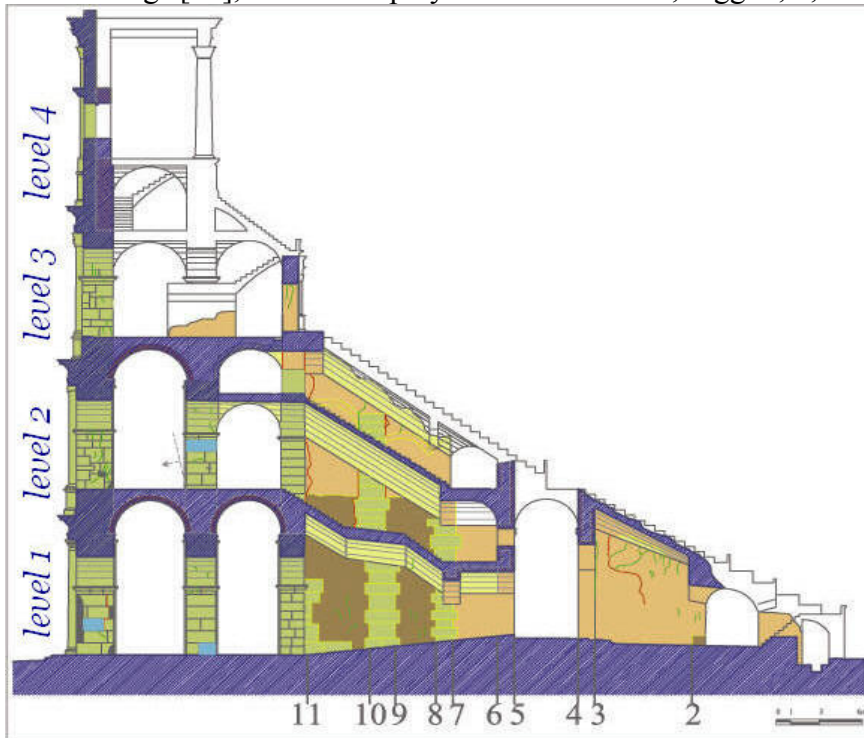


Figure 10. RA XLVII. Disconnections between radial walls 1÷80 and annular walls on the cylindrical vertical surfaces 6÷11, left and right, from outside.

4. Materials

4.1 Accurate analysis

4.2. Homogenization of undamaged concrete

For concrete project as in Figure 11, the homogenized model is adopted; firstly the tests on cubic specimens, having side $a=20$ cm, are performed, with maximum aggregate size $d_{MAX}=2.5$ cm; the ratio $a/d_{MAX}=8$ warrants the independence of mechanical characteristics from random distribution of aggregate inside cubic specimen.

The mechanical characteristic obtained by cube will be used for undamaged reinforced concrete structures, if $a/d_{MAX} > 8$.

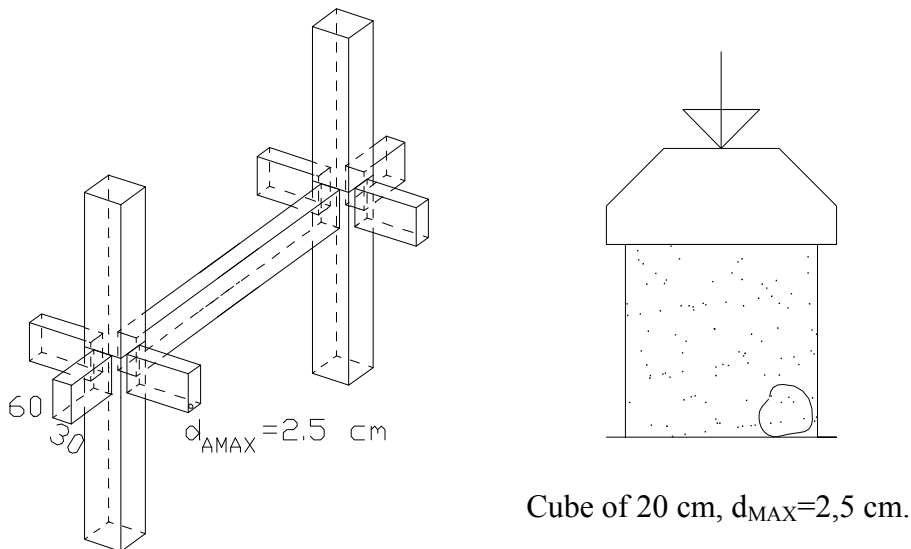


Figure 11. Project of reinforced concrete. Cubic specimen.

4.3. Stiffness matrix: isotropic, symmetric orthotropic, asymmetric orthotropic. Locale and nonlocal continuum.

We start from integer concrete, for which we know all mechanical characteristics at least E_0 , ϵ_F , σ_T are needed. By incremental analysis we arrive to cracking as in Figures 12a and we obtain the local stiffness matrix in the Gauss point, which are:

- 1) symmetric isotropic for integer material;
 - 2) symmetric orthotropic, referred to cracking plane T-T, as in Figure 11c;
 - 3) asymmetric orthotropic, referred to cracking plane T-T if aggregate interlock happens as in Figure 12b, with $\delta_N \neq 0$, $\delta_T \neq 0$.
- The unloading phases are enough complex.

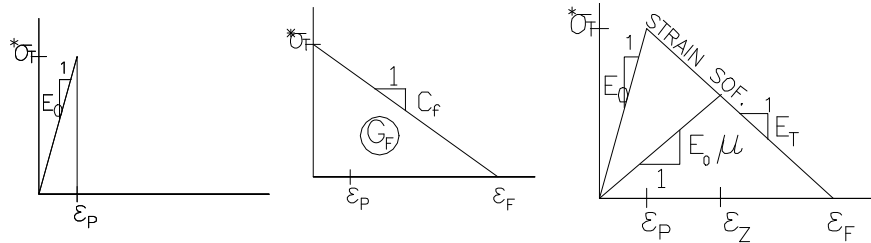


Figure 12a. Fracture: a) Heterogeneous microscopic b-Linear Fracture c-Homogeneous behaviour

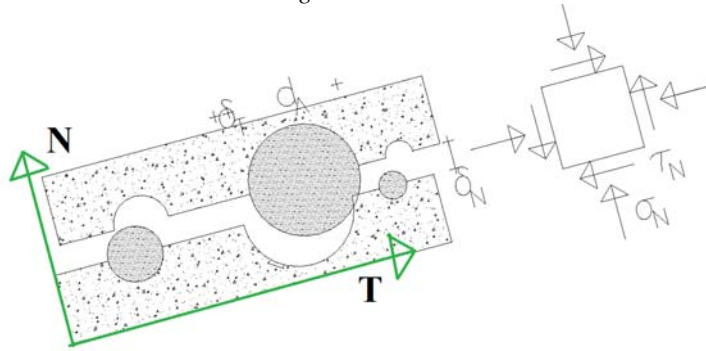


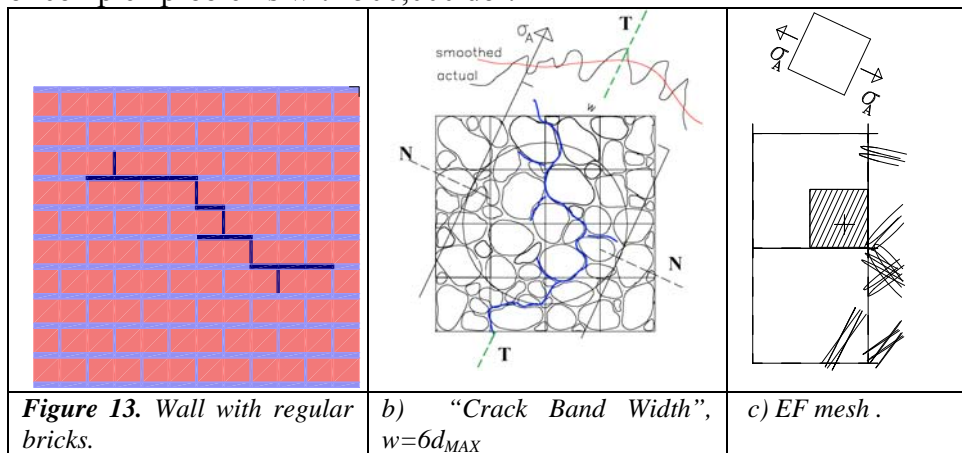
Figure 12b. Aggregate interlock.

4.4 Damagings

But for an ancient concrete wall, the knowledge for integer material of mechanical characteristics is not allowable, surely pre-existing crackings there are: a) crack band width for concrete, b) disconnections of bricks.

The 3D DISS model is used, as in Figure 6 to obtain a map of 350 elasticity moduli, obtained by dynamic identification, in elevation vibration modes and H/V diagrams for foundation and soil.

Since '60 years [51, 52] it was: 1) defined theoretically the geometric and constitutive laws discretizations, 2) foreseeable that the fast electronic and informatic developments would have allowed the solution of complex problems with 500,000 dof.



4.4. Homogenization of damaged walls

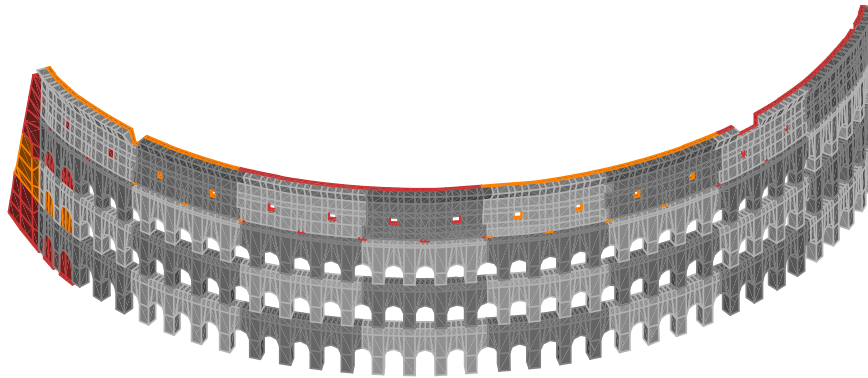


Figure 14. Zones with different elasticity.

The principal evident disconnections were introduced in the mesh, according to existing CISTEC survey [41].

The damagings are not known inside a large depth of a wall.

Finally, only the isotropic linear elastic behaviour may be assumed, with zones having different elasticity moduli E_0 .

The very good analytical-experimental fitting testifies the reliability of the proposed method.

5. Existing tests

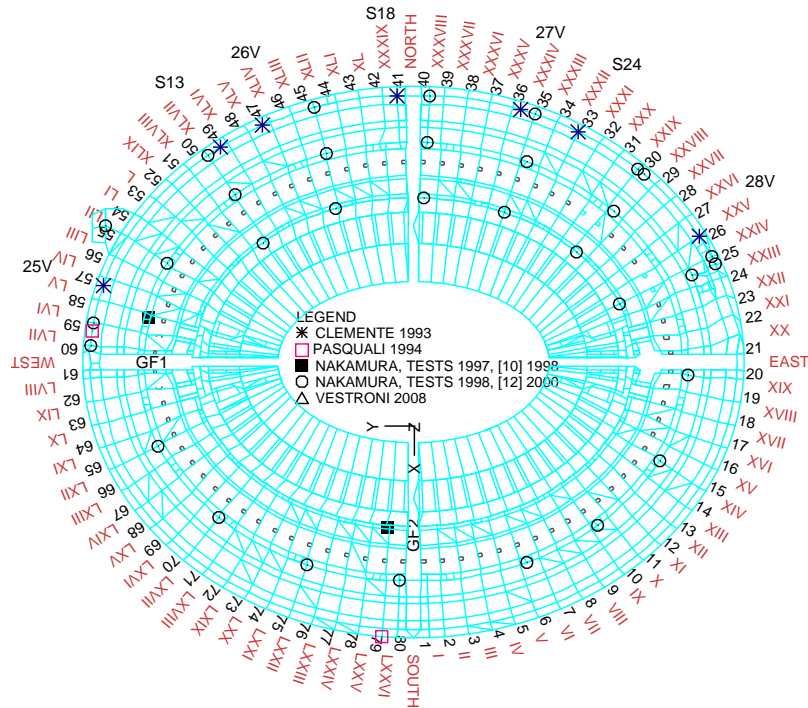


Figure 15. Measurement points on the ground at $Z=0.0$ m, a) radial wall RA with Arabian numbers, b) radial access RA with roman numbers. (n.45 points).

The existing tests were performed in more than 200 points [7, 9, 10, 11, 12, 13, 18, 24, 25, 29, 33, 41]; with seismograms and accelero-grams; with triaxial recordings simultaneously per each level; impact vibration using an instrumented hammer; for short time or long duration. The majority on the northern wall of Colosseum, few on Constantine arch, and few inside the tunnels of Metro B. Nakamura alone performed in about 100 points, in all level and radial sectors of the monument, and in the place around Colosseum, as in Figures 13,..15..

So many experimental data were never compared before in the past with analogous analytical data, that testifies how long and laborious work is needed for this purpose.

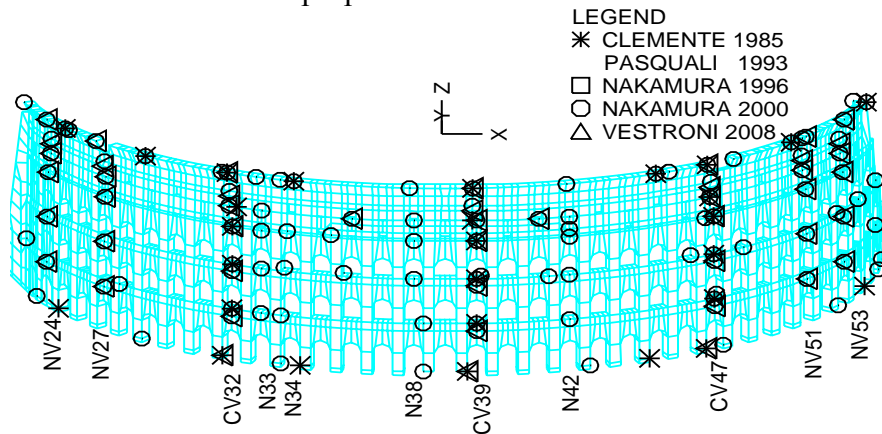


Figure 16. External façade of northern tallest wall, with buttresses; with n. 11 evident vertical alignments, with letters of Authors and number of radial accesses.

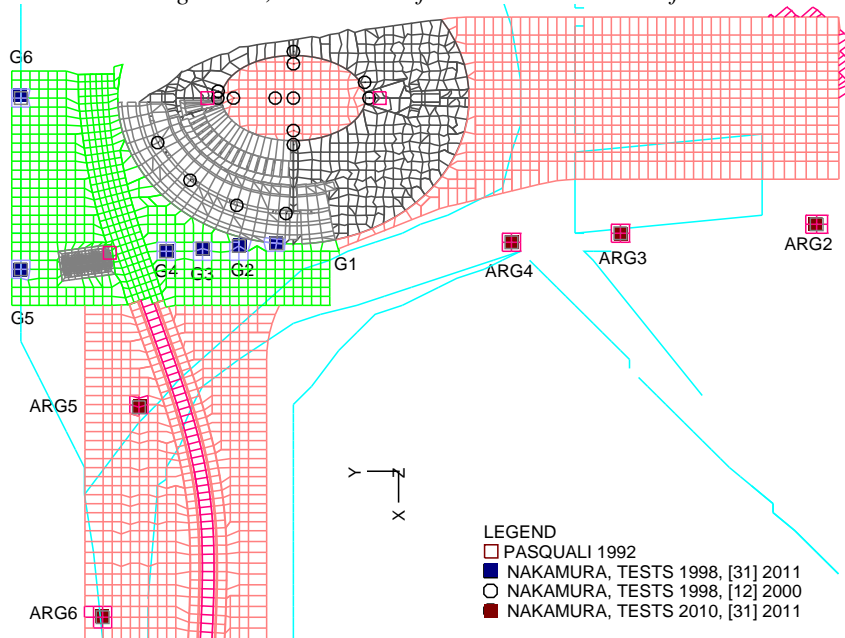


Figure 17. Measurement points on the ground around Colosseum and inside hypogeum (N.25 points).

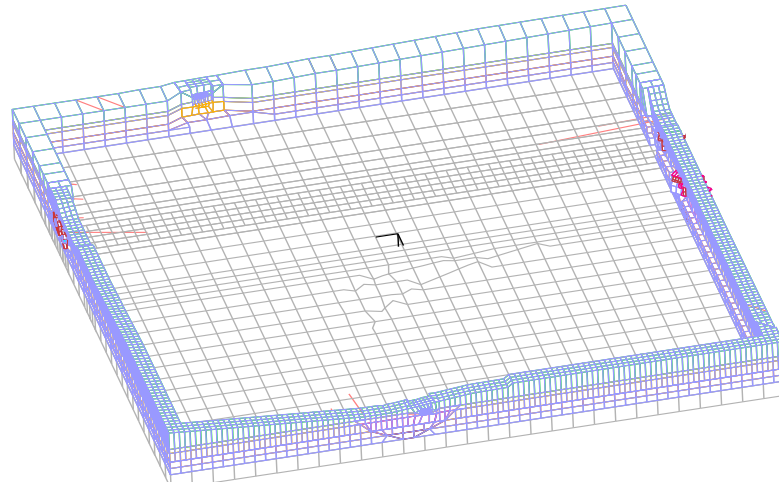


Figure 18. The damping pool Rayleigh=85%, for $f_r=1 \div 10$ Hz.

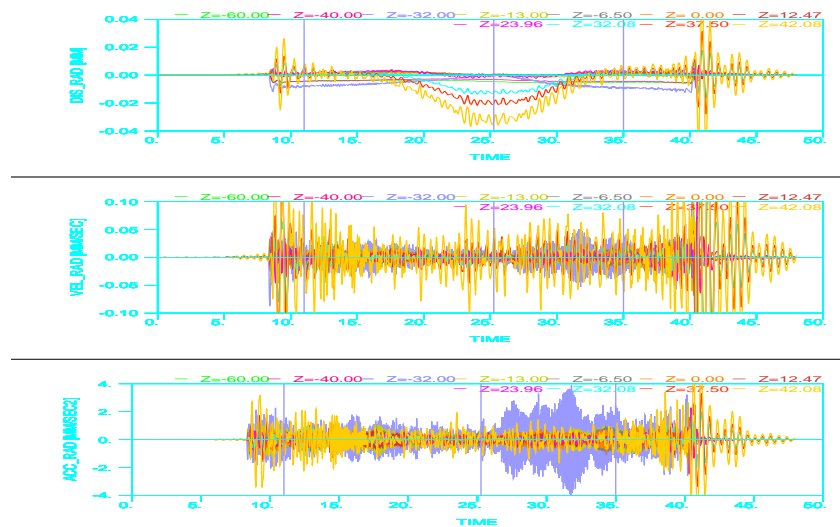


Figure 19. Colosseum section XLVII. Displacements, velocities and accelerations radial values due to the Metro B and C traffic trains.

6. Dynamic analysis

Monument and soil, with the damping pool of Figure 18, stay in a rigid box having five surfaces $x=\pm 300\text{m}$, $y=\pm 300\text{m}$, $z=80\text{m}$, the soil touching the box is fixed orthogonally and free on the surface. The box may move with prescribed displacements by time functions $[\delta_x(t)$,

$\delta_y(t)$, $\delta_z(t)$, $\varphi_x(t)$, $\varphi_y(t)$, $\varphi_z(t)$]; or the box may rest fixed and the accelerations are applied to the model [$a_x(t)$, $a_y(t)$, $a_z(t)$].

We start the analyses by using elasticity modules in references.

Firstly, the model gravity loads are applied in a long time of 10000 secs, and then the external actions are applied with real duration of the transit of four trains in 48 secs.

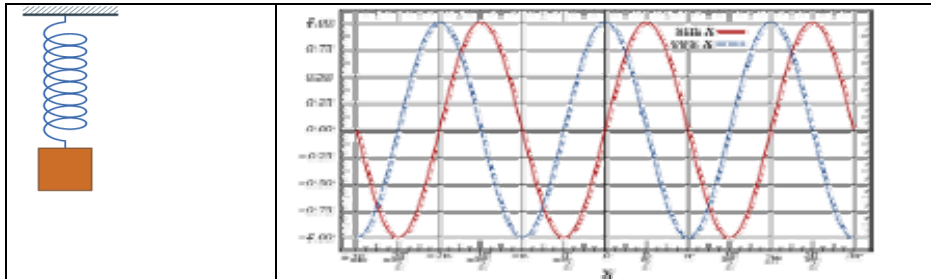


Figure 20. Harmonic vibrations.

The motion equation is used:

$$M \ddot{u} + C \dot{u} + K u = 0 \quad (1)$$

6.1 Harmonic analysis

For the simple oscillator of Figure 20 is:

$$T = 2\pi (M/K)^{1/2} \quad (2)$$

The vibrations due to a vehicle are depending on the load, springs, dampers and path.

From the ambient vibrations measured by tests, several invariant diagrams may be obtained, independent from the external actions, but connected to: j) geometry, k) masses distribution, l) deformability.

These diagrams are obtained by signal analysis and are represented by functions of the monument characteristic frequencies like auto and cross spectra, the vibration modes, the diagrams H/V, they constitute the DNA sequences of the physical reality in examination, in those measurement points.

Then, it is easy to construct an analytical model by FE, having the same geometry and masses of the reality; the deformability alone remains to be evaluated.

We work on the distribution of that deformability of the model, in order to attain the best fitting between tests and analyses for these invariant diagrams, by taking into account the soil-structure interaction.

6.2 Identification of elevation by modal analysis

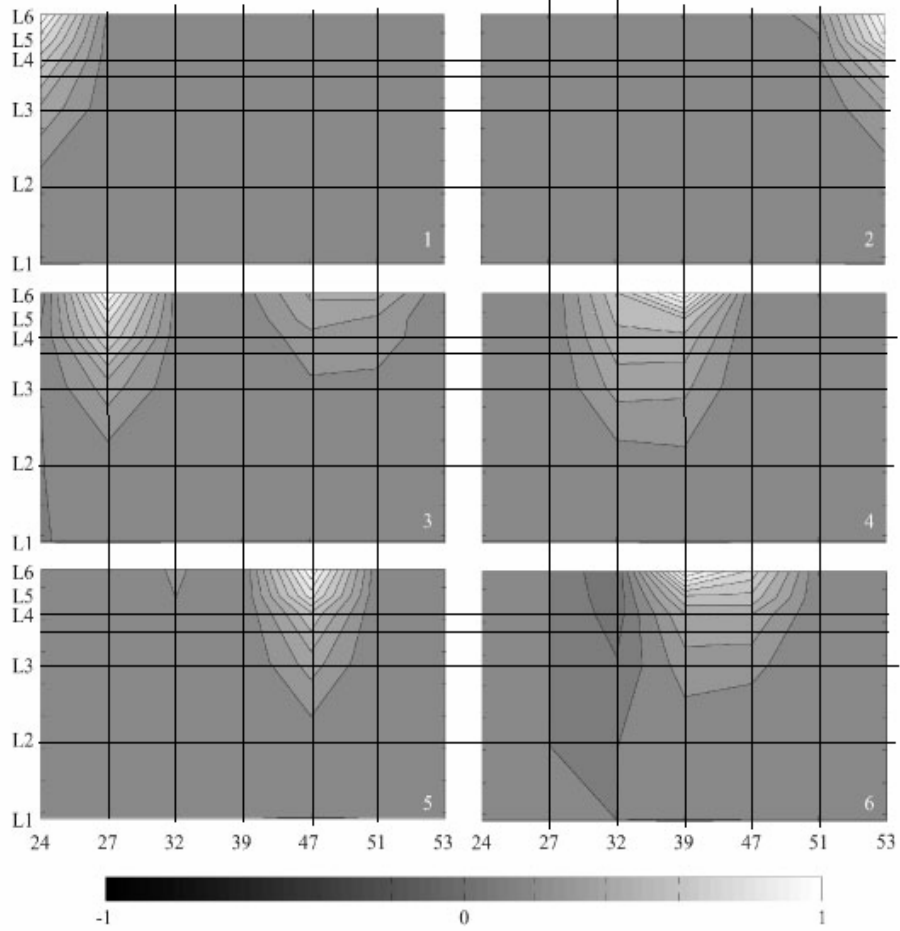


Figure 21. Contour plots of the radial comp. of the first six exp. mode shapes [33].

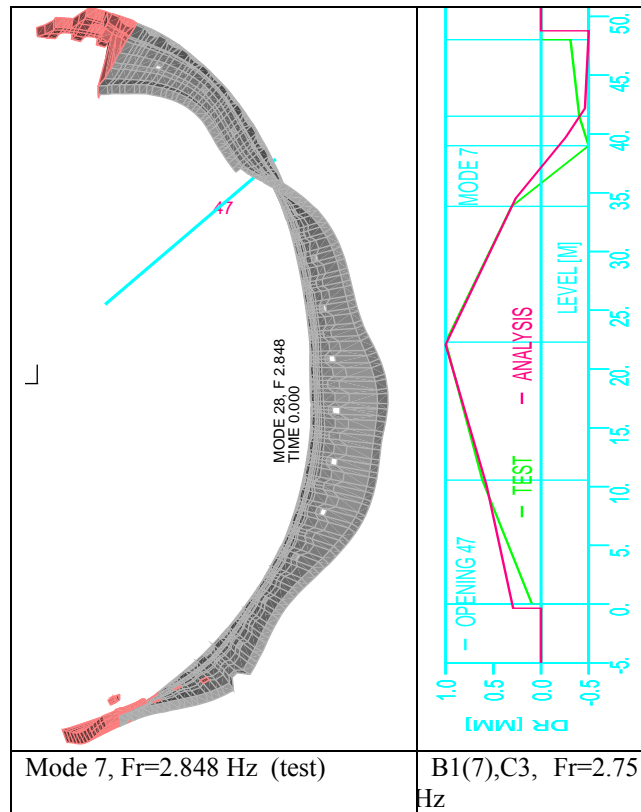


Figure 22. Comparison between experimental and analytical shapes for mode 7. Radial and vertical components; (---) test; (---) analysis. B_z 2.80 Hz.

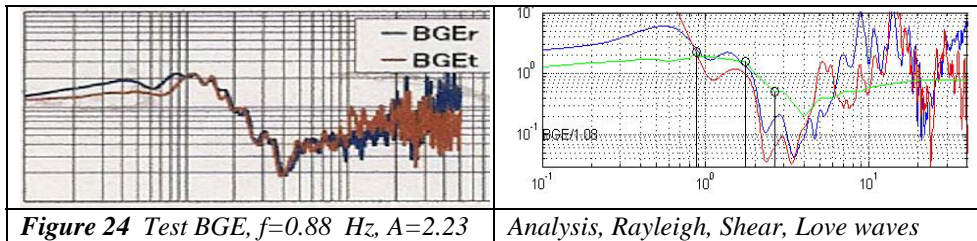
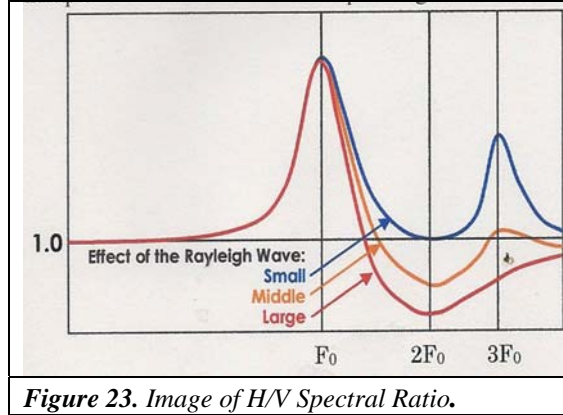
For the monument walls, the map of mean elasticity modules is found by comparison between tests modes shape as in Figure 21 and 22, and the corresponding modes by analysis.

6.3. Identification of soil and foundations by the H/V technique

Figure 23 shows the typical shape of the H/V spectral ratio. The characteristic of H/V for microtremor is summarized as follows. The first peak near F_0 consists of S-wave mainly. The first trough near $2 F_0$ is caused by Rayleigh wave.

Around F_0 there is almost no energy of Rayleigh waves, so the dispersion curves are unstable near F_0 . Rayleigh wave are growing from F_0 ,

and reach the first peak near the $2F_0$. It is verified that the H/V spec The H/V with one remarkable peak is easy to understand as a simple soil layer. In case of neglecting the Rayleigh wave effect, the shape of the H/V could be used as an amplification spectra for wide frequency range. But the other case it is recommend to use the H/V with peak frequency and the peak value.



The stability of H/V spectra was demonstrated for various inputs, different seasons, ambient vibrations and earthquakes. In Figure 24, for point BGE, the results are shown: by the test on the left, by the corresponding analysis on the right.

6.4. Amplification factor (A) and vulnerability index (K)

Horizontal displacement δ_j shown in Figure 25 can be written as in equation (3),

$$\delta_j = \alpha_{sj} / (2\pi F_s)^2 \quad (3)$$

Where δ_j is the horizontal displacement, W is the weight of the j -th floor, h_j is the height of j -th column, α_B , α_G , α_{Sj} are the horizontal acceleration of the basement, ground surface and j -th floor of the structure, respectively, F_s is a predominant frequency of structure.

The story drift angle for j -th story γ_j is expressed as follows:

$$\gamma_j = (\delta_j - \delta_{j-1}) / h_j = (\alpha_{sj} - \alpha_{sj-1}) / (4 \pi^2 F_s^2 h_j) \quad (4)$$

$$\alpha_{Sj} = A_{Sj} \alpha_G = A_{Sj} A_G \alpha_B = A_{SGj} \alpha_B \quad (5)$$

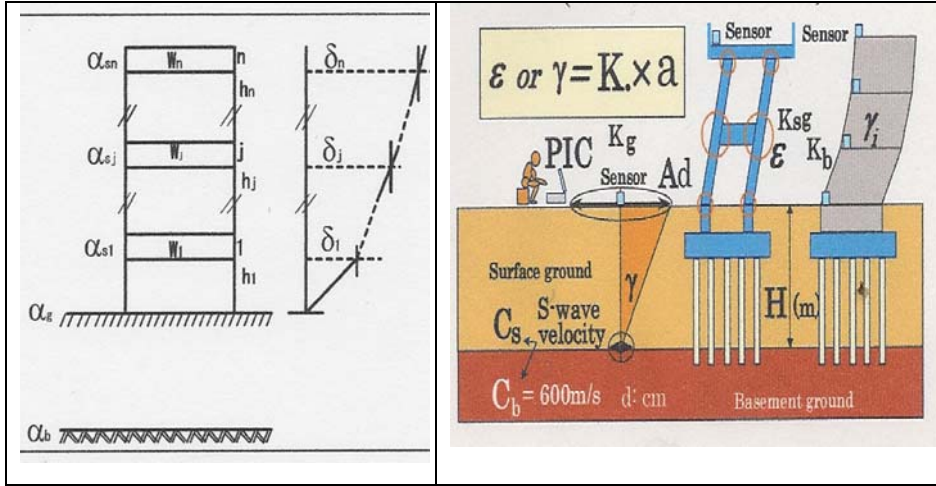


Figure 25. Derivation of mode shapes of n -th floor structures.

Here, A_G and A_{Sj} are an amplification factor for ground and j -th floor of the structure, respectively. α_{Sj} is derived from S_{jH} and S_{GH} which are horizontal spectrum of j -th floor and ground floor respectively. And A_{sgj} is derived from the ratio of S_j and vertical spectrum of ground floor and represents combined amplification factor of surface ground and structure. α_B and α_G are horizontal acceleration of basement and ground surface, respectively.

If unit of drift angle γ_j is 10^{-6} , h_j is meter and seismic acceleration is measured in unit Gal (cm/sec^2), equation (4) can be written:

$$\gamma_j = 10^4 (A_{SGj} - A_{SGj-1}) \alpha_B / (4 \pi^2 F_s^2 h_j) \quad (6)$$

From equation (6) K_{BGJ} value (representing vulnerability index for ground and building) is defined as:

$$K_{BGJ} = 10^4 (A_{SGJ} - A_{SGJ-1}) / (4 \pi^2 F^2 h_j) \quad (7)$$

unit of K values given above become 1/ Gal. From this, vulnerability index for buildings can be written as.

$$K_{BJ} = 10^4 (A_{SJ} - A_{SJ-1}) / (4 \pi^2 F^2 h_j) \quad (8)$$

Maximum allowable acceleration from j-th column α_{baj} (in cm/sec^2) derived from equation (6) is:

$$\alpha_{SAJ} = 10^4 (4 \pi^2 F^2 h_j) \gamma_{AJ} / (A_{SJ} - A_{SJ-1}) \quad (9)$$

Table 2. Experimental natural frequencies, (--) [33], (--) [5], (--) [8]

| RA | XXIV | XXVII | XXXII | XXXIX | XLVII | LI | LIII | f_c |
|----|------|-------|------------------|-------|------------|------|------|-------|
| 1 | 1.00 | 1.00 | | | | | | 1.03 |
| 2 | | | | | | 1.28 | 1.28 | 1.30 |
| 3 | 1.35 | 1.35 | 1.35, 1.46 | 1.46 | 1.35, 1.46 | 1.35 | | 1.49 |
| 4 | | | 1.72 | 1.72 | | 1.72 | | 1.60 |
| 5 | | | 1.80, 1.70, 1.70 | 1.70 | 1.80, 1.70 | | | 1.66 |
| 6 | | | 1.83 | 1.83 | 1.83 | | | 1.75 |
| 7 | | | 2.61, 2.80 | 2.61 | 2.61 | | | 2.75 |

Detailed explanation and examples of the application of this technique can be found in Nakamura [3, 13, 18, 41].

The comparison between tests and analysis, for amplification factors and vulnerability indices, was started but it needs to be developed.

7. Accuracy

Table 3. MAC coefficients between analytical and experimental modes [26].

| a/e | 1 | 2 | 3 | 4 | 5 | 6 | 7 |
|-----|------|------|------|------|------|------|------|
| 1 | 0.94 | 0.10 | 0.27 | 0.03 | 0.01 | 0.03 | 0.05 |
| 2 | 0.10 | 0.97 | 0.11 | 0.02 | 0.00 | 0.06 | 0.11 |
| 3 | 0.14 | 0.12 | 0.56 | 0.23 | 0.49 | 0.51 | 0.17 |
| 4 | 0.12 | 0.05 | 0.28 | 0.73 | 0.64 | 0.50 | 0.31 |
| 5 | 0.13 | 0.02 | 0.69 | 0.20 | 0.72 | 0.62 | 0.21 |
| 6 | 0.15 | 0.09 | 0.37 | 0.47 | 0.45 | 0.49 | 0.37 |
| 7 | 0.04 | 0.08 | 0.32 | 0.12 | 0.37 | 0.18 | 0.88 |



Figure 26. The Colosseum crack due to earthquakes, 1600, Matheo Florimj formis.

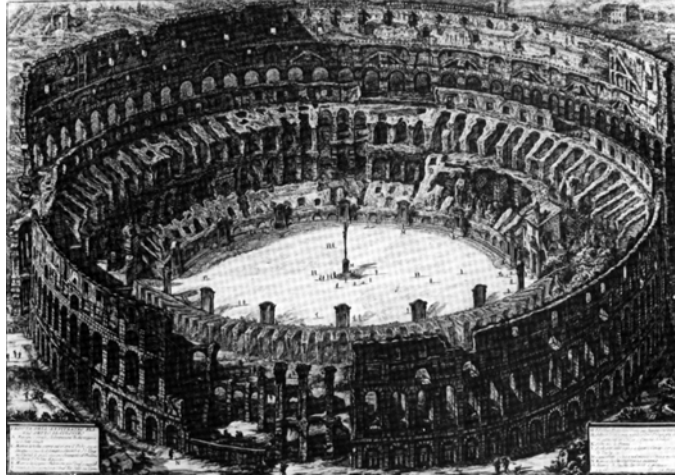


Figure 27 G. B. Piranesi, Via Crucis inside Colosseum, (1751).

The actual accuracies between tests and analyses are:

- a) over 95% for the buttresses Stern and Valadier, which are the most vulnerable elements of the monument;
- b) about 60%, for foundations and soil, because geometry and damaging are not known directly, but we are improving.

We have not yet used the existing experimental results for “vulnerability index” and “amplification coefficient”.

8. Damagings in the past

The sure notices about monument damages by earthquakes are on the years 422, 443, 508, 801, 1349, 1703 and 1812.

Subsequent robberies happened, and other damages are connected to burnings. Often, the damages development were represented by drawings, as in Figures 26, 27.

Table 4. The principal historical happenings in Colosseum.

| Year A.C. | Happenings | Notices |
|------------------|--------------------|---|
| 71-72 | Works start | By Vespasiano |
| 80 | Inauguration | |
| 217 | Burning | 23 August. Due to a thunderbolt |
| 217-223 | Restoration | Upper side in stones |
| 250 and 320 | Burning | Few damages |
| 422 | Earthquake | Collapse of senators floor |
| 429 | Earthquake | 24 August |
| 439 | Earthquake | No exact notices of damages |
| 443 | Earthquake | New collapse as on 422 |
| 508 | Earthquake | Decio Mario Venanzio Basilio "abominandi terrae motus" |
| 610 | Alarico invasion | Stones' metallic connections for weapons |
| 614-617 | Earthquake | No exact notices of damages |
| VIII century | | By Beda: integer monument |
| 801 | Earthquake | Collapse of two arches orders in the upper porticos |
| 847-855 | Earthquake | No exact notices of damages |
| 1044-1073 | Earthquake | No exact notices of damages |
| 1231 | Earthquake | 1 st June |
| 1349 | Earthquake | Petrarca " <i>cecidit aedificarum veterum neglecta civibus, stupenda peregrinis moles</i> ", 7-10 September, VIII MM. |
| 1700 | Repair Clemente XI | Stop salnitrum production for explosives. |
| 1703 | Earthquake | Arches fall, used for Ripetta harbour later |
| 1714 | Restoration | |
| 1803 | Escavations | Pio VII |
| 1812 | Earthquake | Fall of three arches orders |
| 1805-1807 | West buttress | Stern, Pio VII |
| 1824 | East buttress | Valadier, Leone XII |
| 1844-1846 | Restoration | Gregorio XVI |
| 1846 | Restoration | Pio IX |
| 1912 | | n. 33 arches rest in the external ring |
| 1915 | Earthquake | Fucino epicentre. No damages |
| 1946-1950 | Restoration | With injections |

8.1 Principal restoring works

The actual Colosseum is the result of damages from natural events in the past (earthquakes, burnings, vegetation, abandon, etc.) robberies by men, consolidations to save the monument against imminent risks. The greatest damages are concentrated in the period between IX and XV centuries, by the following witnesses:

1) Beda (“*collettanee*”, 745):

*Quamdiu stabit Colyseus
Stabit et Roma
Quando cadet Colyseus
Cadet et Roma
Quando cadet Roma
Cadet et mundus*

2) Petrarca (epistola II del libro X, 7-10 September 1349, VIII M.M.) “*cecidit aedificarum veterum neglecta civibus, stupenda peregrinis moles*”,

3) Luigi Canina (Sul ristabilimento e riparazione della parte media verso l’Esquilino dell’Anfiteatro Flavio”, letta nell’adunanza dell’accademia di archeologia in Roma il 7 aprile 1857), “...io ora non voglio stare a ricercare quando e come siano accadute le rovine principali del monumento medesimo, per esserne occupati dotti scrittori e principalmente il Marangoni nelle sue Memorie sacre e profane dell’Anfiteatro Flavio, ed il Fea nella sua dissertazione sulle rovine di Roma: ma mi limiterò ad osservare che sino dal principio del secolo decimo sesto l’edificio si trovava in circa nel medesimo stato di rovina, cui ora vedesi ridotto, come ne servono di autorevole documento le vedute prospettiche, che ci furono conservate per cura del Marliano, del Kock e del Du Perac; e perciò la rovina maggiore deve essere accaduta tra il nono ed il decimo quinto secolo,....”

4) Rodolfo Lanciani (“Segni di terremoti negli edifici di Roma antica” – Tipografia della R. accademia dei Lincei, 1895) “Non è possibile ammettere una disintegrazione spontanea per vecchiezza, perché, se volgiamo lo sguardo alla metà dell’ Anfiteatro superstite, dalla parte dell’ Oppio, e ne consideriamo la prodigiosa solidità dobbiamo respingere qualunque congettura di disfacimento su larga scala, prodotto da agenti atmosferici o tellurici: ma al tempo stesso può darsi

che il terremoto del 508, o qualcun altro del quale non rimane notizia, abbiano prodotta una fenditura, simile a quella che spacca il cilindro del Pantheon dalla parte di via della Palombella, e che in questa fenditura abbiano messo radici piante arborescenti. Una volta rotto l'equilibrio nessuna forza umana avrebbe potuto arrestare la rovina dell'Anfiteatro..., in questa maniera avrà avuto principio la caduta dei blocchi dell'orlo superiore dell'anfiteatro. Ma, al tempo stesso, non si può negare che, a un dato momento, in un'epoca che non è stata ancora determinata, tutta la parte dell'ellisse dalla parte del Celio cadde a terra, sulla profondità di due ambulacri, creando una montagna di blocchi, che ha servito da cava di materiale per circa sei secoli. La catastrofe è posteriore al secolo VIII, quando il ven. Beda scrisse il famoso proverbio. Forse avvenne nel terremoto del 1 giugno 1231, forse nel terremoto del Petrarca”.

9. The buttresses

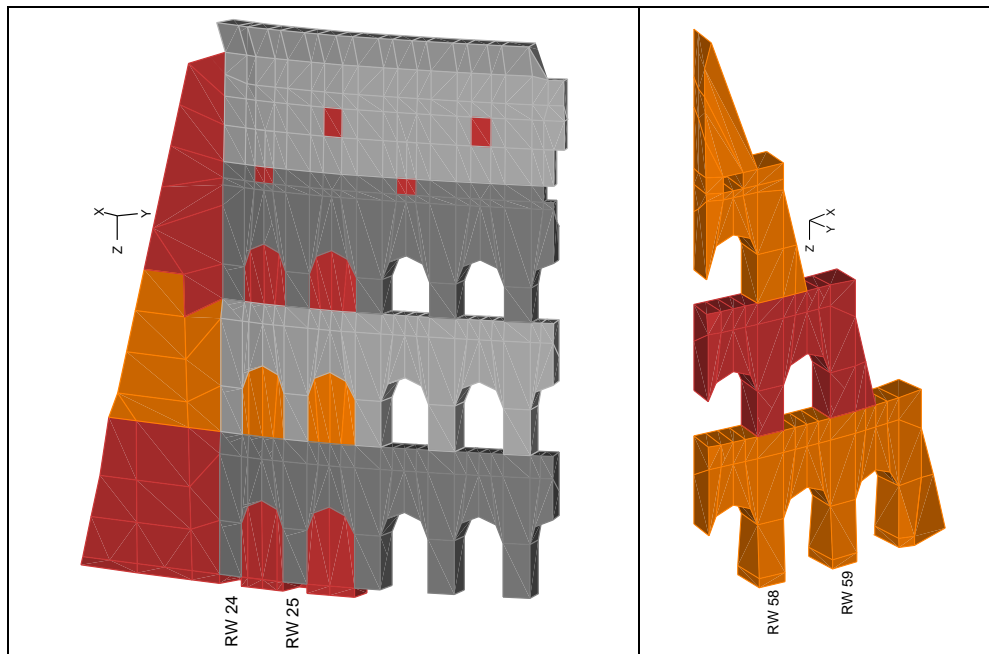


Figure 28. *Buttresses Stern and Valadier.*

It would seem that the actual monument is more vulnerable with respect to the initial integer one, and that the buttresses are the weakest parts, as by following Authors:

A) Nakamura [18]: “For 1349 earthquake the reported modified Mercalli intensity is VIII which correspond to an acceleration of 175 Gal. These values show that, MM VI-VII earthquake which correspond to acceleration about 67 Gal will be enough to cause more damage in vulnerable points of Colosseum”.

B) Pau, Vestroni [33] “The most vulnerable areas of the monument, are the vaults of the second order near Stern’s buttress, and the pillars of the third order near Valadier’s buttress. At these points, the Fourier transforms of the maximum principal stress, exhibit the same pattern and confirm that the first and second modes are mainly responsible for the maximum stress”.

Table 5 Gravity stresses, and their variations for ambient vibrations.

| RW | Order | σ_G | | | $ \Delta\sigma_G _{MAX} \times 1.E+05$ | | | $ \Delta\sigma_{GZ} / \sigma_{GZ} _{MAX}$ |
|----|-------|------------|-------|--------------|--|------|------|---|
| | | x | y | z | x | y | z | |
| | | | | STERN | | | | |
| 24 | 1 | -0.06 | -0.78 | -1.80 | 6.13 | 1.38 | 21.0 | .012 |
| 24 | 2 | -0.05 | .007 | -1.39 | 1.81 | 3.86 | 20.0 | .014 |
| 24 | 3 | -0.17 | -0.18 | -1.00 | 1.41 | 3.93 | 15.0 | .015 |
| 25 | 1 | -0.85 | -0.78 | -2.18 | 4.98 | 5.60 | 14.0 | .006 |
| 25 | 2 | -0.84 | -0.29 | -1.52 | 2.34 | 1.36 | 13.0 | .009 |
| 25 | 3 | -0.59 | -0.18 | -1.05 | 3.30 | 1.74 | 15.0 | .014 |
| 30 | 1 | -1.20 | -0.17 | -1.45 | 2.40 | 2.30 | 15.0 | .010 |
| 30 | 2 | -0.32 | -0.95 | -1.17 | 3.30 | 3.22 | 17.0 | .014 |
| 30 | 3 | -0.44 | -0.40 | -0.95 | 2.01 | 2.24 | 20.0 | .021 |
| | | | | VAL. | | | | |
| 58 | 1 | -0.12 | -0.84 | -0.81 | 6.80 | 8.55 | 76.4 | .093 |
| 58 | 2 | -0.87 | -0.35 | -0.48 | 4.16 | 4.93 | 35.0 | .072 |
| 58 | 3 | -0.49 | -0.06 | -0.21 | 7.30 | 1.63 | 37.6 | .175 |
| 59 | 1 | -0.13 | -0.83 | -0.86 | 6.50 | 8.32 | 70.3 | .082 |
| 59 | 2 | -0.11 | -0.05 | -0.42 | 5.40 | 3.45 | 25.6 | .060 |
| | | MPa | MPa | MPa | MPa | MPa | MPa | % |

From the analysis, for the radial wall 24, 25, 30, 58, 59, on the outer ring, at the first three levels, the followings are obtained:

- a) the ambient vibrations $\Delta\sigma_G$ in the directions x, y, z , in Figure 28 for RW 28, 29 and 30 near Stern Buttress, and Figure 28 for RW 58 and 59 near Valadier buttress;
- b) the Table 5 with the gravity stress $\Delta\sigma_G$, and the ambient vibrations $\Delta\sigma_G$, and the scatters $|\Delta\sigma_{GZ}/\sigma_{GZ}|_{MAX}$.

10. The meaning of this research

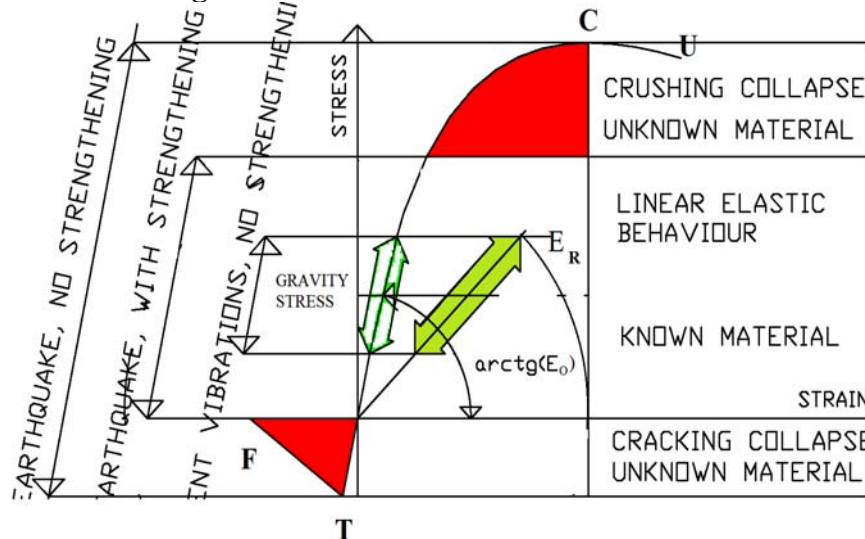


Figure 29. Uniaxial stress-strain relationship for walls. Stresses' ranges:
 a) ambient vibrations $\Delta\sigma = \pm 1/1000$; b) earthquake with strengthening $\Delta\sigma < \pm 20\%$;
 c) earthquake without strengthening $\Delta\sigma = (\sigma_T \div \sigma_C)$.

From the ambient vibrations measured by tests, several invariant diagrams may be obtained, independent from the external actions, but connected to: j) geometry, k) masses distribution, l) deformability.

These diagrams are obtained by signal analysis and are represented by functions of the monument characteristic frequencies like auto and cross spectra, the vibration modes, the diagrams H/V, they constitute the DNA sequences of the physical reality in examination, in those measurement points.

Then, it is easy to construct an analytical model by FE, having the same geometry and masses of the reality; the homogenized damaged elasticity moduli E_R are obtained by identification.

We work on the distribution of that deformability of the model, in order to attain the best fitting between tests and analyses for these invariant diagrams, by taking into account the soil-structure interaction.

11. Physiology, comfort and vulnerability

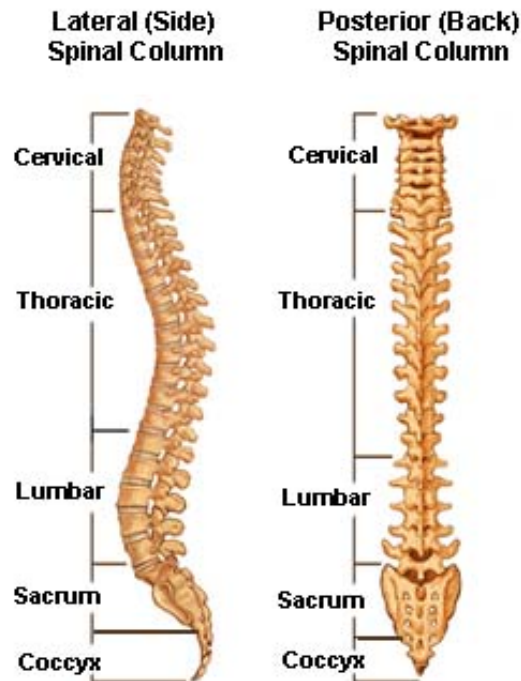


Figure 30. The vertebral column.

The articulations between vertebrae are characterized by semi-mobility. For vertebral column, before the physiology is studied about its movement and the allowable external strength, then the followings are obtained: a) the best sleeping bed having differential support depending on the vertebral zone; b) the neck protection against car crashing, over 200 km/h too, by the limitation of its bending. In the same way, the identification of soil-structure defines the physiology of Colosseum and its soil; and the protection against earthquake consists is the limitation of the vibrations' range $|\Delta\sigma_G / \sigma_G|$, by a suitable distribution of stiffness which acts with differential support.

The corresponding most vulnerable zones are the cervical vertebrae in the vertebral column and the buttresses in the monument.

12. Conclusions

We wished to study the effect of ambient vibrations on the monument.

The actions are transmitted by train to soil and from this to the monument; partial models were yet existing in disciplines of Geophysics, Structural and Transportation Engineering.

The models normally used in Structural engineering are unsatisfying because they concern the monument fixed at the basis, as: a) the L.E.M. with rigid macroelements connected by plastic hinges, treated with static analysis, b) the elastic linear monument alone.

Then, we were sure that these three partial models could be connected in a global model very accurate, but with a work very long and heavy. Finally we realized that the ambient vibrations produce a linear elastic behaviour of the monument.

The present methodology concerns the analysis alone, it rests valid for improved tests at disposal, or for changed geometry by tunnels excavations.

Then the proposed methodology constitutes a tool accomplished in scientific ambient, but ready for the professional use.

References

[1] Perrone, V., "la ferrovia Metropolitana a Roma", *Trasporti pubblici*, nn. 4÷10 1952, nn. 1÷2, 9, 11 1953, nn. 5, 7÷8 1954.

[2] Di Pasquale S.: *L'uso dei modelli nella costruzione della cupola di S. Maria del Fiore*, Università di Firenze, Facoltà di Architettura, Pubblicazione 26/1984.

[3] Nakamura, Y., A Method for Dynamic Characteristics Estimation of Subsurface using Ambient vibration on the Ground Surface, *Quarterly Report of RTRI*, Vol.30, No.1, pp.25-33, 1989.

[4] Croci G., *Studies and research on the Colosseum* (in Italian). Quaderni del Dipartimento di Ingegneria Strutturale e Geotecnica, Rome, Italy, 1990.

[5] ISO 4866 (1990), *Mechanical vibration and shock vibration of buildings. Guidelines for the measurement of vibrations and evaluation of their effects on buildings*.

[6] BS 7385-2 (1993), *Evaluation and measurement for vibration in buildings – Guide to damage levels from groundborne vibration*.

[7] Clemente, P., Bongiovanni, G., (1993) Ambient vibration effects on the Colosseum, *IABSE Symposium on Structural Preservation of the Architectural Heritage*, Rome, pp. 107÷114.

[8] Schingo G., Rea R., “Il progetto di restauro del Colosseo. I sotterranei: assetto idraulico e interventi strutturali tra XIX e XX secolo”, *Bollettino di archeologia*, 23-24 Settembre-Dicembre 1993.

[9] Pasquali, C., (1994) Esperienze e risultati delle campagne di misura per la Metropolitana di Roma, *Giornate Impatto vibro-acustico e ambientale delle ferrovie Metropolitane*.

[10] Funicello, R., Lombardi, L., Marra, F., Parotto, M. (1995) “Seismic damage and geological heterogeneity in Rome’s Colosseum area: are they related?”, *Annali di Geofisica*, 927-937.

[11] Bozzano, F., Funicello, R., Marra, F., Rovelli, A., Valentini, G. (1995) “*Il sottosuolo dell’area dell’anfiteatro Flavio in Roma*”, 405÷422.

[12] Moczo, P., Rovelli, A., Labák, P., Malagnini, L., (1995) Seismic response of the geologic structure underlying the Roman Colosseum and a 2-D resonance of a sediment valley, *Annali di geofisica*, pp. 939÷956.

[13] Nakamura, Y. (1996). “Seismic response of roman Colosseum and its foundation by using micro-tremor measurements”, *The 10th Japan Earthquake Engineering Symposium*, pp. 2625-2630, 1998.

[14] Mertens D., Rea R., Schingo G., Beste H.J., Piraino C., (1998) Il Colosseo: lo studio degli ipogei, “*Sonderdruck aus Mitteilungen des deutschen archaologischen instituts roemische abteilung*“, Vol. 105, 1998, ISBN 3-8053-2459-6.

[15] Clemente P, Rinaldis D. *Protection of a monumental building against traffic-induced vibrations*. Soil Dynamics and Engineering 1998; 17:289–296.

[16] DIN 4150/3 (1999) *Erschütterung im Bauwesen – Einwirkungen auf bauliche Anlagen* (in German).

[17] Coarelli F., Gregori G.L., Lombardi L., Orlandi S., Rea R., Vismara C., “*Il Colosseo*”, Electa, Milano, 1999.

[18] Nakamura, Y., Gurler, E.D., Saita, J., Rovelli, A., Donati, S., (2000) Vulnerability investigation of roman Collisseum using ambient vibration, *12WCEE2000*, paper 2660.

- [19] Pensabene P., Panella C., “*Arco di costantino tra archeologia e archeomentria*”, “L’Erma” di Bretschneider, Roma, 2001.
- [20] Schingo G., “*Gli sterri del 1939 per la costruzione della metropolitana. Dati archeologici inediti dalla valle del Colosseo*”, “L’Erma” di Bretschneider, Roma, 2001.
- [21] Jappelli R., Rea R., Schingo G., “Artificial openings in the foundation of the Colosseum”, *AITES-ITA 2001 World Tunnel Congress, Milano*, June 2001.
- [22] M. Bruner, (2001), “Analisi della marcia di un veicolo di Metropolitana”, *Tesi di laurea, Dpt. Trasporti*, Università di Roma “La Sapienza”.
- [23] Cerone M, Croci G, Viskovic A. The structural behaviour of the Colosseum. International *UNESCO/ICOMOS Congress ‘More than two thousand years in the history of architecture’*, Bethlehem, Palestine, 2001.
- [24] Orlando L., Bernabini M. (2002), “La geofisica nella caratterizzazione delle fondazioni dell’anfiteatro Flavio”, *21° Convegno nazionale, Gruppo nazionale di geofisica della terra solida*.
- [25] Akinci A., Olsen K. B., Rovelli A., Marra F., Malagnini L. (2002) “Simulazioni 3-D e produzione di scenari di scuotimento nella città di Roma”, *21° Convegno nazionale, Gruppo nazionale di geofisica della terra solida*.
- [26] Randall J., Allemang, “*The Modal Assurance Criterion – Twenty Years of Use and Abuse*”, University of Cincinnati, Cincinnati, Ohio, Sound and Vibration, August 2003
- [27] UNI 9916 (2004) *Criteria for the measurements of vibrations and the assessment of their effects on buildings* (in Italian).
- [28] Cerone M., Rovelli A., Valente G. (2004) “Indagine preliminare per l’Identificazione Dinamica del Colosseo”, ANIDIS.
- [29] Pau, A., De Sortis, A., Marzellotta, R., Vestroni, F., “*Health monitoring of cultural heritage using ambient vibrations. In Safety and Security Engineering*”, Brebbia CA, Bucciarelli T, Garzia F, Guarascio M (eds). WIT Press: Southampton, 2005; 331÷340.
- [30] Tertulliani, A., Valente, G., “La meccanica fenomenologica per l’enigma di Noto”, *Conferenza Internazionale CRASC06*, Messina, 20-21 April 2006.
- [31] Valente, G., “Influence of a tunnelling for Metro C to Colosseum in Rome”, *Ist EMAS, Hammamet, Tunisia*, 3-5 May 2006.
- [32] Recommendations ICOMOS/ISCARSAH, 20/05/2007.
- [33] Pau, A., Vestroni, F., (2008) Vibration analysis and dynamic characterization of the Colosseum, *Structural Control and Health monitoring*, Journal of Structural control, Ed. J. Wiley & Sons, Febr.

[34] Crisi, F., Dell'Isola, F., D'Ovidio, G., Valente, G., "Vibrations analysis of Colosseo due to trains' transit", *2.nd EMAS, Hammamet, Tunisia*, May 2008.

[35] Crisi, F., D'Ovidio, G., Valente, G., "Metodologia di analisi delle vibrazioni strutturali dovute al traffico ferroviario: caso di studio dell'area archeologica del Colosseo", March 2009, *Ingegneria Ferroviaria*.

[36] Crisi, F., D'Ovidio, G., Valente, G., "Vibration Analysis on Constantine Arch monument due to the metro train" *Proceedings of 14th International Conference. Transport Means. 2010*.

[37] Crisi, F., D'Ovidio, G., Valente, G., "Flexible Rail Beams Modeling for Soil-Structure Interaction Dynamic Analysis" *Proceedings of 14th International Conference. Transport Means. 2010*.

[38] Caserta A., Cerone M., Crisi F., Delladio A., D'Ovidio G., Govoni A., Marra F., Nakamura Y., Rovelli A. and Valente G., "Dynamic interaction of soil and structure by rail traffic", *Proceedings of Workshop DISS_10, L'Aquila, 19 March 2010, Aracne, ISBN 978-88-548-3693-8*.

[39] Bruner, M., Crisi, F., D'Ovidio, G., Valente, G., "Soil vibration analysis due to the rail bogie motion" *Proceedings of 14th International Conference. Transport Means. 2010*.

[40] Crisi, F., D'Ovidio, G., Valente, G., "Vibrations analysis in the archaeological area of Rome by rail traffic", *4th VI-grade User's Conference - Udine, 18-19 October 2011*.

[41] Nakamura, Y. (2011), "The H/V Technique and Example of its Application for L'Aquila and Rome Area", *Proceedings of the workshop DISS_10, L'Aquila, 19 March 2010, Aracne, ISBN 978-88-548-3693-8*.

[42] F. Crisi, G. D'Ovidio, G. Valente, "Weak vibration of Colosseum area due to the trains running", *Proceedings DISS_12, L'Aquila, March 2012, DISS_Edition, ISBN 9788894011401*.

[43] A. Caserta, P. Clemente, Y. Nakamura, A. Rovelli, G. Valente, "Identification of the mean elasticity modules for soil Colosseum interaction", *DISS_12, L'Aquila, March 2012, DISS_Edition, ISBN 9788894011401*.

[44] F.M.D. Accattatis, M. Bruner, F. Crisi, G. D'Ovidio, G. Valente, P. Vitali, "Railway vehicle dynamics and the soil vibration analysis", *Proceedings DISS_12, L'Aquila, March 2012, DISS_Edition, ISBN 9788894011401*.

[45] F.Crisi, G. D'Ovidio, G. Valente, "Guideway stress comparison due to traffic of wheel-to-rail and MagLev trains", *Proceedings DISS_12, L'Aquila, March 2012, DISS_Edition, ISBN 9788894011401*.

[46] C.I.S.T.E.C. (2000), “*Analisi e documentazione dei dissesti strutturali ed individuazione delle situazioni a rischio*”, le tre Università di Roma.

[47] Maupertuisiana, Hamburg 1753, pag. 203.

[48] D'Ovidio, G. Valente “Dynamic analysis of experimental HTS maglev module based for mass transportation system”, International Conference on Superconductivity and Magnetism 2012, ICSM, Istanbul.

[49] G. D'Ovidio, G. Valente, “Weak vibrations of the Colosseum due to existing and forthcoming underground lines”, 17th International Conference Transport Means 2013, Kaunas University of Technology 24-25 October 2013, Lituania.

[50] Como M., “Statics of Historic Masonry Constructions”, Springer Series in Solid and Structural, Berlin Heidelberg 2013.

[51] Truesdell C.: Hypo-elasticity, *Journal of Rational Mechanics Analysis*, Vol.4, 1955, pp. 83-133.

[52] Zienkiewicz O. C and Taylor R L , *The Finite Element Method for Solid and Structural Mechanics*, ISBN 978-0-7506-6321-2 1967, McGraw Hill, New York.

The importance of defining the geometry of foundations and soil layers for dynamic analysis of Colosseum

Heinz-Jürgen Beste⁶, Paolo Clemente¹, Cinzia Conti⁵,
Gino D'Ovidio³, Yutaka Nakamura⁷, Luciana Orlando⁴,
Rossella Rea⁵, Antonio Rovelli² Gianfranco Valente³

Abstract

By the comparison between tests and analyses, the dynamic characterization was performed, in order to obtain the map of elasticity modules for soil Colosseum interaction. The accuracy for foundations and soil is lower than for monument, due to unknown exact geometry underground. For foundations, a high variability was found of elasticity modules, which was referred to variable damage of concrete for cracking in time. For soil layers, different definitions exist, and we are interested in the best. The vibrations produced by trains are depending on the underground geometry too. The analyses are performed with traditional convoys running on Metro B and C, for the vibrations knowledge on RA XLVII and on ground felt by pedestrians.

1. ENEA Rome, 2. INGV Rome. 3. L'Aquila University. 4. University "la Sapienza" Roma, Italy. 5. Soprintendenza speciale per i Beni Archeologici di Roma.
6. Istituto Archeologico Germanico, Roma, Italy. 7. S.D.R. Tokyo.

1. Introduction

Underground, for foundations and soil layers:

1) the geometry is not visible, the lower surface as regards the foundations,

2) for elasticity modules obtained by the dynamic identification, the accuracy is lower than for monument, and it depends on such geometric uncertainties,

The present interdisciplinary research starts from the necessity to improve this accuracy, with further surveys:

a) geophysical with actual instrumentation inside the five tunnels to define better the lower surface of foundations,

b) the soil layers by new geotechnical surveys for Metro C.

However, this necessity of improvements does not affect:

c) the elasticity modules of monuments are known with great accuracy, over 95% for the buttresses, which are the most vulnerable elements;

d) the vibrations felt by pedestrians, known analytically with accuracy around 80%, and valuable better by instruments on the ground.

Then, new analyses will be performed, for foundations and soil.

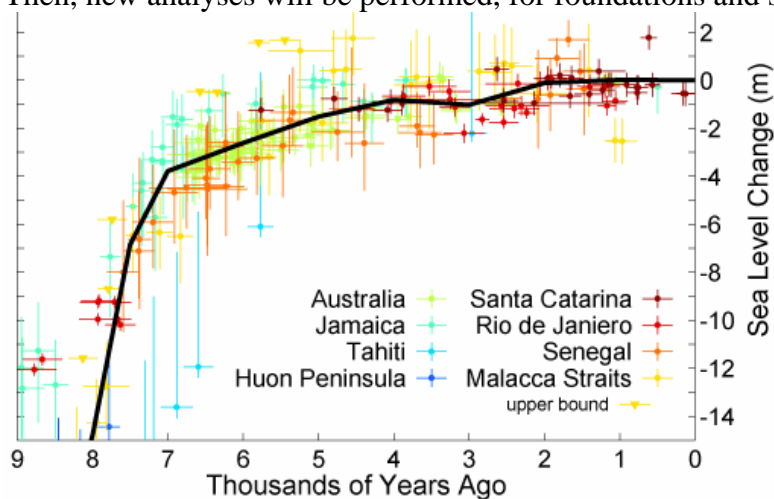


Figure 1. Holocene sea level.

2. Archaeology and Geology

2.1 The last glacial era

During the height of last glacial era (Würm era), *ca* 24,000–10,000 ybp, most of western and central Europe and Eurasia was open steppe-tundra, while the Alps presented solid ice fields and mountain glaciers. Scandinavia and much of Britain were under ice.

The figure 1 shows changes in sea level during the Holocene, the time following the end of the most recent glacial period, based on data from Fleming et al. 1998, Fleming 2000, & Milne et al. 2005. These papers collected data from various reports and adjusted them for subsequent vertical geologic motions, primarily those associated with post-glacial continental and hydrostatic rebound.

The black curve is based on minimizing the sum of squares error weighted distance between this curve and the plotted data. It was constructed by adjusting a number of specified tie points, typically placed every 1 kyr and forced to go to 0 at the modern day.

The deepening of sea level produced a change of the rivers flow to the actual Tiber River, the old path was filled by alluvial deposit, during Holocene era.

The actual ground level around Colosseum is about +23.22 m o.s.l.

2.2. Foundations construction

The “Soprintendenza speciale ai Beni Archeologici di Roma” begun non invasive inspections of Colosseum foundations that are concrete made with “pozzolana” cement and “selce” stones; the upper 6 m are contained by an elliptical wall having depth of 3 m; the travertine pavement has a thickness of 90 cm, see Figures 2 and 3.

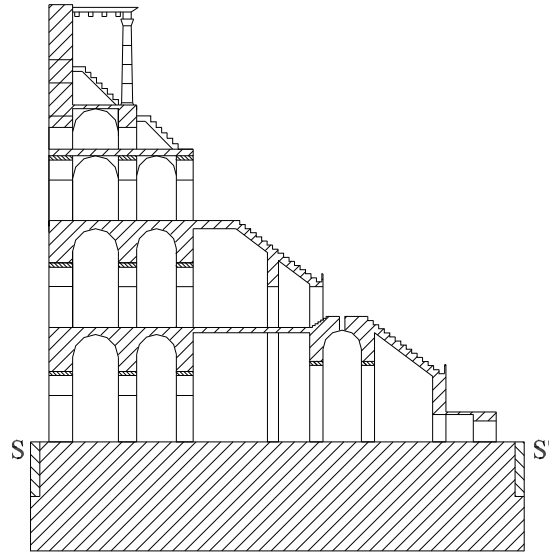


Figure 2. Foundations upper wall

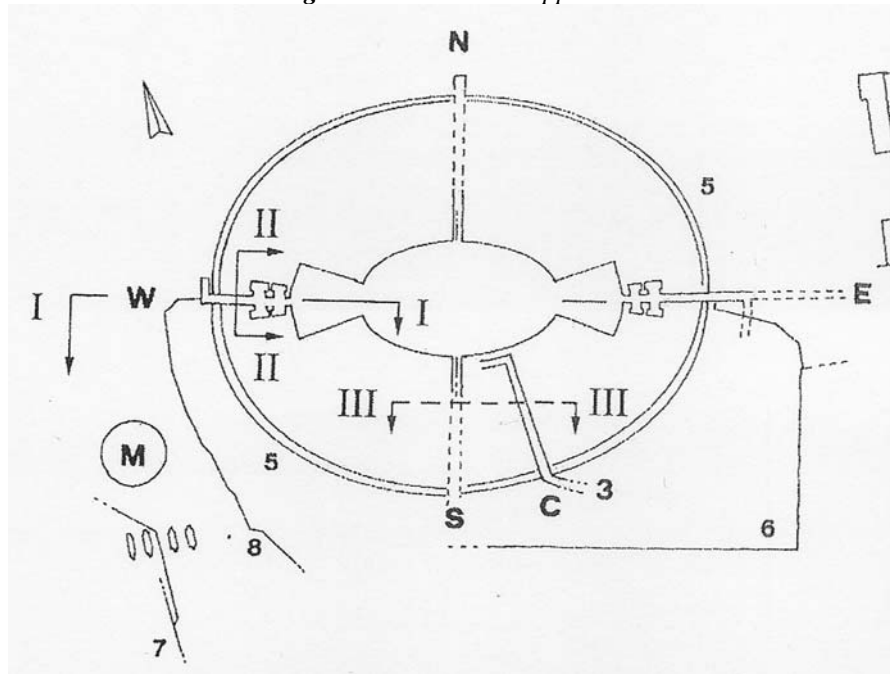


Figure 3 Key map.

3. Geophysical surveys in the past

The Colosseum foundation was investigated with georadar and seismic refraction with the aim to define the thickness of the cover layer and the thickness of foundation. The surveys were mostly located on the southern sector of an amphitheatre, which is currently free of the outcropping of the first two outside ambulatories, which collapsed in the XIV century (Fig. 4).

3.1 GPR survey.

To increase the penetration depth the GPR data were collected with single [35] and multi-fold coverage [35, 36, 37, 38, 39]. The profiles were repeated using different peak frequency antenna and different instruments. The data were collected with PulseEKKO 100 instrument, manufactured by Sensor&Software equipped with 50, 100 and 200 MHz antenna, and SIR 10 by GSSI equipped with 100 and 400 MHz antenna.

The single (red lines) and multi-fold data location (blue lines) are mapped in the figure 4. Corresponding to the Commodo tunnel (Fig. 4), a detailed single fold survey was performed with the 200 MHz antenna of the Sensor&Software instrument. Single-fold data were performed in continuous mode with 200, 100 and 50 MHz antennas of Sensor &Sensor instrument and 400 and 100 MHz antenna of GSSI instrument. The multi fold data were acquired in step mode with WARR geometry using a PulseEKKO100 instrument equipped with 100 and 50 MHz antenna. The maximum offset transmitter-receiver for the multi fold data was 7 m, with receiver offset of 0.2 m and sampling step of 0.2 m. The profiles were acquired mostly in a radial direction with respect to the monument. The radial direction was preferred to the parallel one, so to easily distinguish between air waves and reflections from the ground layers.

The processing of the single fold data was a set time of zero, frequency filter, gain function, background remove the multi fold data included also geometry setting, velocity analysis, normal move-out correction and stacks, the latter was calculated for a velocity of 0.09 m/ns.

The analysis of the radar data has, for the same frequency antenna, underlined that the results in terms of resolution and depth of investigation are analogous for the two types of tools (Fig. 5). They differ in detecting of air waves in the data collected with the Sensor&Software tool because it is equipped with unshielded antennas.

The single-fold data investigated a maximum depth of 2.0-2.5 m which in most part is linked to the cover layer of foundation (Fig. 5). This layer consists of heterogeneous filling sediments, including utilities, travertine blocks, etc. The continuous reflector at a depth of about 0.50 m is due to the ancient ground level and the reflection at 1.5-2.5 m to the top of foundation.

The variation in thickness of the cover layer is due to topography of the ground and to the lateral velocity variation of the material forming that layer.

The single-fold georadar data demonstrated the capability in the investigating with high resolution the cover layer but it was not effective in detecting the bottom of the foundation. The multi-fold data acquired with 50 and 100MHz antennas show reflections up to 220 ns (Figs. 6 and 7). The data shows a lower resolution of the near surface layer and an increase of signal penetration, with respect to the single-fold data. The sloping reflections between 100 and 200 ns are due to the air waves reflected from the walls of the monument, which are also present in the single-fold sections. The continuous and horizontal reflection at 220 ns (around 11 m) is at a more or less the expected depth of the bottom of foundation, considering the 0.090 m/ns propagation velocity used in the Normal Move Out correction.

The interpretation of reflection at 220 ns is validated by two multi-fold profiles (Fig. 7) directed normal to the Colosseum, outside (left) and inside (right) the foundation. The latter is quite similar to the profile of Figure 7 with horizontal reflection at 220 ns interpreted as the foundation bottom, while the left profile, acquired outside the foundation, does not show any reflection at 220 ns.

3.2 Seismic refraction

The seismic refraction gave the thickness of covering layer of the foundation and the P-wave velocities of the cover layer and foundation. We recorded 4 bases (Fig. 4), each sampled with 24 vertical receivers with frequency centred at 10 Hz. The receivers were 2. meters apart and in each base seven shots were fired, located according to the classical scheme: 2 external, two at the ends of the base and 3 inside the base, the consecutive bases overlaps for some geophones.

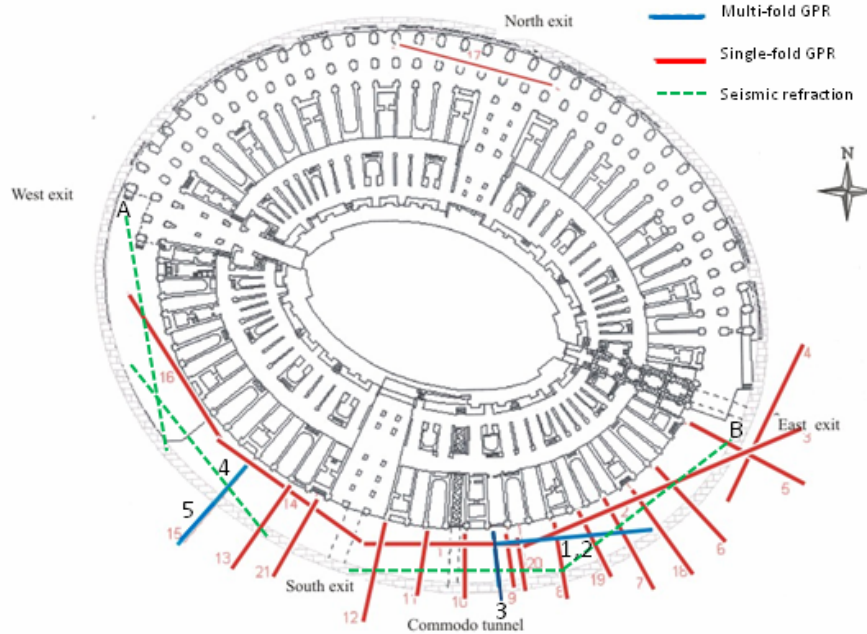


Figure 4. Location of GPR surveys. Single-fold (red lines) acquired with 50, 100, 200 e 400 MHz antenna and multi-fold (blue lines) acquired with 50 and 100 MHz antenna. Seismic refraction location (green lines).

The data were recorded with a 24-channel digital seismograph of Geometrics Corporation. The source was an iron hammer 7 kg weight. The interpretation was based on the intercept method [39, 40] refined according to the method of the 'delay times' [41]. The data (Fig. 8a) show an outcropping layer with a velocity of around 500 m/s and a second one with a velocity of around 3200 m/s. We linked the first one to the cover layer and the second one to the foundation. The top of

foundation is located between a few tens of centimetres and 2.5 m from the ground level.

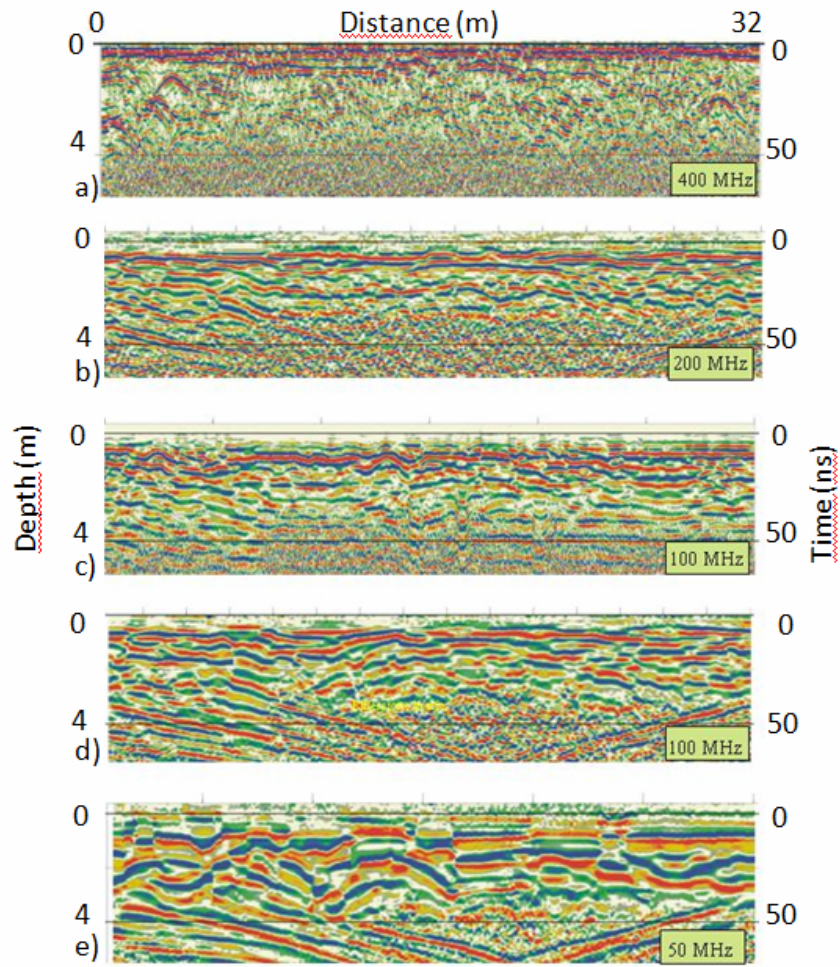


Figure 5. Georadar sections acquired with PulseEkko100 equipped with 200, 100 e 50 MHz antenna (b, d and e) and with GSSI equipped with 400 and 100 MHz antenna (a and e).

The top of foundation shows short period undulations probably due to the travertine blocks and/or coupling of geophones with the ground long period undulations due to the ground level variation.

The superposition of the geometry of the top of foundation obtained with the GPR (Figure 8b) with that obtained by the seismic refraction (Fig. 8a) shows a good overlap and demonstrates as the two methods can provide the geometries of the layer covering the foundation. In detail the GPR allows to reconstruct the thickness of cover layer and the depth of the base of the foundation, instead the seismic refraction gives the thickness of the cover layer and the P-wave velocities of the cover and foundation layers.

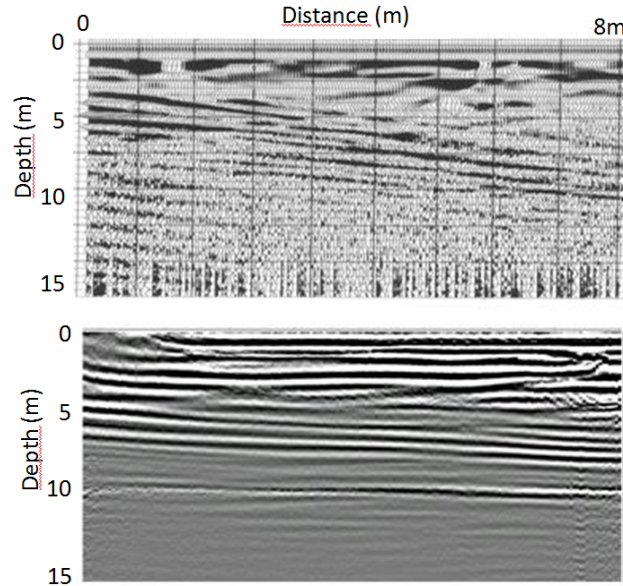


Figure 6. On the top single-fold data and on the bottom multi fold ones acquired with a 50MHz unshielded antenna (Profile 1).

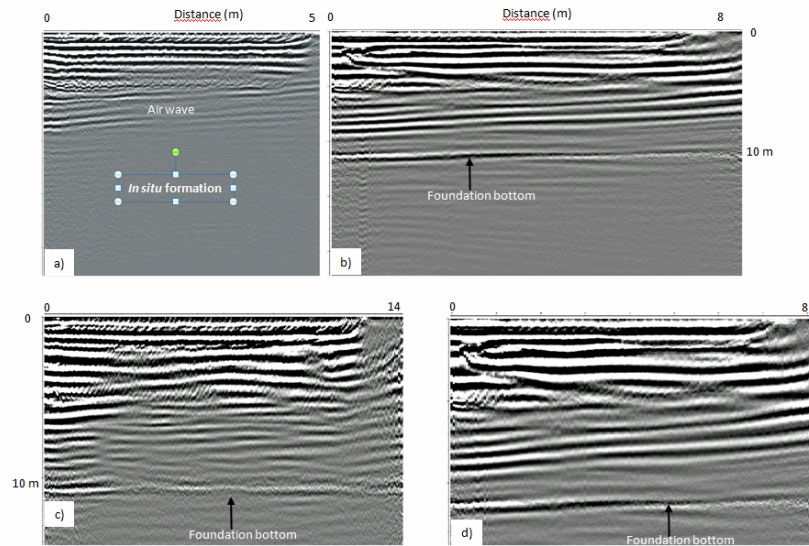


Figure 7. Single-fold profile 5 (a), 4(b), 2(c), 3(d) acquired with a 50 MHz unshielded antenna.

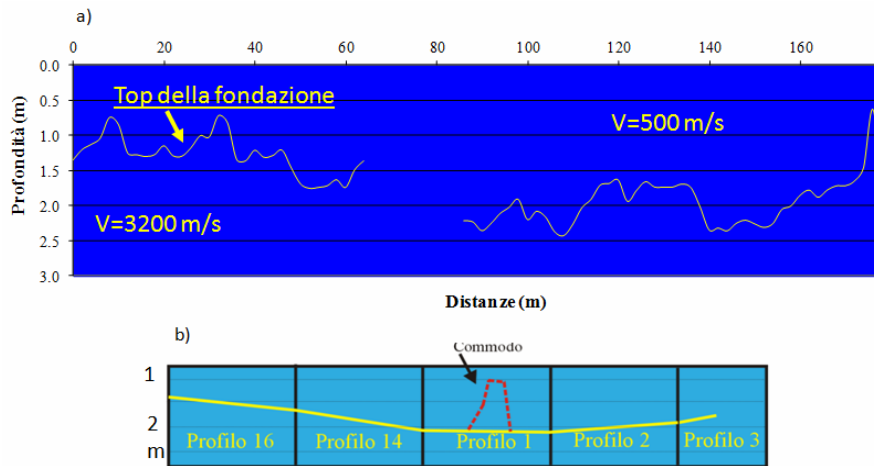


Figure 8. Section of seismic refraction data (a) and Georadar data (b) of the cover layer of the Colosseum foundation between A and B of figure 2.

4. Existing tests H/V

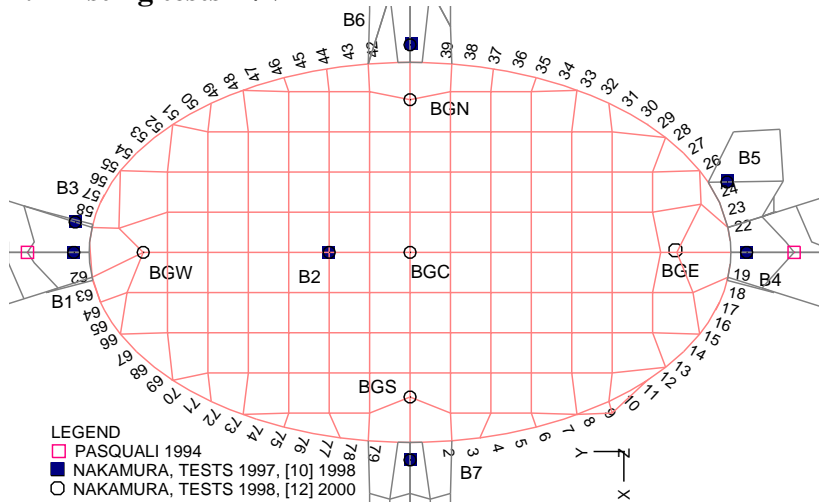


Figure 9. Hypogeum, Z=-6.50 m. (n.14 points).

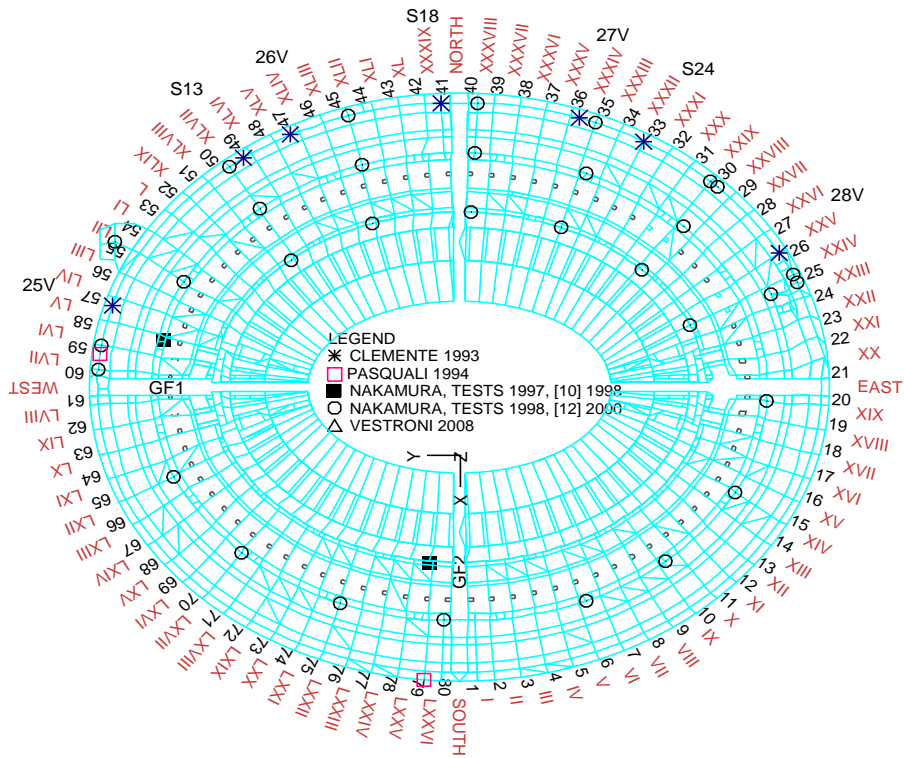


Fig. 10. Measurement points on the ground at $Z=0.0$ m, a) radial wall RA with Arabian numbers, b) radial access RA with roman numbers. (n.45 points).

They were performed in several points on the foundation ring, (B1÷B7, GF1, GF2, BGC, BGN, BGE, BGS, BGW), as in Figures 9 and 10.

5. Numerical models

The foundation was subdivided in n. 4 layers:

- a) travertine pavement, $t \cong 90$ cm, as in Figure 11b;
 - b) upper concrete with four radial cuttings, $t \cong 6.00$ m, as in Figure 11c;
 - c) two lower concrete, $t \cong 2 \times 3.00$ m.
- Upper and lower concrete layers were subdivided in two rings and sixteen radial sectors, with $(3 \times 2 \times 16 + 1 = 97)$ different materials.

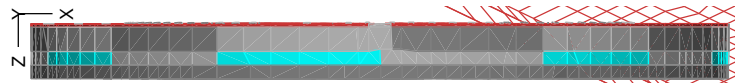


Figure 11a. The lateral projection of foundation layers, $t=(5.00 + 3.50 + 3.50 + 0.80)=12.80$ m.

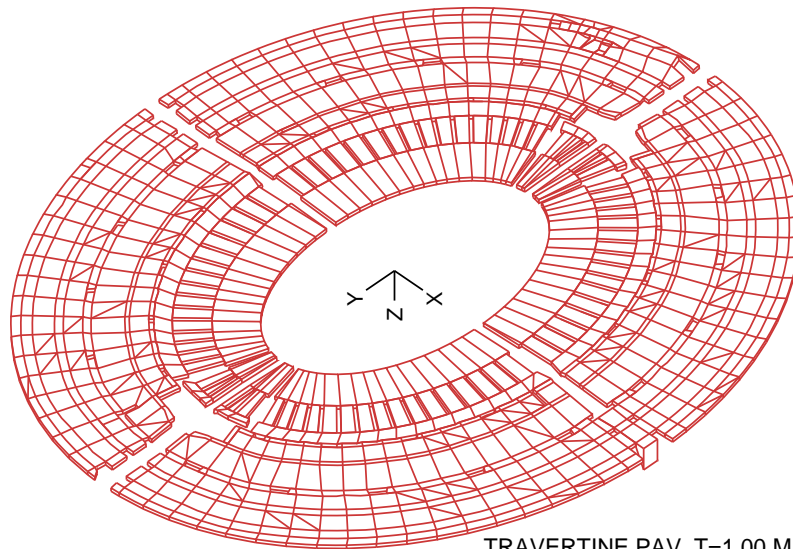


Figure 11b. The travertine pavement, $t=0.80$ m. $E=3640$ MPa

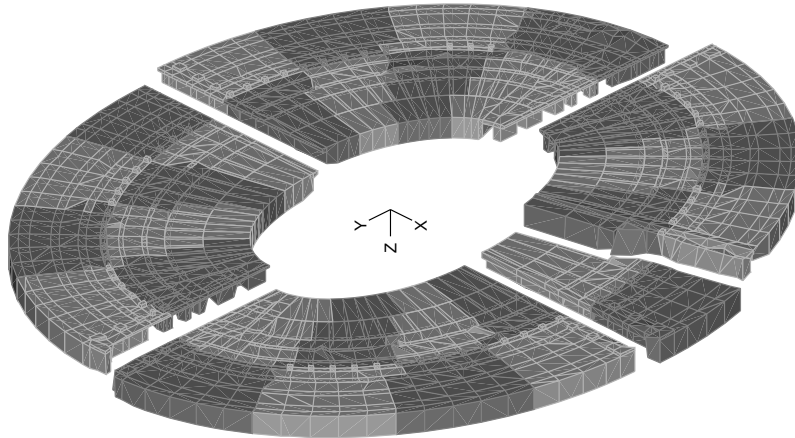


Figure 11c . The mesh of upper concrete layer, with the n.5 tunnels (E, S, W, N and Commodus at SSE).

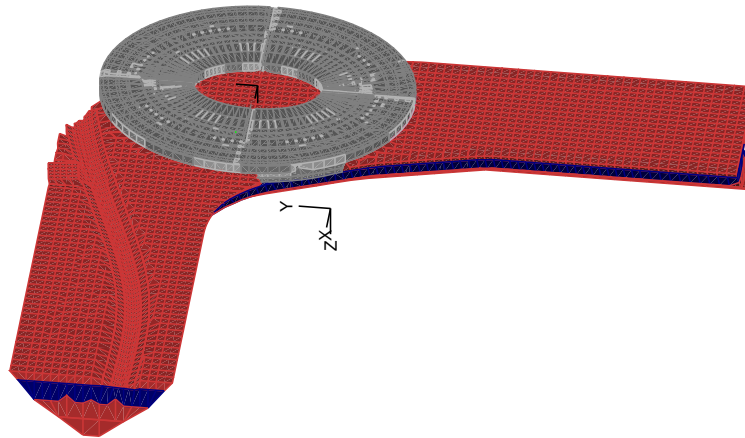


Figure 12 a. Actual[3] and next Holocene (in blue).

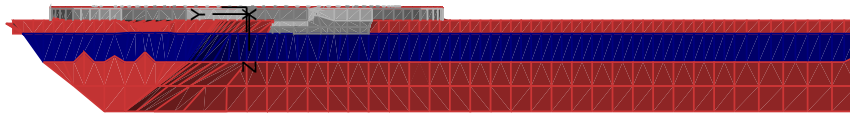


Figure 12b. Lateral view of layers. Holocene: red the used [3], blue the next proposal.

The used Holocene layers are from [3], but a different hypothesis exists for it, principally for the depth $d=17.00$ m instead of the used depth $=45.00$ m.

6. Material characteristics

We perform the dynamic characterization, by the comparison between the tests and the analysis, and we obtain the map of elasticity modules shown in Figures 14a and 14b.

The variability of elasticity modules was referred to variable damage of concrete for cracking, for:

- a) different viscous displacement between Holocene and Pleistocene;
- b) a preferred development corresponding to the four radial cuttings of upper layers.

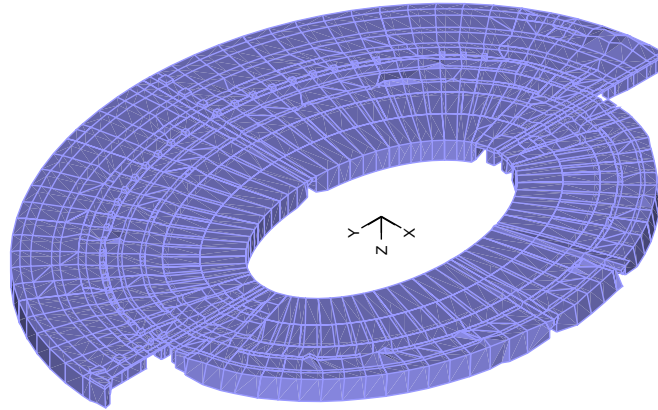


Figure 13. Actual area of wall loading.

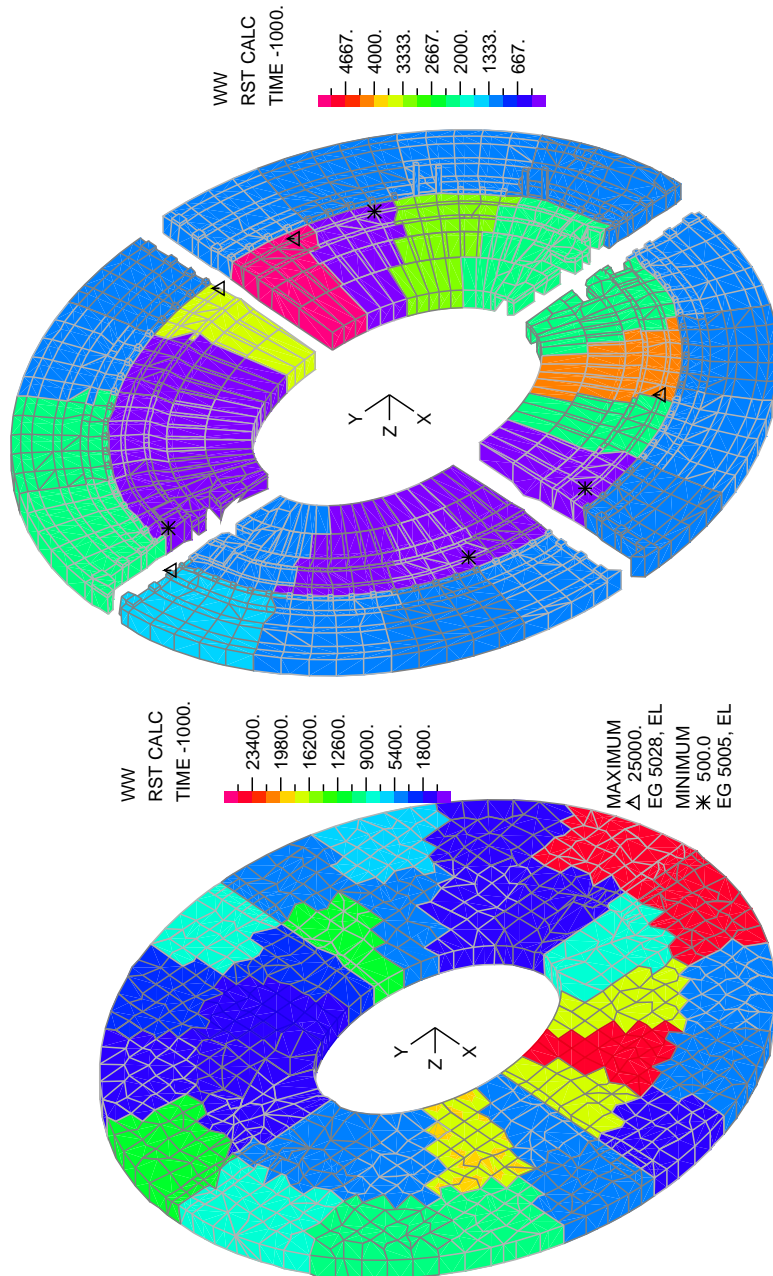


Figure 14 Upper and Lower elasticity modules.

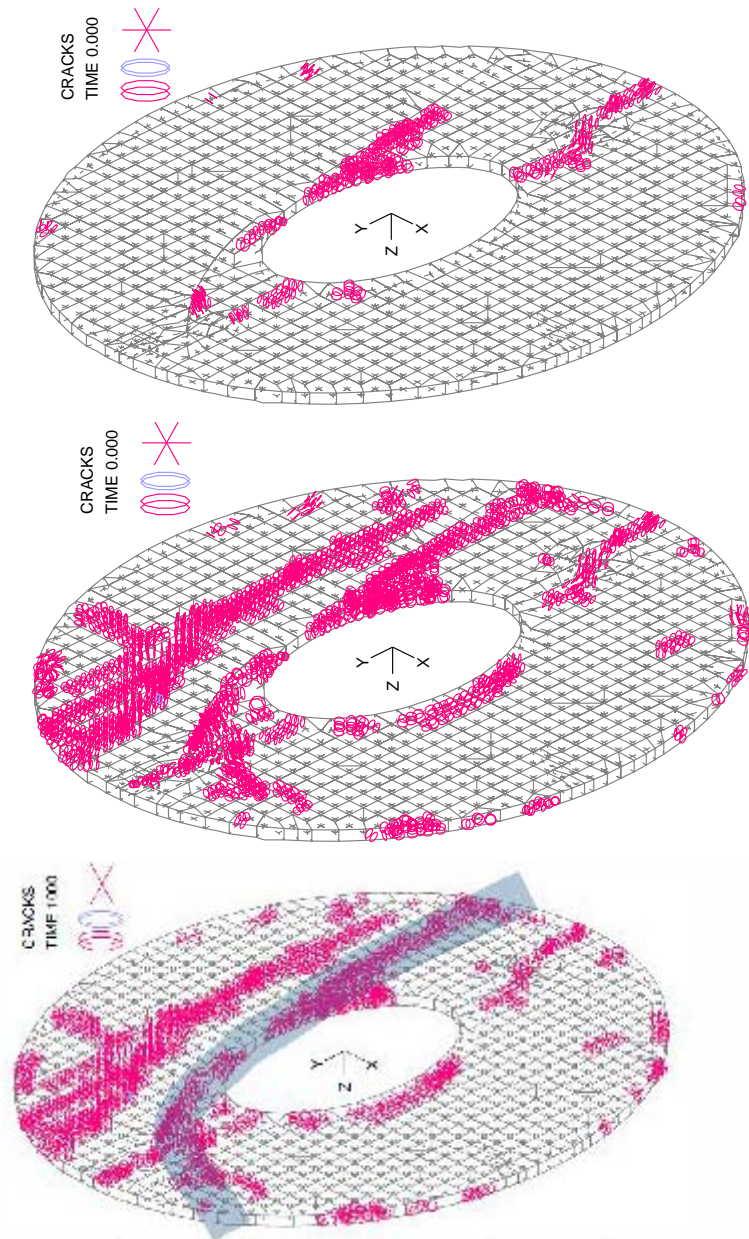


Figure 15. Cracks of lower layer foundations, at phases: 2) full $t=0$; 3) full $t=\infty$; 4) partial $t=\infty$, estimated principal disconnection by tests.

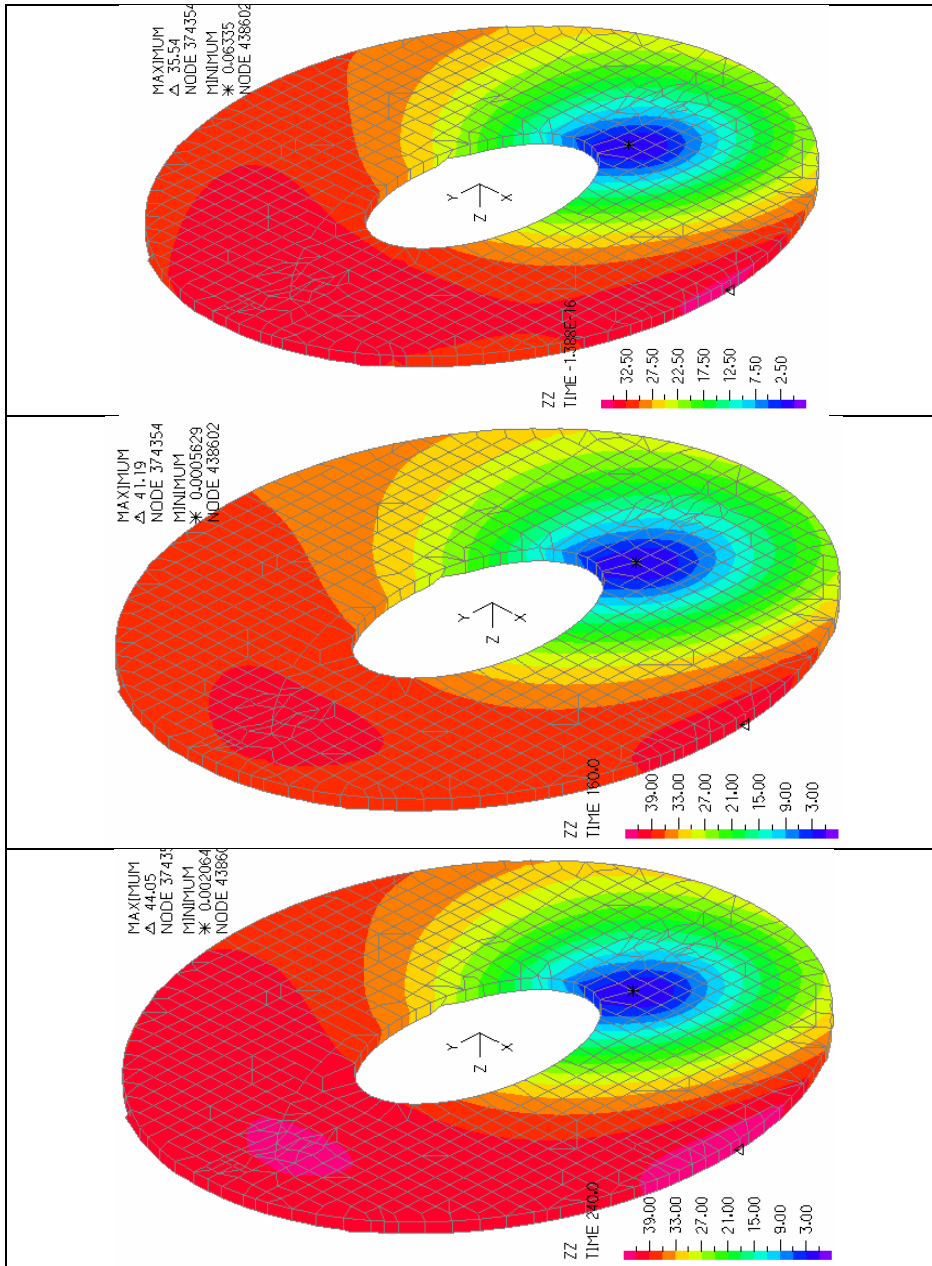


Figure 16. Vertical displacements of foundations, for phases: 1) full $t=0$; 3) viscosity $t=\infty$; 4) partial load $t=\infty$. “Quaranta centimetri di dislivello nella parte sud del Colosseo” (Corriere della Sera 29 luglio 2012).

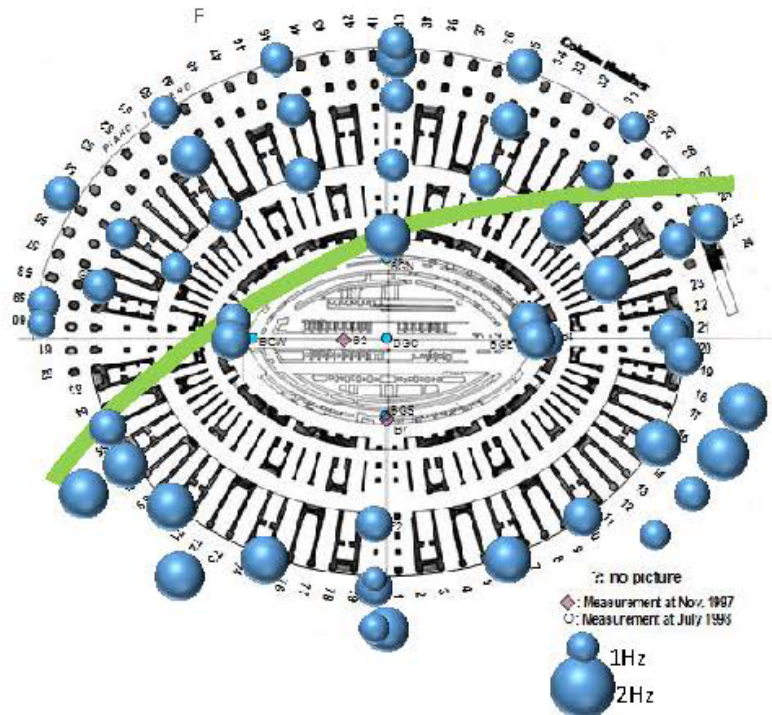


Figure 16a. Predominant frequency distribution of the foundation of Colosseum from frequency range of QTS.

Table 2. Loading sequence.

| Phases | t | E_{CONCR} | E_{SOIL} | Load | Colosseum |
|--------|----------|-------------|------------|------------------|------------------|
| 2 | 0 | E | | foundation | Full |
| 3 | ∞ | 0.5 E | 0.75 E | Found+ el(N+S) | Full |
| 4 | ∞ | 0.5 E | 0.75 E | Found+ el(N+S/3) | Partial, Fig. 15 |

We perform an incremental analysis taking into account different phases, as in Table 2:

a) foundations construction; initially, for undamaged concrete we assume two different constant modules for the two layers, upper $E_{CONCR}^{0_UPPER}=12000$ MPa, lower $E_{CONCR}^{0_LOWER}=24000$ MPa, corresponding to the maximum values obtained by identification

b) monument construction;

c) viscous effect development; at viscous effects exhausted, the final analysis, was performed for the full dead load enclosing the eleva-

tion, half elasticity modules for concrete, 0.75 elasticity modules for the soil:

$$\gamma = 2 \cdot \gamma_0, \quad E_{CONCR} = 0.5 \cdot E_{CONCR_0}, \quad E_{SOIL} = 0.75 \cdot E_{SOIL_0}$$

d) missing of southern walls, the load of elevation acts as in Fig.13. Figures 15.2, 15.3 and 15.4 show the crack patterns, for the phases 2), 3) and 4) respectively;

And Figures 16.2, 16.3 and 16.4 show the vertical displacements for the same phases.

From the tests appears a great difference of dynamic behaviour between northern and southern sides of foundations [1, 8, 13, 22], it could be explained by a principal disconnection as in Figure 15.4.

All these results are depending on the soil layers by [3], if these layers are different all these results will change.

The dead load of foundations is about the same of the elevation.

7. Models of trains

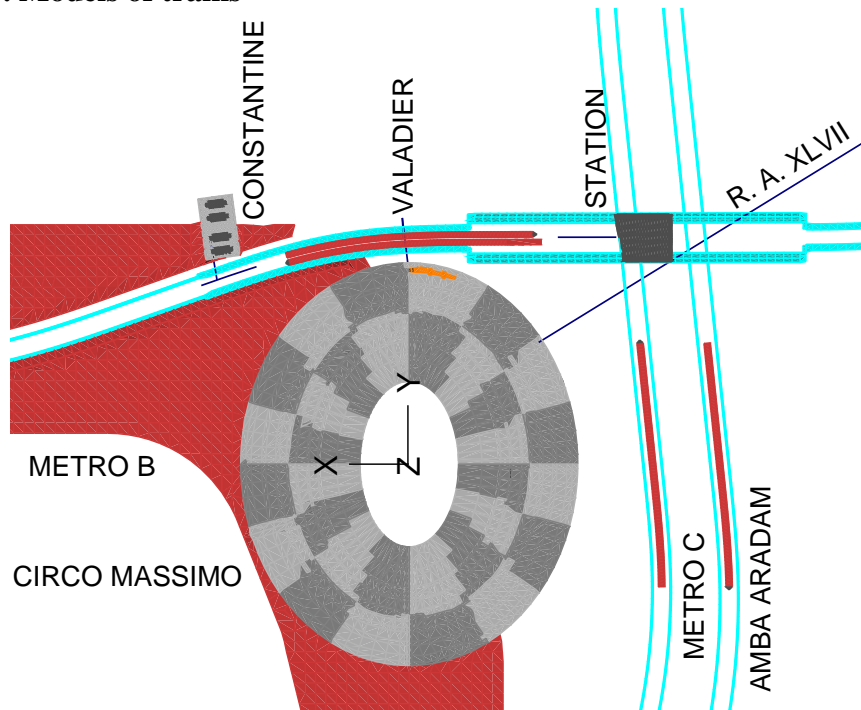


Figure 17. Synchronous placements of the four trains, centred on the referring axes, at mean distances $^x d_b = 109.19 \text{ m}$, $^y d_c = 108.51$ from the station, at time $t = 25.28 \text{ sec}$.

Table 5 concerns the time and space of the n. 4 convoys, in order to arrive synchronously, in axis of the n. 2 principal diameters of Colosseum, as in Figure 17, at time $^{AXES}t_{MAX}= 25.280$ secs.

The summit of the Metro B tunnel touches the pavement of the place; and a pedestrian stopped over the tunnel feels clearly the vibrations for all convoys, then for charged and discharged convoys.

The wagon dead load is 358.88 kN, and the maximum passengers load is 170.10 kN.

For monuments so important it is normal to analyze the vibrations produced by Metro B and C, and to try their reductions [16÷21, 23÷30, 33, 34].

Table 5 – Synchronous paths of the four rails.

| | Time | | |
|---------------------------------|-----------|----------|-----------|
| | Start | On axes | Arrive |
| From Colosseum to Circo Massimo | T=8.250 | T=25.280 | T=44.585 |
| | s=0. | s=109.51 | s=496.092 |
| From Circo Massimo to Colosseum | T=0.065 | T=25.280 | T=35.065 |
| | s=480.949 | s=109.51 | s=0. |
| From Colosseum to Amba Aradam | T=8.250 | T=25.280 | T=44.66 |
| | s=0. | s=108.52 | s=496.11 |
| From Amba Aradam to Colosseum | T=0.0 | T=25.280 | T=35. |
| | s=481.109 | s=108.52 | s=0. |

7.1. Ground vibrations

Table 6. Peak accelerations on the ground, felt by pedestrians.

| Dx | A_H | A_V | A_{TOT} | | A_H | A_V | A_{TOT} | | Sc | | Section |
|-----|----------------------------------|-------|-----------|--|--------------------------------|-------|-----------|--|-------|--|---------|
| 0. | 13.03 | 7.91 | 33.57 | | 3.38 | 4.53 | 12.21 | | 36.37 | | Station |
| 12 | 21.90 | 34.78 | 66.49 | | 4.01 | 14.92 | 15.17 | | 22.82 | | |
| 24 | 22.77 | 36.13 | 65.24 | | 3.32 | 2.56 | 4.57 | | 7.00 | | |
| 100 | 40.42 | 60.27 | 61.17 | | 1.71 | 1.32 | 2.15 | | 3.51 | | Valad. |
| 192 | 47.23 | 65.41 | 71.74 | | 0.29 | 0.25 | 0.37 | | 0.52 | | Const. |
| 240 | 38.58 | 81.52 | 84.90 | | 0.19 | 0.13 | 0.20 | | 0.24 | | MAX |
| m | Metro B+C [mm/sec ²] | | | | Metro C [mm/sec ²] | | | | % | | |

Table 7. Peak velocities on the ground, felt by pedestrians.

| Dx | V_H | V_V | V_{TOT} | | V_H | V_V | V_{TOT} | | Sc | | Section |
|----|-------|-------|-----------|--|-------|-------|-----------|--|----|--|---------|
| 0. | .220 | .292 | .869 | | .057 | .175 | .404 | | 46 | | Station |
| 12 | .356 | .269 | 1.353 | | .089 | .157 | .337 | | 25 | | |

| | | | | | | | | |
|-----|--------------------|------|-------|------------------|------|------|----|--------|
| 24 | .393 | .262 | 1.407 | .076 | .134 | .204 | 14 | MAX |
| 100 | .335 | .528 | .546 | .068 | .053 | .089 | 16 | Valad. |
| 192 | .347 | .494 | .535 | .023 | .008 | .023 | 4 | Const. |
| 240 | .270 | .527 | .543 | .016 | .006 | .016 | 3 | |
| m | Metro B+C [mm/sec] | | | Metro C [mm/sec] | | | % | |

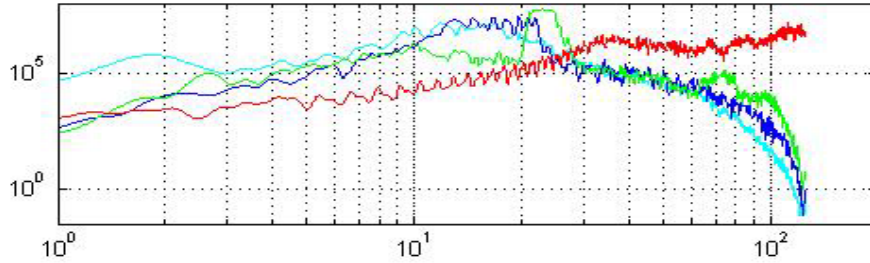


Figure 18. FFT of A_{TOT} felt by pedestrians, due to Metro (B+C). Station cyan, Valadier blue, Constantine green, Max red.

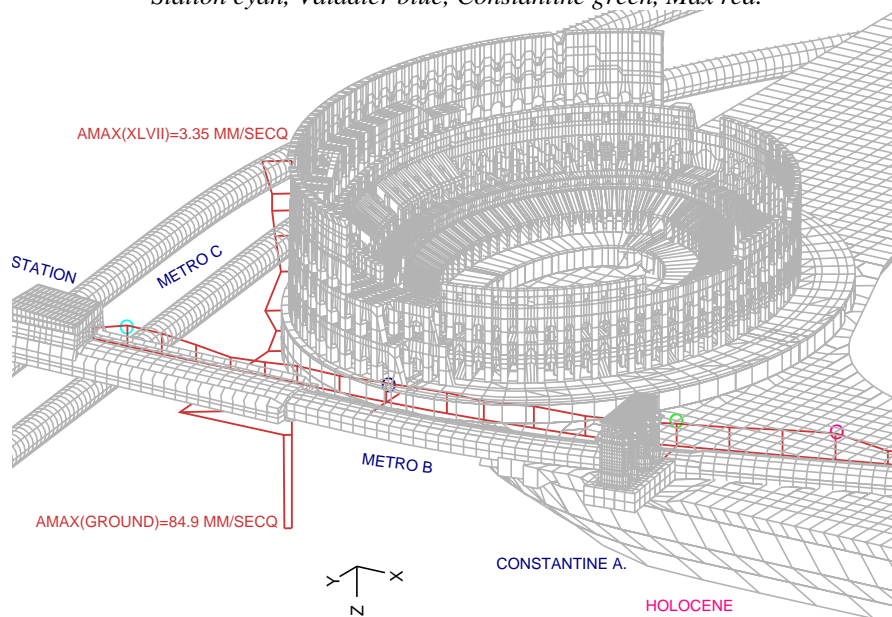


Figure 19. Peak of A_{TOT} on: a) RA XLVII, b) axis of Metro B, felt by pedestrians. Station cyan, Valadier blue, Constantine green, Max red.

About the vibrations on the ground, in axis with Metro B, as in Figure 19, when the two trains arrive both in axis with greater ellipse

diameter, at distance D_x from the step of the station to the end of Constantine arch:

a) the Table 6 and 7 show the maximum velocities and accelerations, in horizontal and vertical directions, with

$$a_H = [(a_x)^2 + (a_y)^2]^{1/2}; \quad a_{TOT} = [(a_x)^2 + (a_y)^2 + (a_z)^2]^{1/2}; \quad a_v = a_z; \quad (2)$$

and analogous equations for velocity components;

b) the last numerical column of Table 6 shows the percentage increasing of Metro C accelerations with respect Metro B vibrations, which is less of 3% in proximity of the monuments.

c) the values A_{TOT} are shown in Figure 17, they arrive to a maximum value around 0.01 g, with fundamental frequencies in the range of 5÷30 Hz, as in Figure 21;

d) the Figure 19 shows the maximum radial accelerations on the RA XLVII, and on the ground over the tunnel of Metro B.

The lower limit of vibrations perceptible to people is set by observation and experiment at approximately 0.0017g or 1 cm/sec (from National Information Service for Earthquake Engineering, University of California, Berkeley, "*The Nature of Ground Motion and its Effect on Buildings*", Christopher Arnold, A.I.A., 1982).

Whole-body vibrations in the range of 3-10 Hz are particularly critical because large body organs within the rib cage and abdomen resonate within this frequency range and it is within this general range that the inherent vibration isolation capability of the body is least effective (Grether, W. F., "*Vibration and Human Performance*," *Human Factors*, Vol.13, No. 3, 1971, pp. 203-216).

Man is sensitive to mechanical oscillations ranging in frequency from well below 1 Hz up to at least 100 kHz. Guignard, J. C., *Journal of Sound and Vibration*, Volume 15, Issue 1, 03/1971.

The maximum accelerations overcome this threshold of human perceptibility; instead the maximum velocities are near the limit of perceptibility for pedestrians.

The analyses should be deepened for different convoys passages, besides the proposed four convoys simultaneously centred on the two diameters; however, in order not to feel any vibration by pedestrians, from the analysis the reduction factor is requested $\chi \cong 85/17=5$.

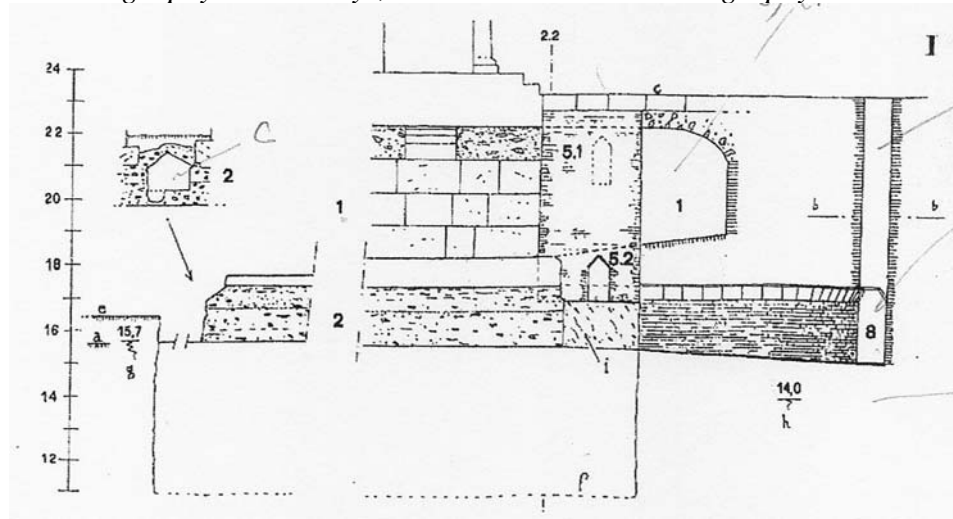
If we consider a single point centred on the axis of Metro B, the simultaneous passage of two convoys is a rare event, instead for one convoy alone the interval time is around few minutes; so we could be satisfied of the reduction factor requested $\chi \cong 2.5$, for a single convoy.



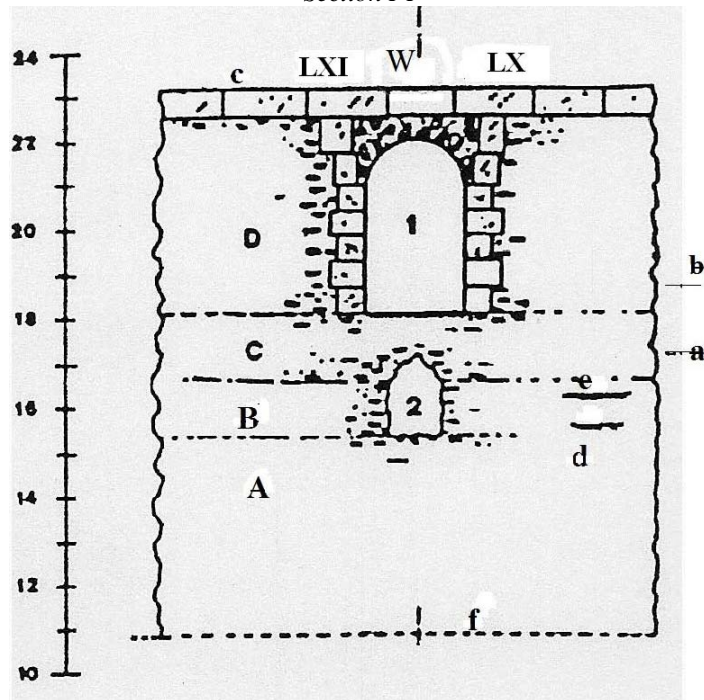
Figure 20. Plan of eastern cryptoporticus: a) red $Z=16.51$ m, b) green $Z=17.59$ m, c) blue wall, d) orange hypogeum $Z=16.20\div 16.80$ m.

8. Future developments

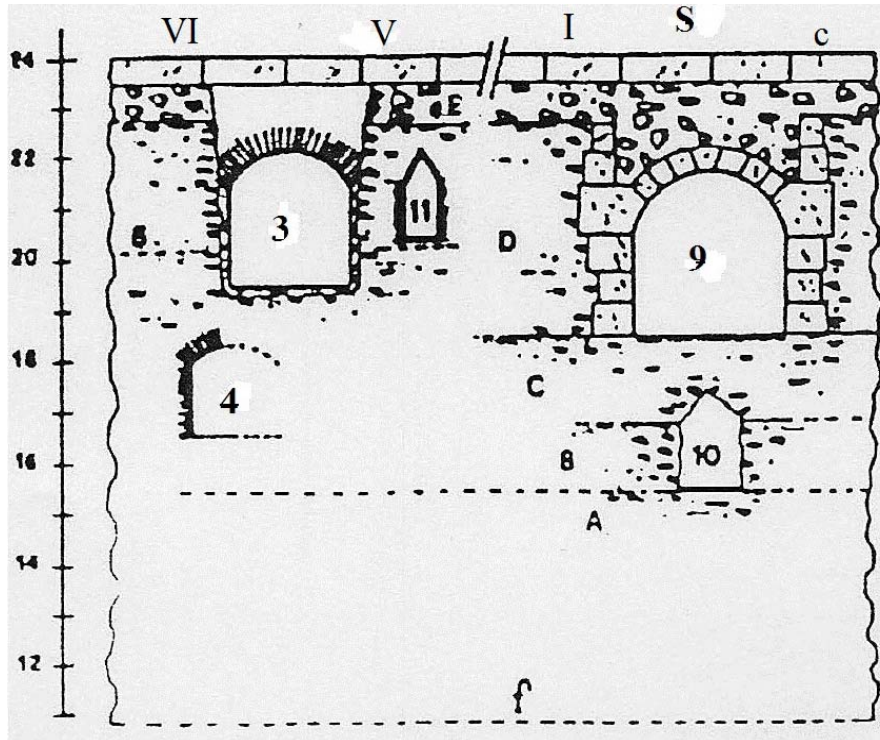
8.1 New geophysical surveys, electric and seismic tomography.



Section I-I



Section II-II.



Section III-III

Figure 21. 1) West cryptoporticus 2.34 x 4.12 m Z=17.59 m;
 2) culvert 1.25 x 1.70 m; 3) Commodus passageway 2.52 x 2.75 Z=19.50 m;
 4) unidentified opening; 9) S cryptoporticus 2.95 x 3.15 Z=18.30 m Z=17.59 m,
 10) S culvert 1.30 x 1.90 m Z=15.40 a) ante Neronian GL,
 b) Neronian post 64 a.D. GL, c) present square GL Z=23.22 m, d) Flavian GL,
 e) hypogea L. Z=16.20÷16.80 m, f) foundation mat bottom Z=10.22 m;
 g) A÷D concrete layers, h) GWL Z=16.00.

The good quality of numerical analyses depends on the knowledge of geometries and physical parameters of the archaeological structures and sub-soil. In this particular case the physical parameters necessary for the model are about elasticity, density and geometry. Such parameters may be obtained by integrated interpretation of data inferred by direct methods, as wells and indirect methods such as geophysical ones.

In the particular case of the Colosseum, the integration of direct and indirect surveys is of paramount importance given the complexity of the subsurface setting and lack of knowledge of the foundation.

On the basis of surveys carried out at the site in the late nineties and on the basis of new instrumentation and processing techniques now available, we are able to design and perform detailed investigations that can bridge the gap of knowledge still in place and provide adequate information on parameters needed for the numerical models and archaeological studies.

In detail, we believe that the evaluation of elastic modulus and geometry of the strata can be carried out from high-resolution multi-fold seismic reflection method with P- and S waves sources. This type of investigation can be used on both on the foundation and on the area outside the monument for characterizing the foundations and subsoil.

Two and three dimensional electrical investigations can be applied on the foundation and outside the monument to define the geometries and lithologies of the sediments. These surveys will provide useful information on the presence of sediment silt-clay layer and location of the aquifer.

On the foundations multi-fold GPR surveys can perform with the aim to define the geometries of the foundations. The investigations of the '90s showed that this kind of investigation is able to increase the penetration depth and detect the base of the foundations.

Down-hole surveys of P and S waves can be carried out in the holes drilled in the '90s and if it is necessary new ones can be planned for the stratigraphic reconstruction of areas not yet explored and for defining the P and S profiles.

This activity could be part of a research project because of its complexity and not complete standardization of acquisition and data inversion.

These tests will be performed inside cryptoportici as in Figures 20 and 21, with the purpose to know better the foundation mat bottom in the neighbourhood of the same cryptoportici.

8.2 Dynamic tests inside tunnels of Metro B and C

These tests could be suitable inside a ray of 400m from Colosseum, in order to better define the mechanical characteristics of soil.

8.3 Dynamic tests inside and around Constantine arch

These tests could be suitable in various points of the monument at different floors, and on the place around the monument, in order to define completely the mechanical characteristics of monument and soil in archaeological area.

9. Conclusions

The geometry knowledge for the underground is not accurate, as regards the lower surface of foundations and the soil layers.

Then for soil, the scatter between dynamic tests and analytical results is larger than for elevation.

The next improvements will be performed:

- 1) conclusive experimental tests, oriented to soil-monument interaction, on Colosseum, the ground and all running tunnels, Metro B and C too, Commodo passage, ancient sewers, Constantine arch.
- 2) new geophysical surveys to define the thickness of foundation with the instrumentation available today;

10. Acknowledgements

We thank the “*Soprintendenza Speciale per i Beni Archeologici di Roma*” having allowed the execution of the geophysical investigations and Eng. Roberto Scauzilli for the help in the acquisition and data processing.

References

[1] Nakamura, Y., A Method for Dynamic Characteristics Estimation of Subsurface using Microtremor on the Ground Surface, Quarterly Report of RTRI, Vol.30, No.1, pp.25-33, 1989.

[2] G. Schingo, R. Rea, Il progetto di restauro del Colosseo. I sotterranei: assetto idraulico e interventi strutturali fra XIX e XX secolo,

Bollettino di Archeologia, Min. BB.CC.AA. 23-24 Settembre-Dicembre 1993.

[3] Funicello, R., Lombardi, L., Marra, F., Parotto, M. (1995) "Seismic damage and geological heterogeneity in Rome's Colosseum area: are they related?", *Annali di Geofisica*, 927-937.

[4] Bozzano, F., Funicello, R., Marra, F., Rovelli, A., Valentini, G. (1995) "Il sottosuolo dell'area dell'anfiteatro Flavio in Roma", 405÷422.

[5] Moczo, P., Rovelli, A., Labák, P., Malagnini, L., (1995) Seismic response of the geologic structure underlying the Roman Colosseum and a 2-D resonance of a sediment valley, *Annali di geofisica*, pp. 939÷956.

[6] R. Rea, *Anfiteatro Flavio*, Ministero BB.CC.AA., 1996, n.37.

[7] Sugiura T., Tashiro M., Uematsu Y. and Yoshizawa M.: Mechanical Stability of a High-Tc Superconducting Levitation System: *IEEE Trans. Appl. Supercond* 7(2), 1997 pp 386-389.

[8] Nakamura, Y. (1996). "Seismic response of roman Colosseum and its foundation by using micro-tremor measurements", The 10th Japan Earthquake Engineering Symposium, pp. 2625-2630, 1998.

[9] D. Mertens, R. Rea, G. Schingo, H.J. Beste, C. Piraino, (1998) Il Colosseo. Lo studio degli ipogei, *Bollettino dell'Istituto Archeologico Germanico Sezione romana*, Vol. 105, 1998.

[10] Clemente P, Rinaldis D. Protection of a monumental building against traffic-induced vibrations. *Soil Dynamics and Engineering* 1998; 17:289–296.

[11] Futamura M., Maeda T., Konishi H.: Damping Characteristics of a Magnet Oscillating above a YBCO Superconductor: *Jpn. J. Appl. Phys.* 37: 1998 pp 3961-3964.

[12] Hull J.R. and Cansiz A.: Vertical and lateral forces between a permanent magnet and a high-temperature superconductor *J. Appl. Phys.* 86(11): 1999 pp 6396-6404

[13] Nakamura, Y., Gurler, E.D., Saita, J., Rovelli, A., Donati, S., (2000) Vulnerability investigation of roman Collisseum using micro-tremor, *12WCEE2000*, paper 2660.

[14] R. Jappelli, R. Rea, G. Schingo, Artificial radial accesses in the foundation of the Colosseum, Congresso *AITES-Ita World Tunnel Congress*, 2001.

[15] G. Schingo, Gli sterri del 1939 per la costruzione della Metropolitana. Dati archeologici inediti dalla valle del Colosseo, *Bollettino della Commissione Archeologica Comunale di Roma*, 2001.

[16] D'Ovidio G., Lanzara G., Crisi F.: *Italian patent 0001385998*, 2007.

[17] Crisi, F., Dell'Isola, F., D'Ovidio, G., Valente, G., "Vibrations analysis of Colosseo due to trains' transit", 2.nd EMAS, Hammamet, Tunisia, May 2008.

[18] Crisi, F., D'Ovidio, G., Valente, G., "Metodologia di analisi delle vibrazioni strutturali dovute al traffico ferroviario: caso di studio dell'area archeologica del Colosseo", March 2009, Ingegneria Ferroviaria.

[19] Crisi, F., D'Ovidio, G., Valente, G., "Vibration Analysis on Constantine Arch monument due to the metro train" Proceedings of 14th International Conference. Transport Means. 2010.

[20] Crisi, F., D'Ovidio, G., Valente, G., "Flexible Rail Beams Modelling for Soil-Structure Interaction Dynamic Analysis" Proceedings of 14th International Conference. Transport Means. 2010.

[21] Caserta A., Cerone M., Crisi F., Delladio A., D'Ovidio G., Govoni A., Marra F., Nakamura Y., Rovelli A. and Valente G., "Dynamic interaction of soil and structure by rail traffic", Proceedings of Workshop DISS_10, L'Aquila, 19 March 2010.

[22] Nakamura, Y. (2011), "The H/V Technique and Example of its Application for L'Aquila and Rome Area", Proceedings of the workshop DISS_10, L'Aquila, 19 March 2010.

[23] Bruner, M., Crisi, F., D'Ovidio, G., Valente, G., "Soil vibration analysis due to the rail bogie motion" *Proceedings of 14th International Conference. Transport Means. 2010.*

[24] F. Crisi, G. D'Ovidio, G. Valente "Vibrations analysis in the archaeological area of Rome by rail traffic, the 4th VI-grade User's Conference Udine, October 2011.

[25] D'Ovidio G., Crisi F., Lanzara G.: Design and Optimization of UAQ4 Experimental Maglev Module" *Journal of MSF in Applied Electromagnetic Engineering* Vol. 670, 2011 pp 42-47

[26] Francesco Crisi, Gino D'Ovidio, Gianfranco Valente, “*Weak vibration of Colosseum area due to the trains running*”, Proceedings of 2.nd International Workshop DISS_12, L'Aquila, 29 March 2012.

[27] F.M.D. Accattatis, M. Bruner, F. Crisi, G. D'Ovidio, G. Valente, P. Vitali, “*Railway vehicle dynamics and the soil vibration analysis*”, Proceedings of 2.nd International Workshop DISS_12, L'Aquila, 29 March 2012.

[28] F.Crisi, G. D'Ovidio, G. Valente, “*Guideway stress comparison due to traffic of wheel-on-rail and maglev trains*”, Proceedings of 2.nd International Workshop DISS_12, L'Aquila, 29 March 2012
DISS_Edition, ISBN 978-88-940114-0-1.

[29] F. Crisi, D'Ovidio, G. Valente “Dynamic analysis of experimental HTS maglev module based for mass transportation system”, International Conference on Superconductivity and Magnetism 2012, ICSM, Istanbul.

[30] G. D'Ovidio, G. Valente, “Weak vibrations of the Colosseum due to existing and forthcoming underground lines”, 17th International Conference Transport Means 2013, Kaunas University of Technology 24-25 October 2013, Lituania.

[31] Orlando L., Bernabini M. (2002), “La geofisica nella caratterizzazione delle fondazioni dell'anfiteatro Flavio”, 21° Convegno nazionale, Gruppo nazionale di geofisica della terra solida.

[32] Akinci A., Olsen K., B., Rovelli A., Marra F., Malagnini L. (2002) “Sumulazioni 3D e produzione di scenari di scuotimento nella città di Roma”, 21° Convegno nazionale, Gruppo nazionale di geofisica della terra solida.

[33] *VI-Rail 13.0 Documentation*, pages 222÷231, 2010.

[34] ORE B176 RP1, Vol. 1: *Preliminary studies and specifications* – Vol. 2: Specification for a bogie with improved curving characteristics – Vol. 3: Specifications for a bogie with improved curving characteristics for body tilt, 1989.

[35] Fisher E., Gorge M., Annan P. “Acquisition and processing of wide-aperture round penetrative radar data”, *Geophysics*, vol. 57, n.3, pp. 495-504, 1992.

[36] S. Malagodi, L. Orlando, S. Piro, “Improvement of signal to noise ratio of ground penetrating radar using CMP acquisition and

data processing”, *Proceedings of Fifth International Conference on Ground Penetrating Radar, Ontario, Canada*, pp. 689-699, 1994.

[37] Orlando I. (2009). Multi-fold GPR data to study the foundation of the Flavi Amphitheatre. Proceeding of *IWAGPR, Granada , Spain*, 155-158.

[38] M. Pipan, I. Finetti, F. Ferigo, “Multi-fold GPR techniques with applications to High resolution studies: two case histories”, *European Journal of Environmental and Engineering Geophysics*, 1, pp 83-103, 1996.

[39] M. Pipan, L. Baradello, E. Forte, A. Prizzon , I. Finetti, “2D and 3D processing and interpretation of multi-fold ground penetrating radar data: a case history from an archaeological site”, *Journal of Applied Geophysics*, vol. 41, pp. 271-292., 1999.

[40] B.A. Berard and J.M. Maillol, “Multi-offset ground penetrating radar data for improved imaging in areas of lateral complexity - Application at a Native American site”, *Journal of Applied Geophysics*, vol. 62, pp. 167-177, 2007.

[41] L. Gardner, “An area plan of mapping subsurface structure by refraction shooting,” *Geophysics*, vol. 4, pp. 247–250, 1939.

[42] F. S. Grant and G. F. West, *Interpretation Theory in Applied Geophysics*, McGraw-Hill, New York, NY, USA, 1965.

[43] M. Bernabini, “Alcune considerazioni sui rilievi sismici a piccole profondità,” *Bollettino di Geofisica Teorica e Applicata*, vol. 26, pp. 106–118, 1965.

SHM experiences of monuments in different structural, use and environmental conditions

Claudio Modena¹

Abstract

In the last decades the need for an effective seismic protection and vulnerability reduction of strategic structures and particularly the architectural heritage determined a growing interest in Structural Health Monitoring (SHM) as a measure of passive mitigation of earthquake effects. The object of monitoring is to identify, locate and classify type and severity of damages induced by external actions or degradation phenomena and to assess their effects on the structural performance. In this way it is possible to take appropriate measures to reduce the danger of collapse and, when necessary, perform strengthening interventions to improve the structural and seismic capacity. Motivated by the above reasons, the paper provide a contribution to the application of integrated methodologies and techniques, based on SHM, for the assessment and protection of Cultural Heritage (CH) buildings and monuments. Selected case studies, equipped with distributed sensors and acquisition systems, allowed the definition and successive validation of SHM as a knowledge-based assessment tool, implemented to evaluate intervention needs, following an incremental approach during their execution, and to control the damage states of buildings in a post-seismic scenario. In order to maximize the benefits of SHM and optimize the entire process, dedicated software for static monitoring and automated algorithms for modal parameters identification have been developed, able to provide almost real time information on the health state of the monitored structure. Finally integrated procedures based on robust statistical and numerical models have been implemented to interpret and exploit SHM outputs to assess the structural conditions of the investigated CH buildings.

¹ Università degli Studi di Padova, Dipartimento di Ingegneria Civile, Edile e Ambientale, Italy

1. Introduction

For several years the Department of Civil, Architecture and Environmental Engineering of the University of Padova, in line with the needs for the conservation of monuments, has been employing SHM systems on representative historical constructions and monuments. The final aim is the assessment of their structural behaviour, especially with reference to the seismic performance, integrating monitoring techniques, inspections and structural analyses.

In this framework, designated case studies cover different types of problems concerning specific objectives and applied methodologies. The different problems identified are a consequence of the meaningful differences shown by case studies with regards to construction typologies, seismicity of the sites, quality of the construction materials and techniques, damage conditions, effects of past or recent earthquakes and effectiveness of possible performed strengthening interventions. CH buildings, currently equipped with SHM systems, are listed hereafter:

- Roman Arena of Verona (Verona, Italy)
- Scrovegni Chapel (Padova, Italy)
- Cansignorio stone tomb (Verona, Italy)
- S. Sofia church (Padova, Italy)
- Roman bridge of S. Lorenzo (Padova, Italy)
- Spanish Fortress (L'Aquila, Italy)
- S. Marco church (L'Aquila, Italy)
- S. Biagio / S. Giuseppe churches (L'Aquila, Italy)
- Civic tower (L'Aquila, Italy)
- S. Agostino church (L'Aquila, Italy)
- S. Silvestro church (L'Aquila, Italy)

Thanks to the implementation of a large number of monitoring systems to CH structures it was possible to define a methodology of application according to the final aim of monitoring within each selected case history. Following this approach monitoring represents an essential step in the assessment and protection processes of historical constructions, regarding, in particular, the following problems:

- a) Increasing the knowledge on the structural behavior using SHM to assess strengthening needs and avoid the execution of unnecessary interventions;
- b) Applying an incremental approach to the execution of strengthening interventions using SHM before, during and after the implementation, validating eventually their effectiveness;
- c) Post-earthquake controls on severely damaged buildings using SHM to control the evolution of damage and verify the effectiveness of provisional strengthening measures.

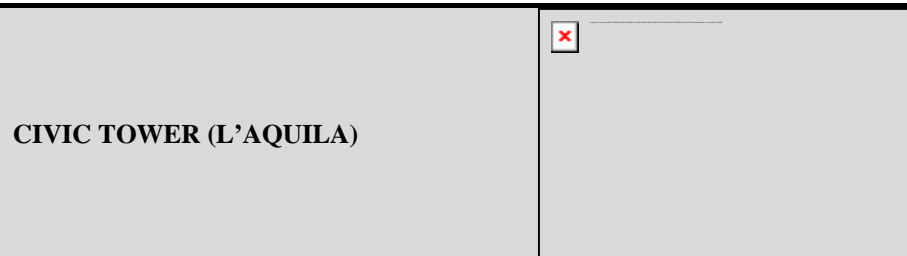
In the following section monitored CH buildings are briefly presented, highlighting aims and problems that SHM tries to face and solve.

| | |
|--|--|
| ARENA OF VERONA |  |
| INSTALLATION PERIOD | December 2011 |
| SHM TYPOLOGY | Static/Dynamic system |
| PURPOSE OF MONITORING | Alternative to the execution of interventions |
| SCROVEGNI CHAPEL |  |
| INSTALLATION PERIOD | August 2013 |
| SHM TYPOLOGY | Static/Dynamic system |
| PURPOSE OF MONITORING | Protection of immovable CH goods (Giotto's frescos) |
| CANSIGNORIO STONE TOMB (VERONA) |  |
| INSTALLATION PERIOD | December 2006 |
| SHM TYPOLOGY | Static/Dynamic system |

PURPOSE OF MONITORING Structural controls before, during and after interventions



| | |
|-----------------------|--|
| INSTALLATION PERIOD | 1999 (1st installation); 2008 (1st upgrade); 2010 (2nd upgrade) |
| SHM TYPOLOGY | Static/Dynamic system |
| PURPOSE OF MONITORING | Structural controls before, during and after interventions |



| | |
|-----------------------|--------------------------|
| INSTALLATION PERIOD | July 2010 |
| SHM TYPOLOGY | Static/Dynamic system |
| PURPOSE OF MONITORING | Post-earthquake controls |



| | |
|-----------------------|--------------------------|
| INSTALLATION PERIOD | December 2009 |
| SHM TYPOLOGY | Dynamic system |
| PURPOSE OF MONITORING | Post-earthquake controls |

| | |
|-----------------------------------|--|
| S. MARCO CHURCH (L'AQUILA) |  |
|-----------------------------------|--|

| | |
|-----------------------|--------------------------|
| INSTALLATION PERIOD | August 2009 |
| SHM TYPOLOGY | Static/Dynamic system |
| PURPOSE OF MONITORING | Post-earthquake controls |

| | |
|--|--|
| S. BIAGIO & S. GIUSEPPE CHURCHES (L'AQUILA) |  |
|--|--|

| | |
|-----------------------|--------------------------|
| INSTALLATION PERIOD | December 2010 |
| SHM TYPOLOGY | Static/Dynamic system |
| PURPOSE OF MONITORING | Post-earthquake controls |

| | |
|--------------------------------------|---|
| S. AGOSTINO CHURCH (L'AQUILA) |  |
|--------------------------------------|---|

| | |
|-----------------------|--------------------------|
| INSTALLATION PERIOD | July 2010 |
| SHM TYPOLOGY | Static/Dynamic system |
| PURPOSE OF MONITORING | Post-earthquake controls |

| | |
|---------------------------------------|--|
| S. SILVESTRO CHURCH (L'AQUILA) |  |
|---------------------------------------|--|

INSTALLATION PERIOD July 2010
 SHM TYPOLOGY Static/Dynamic system
 PURPOSE OF MONITORING Post-earthquake controls

2. General knowledge-based methodology

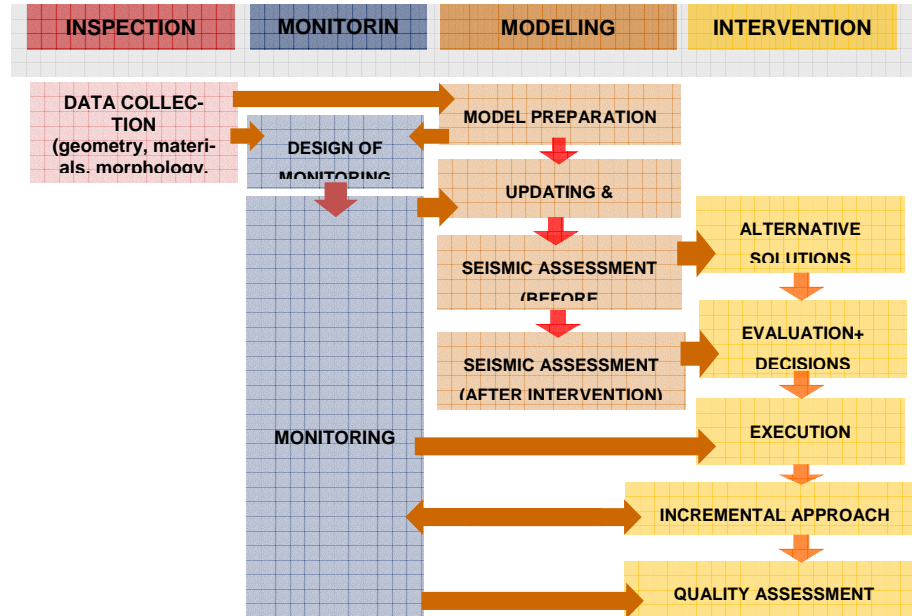


Figure 1 - General knowledge-based strategy for the study and assessment of CH buildings (WP9, NIKER Project 2012)

Knowledge-based methodologies for the study of heritage buildings are based on the exploitation and integration of different approaches including historical research, inspections, monitoring and structural analysis. Monitoring, in particular, is carried out across the entire process and may be utilized not only for diagnosis but also as an auxiliary tool during the intervention and even during the later post-intervention period for control and preventive maintenance purposes. In the complex knowledge process of historic buildings four different activities are developed in a parallel and interconnected way. The proposed general strategy, as represented in Figure 1, includes:

- (i) Inspection

- (ii) Monitoring
- (iii) Modeling (or structural analysis)
- (iv) Intervention

Looking more in detail at the role of monitoring within the previous defined general strategy for the study and assessment of historic buildings, it is possible to identify different phases according to the nature of activities carried out on the investigated building. In each phase monitoring plays a fundamental and active role.

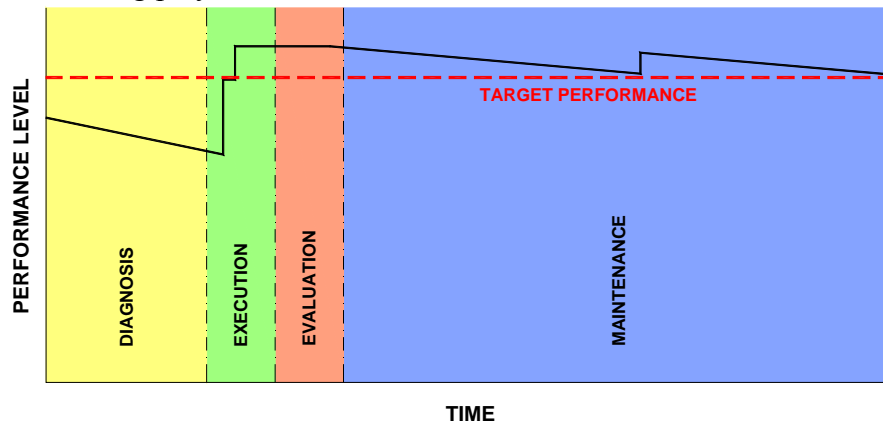


Figure 2 - Monitoring phases across the knowledge-based process for the assessment and protection of CH buildings (WP9, NIKER Project 2012)

The different phases considered are:

- (i) Investigation phase
- (ii) Intervention phase
- (iii) Evaluation phase
- (iv) Maintenance phase

In spite of the distinction between the different phases, they are intimately connected and any general action on a historical structure should plan all of them according to unified approaches and criteria. Figure 2 schematizes the subsequent phases in the process involving the study, intervention and later control of a cultural heritage structure.

3. Application of SHM to selected case studies

This paragraph presents and analyses some selected case studies, showing aims and needs of monitoring and presenting preliminary inspections and the successive design and installation phases of the monitoring systems.

Case studies selection was performed according to the following aspects: (i) choice of a sufficiently wide range of CH buildings, characterized by different typologies, structural features, seismic vulnerabilities; (ii) seismicity levels of the sites; (iii) aims of monitoring to face different problems, following the methodology previously described:

- a) SHM as an alternative to strengthening: Arena of Verona and Scrovegni Chapel (Padova)
- b) SHM for vibration controls: Roman bridge of S. Lorenzo (Padova)
- c) SHM applied before, during and after interventions: Cansignorio stone tomb (Verona)
- d) SHM for post-earthquake controls: Civic tower and Spanish Fortress (L'Aquila).

3.1. SHM as an alternative to strengthening: Arena of Verona



Figure 3 - The Roman Arena of Verona

3.1.1 Geometric and structural features

- Ellipse with four focuses (152.43m x 123.23m)
- Two annular galleries and 73 radial masonry walls
- Inner masonry: multi-leaf with inner core
- ‘Wing - Ala’: freestanding structure remaining four arches of the outer ring, h=30.75 m.

- Outer leaf of the perimeter stone wall
- The ‘wing’: most vulnerable structural element

| MO DE | AVT - Oct 2011 | | | | FVT - 1996 | | AVT vs. FVT | |
|----------|----------------|----------|-----------|------|------------|-----------|-------------------|--------|
| | FDD | EFDD | | MAC | | | Average error [%] | |
| | f [Hz] | f [Hz] | ξ [%] | | f [Hz] | ξ [%] | f | ξ |
| 1 | 1,93 | 1,92 | 1,36 | 1 | 1,92 | 1,4 | 0 | 2,94 |
| 2 | 2,64 | 2,65 | 1,12 | 0,99 | 2,61 | 1,3 | 1,51 | 16,07 |
| 3 | 5,08 | 5,08 | 1,07 | 0,99 | 4,83 | 1,8 | 4,92 | 68,22 |
| 4 | 5,88 | 5,98 | 3,86 | 0,99 | 5,87 | 6,9 | 1,84 | 78,76 |
| 5 | 7,30 | 7,29 | 2,07 | 0,99 | 7,10 | 2,3 | 2,61 | 11,11 |
| 6 | 9,30 | 9,30 | 0,43 | 0,99 | 8,62 | 1,1 | 7,31 | 155,81 |
| 7 | 10,94 | 10,92 | 1,06 | 0,99 | 10,65 | 2,6 | 2,47 | 145,28 |



Figure 5 - Results of modal analysis.

Operational modal analysis

- Select optimal layout of dynamic system
- Identification of the dynamic behaviour of the ‘Wing’ and model updating
- Comparison of results using different OMA/EMA techniques
- Sampling frequency: 100 Hz; 131’072 points; record length: 21’51’’
- System identification: decimation; segment length 2048 points, 66.67% overlap; selected methods: FDD and EFDD

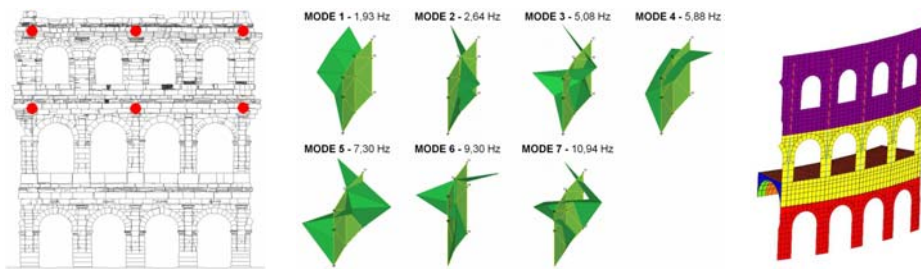


Figure 6 - Results of modal analysis and FE model creation

3.1.4 The monitoring system

Needs of monitoring

- Increase the knowledge on the structural behaviour using SHM to assess strengthening needs and avoid the execution of unnecessary interventions
- Control the structural response to different external actions, considering the relevant use/exploitation of the monument
- SHM in the framework of a complex maintenance program of the Arena to guarantee appropriate safety conditions
- Assessment and minimization of the seismic risk; Calibration of reference behavioural models
- Acquisition of vibration characteristics of the monument and control of the surveyed crack pattern under operational conditions and in case of exceptional events and concerts.

Static monitoring

- 20 displacement transducers
- 4 integrate sensors of temperature and relative humidity

Dynamic monitoring

- 16 Single-axis accelerometers

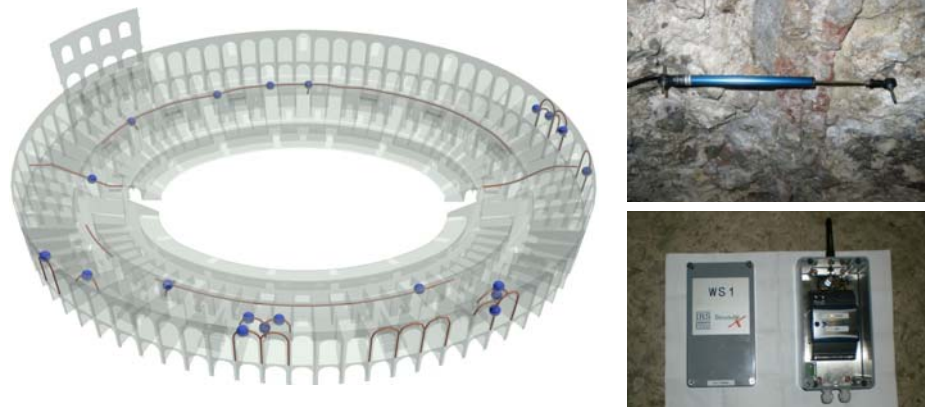


Figure 7 - Static monitoring system layout

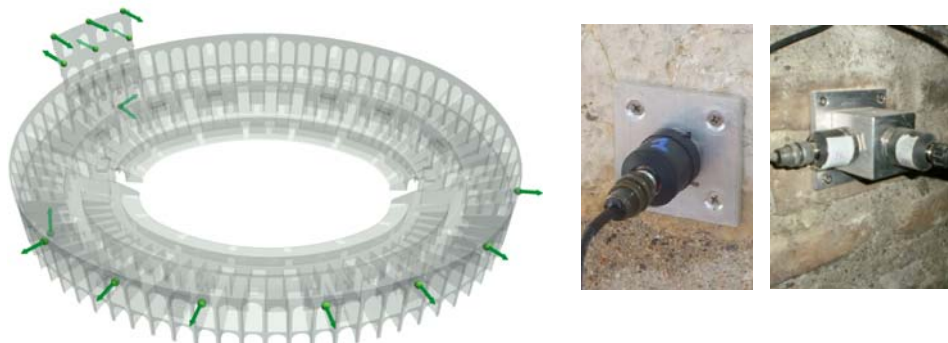


Figure 8 - Dynamic monitoring system layout

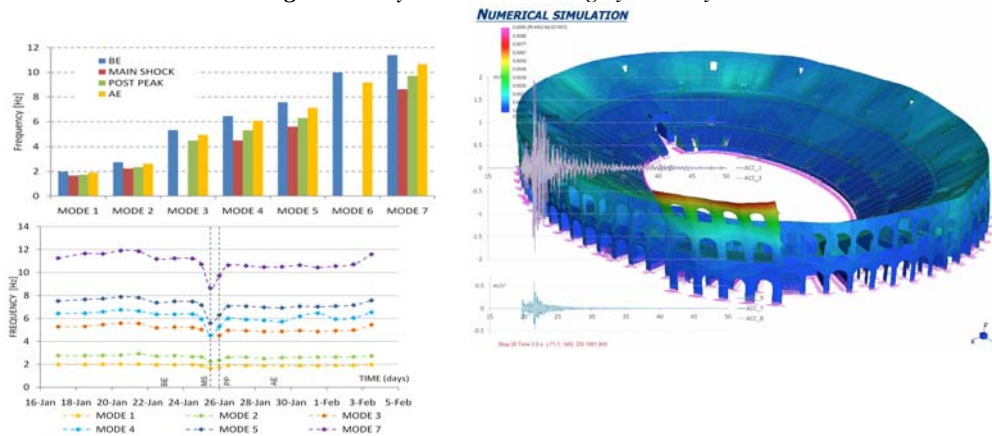


Figure 9 - Monitoring data analysis

3.1.5 Post-processing and data analysis

Model driven approach; exploit SHM and dynamic identification results to calibrate and validate reference numerical models:

- Implementation of modal matching procedures
- Model updating targets: material properties, geometry, morphology, connections, boundary conditions, soil-structure interaction, damage distribution, ect.
- Identification of morphology and materials
- Definition of initial values of elastic mechanical properties
- Iterative variation of mechanical properties/boundary conditions within a predefined range until reaching the final calibration

Seismic monitoring

- Analysis of ground motion records
- Evaluation of the PGA and analysis of the frequency content of the input
- Evaluation of the structural response
- Modal analysis and evaluation of the modal parameters change during and after the earthquake
- Numerical simulation of the earthquake

3.2. SHM to protect immovable CH goods: Scrovegni Chapel (Padova)



Figure 10 - The Scrovegni Chapel with the Giotto's frescos

3.2.1 Historical notes - past interventions:

The Scrovegni Chapel, dedicated to St. Mary of the Charity, frescoed between 1303 and 1305 by Giotto, is one of the most important masterpieces of Italy. The frescoes, which narrate events on the lives of the Virgin Mary and Christ, cover the entire walls.

XX c. Strengthening interventions:

- 1957 Strengthening interventions of the façade through the insertion of 3 horizontal ties;
- 1961-63 Substitution of the old steel ties;
- 1961-63 Substitution of the wooden trusses of the roof;
- 2006-08 important consolidation interventions

3.2.2 Preliminary inspections

- Crack pattern survey
- Dynamic test on steel ties
- Operational modal analysis on the frescoed barrel vault

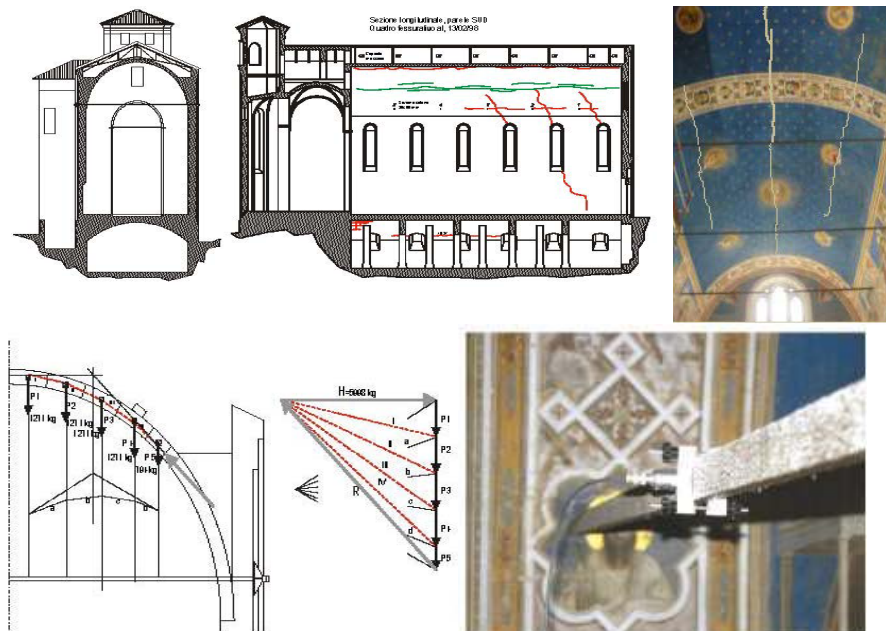


Figure 11 - Crack pattern survey and dynamic test on steel ties

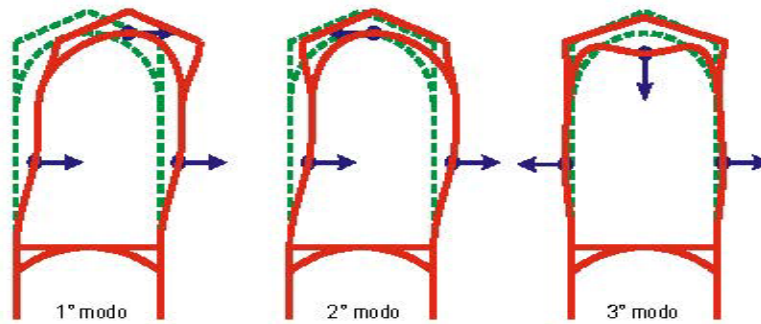


Figure 12 - Dynamic identification of the structural response

Static monitoring

- 8 displacement transducers
- 2 Inclinometers
- 2 integrated sensors of temperature and relative humidity

Dynamic system

- 8 Single-axis accelerometers
- 1 acquisition unit equipped with an internet router for data transmission

3.2.3 The monitoring system

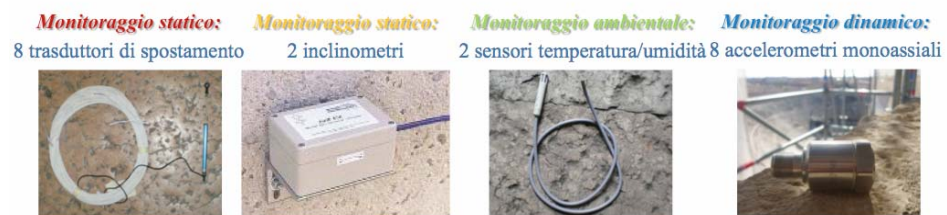
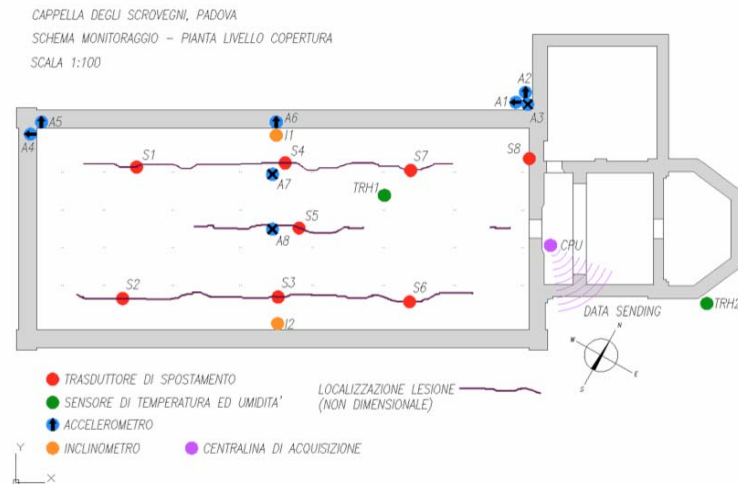


Figure 13 - Layout of the monitoring system

3.2.4 Post-processing and data analysis

- Creation of numerical and analytical models of the structure
- Structural analyses (wind and seismic verifications)
- Monitoring data analyses

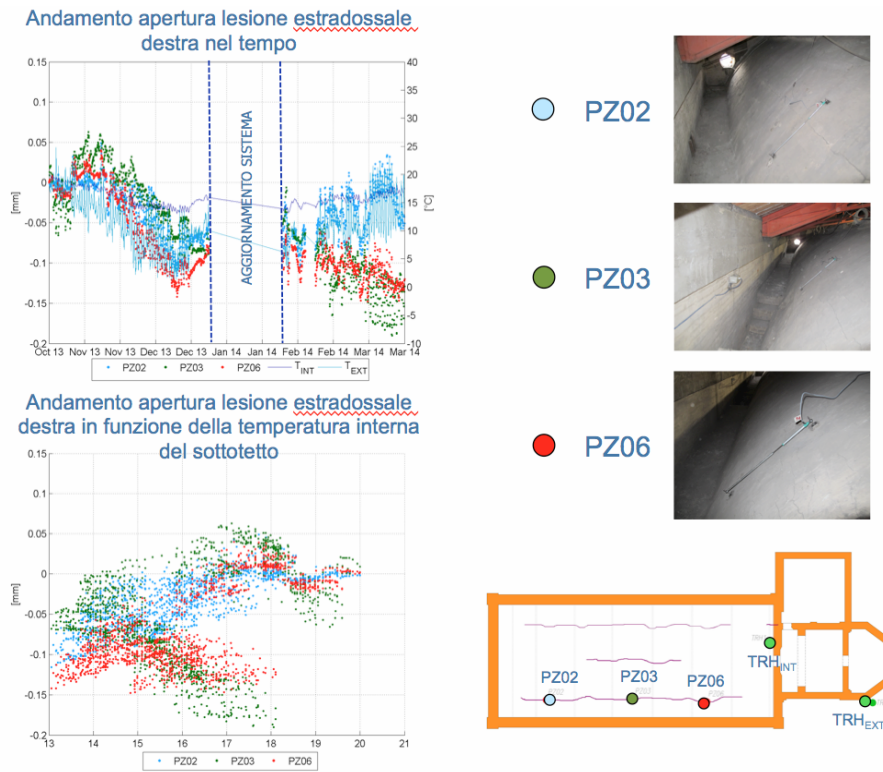


Figure 14 - Monitoring data analyses

3.3. SHM for vibration controls: Roman bridge of S. Lorenzo (Padova)

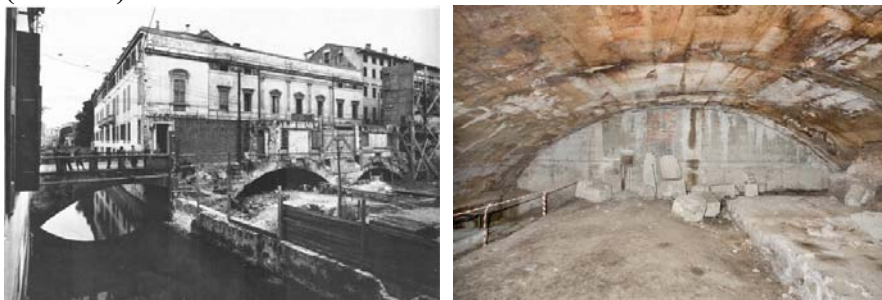


Figure 15 - S. Lorenzo bridge: historic picture and view of the arch intrados

3.3.1 Historical notes

- The Roman Bridge of S. Lorenzo is the best preserved and most famous Paduan bridge remaining from Roman times
- The bridge has been restored several times over centuries
- In 1938 an archaeological excavation was undertaken, in consequence of the laying of the foundations for the new wing of the University (the Bò)
- In 1959 the first arch of the bridge was partially buried as a result of the filling of the Canal

3.3.2 Geometric and material features:

- The bridge is about 53.30 metres (180 Roman feet) long, 44 metres without the access road, and 8.35 metres wide, while the roadway was 7.40 metres (about 25 Roman feet) wide
- The need to facilitate the passage of the boats help to explain the exceptional structure of the bridge, including the high, narrow piers and unusually flat arches.
- The bridge has three arches using blocks of trachite from the Euganean Hills and armille and limestone from Costozza

3.3.3 The monitoring system

Monitoring strategy

- Analysis of traffic-induced vibrations
- 10 day of continuous dynamic monitoring
- 18 single-axis accelerometers
- 1 basis (3 sensors in x,y,z directions) at the pile's basement
- 3 basis (3 sensors x,y,z) in the 1st span at different heights
- 1 basis (3 sensors x,y,z) in the 2nd and 3rd span at arch's top

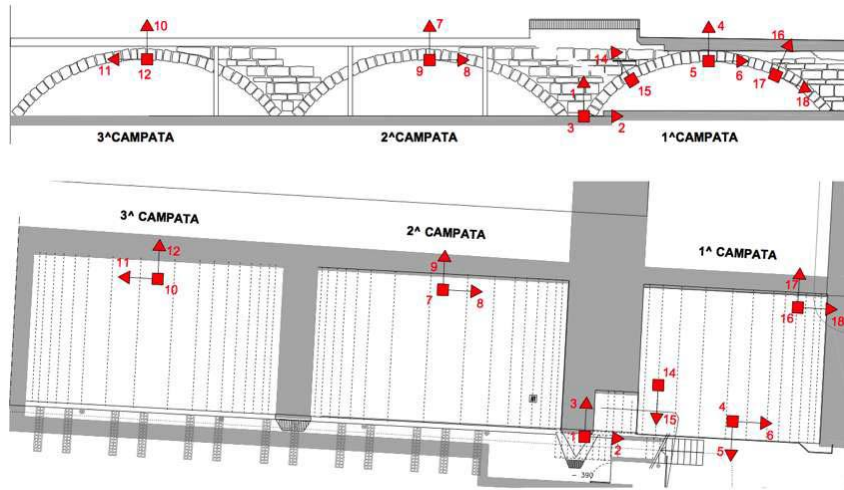


Figure 16 - Layout of the dynamic monitoring system

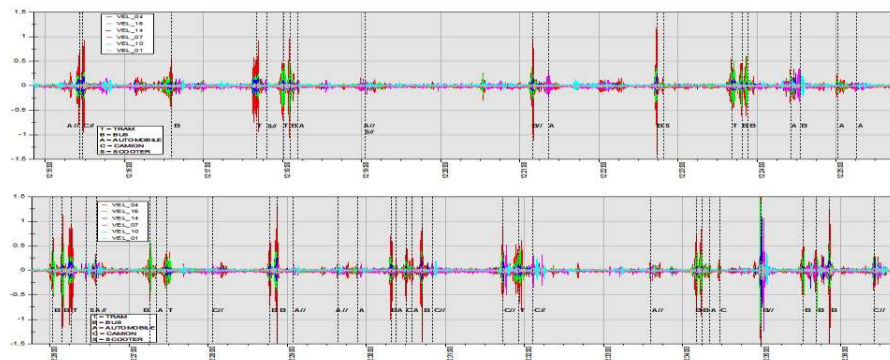


Figure 17 - Time history of velocities: vertical direction. Identification of the type of vehicles

3.3.4 Monitoring results

Visual monitoring

- Acceleration measurement - sampling frequency 100 Hz
- High-pass filtering of the signals - cutoff frequency 1 Hz
- Numerical integration of the signal to convert accelerations into velocities

- Successive High-pass filtering of the signals - cutoff frequency 1 Hz

Analysis of traffic-induced vibration

- Traffic-induced vibrations are generally not of high intensity:
- Bus passage causes in some traffic conditions, vibrations intensity above the threshold (maximum 3.43 mm/sec).
- Tram passage generally induces less vibrations amplitude (up to 1.41 mm/sec).

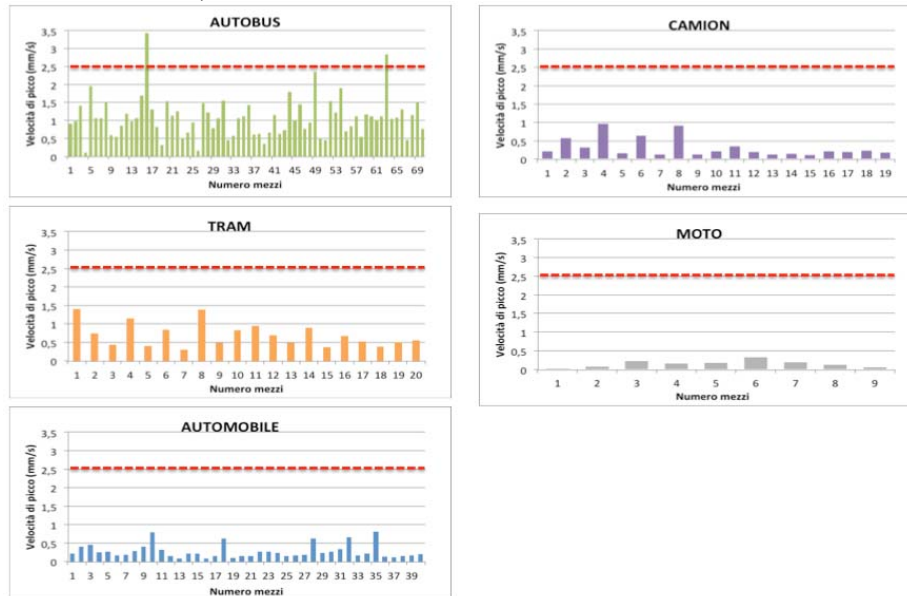


Figure 18 - Analysis of traffic-induced vibrations

Analysis of recorded velocities over the entire period (10 days)

- 3% of vehicles exceed the DIN 4150 - Threshold (2.5 mm/s)
- 12% of vehicles exceed the SN 640312 - Range (1.5 - 3.0 mm/s)

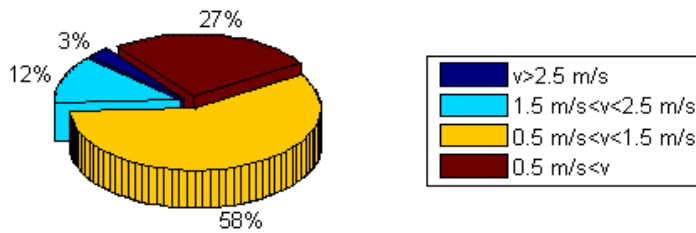


Figure 19 Analysis of vibrations and verifications in terms of recorded velocities over the entire monitoring period (10 days)

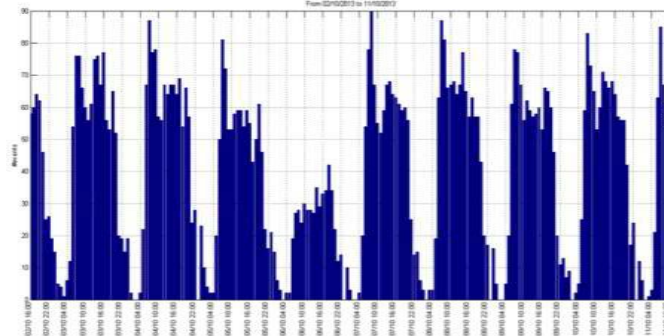


Figure 20 - Distribution of traffic intensity level during 10 days of continuous monitoring

3.4. SHM to validate the effectiveness of interventions: Cansignorio stone tomb (Verona)



Figure 21 - Cansignorio stone tomb in Verona

3.4.1 Geometric and material features:

- Placed in the monumental area of S. Maria Antica;
- Funerary monument of ‘Scaligeri’ family, in the Gothic style;

- Hexagonal plan, full of sculptures, spired tabernacles and decorations; equestrian sculpture on the top
- Soft limestone (gallina), red Verona marble, marble of Candoglia.

3.4.2 Historical notes - past interventions:

- 1374-1376: Construction following the drawings of Bonino da Campione;
- from 1676: periodical restoration works;
- 1915-19, 1940-45: anti-aircraft protections;
- 2006-08: important consolidation interventions

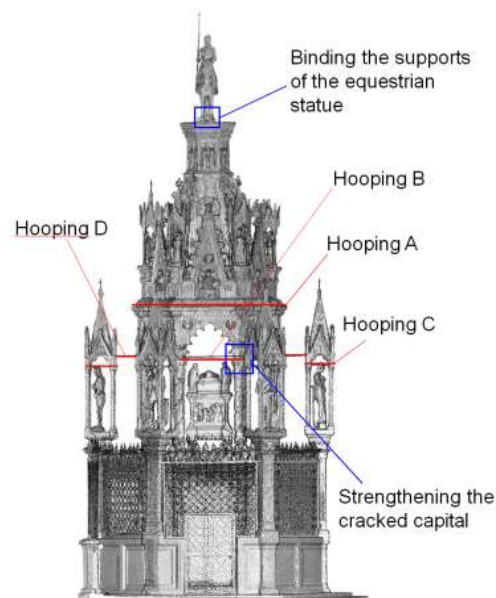


Figure 22 - Strengthening interventions performed in 2006-2008

3.4.3 Preliminary inspections

Operational modal analysis (OMA)

- Definition of the optimal layout of the dynamic system
- Identification of the dynamic behaviour of the monument
- Model updating

- SF 100 Hz; 131'072 points; record length: 21'51'' sec
- System identification: decimation; segment length 2048 points, 66.67% overlap; selected method: FDD

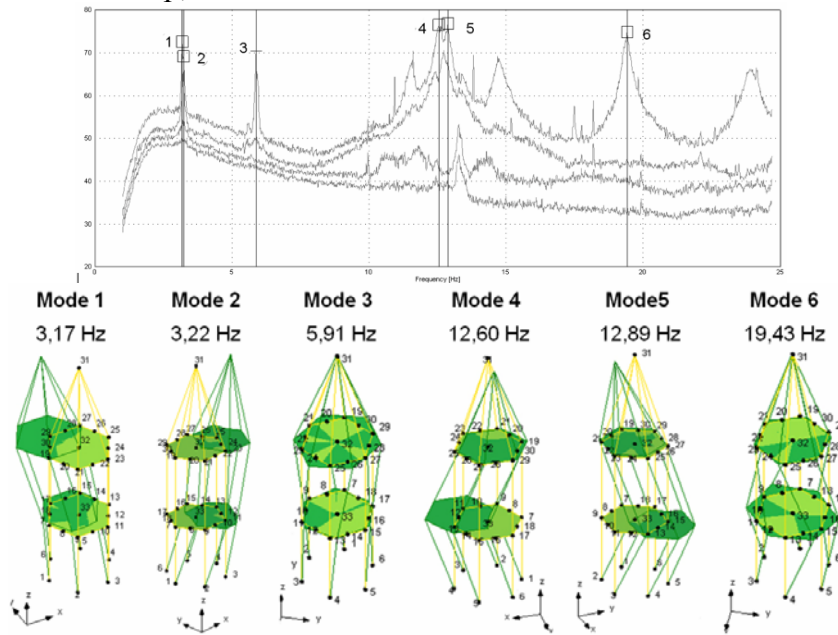


Figure 23 - Ambient vibration tests and modal analysis performed on the tomb

Needs of monitoring:

- Application of SHM before, during and after interventions' execution
- Evaluate on-site the effectiveness of performed strengthening interventions
- Assessment of possible upgrading solutions
- Application of an incremental approach to interventions

3.4.4 The monitoring system

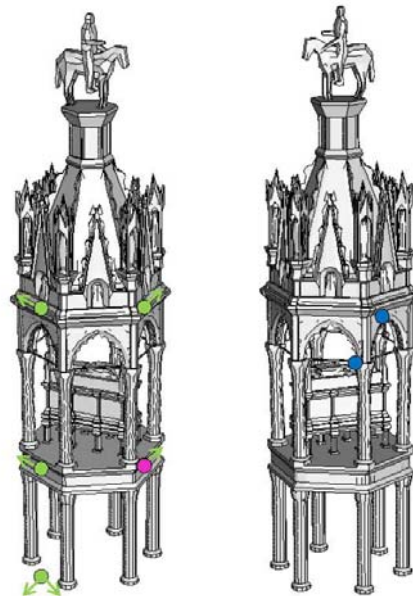


Figure 24 - layout of the static and dynamic monitoring system

Dynamic monitoring

- 4 Single-axis accelerometers

Static monitoring

- 2 Displacement transducers
- 1 Temperature/Relative humidity sensor

3.4.5 Monitoring results

Dynamic monitoring: evolution of the natural frequencies over 7 years

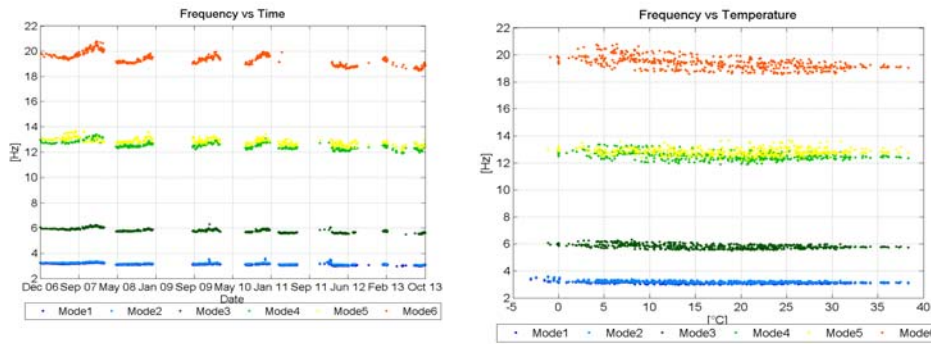


Figure 25 - Evolution of the natural frequencies in function of time and temperature

Static monitoring: evolution of cracks opening

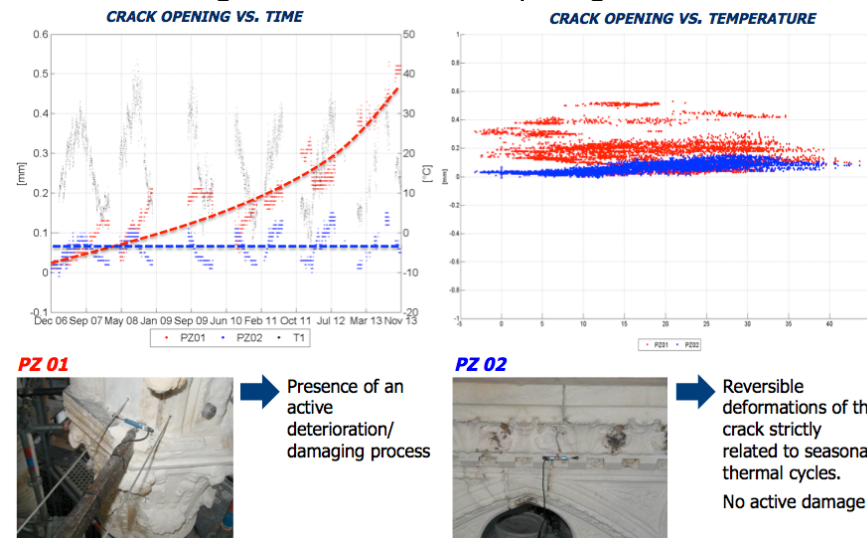


Figure 26 - Crack opening vs time and vs. temperature of the two monitored lesions

3.5. SHM for post-earthquake controls: L'Aquila case studies

Needs of monitoring:

- Evaluate quantitatively the progression of the damage pattern
- Design effective and urgent provisional interventions to prevent further collapses

- Define an early warning procedure for the safety of the workers employed in the strengthening interventions □ Schedule the execution of definitive interventions (heavy reconstructions)

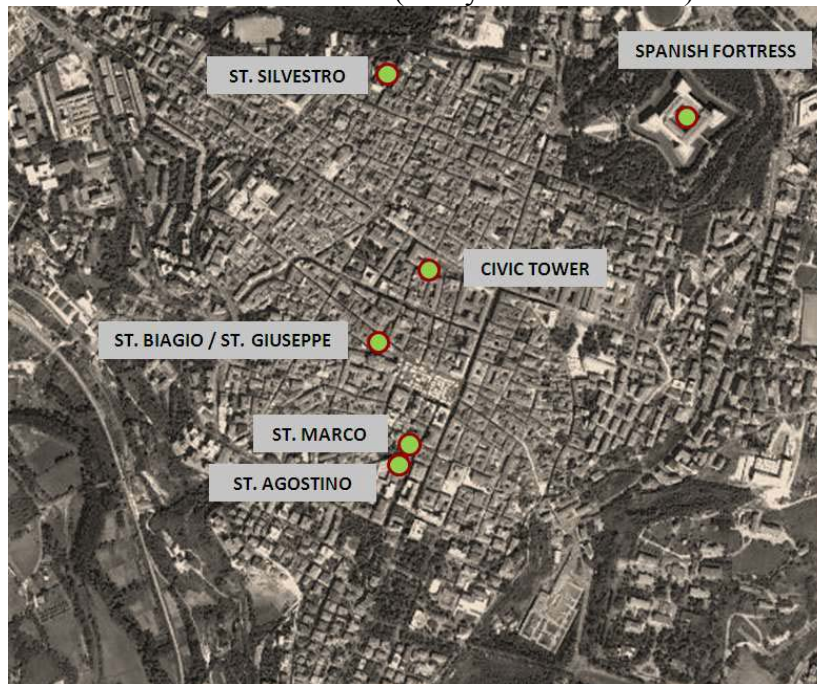


Figure 27 - L'Aquila SHM network (University of Padova & Nagoya University - Japan)



Figure 28 - The Spanish Fortress in L'Aquila

3.6. SHM for post-earthquake controls: the Spanish Fortress

The Spanish Fortress is located in the north-east part of the city of L'Aquila. It is one of the most impressive Renaissance castles in Central and Southern Italy.

3.6.1 Geometric and material features:

- Composed by 4 bastions connected through massive defensive walls (60 m long, 20m thick at the base and 5m thick at the top)
- Surrounded by a deep ditch 23 m wide, 14 m deep
- Perimeter walls: irregular stone masonry with external covering made of travertine.

3.6.2 Historical notes – past interventions

- XV sec.: L'Aquila is the second most powerful city of the Naples' Kingdom, under Spanish domination
- 1534: beginning of the fortress' construction, designed by a Spanish architect
- 1949-1951: restoration works; the fortress became the seat of the National Museum of Abruzzi.

3.6.3 Earthquake induces damages:

- Out of plane overturning of the longitudinal walls
- Collapse of the main façade's and of the roof
- Shear damages and collapses in the inner walls
- Damage to arches, local collapse of vaults and floors
- Overturning mechanisms of the pillars



Figure 29 - Damaged induced by the 6 April 2009 earthquake

3.6.4 Provisional interventions



Figure 30 - Provisional strengthening interventions performed during the emergency phase

- Structural stability provided by relying on the remaining strength of the resisting elements, i.e. connecting the internal and external façades of the damaged wings by means of stainless steel cables, to avoid overturning mechanisms.
- Reconstruction of the roof, using steel trusses and a light covering structure made of wood

3.6.5 Preliminary inspections

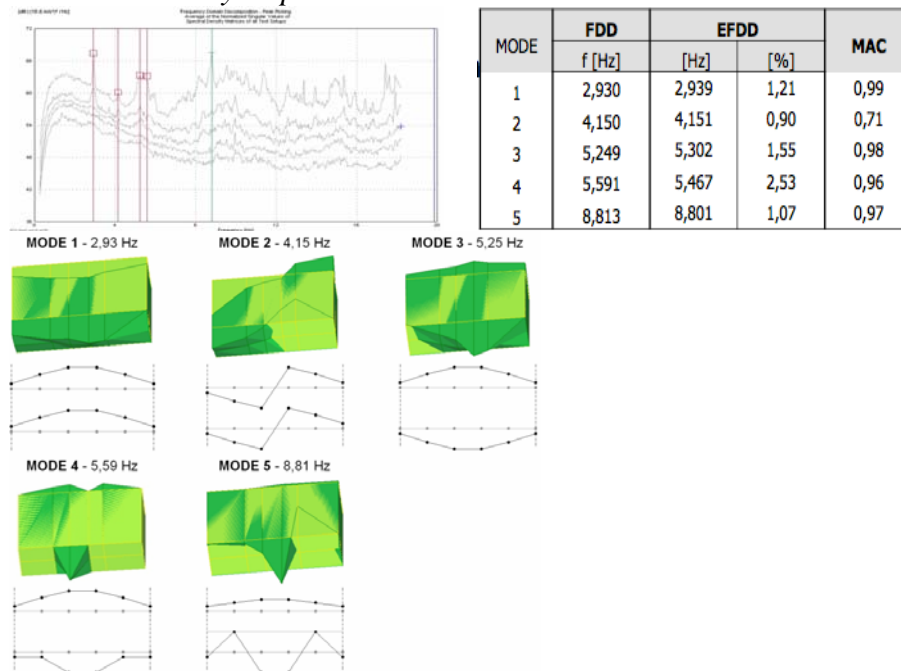


Figure 31 - Preliminary ambient vibration tests on the SE wing on the fortress

Operational modal analysis (OMA):

- Execution of AVT on the SE wing of the fortress
- Identification of the dynamic response in the damaged state:
- assess if the structure has still a unitary dynamic behaviour
- Definition of the optimal layout of the dynamic monitoring system
- Model updating
- SF 100 Hz; 131'072 points; record length: 21'51'' sec

- System Identification: FDD and EFDD OMA techniques

3.6.6 The monitoring system

8 Single-axis accelerometers

The dynamic monitoring system is composed by an acquisition unit connected to eight high sensitivity piezoelectric accelerometers. The central unit, located at the second floor of the fortress, in the South-East wing, is provided with a Wi-Fi router for remote data transmission.

A couple of reference sensors is fixed at the base of the structure for the record of the ground acceleration both in operational conditions and during seismic events.

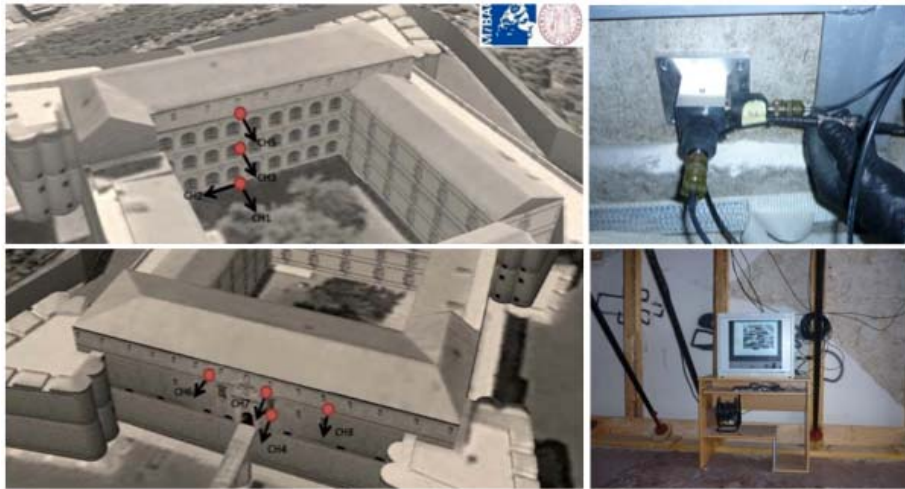


Figure 32 - Layout of the dynamic monitoring system installed on the SE wing of the fortress

3.6.7 Monitoring results

Natural frequencies variation over 3 years

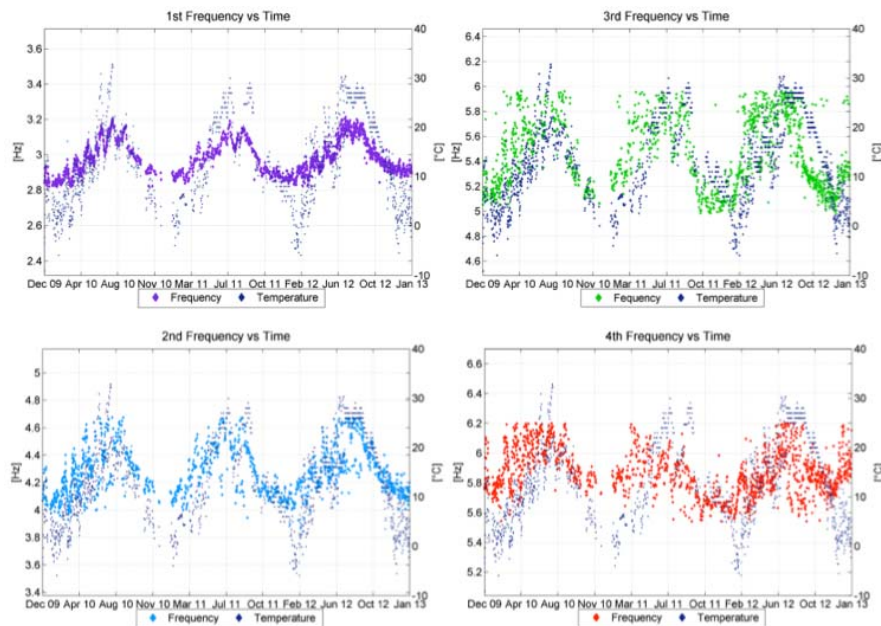


Figure 33 - Natural frequencies and temperature variation over 3 years of monitoring

3.6.8 Structural assessment and damage detection based on SHM

- Definition of clear procedures to interpret, post-process and exploit SHM results
- Data driven approach: Modelling environmental effects through black box models
- Aim: Filter out environmental effects from recorded data and extracted features: decompose the measurements into their reversible and irreversible component and provide object criteria for damage detection
- Application of regression analysis to establish relationships between observed environmental factors (inputs) and estimated natural frequencies (outputs)
- Modelling environmental effects through black box models: implementation of dynamic models □ ARX models (Auto-Regressive output with an eXogenous input) (Ljung 1999)

Description of the procedure

| | | |
|--------------------------------|---|--|
| CORRELATION ANALYSIS | • SELECTION OF ARX MODEL PREDICTORS | $\hat{r}_{xy} = \frac{COV(x_k, y_k)}{\sigma_x \sigma_y}$ estimated covariance estimated standard deviation |
| DATA NORMALIZATION | • MEANS REMOVAL FROM INPUTS AND OUTPUTS | $x_{k,norm} = \frac{x_k^m - \bar{x}_k}{\sigma_{x_k}}$ $y_{k,norm} = \frac{y_k^m - \bar{y}_k}{\sigma_{y_k}}$ |
| ARX MODELS CONSTRUCTION | • ESTIMATION OF ARX SISO MODELS AND THEIR STATISTICAL PROPERTIES | ARX $[n_a, n_b, n_k] = [1: 10, 1: 10, 1: 10]$ |
| BEST MODEL SELECTION | • QUALITY CRITERIA (LJUNG 1999) | Loss Function; Akaike's Final Prediction Error FPE; Coefficient of determination; Autocorrelation functions of residuals |
| RESPONSE PREDICTION | • SIMULATION OF THE RESPONSE BASED ON NEW ENVIRONMENTAL DATA | |
| RESIDUAL ANALYSIS | • CALCULATION OF SIMULATION ERROR AND ITS STATISTICS | $e_k = y_k - \hat{y}_k$ and $\hat{\sigma}_y$ |
| CONFIDENCE INTERVALS | • CALCULATION OF 95% CI USING A STATISTICAL TABLE OF THE T-STUDENT DISTRIBUTION | $[\hat{y} - t_{\alpha/2, \nu} \hat{\sigma}_y, \hat{y} + t_{\alpha/2, \nu} \hat{\sigma}_y]$ |
| DAMAGE DETECTION | • CI AS AN OBJECT CRITERION FOR DAMAGE DETECTION (OUTLIERS ANALYSIS) | |

- Monitoring period: 22/12/2009 - 22/01/2013 → 3 years
- Construction of ARX models on the first 4 natural frequencies

Residual analysis and damage detection

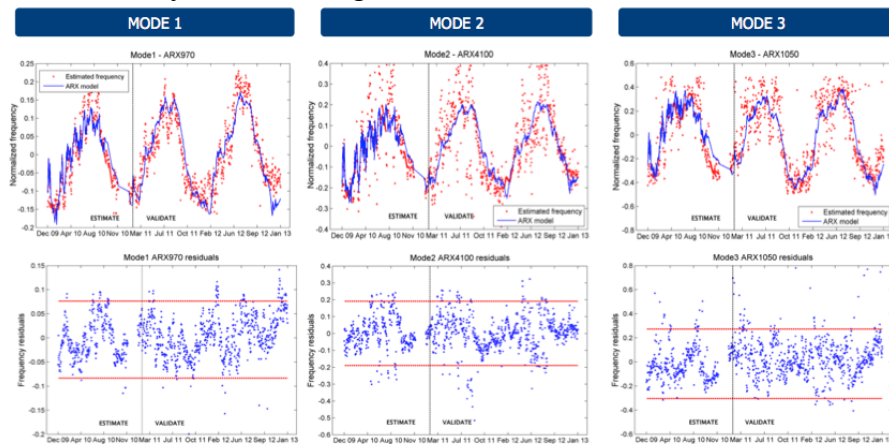


Figure 34 - Residual analysis and damage detection based on ARX models and confidence intervals

- Natural frequencies of the first 4 structural modes are generally included within confidence intervals
- The damage pattern induced by the earthquake is stable during the validation period (last 2 years of SHM)
- Provisional strengthening interventions are effective and prevented further damages/collapses

3.7. SHM for post-earthquake controls: the Civic Tower

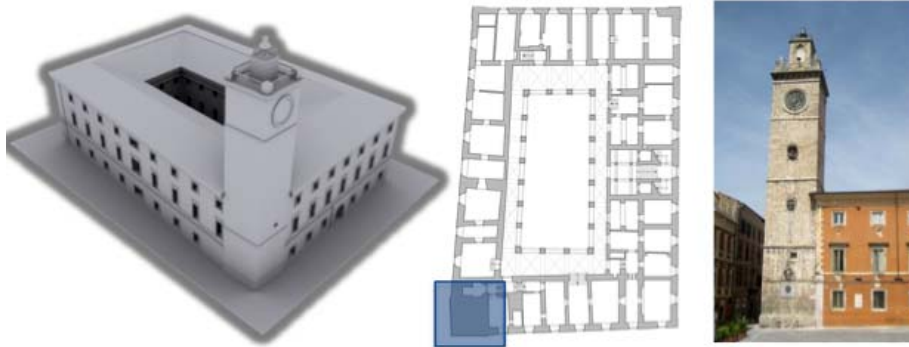


Figure 35 - The Civic Tower in L'Aquila

The Civic Tower is located in the heart of the historical city center of L'Aquila and it's part of the complex of the L'Aquila City Hall composed by two bodies: the Margherita Palace and the Tower.

3.7.1 Geometric and material features

- 6,27m long, 6,42m wide, 42m high
- Covering: calcareous stone blocks
- Presence of some orders of bricks at the second level
- Presence of ancient tiles

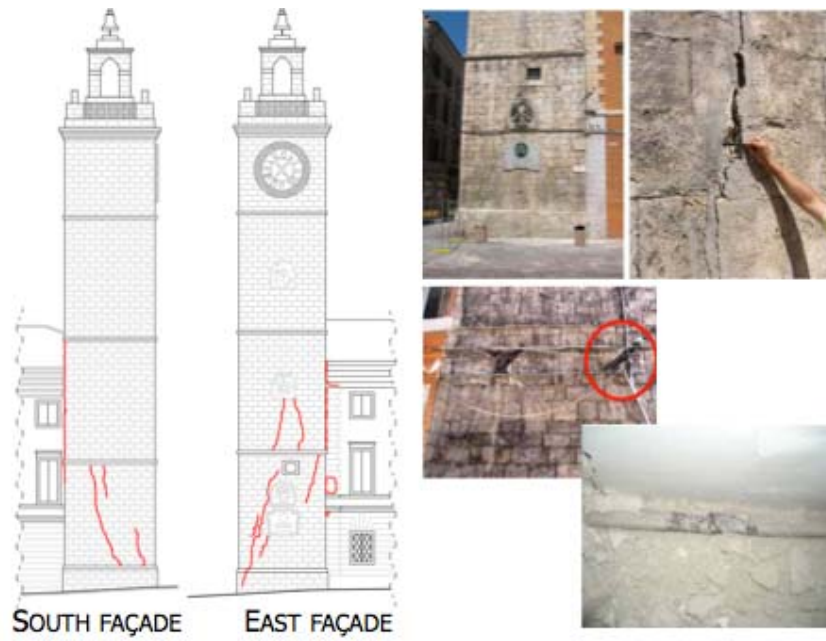


Figure 36 - Earthquake-induced damages



Figure 37 - Provisional strengthening interventions performed immediately after the earthquake

3.7.2 Historical notes - past interventions

- XIII sec.: first construction of the tower, originally conceived as an isolated element
- 1294: construction of 'Margherita' palace
- 1349, 1461 and 1703: strong earthquakes induced several damages/collapses

3.7.3 Earthquake-induced damages

- West façade: vertical cracks
- East and South façades: cracks at the bottom of the tower due to stress concentrations
- South façade: failure of an existing tie
- Detachment of the tower from the Palace

3.7.4 Provisional interventions

- Confinement system of the tower (steel beams, ties and timber frames)
- Improvement of the tower-palace connection
- Propping system of the palace's perimeter walls to prevent out-of-plane overturning

3.7.5 Preliminary inspections

Operational modal analysis (OMA):

- Definition of the optimal layout of the dynamic system
- Identification of the dynamic behaviour in the damaged state
- Model updating
- SF 80 Hz; 144'000 points; record length: 30'
- SI: decimation; selected OMA techniques: FDD, EFDD, pLSCF

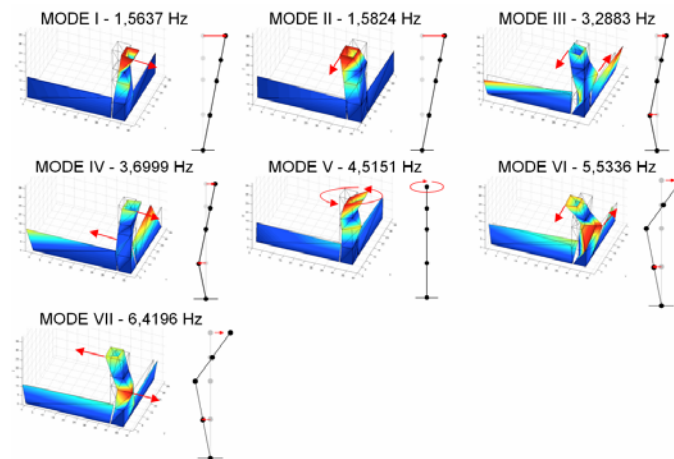


Figure 38 - Mode shapes and natural frequencies identified from ambient vibration tests

3.7.6 The monitoring system

Static system

- 5 Linear displacement transducers
- 6 Strain gauges
- 1 Inclinometer
- 6 Thermo couples

Dynamic system

- 8 single axis accelerometers

3.7.7 Monitoring results

During the first 1,5 years of monitoring the crack pattern of the tower was kept rather stable

Starting from February 2012 the equilibrium conditions of the tower underwent a significant change due to a slight rotation/displacement of the tower toward the palace.

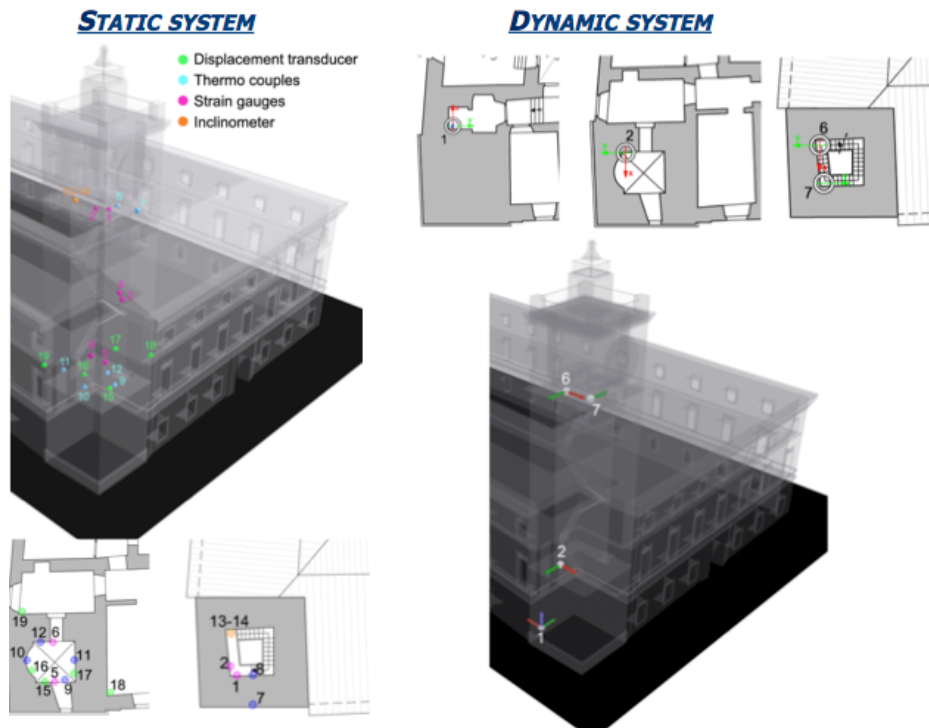


Figure 39 - Layout of the static and dynamic system

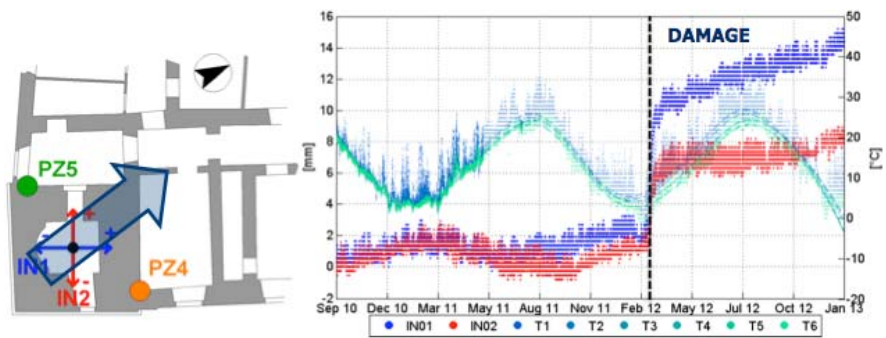


Figure 40 - Anomalous displacement/rotation of the tower toward the palace in Feb 2012

3.7.8 Structural assessment and damage detection based on SHM

- Monitoring period: 22/07/2010 - 09/01/2013 □ 2,5 years

- Construction of ARX models on the first 5 natural frequencies
- Until Feb 2012 □ damage is stable since the residuals are always included within confidence intervals
- From Feb 2012 □ the equilibrium condition of the tower changed due to a displacement of the tower
- It was possible to detect damage/modification of the structural layout demonstrated by an increment of frequencies

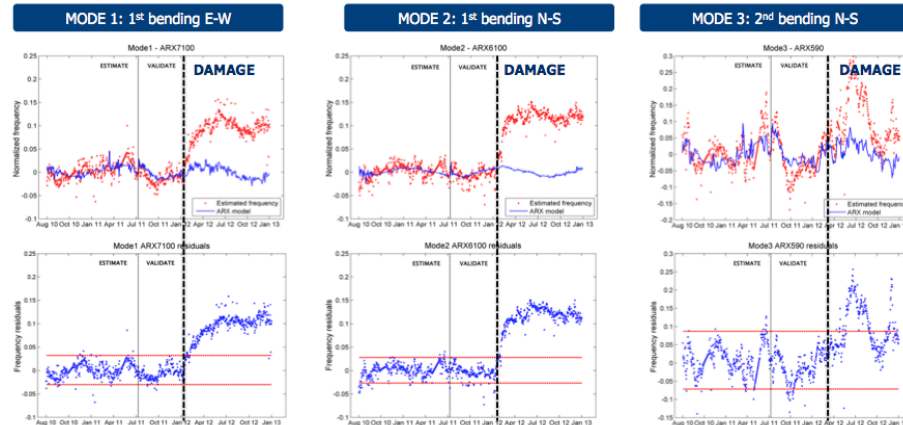


Figure 41 - Residual analysis and damage detection based on ARX models

4. Conclusions

Monitoring is being more and more considered, in the field of cultural heritage buildings, as a key activity in order to increase the knowledge on the structural functioning of monuments and therefore to have a deeper insight on their conditions. In case of a seismic event, monitoring can furthermore prove its usefulness in quantitatively assess the real entity of structural damages.

The combined use of “global” dynamic identification procedures and “local” controls (besides the monitoring of the environmental parameters), providing quantitative information on local conditions of structural elements (e.g. cracks opening), can be an important asset in the effort of attaining a deeper degree of awareness on the real structural functioning of monuments.

The paper reported a sound methodology for the application of SHM to CH buildings and monuments and its validation on several case studies subjected to different structural, use and environmental conditions. The central core of the research is the exploitation of features and information extracted from monitoring data to assess the structural conditions of the monitored buildings. The idea is to interpret and post-process those data in the general framework of increasing the knowledge level of historical buildings, trying to assess their static/seismic capacities and in case intervene through some structural improvements.

This fundamental objective was successfully achieved through the analysis of different but interconnected problems:

- Control the structural behavior of the monitored buildings under operational conditions;
- Calibrate and validate reference behavioral numerical models;
- Study and characterize the structural response in case of exceptional events.

One of the most important conclusions that can be traced from this research experience is that SHM represents a necessary tool for the study and assessment of CH buildings. In order to achieve successfully this ambitious objective it seems that the multi-model approach is the key solution. This means that the implementation of rigorous statistical models based on data-driven approaches on the one hand and the construction and constant updating of reliable numerical models on the other hand provide sufficient tools to exploit and combine the results of SHM in the general framework of the assessment and protection of historical constructions.

References

- [1] Beschi L. (1960), Verona romana. I monumenti in Verona e il suo territorio, vol. I, Istituto per gli studi storici veronesi, Verona.
- [2] Binda L., Modena C., Casarin F., Lorenzoni F., Cantini L., Munda L. (2010). Emergency actions and investigations on Cultural Heritage after the L'Aquila earthquake: the case of the Spanish For-

tress. *Bulletin of Earthquake Engineering*, vol. 9; p. 105-138, ISSN: 1570-761x, DOI: 10.1007/s10518-010-9217-3.

[3] Casarin F, Valluzzi M.R., da Porto F., Modena C. (2008), Structural monitoring for the evaluation of the dynamic response of historical monuments, RILEM Symposium on On Site Assessment of Concrete, Masonry and Timber Structures - SACoMaTiS 2008, eds.L.

[4] Binda, M. di Prisco, R. Felicetti, ISBN 978-2-35158-061-5, pages 787 - 796, Publisher RILEM Publications SARL.

[5] Casarin F., Modena C., Aoki T., da Porto F., Lorenzoni F. (2011). Structural Health Monitoring of historical buildings: preventive and post-earthquake controls. 5th International Conference on Structural Health Monitoring of Intelligent Infrastructure (SHMII-5) 2011, 11-15 December 2011, Cancún, México.

[6] Directive of the Prime Minister (2007) "Guidelines for the evaluation and mitigation of the seismic risk for Cultural Heritage buildings – in line with the new Technical Standards for Constructions" (Italy).

[7] Gaudini G., Modena C., Casarin F., Bettio C., Lucchin F. (2008), Monitoring and strengthening interventions on the stone tomb of Cansignorio della Scala, Verona, Italy, 8th International Conference on Structural Analysis of Historical Constructions, 2-4 July 2004, Bath, UK.

[8] ICOMOS/ISCARSAH (2003) - Recommendations for the analysis, conservation and structural restoration of architectural heritage, International Scientific Committee for Analysis and Restoration of Structures of Architectural Heritage.

[9] Lorenzoni F, Aoki T., Casarin F, Modena C., da Porto F., Sabia D., Sumini V. (2012). Post-earthquake assessment of the Civic Tower in L'Aquila: Ambient Vibration Tests and Structural Health Monitoring. 8th International Conference on Structural Analysis of Historical Constructions, 15-17 October 2012, Wroclaw, Poland.

[10] Lorenzoni F. (2013), Integrated methodologies based on Structural Health Monitoring for the protection of Cultural Heritage buildings, Ph.D. Thesis, University of Trento, Trento, Italy.

[11] Lorenzoni F, Casarin F, Modena C, Caldon M, Islami K, da Porto F (2013). Structural Health Monitoring of the Roman Arena of

Verona. *Journal of Civil Structural Health Monitoring*, 3:227-246, ISSN 2190-5452, DOI 10.1007/s13349-013-0065-0.

[12] Modena C., Casarin F., Valluzzi M. R., Da Porto F. (2008), *Structural monitoring for the evaluation of the dynamic response of historical monuments, Masonry and Timber Structures*, Publisher RILEM Publications.

[13] Morandi R. (1956). *Il rafforzamento dell'Ala dell'Arena di Verona mediante precompressione*, *L'industria Italiana del Cemento*, Anno XXVI, n.2, Febbraio 1956, pp. 39-41 (in italian).

[14] NIKER (2010-2012), *New Integrated Knowledge-based approaches to the protection of Cultural Heritage from Earthquake-induced Risk*, funded by EC under the 7th Framework program, contract n. ENV2009-1-GA244123.

Dynamic Characteristics of Great Bronze Buddha of Kamakura using microtremor

Yutaka Nakamura¹, Jun Saita¹, Mitsuhiro Tachibana¹ and
Tsutomu Sato¹

Abstract

The second largest bronze Buddha in Japan built in around 1250AD at Kamakura immediately above the focal region of the 1923 Kanto earthquake. Great Buddha of Kamakura has still remained basically its original shape, though it has been suffered several natural disasters as losing its hall. Especially, although the 1703 and 1923 Kanto earthquakes caused settlement and sliding of the basement over 0.3 m, the body has been not suffered serious damage. This statue was casted in order from the bottom with many joints. The joint between the head and the body was noticed because it is reinforced by FRP, Fiber Reinforced Plastic, at the time of the last major repair in 1961. And ingenuity was exercised to fence off the earthquake motion over 400 Gal with sliding the body on the basement, to reduce the load for the neck during earthquake. This is the first example of the earthquake isolation system for cultural properties in Japan. Over 50 years passed after the last major repair, deterioration of FRP is feared. Concerning safety during earthquake motion, microtremor measurement was conducted. As a result of the preliminary investigation in 2009, the surrounding ground was estimated that liquefaction was occurred at the front and right sides of the basement and the basement suffered damage as settlement. However, it is considered that the propagation of the earthquake motion for the statue was interrupted because of the liquefaction. Thus, it seems that the damage for the statue itself was prevented because of namely the natural isolation system. Additionally in 2013, microtremor of the statue itself was measured for making clear the connection status between the body and the head.

¹ System and Data Research, Tokyo, Japan.

1. Introduction

Great Buddha of Kotokuin Temple in Kamakura (see Figure 1) is the second largest bronze Buddha in Japan built in around 1250AD. Kamakura locates at the high earthquake activity area in Japan as Figure 2.

Repair report of Showa era (1926-1989) says that although Great Buddha of Kamakura has repeatedly been attacked by several disasters as earthquake, rain storm or flood, the statue itself has still remained its original shape without serious damage until today. Although this statue is outside at present, it had its hall at first and finally lost the hall at the time of disaster in 14 or 15 century. Great Buddha of Kamakura suffered many large earthquakes. At least at the time of the 1703 Kanto earthquake (M7.9 to M8.2) and the 1923 Kanto earthquake (M7.9), these focal regions are shown in Figure 2, although the damage as collapse of the basement and shift and settlement of the statue was reported, the statue itself was not damaged severely. It is interesting why this Great Buddha has not suffered severe damage and

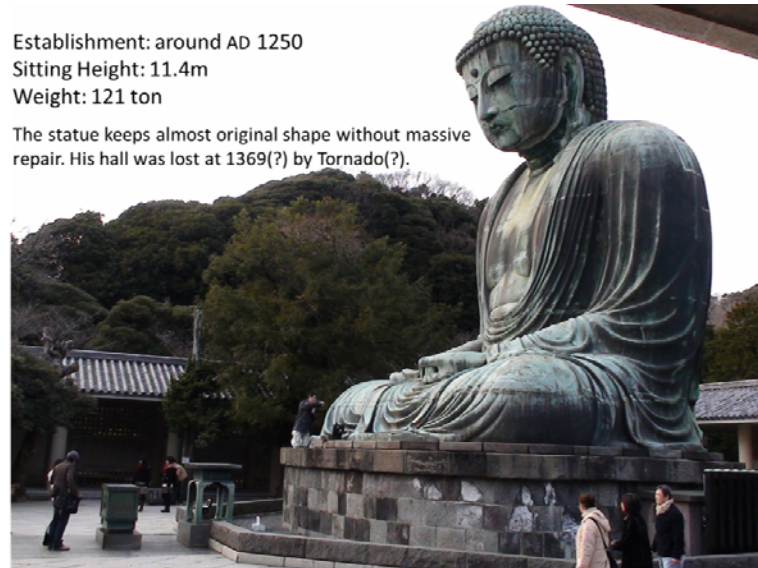


Figure 1. Great bronze Buddha of Kamakura

remained the original shape in spite of suffering large earthquake motion repeatedly and collapse of surrounding buildings.

The damage of the 1923 Kanto earthquake was soon repaired, and additionally a major repair in Showa era was done in 1960 to complement the repair for the 1923 damage. At the time of Showa major repair, the neck of the statue was reinforced by FRP, Fiber Reinforced Plastic. With reinforcing the basement and the bottom of the statue by concrete, a stainless steel plate was applied under the reinforced concrete of the bottom of the statue to slide on the granitic block with bush-hammering attached above the basement during large earthquake motion (see Figure 3). This ingenuity is known as the first seismic isolation system for cultural properties in Japan.

Momentum to consider countermeasures for Great Buddha of Kamakura against earthquake motion is increasing again covering the confirmation of the degradation situation of FRP reinforcement for the neck more than 50 years after execution. This paper reports the result

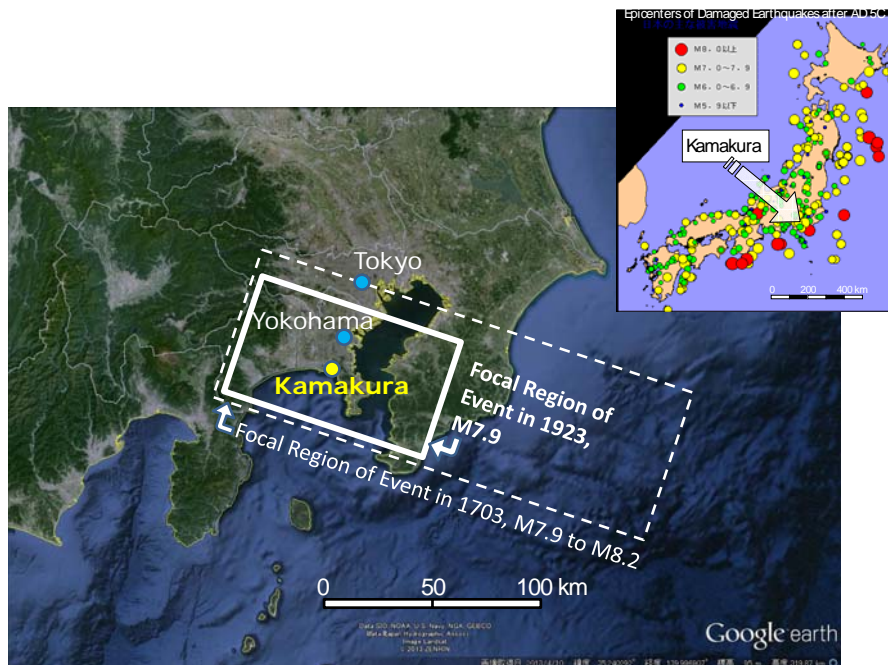


Figure 2. Location of Kamakura and its surrounding seismicity

of the microtremor measurement of the statue taken in the result of the preliminary microtremor measurement of the statue and surrounding ground.

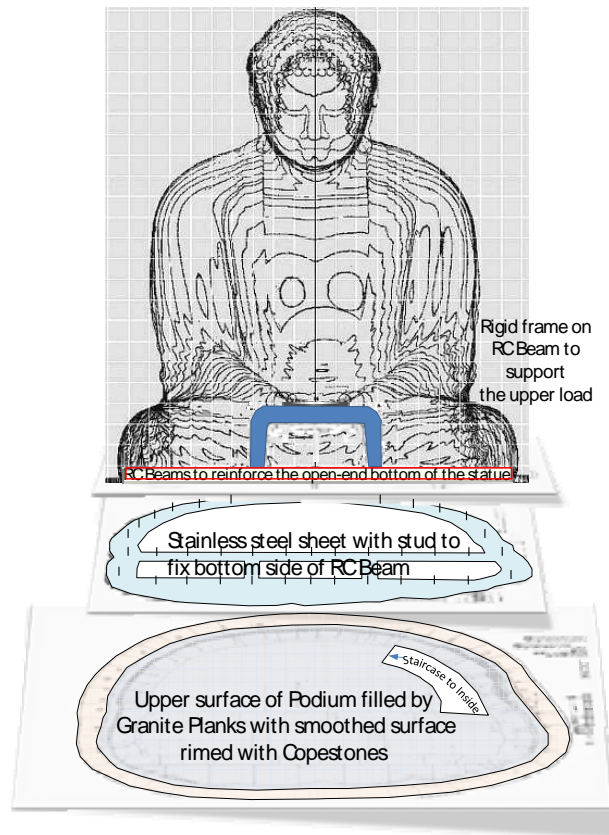


Figure 3. Base isolation system for the Great Buddha of Kamakura

2. Summary of results of the preliminary microtremor measurement of the statue and surrounding ground [2]

Figure 4 shows a distribution of points for microtremor measurement on ground. Figure 5 is QTS (H/V) derived from measurement results. Figure 6 shows the predominant frequency F and amplification factor A corresponding to the measured location with the value follow-

ing to the size of the bubble. This figure shows that the ground becomes softer from west to east or from north to south. This is also confirmed from Figure 7 as the distribution of Kg value, derived from F and A as Equation (1).

$$Kg = A^2/F \tag{1}$$

Here, Kg value can roughly estimate the strain of the surface ground multiplying the maximum acceleration value at base ground, so large Kg value corresponds to large shear strain of surface ground caused by earthquake motion.

Next, the relationship between Kg value and the earthquake damage is concerned. The 2011 off the Pacific coast of Tohoku Earthquake occurred two years after the preliminary investigation. This earthquake caused damage for this temple as turnover of some stone lanterns, but some of bronze lanterns were survived. Figure 8 shows the relationship between the damage situation and Kg value measured at near point. Large Kg value is measured near the turnover and small

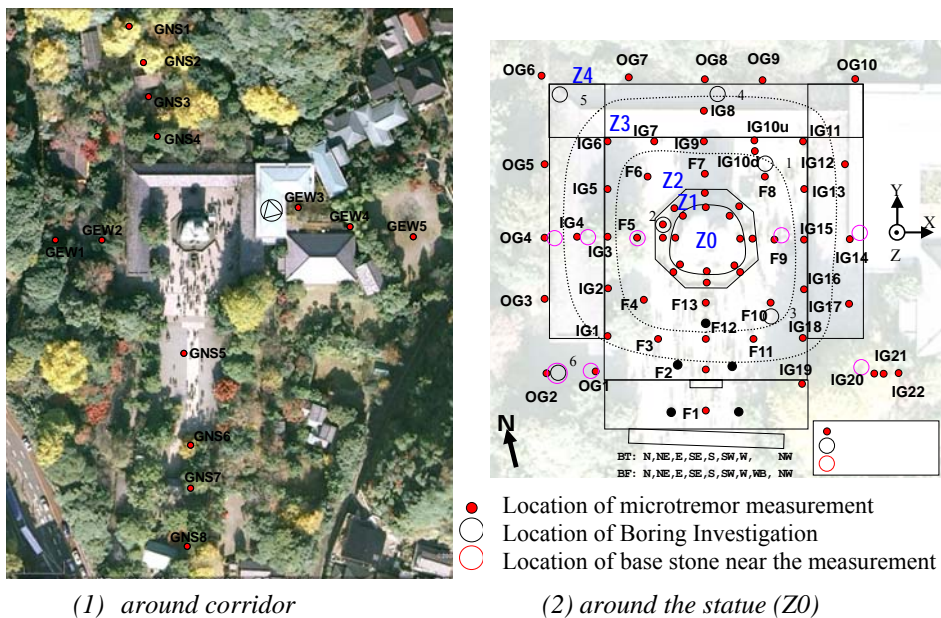


Figure 4. Measurement points of microtremor on ground of Kotokuin Temple

K_g value is closed to survived bronze lanterns.

Figure 9 shows K_g value as a size of bubble at a location corresponding to the damage pictures of Great Buddha at Kamakura shot from three direction at the time of the 1923 Kanto earthquake. It is confirmed that K_g value shows good correlation with earthquake damage level or situation. Although K_g value around the basement is about 10 at maximum and not so large value, the acceleration was possibly over 500 Gal and the shear strain might reach a few 1000 μ . Therefore, the settlement of the basement over 30cm was estimated to be caused by liquefaction.

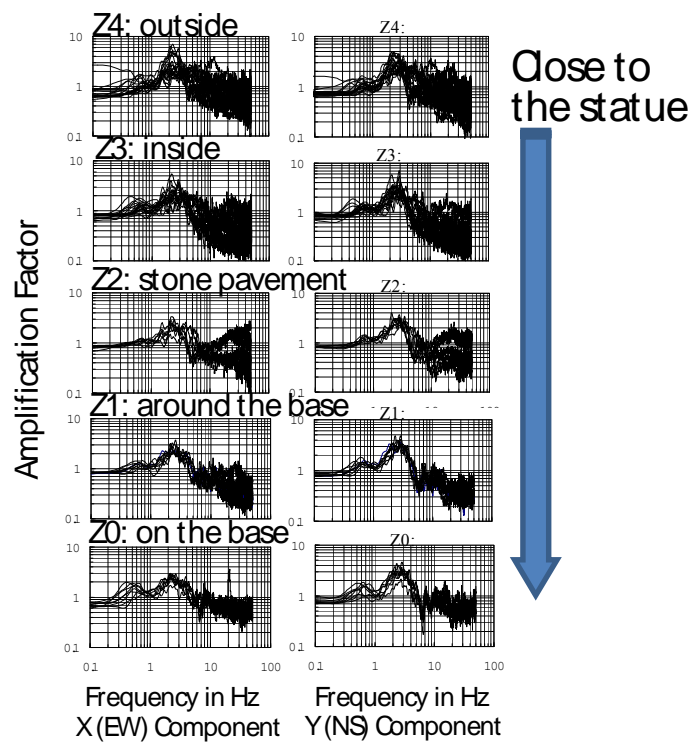


Figure 5. QTS (H/V spectral ratio) for around of cloister

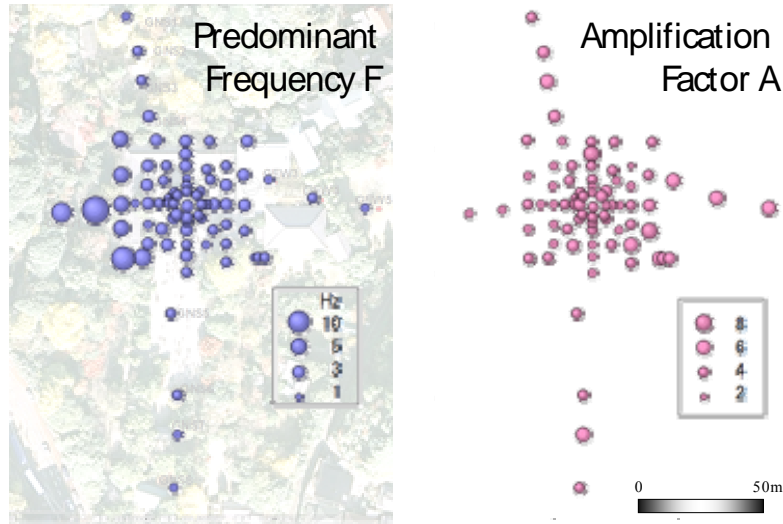


Figure 6. predominant frequency F and its amplification factor A

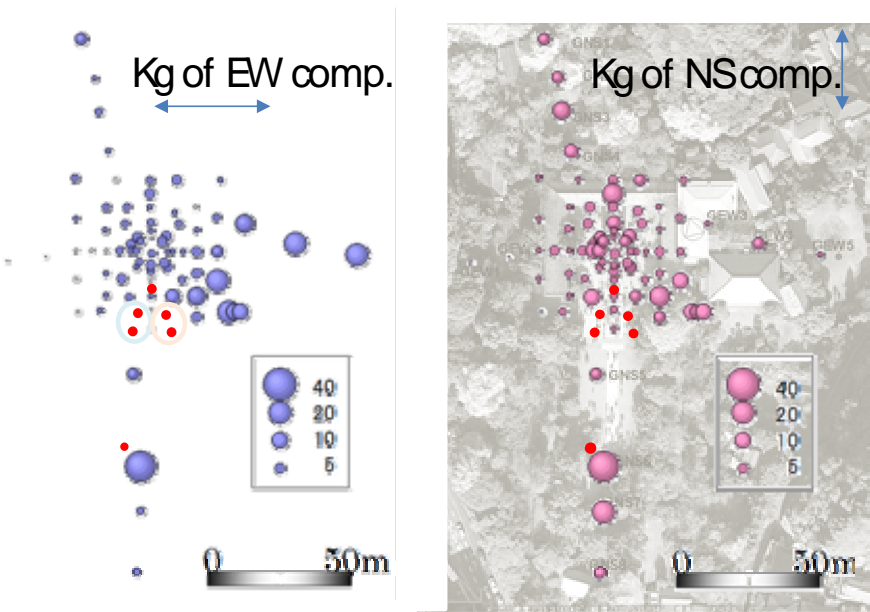
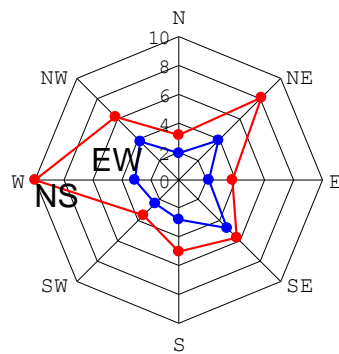


Figure 7. Kg-values distribution



Figure 8. Damage example by the 2011.3.11 Tohoku earthquake



Kg-values around the podium

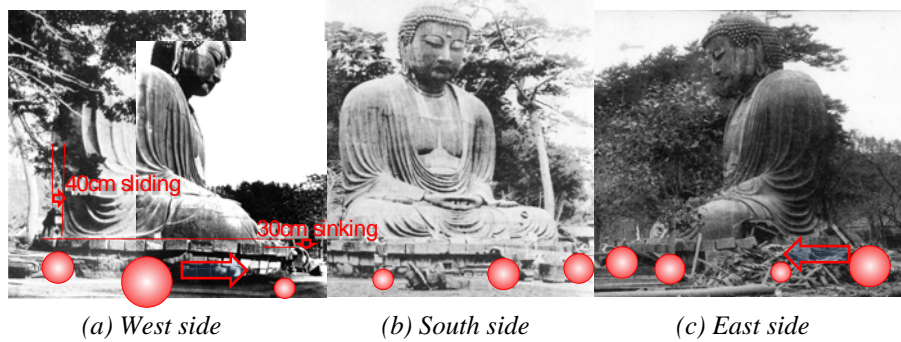


Figure 9. Comparison between Kg-values and Damage caused by the 1923 earthquake of M7.9

3. Measurement situation and analysis method of the Great Buddha

The microtremor measurement was carried out on July 23-25, 2013. Figure 10 shows the distribution of the microtremor measurement points for the main body of the Great Buddha. Figure 11 and Figure 12 show the appearance around measurement points. Here, the

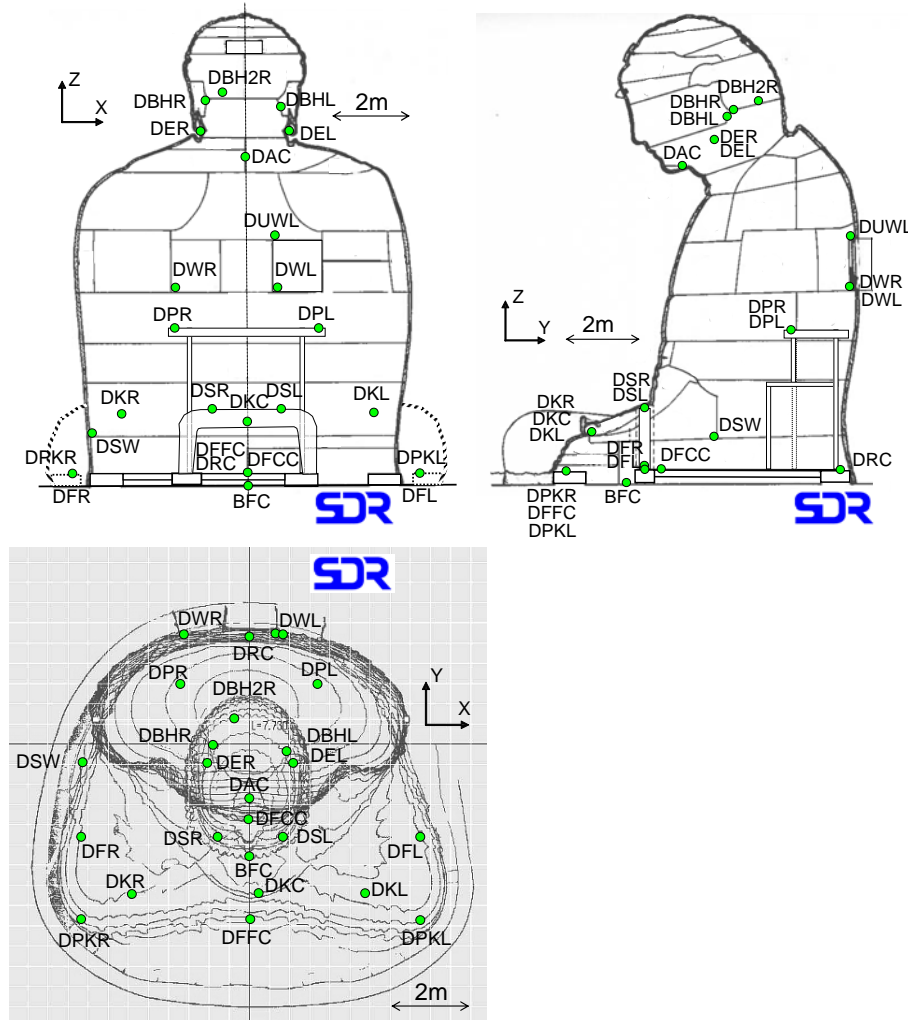


Figure 10. Microtremor measurement points in the Great Buddha of Kamakura

three-digit number after the site code indicates the date of measurement, for example, 723 means July 23. It was impossible to set the sensor immediately because a small Buddha was placed inside the jaw of the Great Buddha and a money offering was deposited during opening a platform having honor of seeing. However they are removed in the morning at July 25 and it became possible to measure microtremor. The total weight of a small Buddha and a money offering were 155 kg.

On July 25 after removing the small Buddha and a money, microtremor was recorded again at the earlobe measured before July 23 to grasp the change of the dynamic characteristics caused by the variation of the weight, and the vibration characteristics are compared between before and after removing and the change are considered. Also the small Buddha (the weight is 40.4 kg) was put back into place at July 26.

Continuous measurement was carried out at the point DRC under the platform, and the measurement at the other two points was carried out simultaneously standardized by the point DRC. So microtremor of each three points shown in Figure 10 was measured simultaneously to

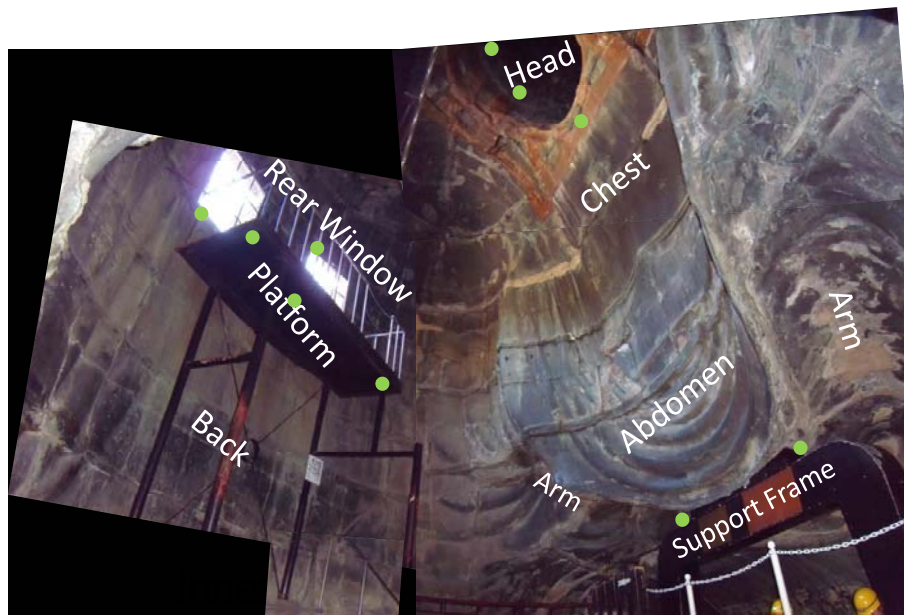


Figure 11. Inner view of Great Buddha of Kamakura

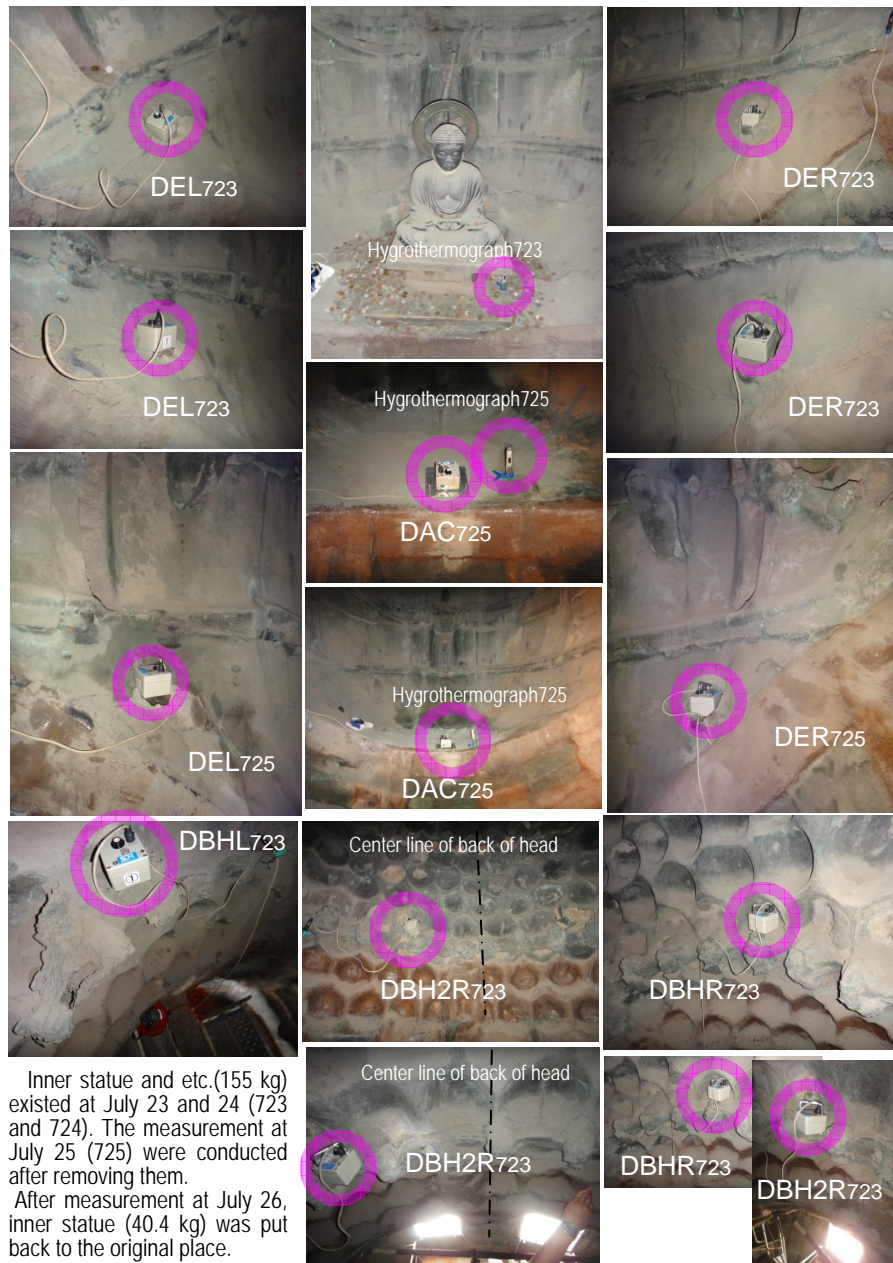


Figure 12. Measurement points in Head

device to have same result of frequency analysis measuring all the point at the same time.

Sampling frequency was set 100 Hz and generally microtremor was recorded for five minutes. More than five analysis sections with 40.96 seconds were chosen from each recorded microtremor and applied frequency analysis, and then an averaged spectrum was calculated

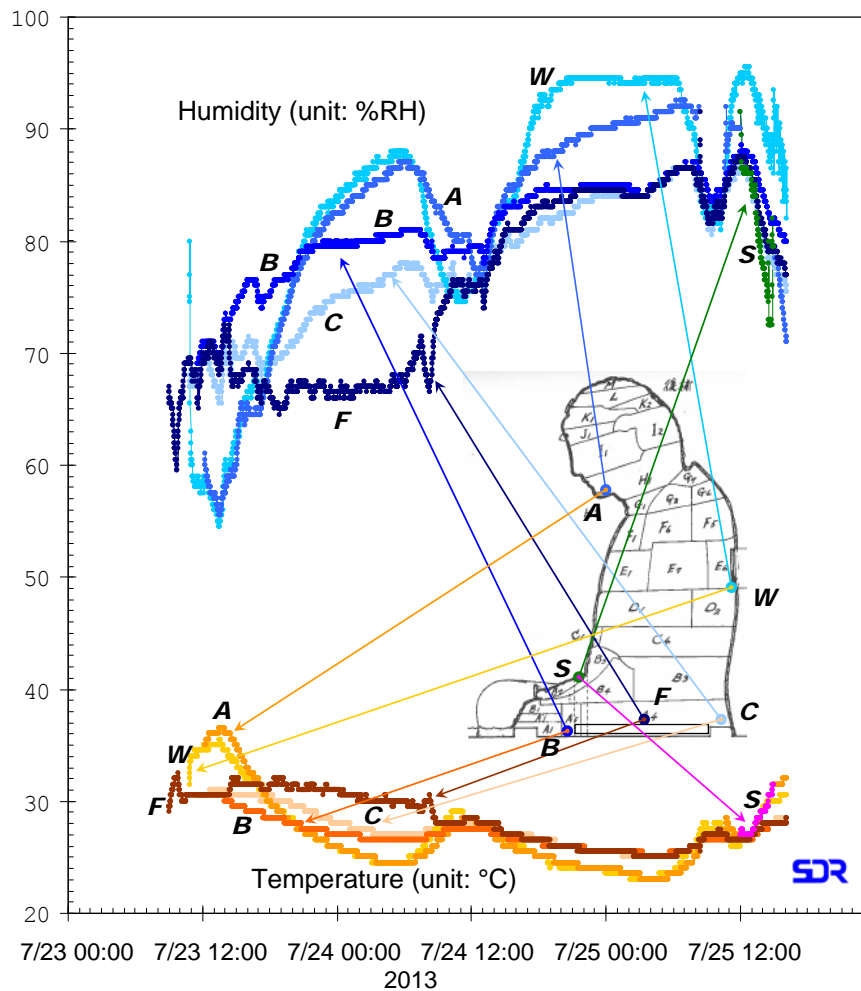


Figure 13. Change of temperature and humidity at the period of microtremor measurement

from three to five sections.

On the other hand, because a vibrational trajectory is known to be effective to understand the vibration characteristics [1], here the velocity locus of 60 seconds was drawn and considered to grasp the whole motion.

Microtremor was measured moving points in the daytime and then measured at point DRC and the other point continuously till the next morning. Microtremor was measured at the points DRC, DUWL and DBH2R from the evening of July 23 to the morning of July 24, and at the points DRC, DSL and DSR from the evening of July 24 to the morning of July 25.

A fireworks festival in Kamakura was held 2 km south from the Great Buddha in the evening of July 23 and the vibration of fireworks were also measured. Continuous measurement aimed to observe not only seismic events but also the other vibrations as frictional vibration caused by the change of temperature between the morning and the evening but there was no seismic event.

Because the differences of temperature was not so large shown in Figure 13, the existence of frictional vibration was also not clear. Here, Figure 13 shows the change of the temperature and humidity in every minutes with 0.5 °C and 0.5 %RH resolution during microtremor measurement specifying the location of the sensors. It is confirmed from this figure that both temperature and humidity show different behavior at each measurement point in the body.

Although the relationship between the vibration characteristics and the change of temperature or humidity, or the vibration of the fireworks are impressive topics, they will be discussed for another day, not in this article.

4. Result of analysis

4.1 Locus of microtremor

Figure 14 shows the locus of microtremor at all the measurement points, projecting to an elevation, a profile and a plan. Background figures of an elevation and a profile are figures of casting joints (see

[3]). For a plan background figure is contour map based on the three-dimensional measurement [7]. Locus in warm color and cold color indicates the points at right side and center or left side, respectively. According to this figure, it is possible to grasp the vibration situation of each point mentioned below. Notice that these figures include an error with drawing so the center of the locus may not correspond to the measurement point.

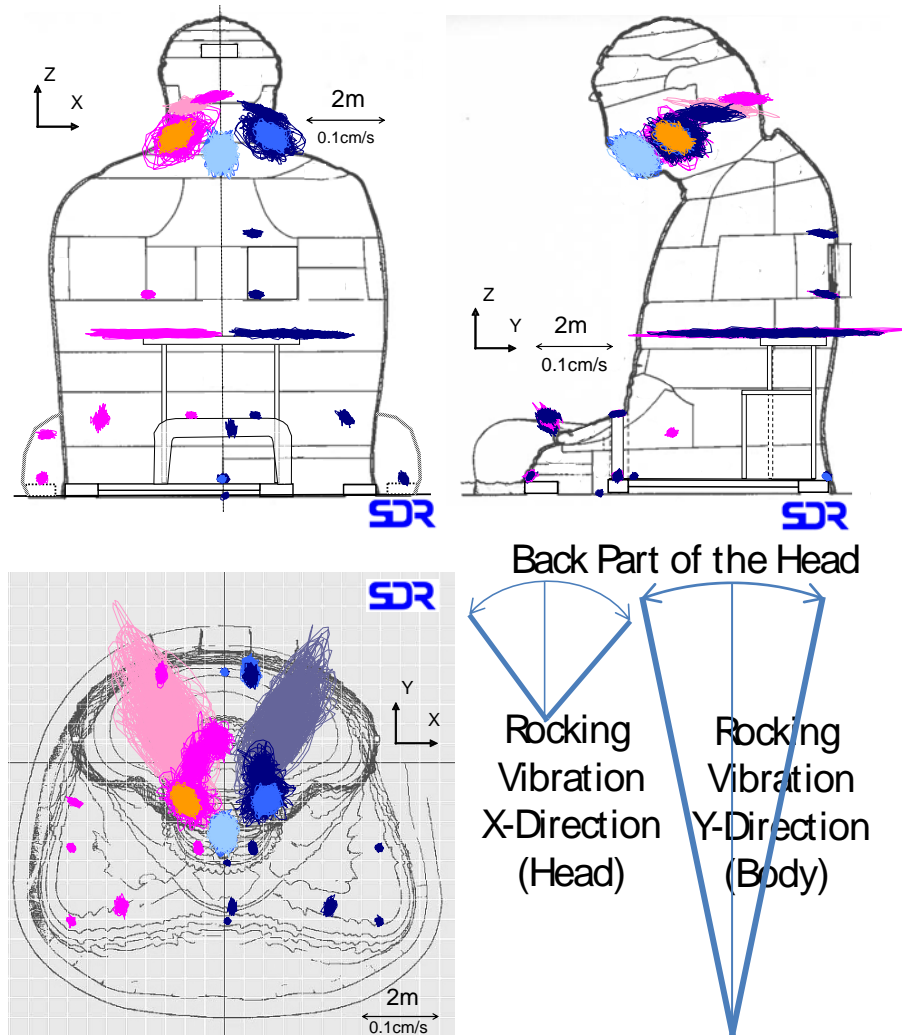


Figure 14. Locus of microtremor in Great Buddha of Kamakura

4.1.1 The vibration of a platform having honor of seeing for the inner small Buddha

This platform is a stage inside the body to having honor of seeing for the inner small Buddha and can access the window at the backside. This platform has been not opened to public and removed its stairs about ten years ago. At the time of measurement in 2009, the authors found an evidence that this platform had contacted to the inner wall of the body and it can be estimated that this platform may swing widely during large earthquake motion and attack the inner wall. For this reason, microtremor measurement was carried out for the platform.

The locus of the microtremor is shown in Figure 14, and it can indicate the structural characteristics of this platform. Because the platform consists of the other vibration system from that of the body of the Great Buddha and it is available to show that the structural characteristics appears at the microtremor characteristics, it is explained in rather detail.

The platform is supported by four columns as Figure 11, and the span of the column width is forced to enlarge at left side of the inner body because of the location of the stairs from the entrance putting the column on the intercepting beam. On the other hand, the column span corresponds to the width of the stage and is rather narrow at the right side of the inner body. The horizontal motion predominates in the vibration of the stage, and reflecting the difference of the structure, the locus projected to a profile is seemed falling forward slightly because of a vibration like the rocking vibration in the right side whereas the locus shows almost horizontal shape with slight small horizontal amplitude except for tiny vertical motion because the supporting span is comparatively long in the left side. The tiny vertical motion in the left side seems to be affection of the structure of the column supported by the beam.

As mentioned above, the difference of the structure appears clearly at the microtremor. And it can be understood that sway and torsional vibrations appear clearly on the vibration of the platform projected horizontal plane.

4.1.2 The vibration of the body of the Great Buddha

The vibrations in left and right direction of the body are almost same amplitude regardless of the measured points and it shows well the characteristics of the body of the Buddha broad in left and right direction as the rigid body.

On the other hand, a remarkable tendency can be seen that the vibration in back and forth direction becomes larger toward to higher point of measurement, and it can be estimated appearing the bending vibration including the rocking vibration with the rocking center at the lower part of the basement or the shear vibration.

Anyway, this vibration shows the characteristics of the structure at the measured point and shows comprehensible behavior as rather predominating the vibration corresponding to the motion of the rack where locates in the back of the hand with mudra or crossing leg.

4.1.3 The vibration of the head of the Great Buddha

Six measurement points could be installed in the head as three points at back of the head, one point in jaw and two points at the base of the earlobe. The microtremor locus in velocity is highly distinguishing for each measurement point. One minute long locus of horizontal motion of each point shows mainly ellipse shape with various vibrations inside the ellipse. It shows that the head moves in various amplitudes and the maximum amplitude is the outmost ellipse.

Although the size of the outmost ellipse was larger at the earlobe before removal of the inner small Buddha, it became almost similar to each point after removal. It can be understood that the fixing in the horizontal plane of the head has a certain level of flexibility and the fixing is not so differ from the measured points.

On the other hand, the locus projected at the elevation or side plane is quite differ between the three points at back of the head and the three points at the jaw and the earlobe. The vibration at back of the head draws a locus as constricted vertical motion and a forward-and-backward and a left-and-right motions seem to draw a locus of rocking vibration mainly consisted of the vibration of the body and the head, respectively. Both a back-and-forth vibration and a left-and-right vibration of the jaw and the earlobe draw a large ellipse locus predominating vertical motion.

A load is differ about 155 kg before and after removal of the inner small Buddha and other deposits. Microtremor at the jaw and the ear-lobe was measured before and after removal, and the locus of microtremor after removal is drawn in light color. This shows that the vibration after removal, decreasing the load about 155 kg from on the jaw, becomes not only significantly smaller amplitude but also smaller scattering. Right side vibrates obviously larger before removal and it

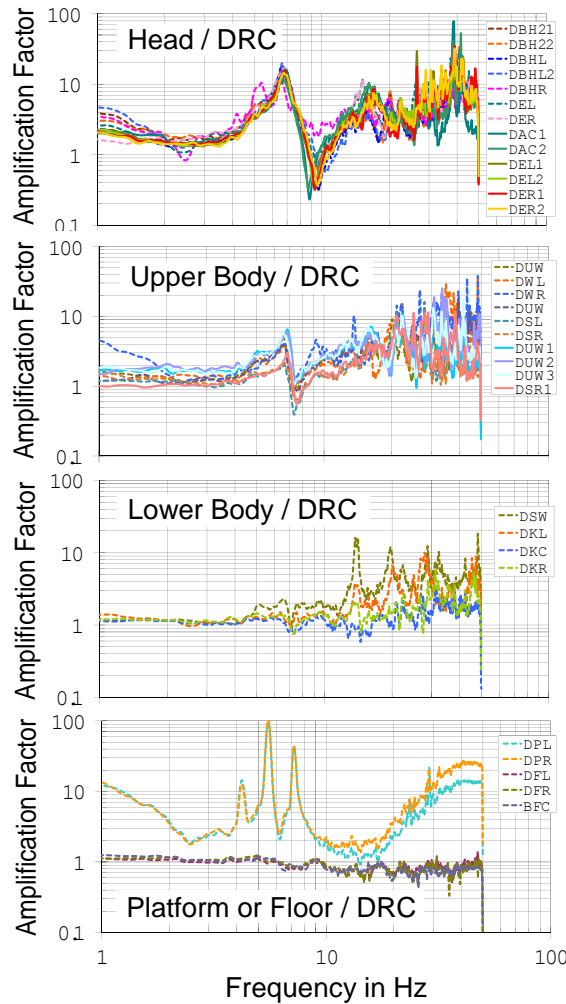


Figure 15. Spectral Ratios against DRC Spectrum for X-component

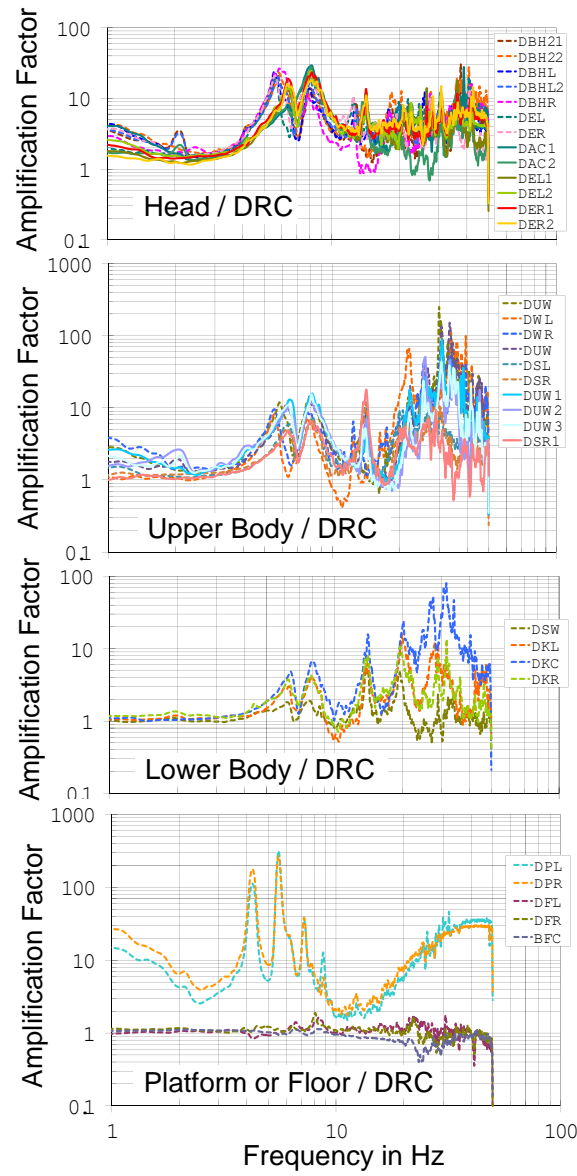


Figure 16. Spectral Ratios against DRC Spectrum for Y-component

seems that there becomes a little difference between right side and left side vibration after removal. It is not apparent how the vibration at back of the head changed after removal because the measurement was carried out only at the jaw and the earlobe after removal.

This apparent change of the characteristics is estimated roughly from overlapped one-minute long amplitude fluctuating in time, and this is considered in detail resolving into each frequency in the next section.

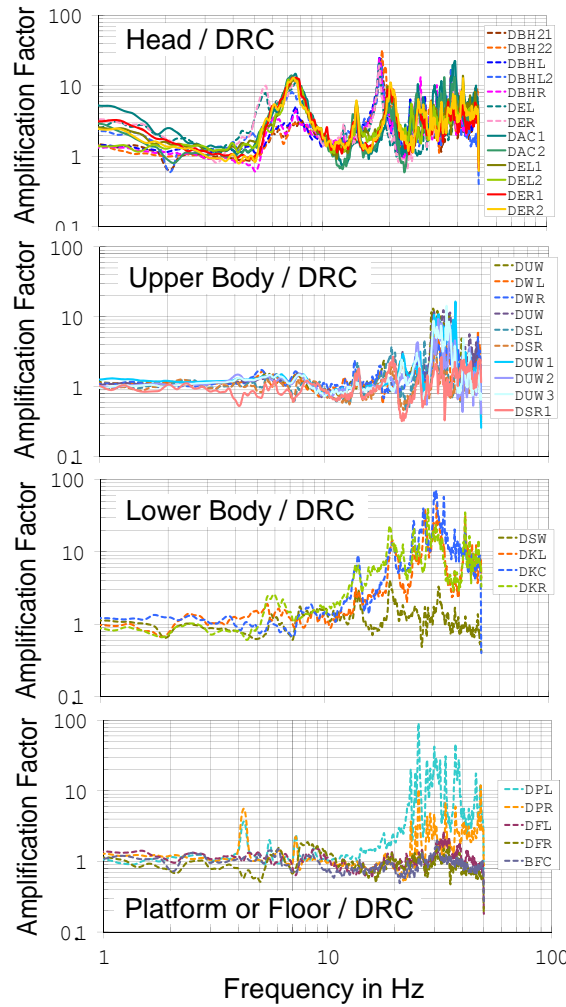


Figure 17. Spectral Ratios against DRC Spectrum for Z-component

4.2 Result of the frequency analysis

Figure 15 to Figure 17 show the result of the transfer function analysis of the microtremor measured at each point as standardized spectral ratio with the point DRC, separated in the head, in the upper body, in the lower body, on the floor and on the platform. These figures show the measured spectra in dotted and solid line before and after removal of the inner small Buddha and other deposits, respectively. This shows that each points at the body of the Buddha has slightly differ vibration peak for each other. The vibration characteristics of the head and the body have big difference for each other.

The vibration less than 10 Hz predominates only at the head and that over 20 Hz shows many peaks predominating at both the body and the head. It represents the high rigidity with corresponding that the body and the head is collective entity consisted of many members, and it indicates that the joint between the body and the head is relative loose.

Figure 18 is a kind of vibration mode diagram indicating the amplification factor corresponding to various predominant frequencies shown in Figures 15 to 17 with the height of the measurement point. The difference of the amplification factor at each point can be grasped by this figure.

Figure 19 shows the spectral ratio using the left side as base in case of the measurement at both left and right side and it corresponds to the situation before removal the inner little Buddha and other deposits.

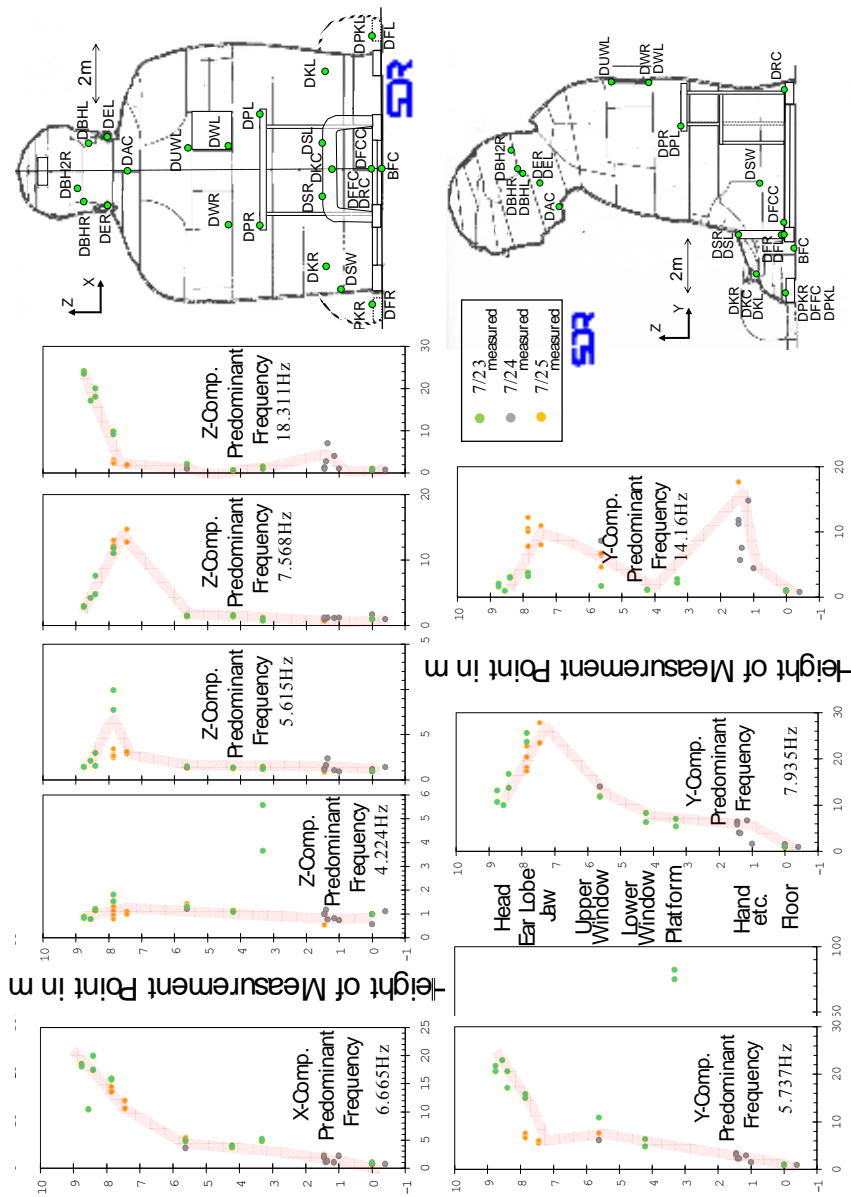
Figure 20 shows the amplification spectra of earlobe based on the point DRC and the spectral ratio at the point left and right side earlobe based on the left side for before and after the removal.

Hereinafter, the frequency characteristics of the Great Buddha are considered for each vibration component referring these figures.

4.2.1 Left and right direction (*X*-component)

In case of left and right direction, each points at the head, the upper body, the lower body, the floor and the platform show different characteristics.

There are six measurement points in the head and all the points shows same characteristics at least less than 10 Hz. It means that the head behaves monolithically. The predominant frequency is about 6.7



Amplification Factor against DRC
 Figure 18. Vibration modes of the Great Buddha at Kamakura

Hz with amplification factor more than 10. It is considered as resonance combined the head and the upper body motion shown in Figure 18, and the predominant frequency was not so changed by decreasing the weight of 155 kg from the jaw.

At that time the amplitude at the body is considerably smaller than that at the head. Therefore the body is assumed as rigid and setting Kh as the spring constant of horizontal spring connecting the body and the head, the mass relating to the vibration M and the decreased mass m , the estimation of Kh and M is attempted. When the predominant frequencies before and after decreasing the weight are f and f' , they can be expressed as follows.

$$\begin{aligned}(2\pi f)^2 &= Kh/(M + m) \\ (2\pi f')^2 &= Kh/M \\ (f'/f)^2 &= (M + m)/M = 1 + m/M \\ \therefore M &= \frac{m}{(f'/f)^2 - 1}\end{aligned}\tag{2}$$

If the frequency was changed as same level of the minimum dissolution about 0.0244 Hz from 6.690 Hz although the change of the frequency can not be recognized by decreasing the load, it is possible to estimate the mass relating to this vibration as follows.

$$M \approx 21.2 \text{ tons}$$

This is almost same level of the estimated mass of the head, 20 tons. It also suggests that this is the vibration of entire head part. Here the spring constant of connection spring Kh is estimated as follows.

$$Kh = (2\pi f)^2 M \approx 37.7 \text{ MN/m} = 38.5 \text{ ton/cm}$$

Although this result coincides with estimation from the frequency f Hz using estimated mass of the head and suggests the hypothesis used in this estimation is proper, the detail will be examined hereafter.

In addition, a number of peaks over 10 Hz can be recognized at the body. These high frequencies seem to reflect the vibration characteristics of the parts of the body, and there are basically only high frequencies at the lower body.

All the points at the floor show almost same vibration characteristics to the basing point and it suggests high rigidity of the floor.

There are three predominant frequencies, 4.2 Hz, 5.6 Hz and 7.2 Hz at the platform. The amplification factors are roughly 15, 75 and 45, and that corresponding to 5.6 Hz is the largest.

The predominant frequency of each part of the left and right component has not changed after decreasing the load at least less than 10 Hz.

4.2.2 Back and forth direction (*Y*-component)

In case of backand forth direction, there are two significant peaks less than 10 Hz except at the floor and the platform. Although the vibration around 8.0 Hz has changed little by decreasing the load from the jaw, that around 5.7 Hz has shifted to around 6.4 Hz by decreasing the load. The vibration modes of them at the head are distinguishing.

The amplification factor after shifting to 6.4 Hz from 5.7 Hz by decreasing the load is relative small as 5.5 at the jaw, but it becomes larger as around 20 at back of the head.

On the other hand, the amplification factor corresponding to the vibration around 8.0 Hz is increased more than 20 excited by the body at the jaw, but it becomes about 10 at back of the head smaller than that of the upper part of the body at the back side.

This means that although these two frequencies predominate at the head, the one around 5.7 Hz shifted to around 6.4 Hz by removal the load and make the part back of the head vibrate largely, and the other one around 8.0 Hz has changed little by decreasing the load and make the jaw vibrate largely. Because the vibration around 6 Hz is responsive to the variation in weight of the jaw, this vibration seems to relate to only some portion of the head. Whereas, the vibration around 8 Hz is resonance of the body and it is estimated that the vibration is little affected by the change of the weight of the jaw because the head vibrates as dragged by this motion.

Also the vibration over 10 Hz observed at the upper body is estimated as the localized motion at each portion.

4.2.3 Up and down direction (Z-component)

In case of up and down direction, the vibration less than 10 Hz predominates only at the head and that over 15 Hz predominates at the body. The amplification factor distributes under 15 for the vibration less than 10 Hz at the head, and the amplitude is smaller than that of the horizontal motion.

Significant peaks for the head appear around 5.6 Hz, 7.6 Hz and 18.3 Hz. The peak at 5.6 Hz can be seen only at the point DER or DEL at the base of the earlobe before removal and its amplification is about 8. The body moves little by the vibration at 7.6 Hz and the amplification factor becomes larger from back of the head to the jaw and exceeds 10. Contrary to this, the amplification factor of the vibration around 18.3 Hz exceeds 20 toward to back of the head.

The vertical motion at 7.6 Hz has changed little after removal and is confirmed to have high correlation with the vibration of back and forth direction. The vibration at 5.6 Hz and 18.3 Hz has shifted to higher frequency as around 6 Hz and 20 Hz after removal. The vibration at 18.3 Hz is a motion that the head moves up and down dominantly and the motion at the body is considerably small without that behind the knee.

Therefore assuming the body as rigid and the weight of the head as 20 tons same as a back and forth motion, the spring constant of connecting spring for vertical motion to the head K_v can be estimated as follows.

$$K_v = (2\pi f)^2(M + m) \cong 264 \text{ MN/m} = 269 \text{ ton/cm}$$

This is 7 times more than the spring constant K_h of horizontal spring, and the properness of this result will be validated hereafter.

4.2.4 Measurement points corresponding between left and right side

Figure 19 shows the spectral ratio referenced by the left side point in case of the measurement corresponding between left and right side.

This figure shows a situation before removal of the inner small Buddha and other deposits. And Figure 20 shows the similar spectral ratio of the measurement at the earlobe before and after the removal and additionally shows the amplification spectra against the point DRC. Here the consideration is advanced noticing the frequency range displaying large amplification.

With Figure 19, L/R ratio of vertical motion shows similar shape for the points DBHL and DBHR at back of the head and the points DEL and DER at the earlobe and slightly different shape for the points DKL and DKR at the knee. And the ratio becomes about 1 at frequency range less than 20 Hz same as the points DSL and DSR at the supporting frame work, which means that the motion is almost same for both left and right side. It is estimated that the supporting

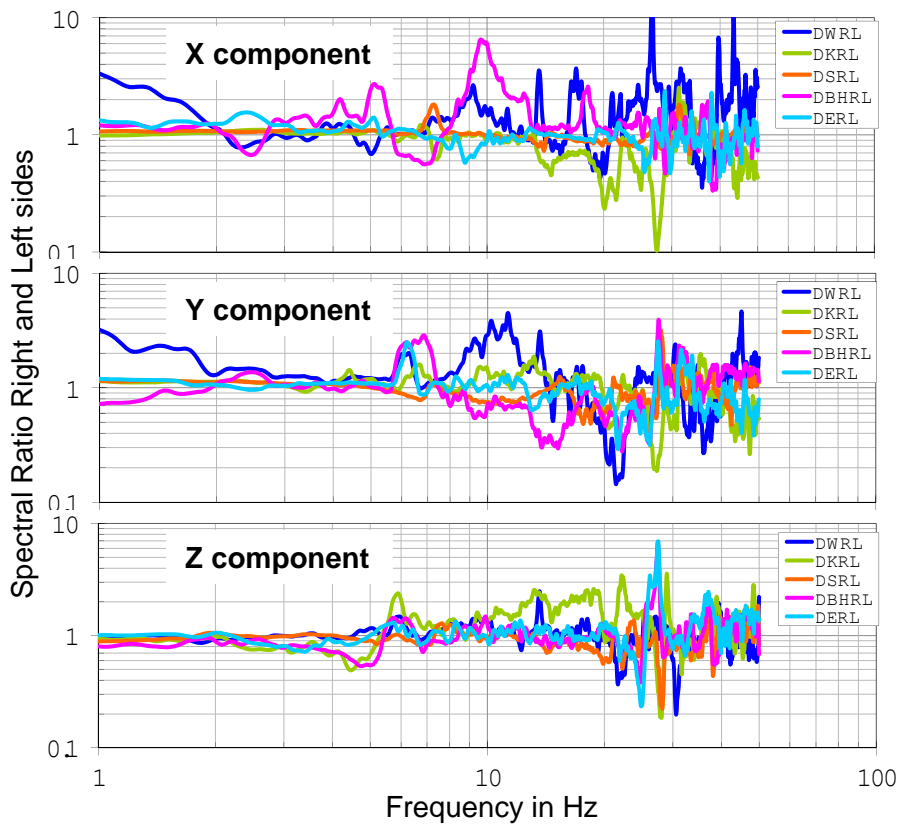


Figure 19. Spectral ratio of right and left sides (before removal of weight)

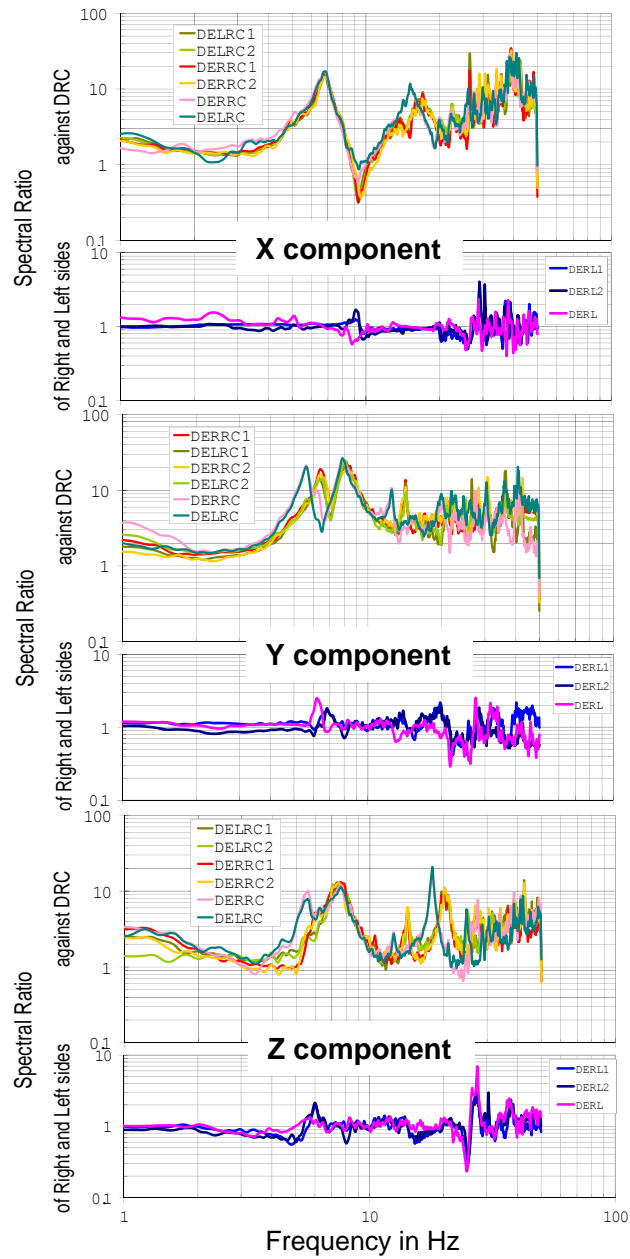


Figure 20. Spectral ratios between earlobes and DRC, and spectral ratio between right and left of earlobe (before and after removal of weight)

situation of the head on the vertical direction is mostly same for both left and right side.

The left and right motion is differing little from the points at left and right side at the earlobe or the points DSL and DSR at the supporting frame work. However, R/L ratio is about 0.6 at around 6.7 Hz, which estimated to be the resonance of the head, and it means that the left side motion at back of the head is 1.7 times larger than the right side motion. Also in case of back and forth motion, the left side motion is rather large at around 8 Hz as the predominating frequency range of it. These phenomena are noticed relating to the fact that the connecting situation to the body is differing between the left and right sides.

Hereafter, the authors will consider this situation in detail because the difference of the vibration characteristics for left and right side relate to the connecting situation of casting.

4.2.5 For a further understanding

Finally, an animation is developed as an attempt to grasp visually the total vibration characteristics of whole the Great Buddha with projecting not only the vibration mode of each component but also the vibration locus for each frequency to XY, YZ and XZ plane [6]. This animation draws a vibration locus considering the degree of correlation for the vibration direction component at each plane. Therefore, note that the movement at each plane is independent for each other and this animation does not draw one motion projecting to each plane. Also because the locus on this animation is drawn back to the measured point after one period, the drawing direction of the locus can be confirmed.

As mentioned above, it is confirmed from this animation that the vibration less than 10 Hz mainly makes the head move largely and various frequencies are appeared as a large motion of various portion continuously. Although this Great Buddha is bilaterally symmetric seating statue, the vibration characteristics are slightly differ between right and left sides and it is estimated to reflect the characteristics of this Great Buddha with a lot of connection.

The change of the characteristics caused by removal of the load on the jaw is unexpectedly large. However it is expected to be able to

grasp precisely the local situation with grasping the vibration characteristics by changing the load actively. Hereafter, the authors would like to continue research in detail keeping in mind these points.

5. Concluding remarks

It is quite important for the Great Buddha of Kamakura to understand the vibration characteristics of the head because it relates to integrity of the connection between the body and the head.

The report of a major repair in Showa era was done in 1960 says that the problem of the connection exists mainly at back of neck and there is little problem from the chest to front of neck. And it also says that although the portion back of neck at right side (west side) was almost succeeded to connect at the time of casting, that at left side (east side) was almost failed to connect and it was repaired by tinkering or other technique after casting.

As a result of microtremor measurement at some points in the head, the vibration less than 10 Hz predominates at the head. Also it is cleared that the vibration over 20 Hz predominates at the body and the predominant frequency of the vibration related to the connection between the body and the head is lower frequency less than 10 Hz.

The weight of the head has been estimated about 20 tons and it is remarkable that the vibration characteristics is significantly affected by change of the load about 155 kg with removal of the inner small Buddha and other deposits. It suggests that the welding connection moves with a certain level of degrees of freedom but the head vibrates as a unit. Therefore, it pointed out the necessity to consider carefully the connecting situation at each portion in the head. Hereafter it is expected to carry out more detailed measurement with increasing the number of measurement points around the connection between the head and the body to grasp the dynamic situation. It seems that it is necessary to take a proper countermeasure based on the result of this detailed measurement.

The frequency of the horizontal motion at the platform is 4.2 Hz, 5.6 Hz and 7.2 Hz, and these vibrations are torsional vibration except that at 4.2 Hz. So, sway vibration at 4.2 Hz of back and forth direction

is estimated to predominate during earthquake motion. In this time the amplification factor becomes large value 175 at the right side.

The gap between the stage and the body of the Great Buddha is about 2 cm and the amplitude of the motion at the stage might be estimated about 2 cm in maximum if the earthquake motion reaches 8 Gal or Japanese Seismic Intensity 3 at the floor of the Great Buddha, assuming that the amplification factor is kept during the earthquake motion. The earthquake motion larger than this has a possibility of collision against the body of the Great Buddha. It seems that it is necessary to take a countermeasure for conservation of the Great Buddha.

Acknowledgement

This investigation was conducted under the committee of repair for Great Buddha of Kamakura. The authors would like to express our deepest appreciation to the committee and relations.

References

- [1] Nakamura, Y., Saita, J., and Sato, T.: Application to World Heritage Sites, Workshop Proceedings on Increasing Seismic Safety by Combining Engineering Technologies and Seismological Data, Edited by M. Mucciarelli, M. Herak and J. Cassidy, Springer, pp.293-324, 2009.
- [2] Nakamura, Y., Saita, J., Tachibana, M., Morii, M., Inoue, S. and Ohmachi, T.: On the Dynamic Characteristics of Great Buddha of Kamakura and its surroundings (in Japanese with English abstract), Proceedings of the 13th Japan Earthquake Engineering Symposium, 2006.11.
- [3] Sekino, M. (editor): Report on Conservation of the Great Image of Buddha, National Treasure, Kotokuin-Temple at Kamakura (in Japanese with English summary), Kotokuin-Temple, 1961.7.
- [4] Sekino, Masaru: Seismic Reinforcement using Fiber Reinforced Plastic for the Great Buddha of Kamakura (in Japanese), "Seisan-Kenkyu" Monthly Journal of the Institute of Industrial Science, University of Tokyo, Vol.13, No.2, 1961.2.

- [5]Sato, Takao: Damage Pictures of Lanterns in Area of Kotokuin-Temple (in Japanese), private communication with the chief priest of Kotokuin-Temple, 2011.3.24.
- [6]SDR: Vibration Mode of the Great Bronze Buddha at Kamakura, www.sdr.co.jp/eng_page/paper.html, 2014.4.
- [7]CAD CENTER, www.cadcenter.co.jp.

Cracking pattern and seismic performance assessment of the Orvieto cathedral

Gerardo De Canio¹

Abstract

In this paper are described the in situ cracking pattern measurement and ambient vibration monitoring for the seismic performance evaluation of the Orvieto Cathedral, Italy, according the displacement based safety assessment. This requires, as a first step, the direct measurement of the cracking patterns and dynamic response of the structural macro elements of the cathedral due to weak vibrations induced by traffic and seismic micro tremors. Seismic assessment for this type of structure requires also the proper limit states definitions. In fact, in the case of historic monuments like churches, due to the presence of specific typology of macro elements: rigid blocks, complex vault systems, slenderness of the walls, presence of wide halls, domes and drums with particular geometry, is necessary to define the proper assessment procedures which are slightly different with respect those required for conventional civil or industrial buildings. Regarding the Ambient vibration monitoring, a new approach to estimate the participating masses associated to the macro element kinematics is defined: it is based on the frequency contribution to the Root Mean Square Acceleration, obtained by numerical integration of the Power Spectral Density (PSD) function. This information, when associated to the analysis of the Real and Imaginary part of the Cross Spectral Density (CSD) function between the acceleration time histories at different points, allow to identify the principal (at least first and second) mode shapes of the structure.

¹ ENEA, Roma, Italy.

1. Introduction

The Orvieto Cathedral is one of the most significant monuments representative of the roman architecture of the late XII century in Italy. According to the historic documents available at the Archive of the *Opera del Duomo di Orvieto* (OPSM), the first stone of the cathedral was positioned the year 1290. The work continued up to the crisis occurred the year 1308, when the architectural asset of the cathedral had a strong modification with the adjoin of massive counterforts and arches to contrast structural instability of the transept. Successively, by means of the architect “universalis magister” Lorenzo Maitani (Siena 1270-75, Orvieto 1330), the counterforts and arches were transformed in the walls of the St. Brizio Chapel, where Luca Signorelli (XV century) realized the pre-Michelangelo “Giudizio Universale”, and the Corporale Chapel hosting the reliquary of the “Miracle of Bolsena”. Also the original design of the mono-cusped facade was redesigned and transformed by Maitani in the actual magnificent tricuspid facade. Therefore the actual architectural configuration of the cathedral consists of three principal corpus composed by the tricuspid facade, the main nave and the massive transept. The three corpus have different masses and stiffness and dynamically interact each other. The cracking pattern of the three corpus, together with their dynamic characterization is the first step for assessing the seismic vulnerability of the cathedral. Due to the multidisciplinary mix of knowledge and competences required, the following integrated technologies are applied by ENEA (the Italian National Agency for the New technologies, Energy and Sustainable Economic Development) for the cracking pattern identification and structural characterization to assess the seismic vulnerability the Orvieto Cathedral:

- RFI (Radio Frequency Identification)
- FBG (Fiber Bragg Grating)
- 3D Colours Lidar
- Scan Laser
- Sonic Tomography
- Dedicated array of seismic stations
- Ambient vibration monitoring
- SAR (Synthetic Aperture Radar)



Figure 1. The Orvieto Cathedral.

To achieve the Seismic Safety evaluation LV3 defined by the Italian guidelines **D.P.C.M. 09.02.11**, “Linee Guida per la valutazione e riduzione del rischio sismico del Patrimonio Culturale tutelato con riferimento alle **NTC 2008**”, (in accordance with the text approved by the Consiglio Superiore dei Lavori Pubblici (CSLP) the 2010 July 30 and with **DM 14.01.2008**), the following steps are applied:

- Global 3D model (linear elastic FEM to identify the zones of max strain energy).....
- Macro element identification : distribution of the seismic action between the macro elements , depending on the different mechanic characteristics;

The distribution of the seismic forces must guaranty the equilibrium regarding the horizontal actions (longitudinal and transversal). The fig. 2 show two of the principal collapse mechanisms defined in the D.P.C.M. and identified for the Orvieto cathedral, together with the out of plane instability of the façade.

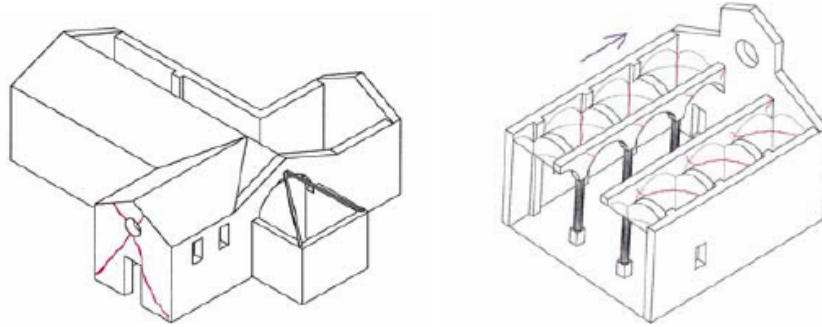


Figure 2. Principal collapse mechanisms of structural macro elements for a church: shear stresses for the wall of transept; longitudinal response of the main nave.
From the Abacus of the collapse mechanisms of a church, D.P.C.M. 09.02.11

The three main corpus of the Orvieto Cathedral (and their connections) are represented in fig.3, they correspond to three structural macro elements: Façade, Main Nave, Transept.

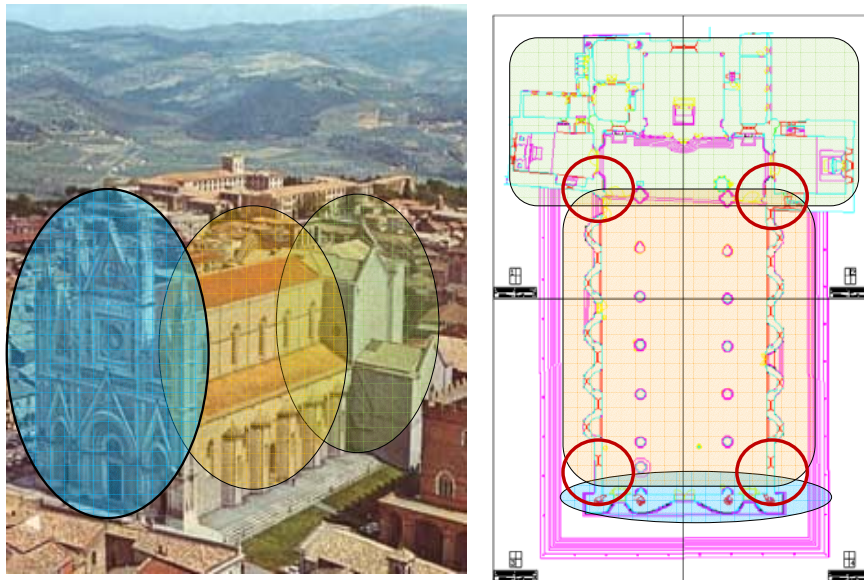


Figure 3. The three macro elements of the Orvieto Cathedral: facade, nave, Transept.



Figure 4. Orvieto Cathedral: the tri cusped façade connected to the main nave



Figure 5. Orvieto Cathedral: the main nave



Figure 6. Orvieto cathedral: The transept counterforts built after the crisis of the year 1308 become the walls of the Corporale Chapel realized by Lorenzo Maitani.

2. Study and monitoring the crack pattern of the Orvieto cathedral

In this chapter is illustrated the approach to identify the Crack pattern of the columns and walls of the main nave to assess its structural vulnerability. The first step was to define a taxonomic identification of each crack at the base of the columns and at the connections nave-façade (West side) and nave-transept (East side), and then monitor the evolution during time. The crack pattern has been identified by means of high resolution photogrammetry imported and superposed to vector drawing CAD. Furthermore, a thermograph image restitution of the walls of the nave defined the degradation zone.



Figure 7. Orvieto cathedral: Degradation of the walls at the North-East connection between the Main Nave and the Transept

Regarding the columns, the following taxonomic definition is defined:

- 2D drawing representation of the column and definition of eight sectors : S, SE, E, NE, N, NW, W, SW.
- identification number of the fracture, the level and chromatic identification of the stone, the type of fracture (e.g. crack of a stone or crack of the joint between stones)
- length and thickness measurement of each fracture .

Table 1: Taxonomy identification of the fractures for the column N°1

| Sector | Chromatic level | fracture | Foto | Single/multiple S/M | Stone/Jointo P/G | thickness mm |
|--------|-----------------|----------|------|---------------------|------------------|--------------|
| SE | 4B | 1 | A | M2 | P | 0 |
| SE | 5N | 1 | A | S | G | 0 |
| SE | 6B | 1 | A | S | P | 0 |
| E-NE | 1N | 2 | B | M2 | G | 0 |
| E-NE | 2B | 2 | B | M2 | P | 1 |

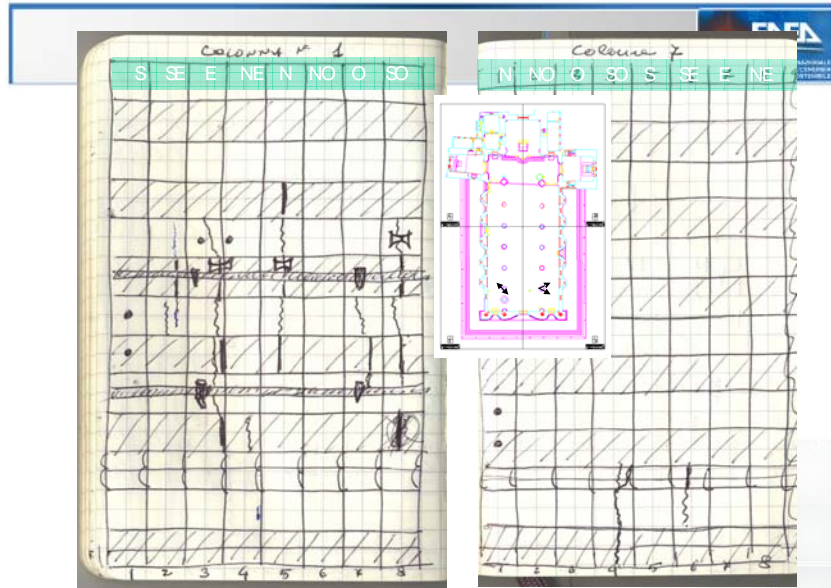


Figure 8. Orvieto cathedral: first representation of the Crack pattern and orientation relative to the columns N° 1 and N°7 of the main nave

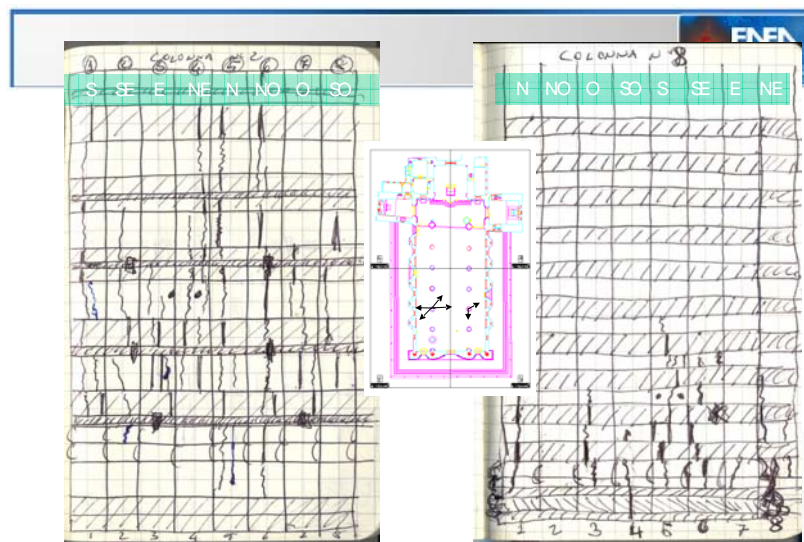


Figure 9. Orvieto cathedral: first representation of the Crack pattern and orientation relative to the columns N° 2 and N°8 of the main nave

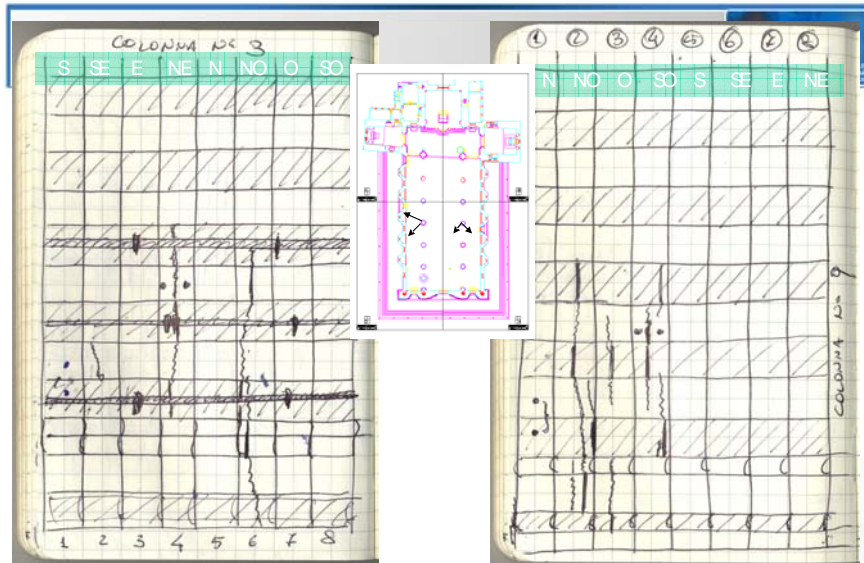


Figure 10. Orvieto cathedral: first representation of the Crack pattern and orientation relative to the columns N° 3 and N° 9 of the main nave

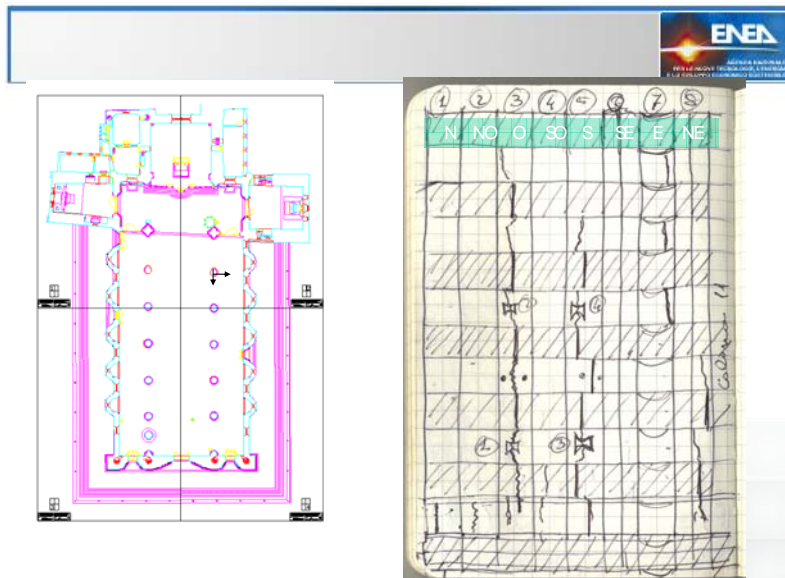


Figure 11. Orvieto cathedral: first representation of the Crack pattern and orientation relative to the column N° 11 of the main nave; no cracks for the column N° 10.

The following considerations arisen after this first phase of the crack monitoring:

- New Cracks occurs on the columns after 2009 April 6
- The new cracks involved the north and south nave columns
- NE-SW orientation of the cracks
- Large cracks at the base of Columns N°2 and N°11. New cracks at the base of the column N° 8 due to the L'Aquila earthquake.
- Need to urgent reinforce the columns N° 2, 8, 11

3. Seismic Safety evaluation LV3 for the Orvieto Cathedral

To achieve the Seismic Safety evaluation LV3 the Italian *guidelines allow*:

- Global 3D model (linear elastic FEM to identify the zones of max strain energy).....
- Macro element identification : distribution of the seismic action between the macro elements , depending on the different mechanic characteristics;

The distribution of the seismic action by macro elements must guaranty the equilibrium regarding the horizontal actions (longitudinal and transversal). The figures 12-19 illustrate the Abacus of collapse mechanisms for the Orvieto Cathedral according to abacus defined in the D.P.C.M. 09.02.11.

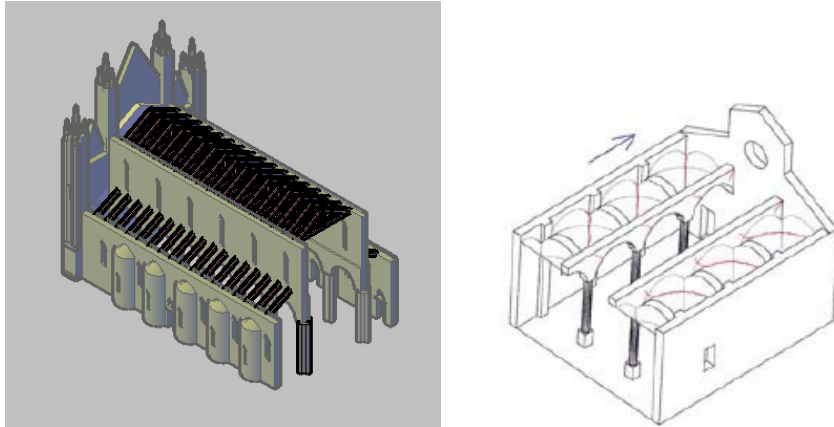


Figure 12 . Orvieto Cathedral : Longitudinal instability of the main Nave columns and out of plane mechanisms for the facade

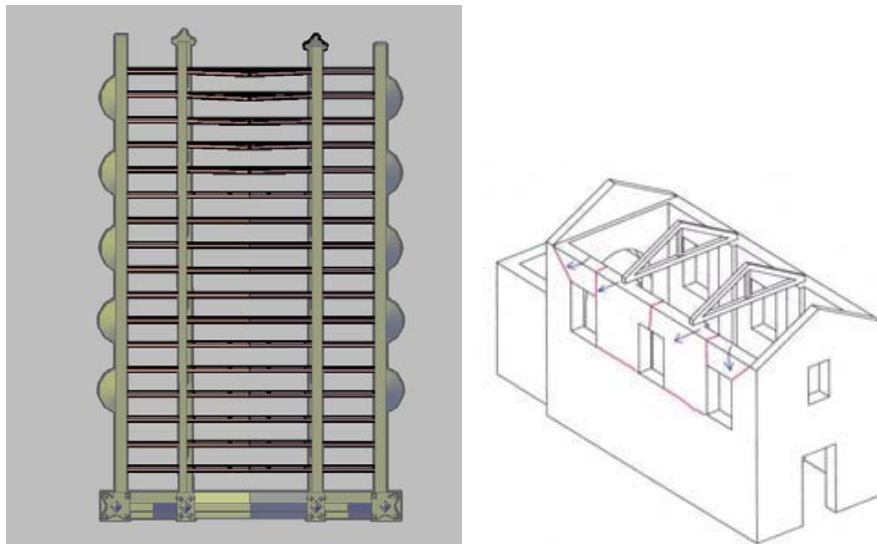


Figure 13. Orvieto Cathedral : Roof wooden Elements of the main and lateral nave

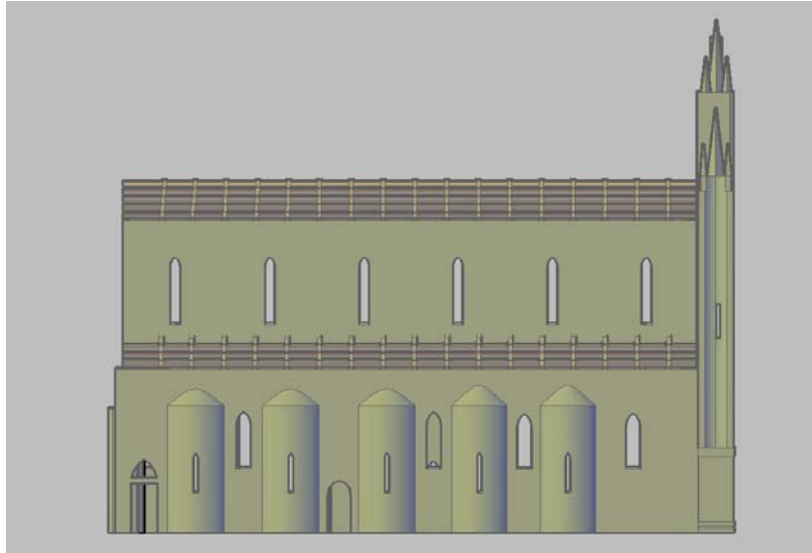


Figure 14. Orvieto Cathedral : North side main nave and North side lateral nave with cylindrical chapels

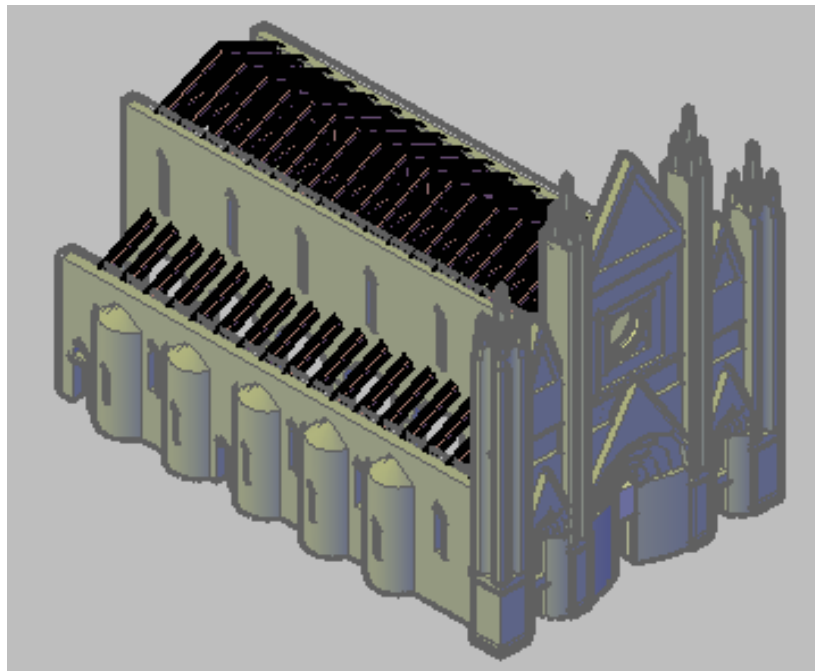


Figure 15. Orvieto Cathedral : The nave roofs and three cusped facade

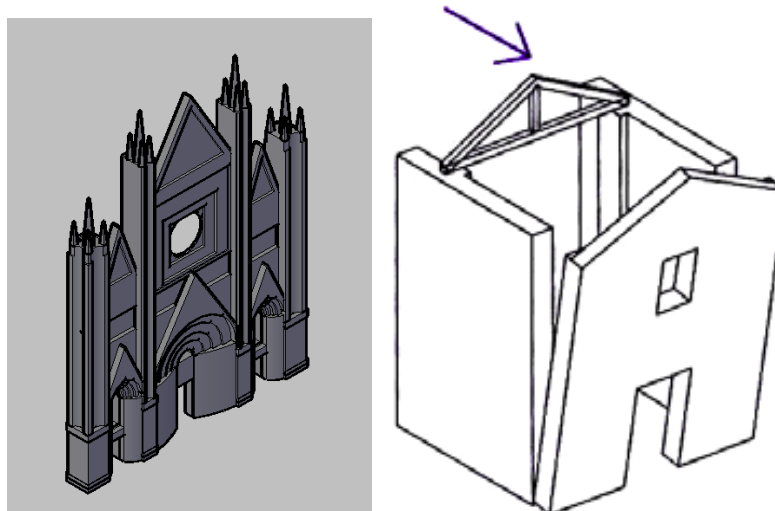


Figure 16. Orvieto Cathedral: Out of plane overturning mechanism of the facade

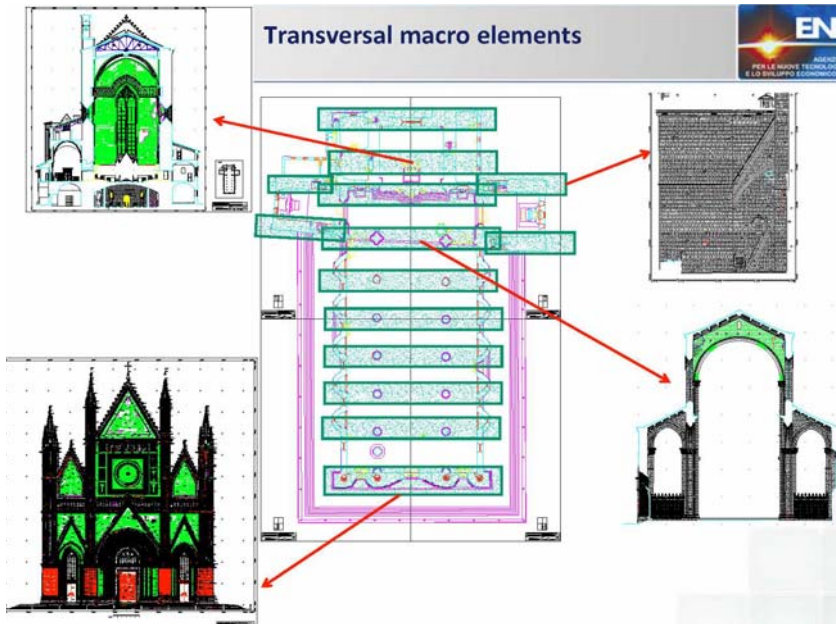


Figure 17. Orvieto Cathedral: Transversal macro elements

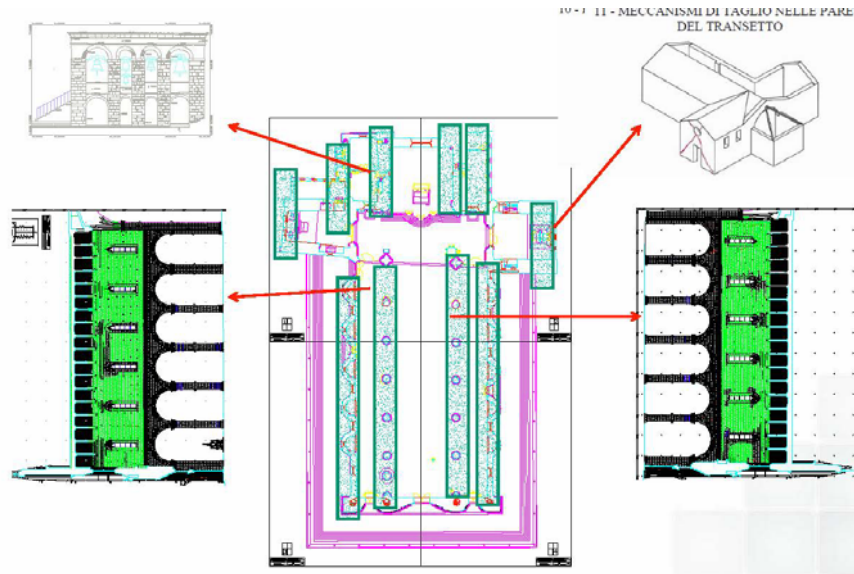


Figure 18 Orvieto Cathedral: Longitudinal macro elements

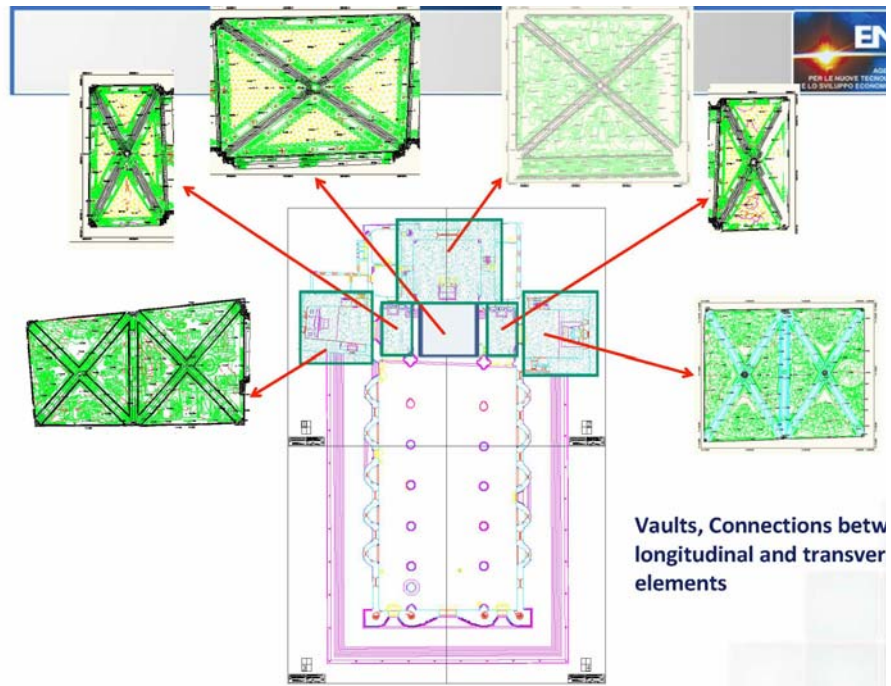


Figure 19 Orvieto Cathedral: Transept Vaults macro element

4. The FE model of the facade

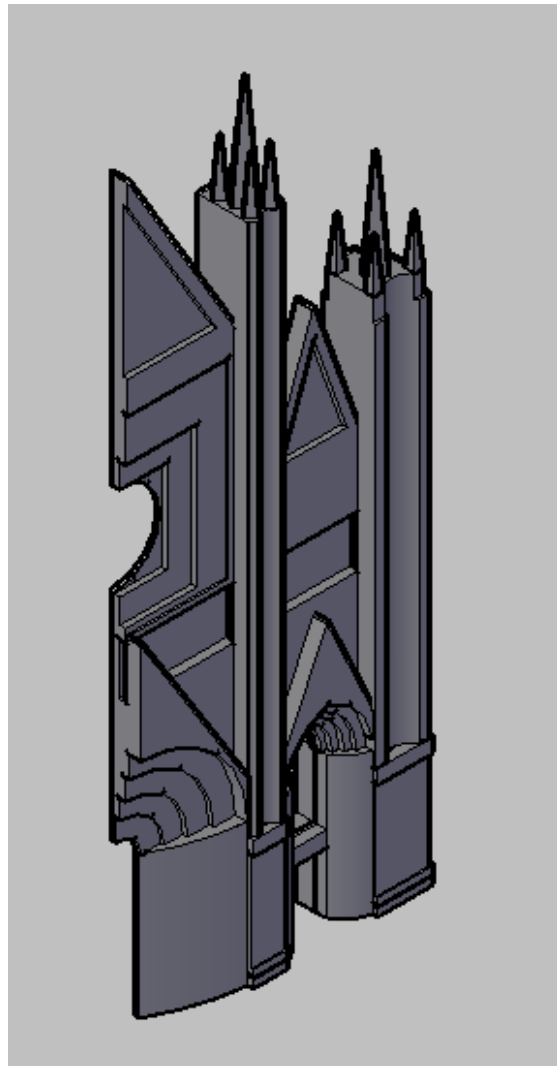


Figure 20. Orvieto Cathedral: 3D CAD drawing for the FE model of the facade

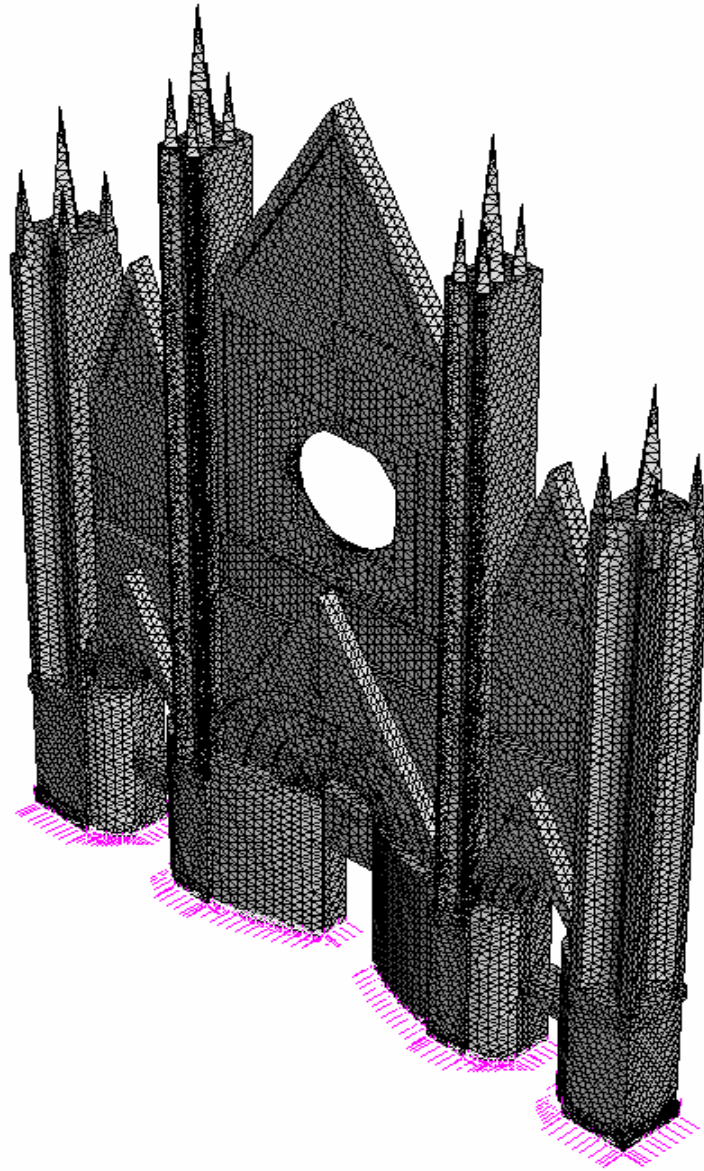


Figure 21. Orvieto Cathedral: 3D mesh for the FE modeling of the facade

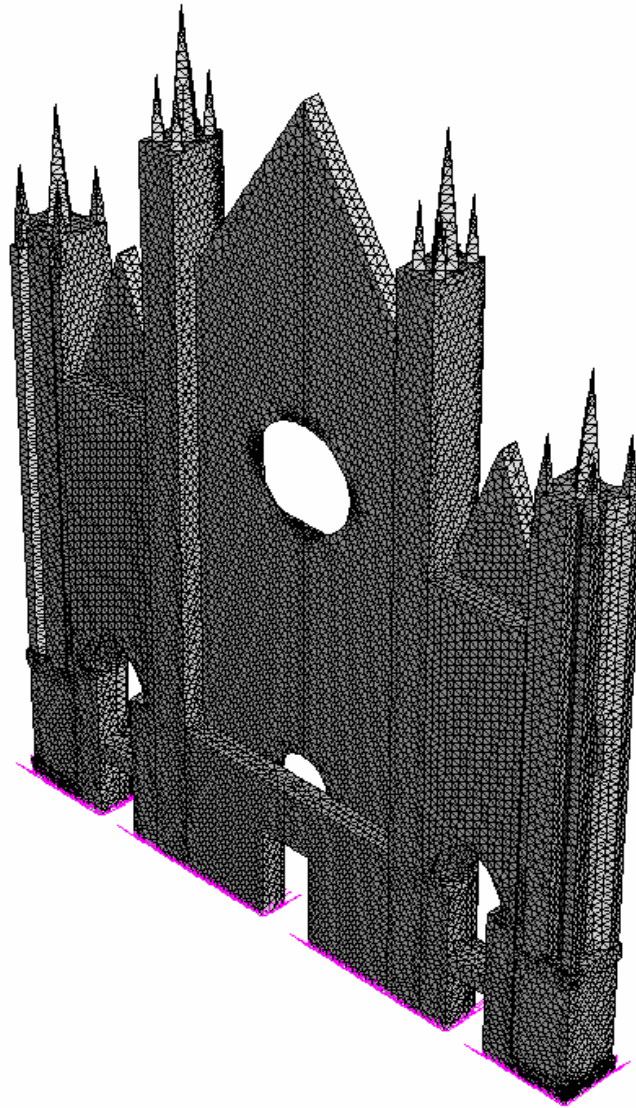


Figure 22. Orvieto Cathedra: *contra façade* (internal side of the *façade*)

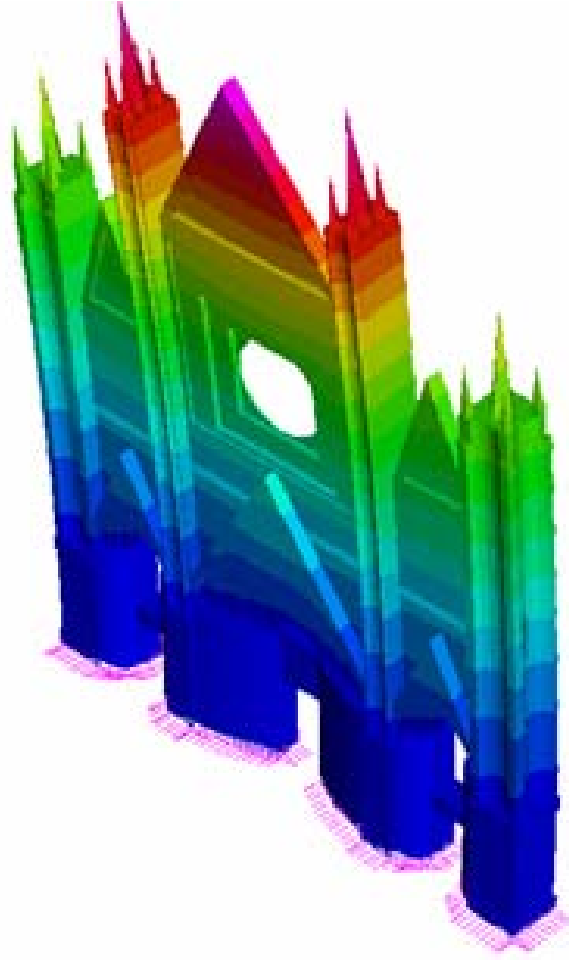


Figure 23. Orvieto Cathedral: FE Analysis of the facade. First mode

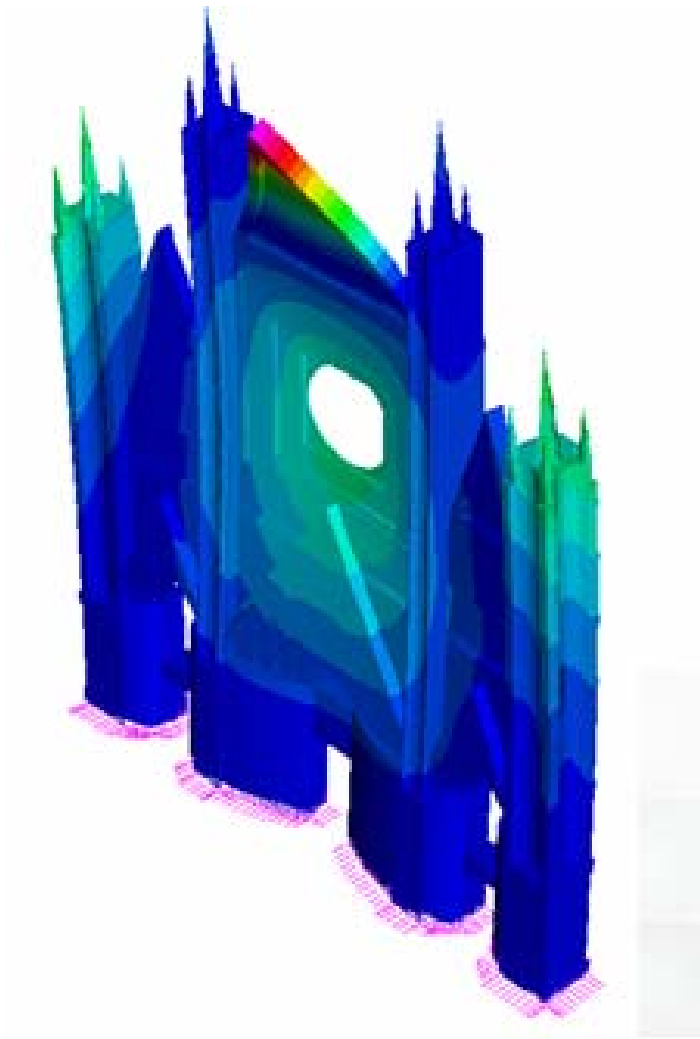


Figure 24. Orvieto Cathedral: FE Analysis of the facade. Second mode

4. Monitoring of the ambient vibrations and dynamic characterization of the macro elements

To achieve the Seismic Safety evaluation LV3 must define the Ultimate limit state ground acceleration, i.e. the ULS seismic input. Therefore 3 dedicated seismic stations have been installed (using velocimeters model SL06 of the SARA electronic instruments s.r.l). The first was positioned at the base of the Orvieto Cliff, the second in a cave close to the cathedral and the third in the crypt at the east side of the cathedral



Figure 25. Orvieto Cathedral: Velocimeters' placement of the three stations seismic array

Ambient seismic noise (HVSR)
 (amplitudes 10^{-4} - 10^{-2} mm)
 Sensor: 3D velocimeter
 Scope: HVSR Analysis
 $f = V_s / 4H$
 f = frequency
 V_s = S wave velocity

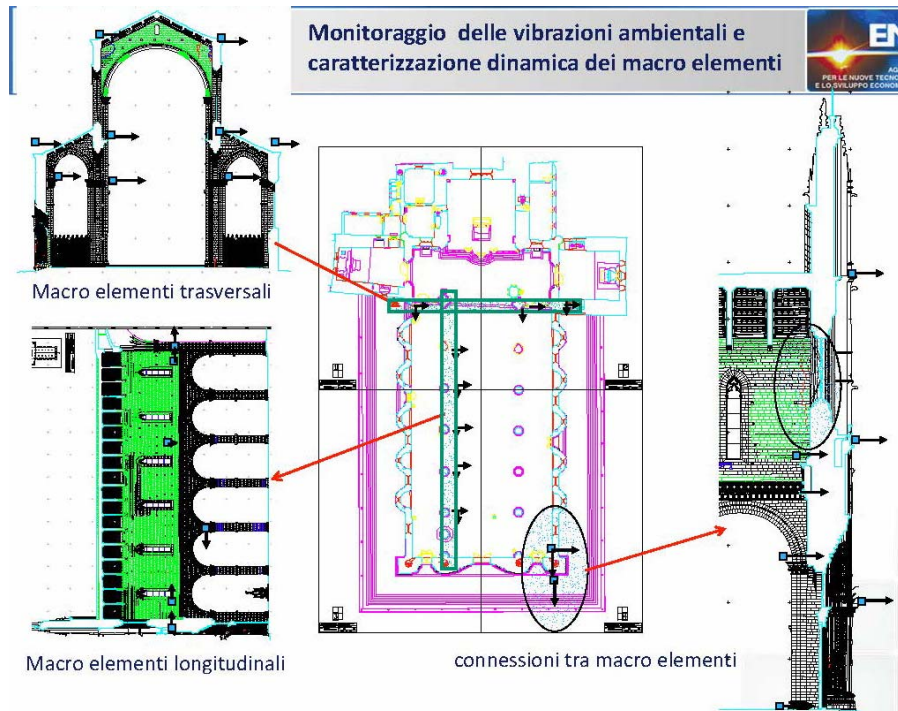


Figure 26. Orvieto Cathedral: monitoring the connection between macro elements

Measurement points:

- 1 South Column of the main arch
- 2,3,4 South nave wall
- 5,7 Contra fachade
- 8,9,10 North Nave wall
- 11 Central arch pile
- 6 south tower
- 12 north tower
- 13 Triassiale Colonna N° 8
- 14 Triassiale Colonna N° 2

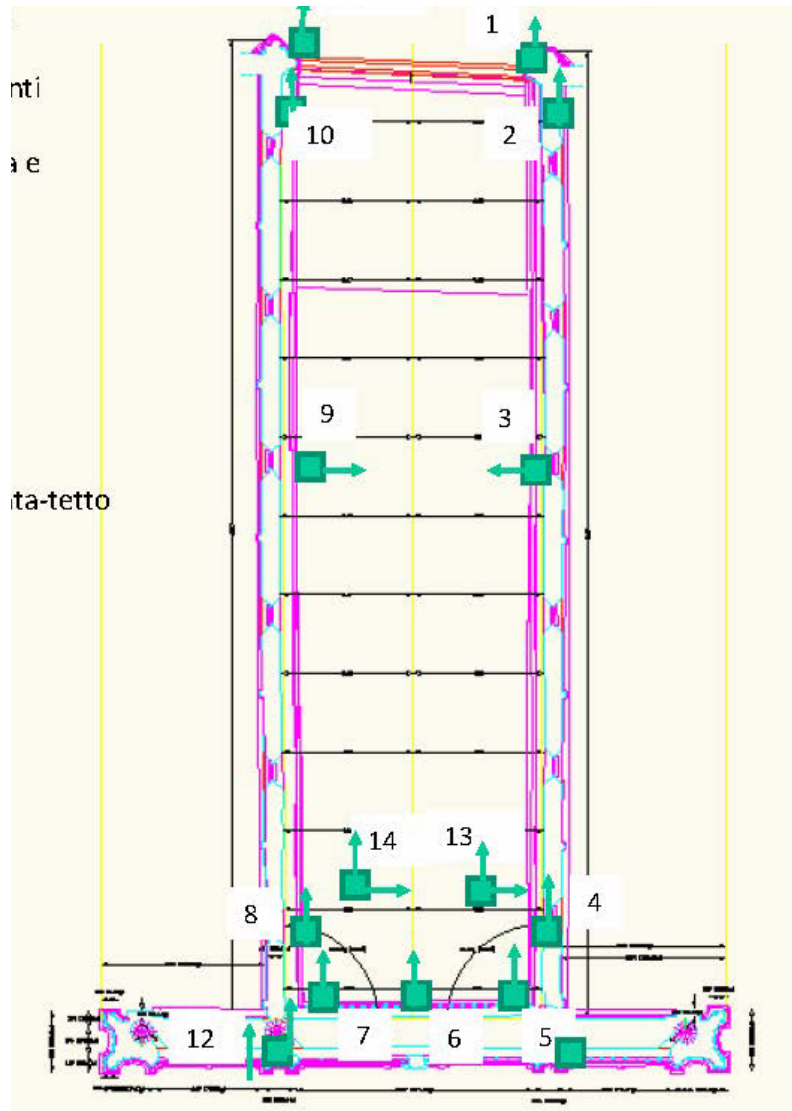


Figure 27. Orvieto Cathedral: measurement points of the accelerometers for ambient vibrations

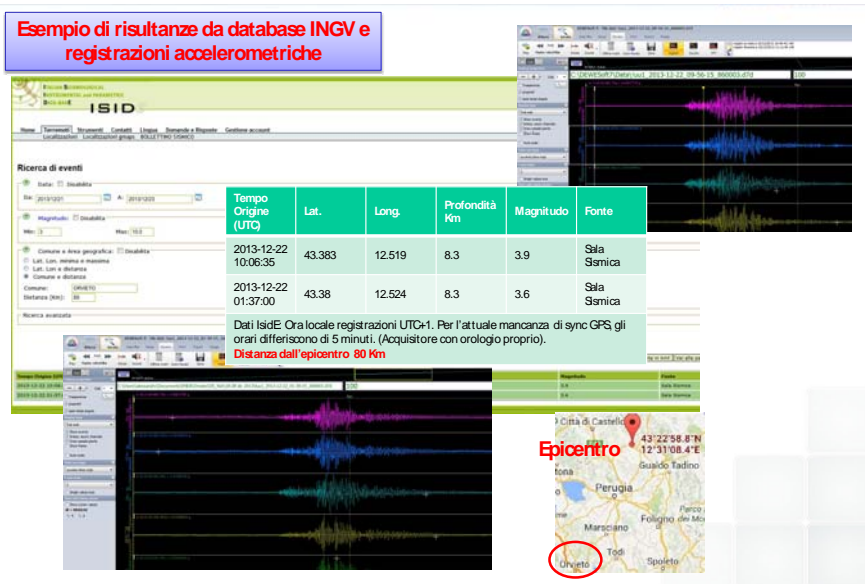


Figure 28. Orvieto Cathedral: time histories of the event 2013 dec 22, 01:37UTC at Città di Castello.

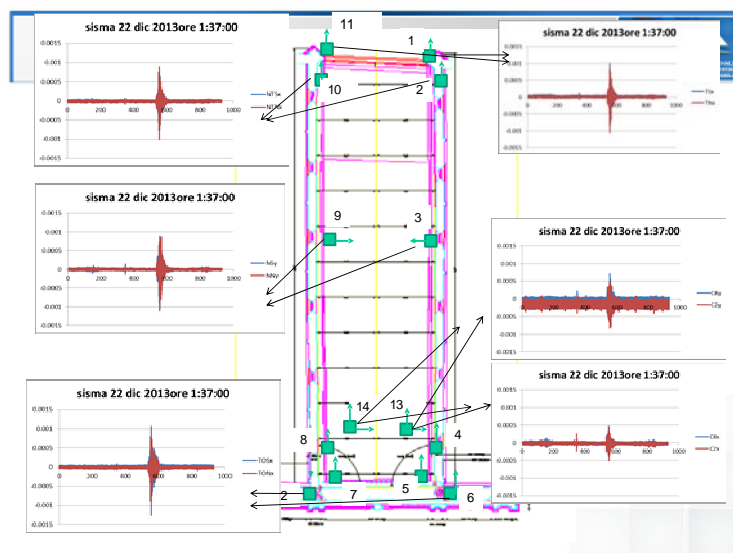


Figure 29. Orvieto Cathedral: time histories recorded the 2013-12-22, 01:37UTC.

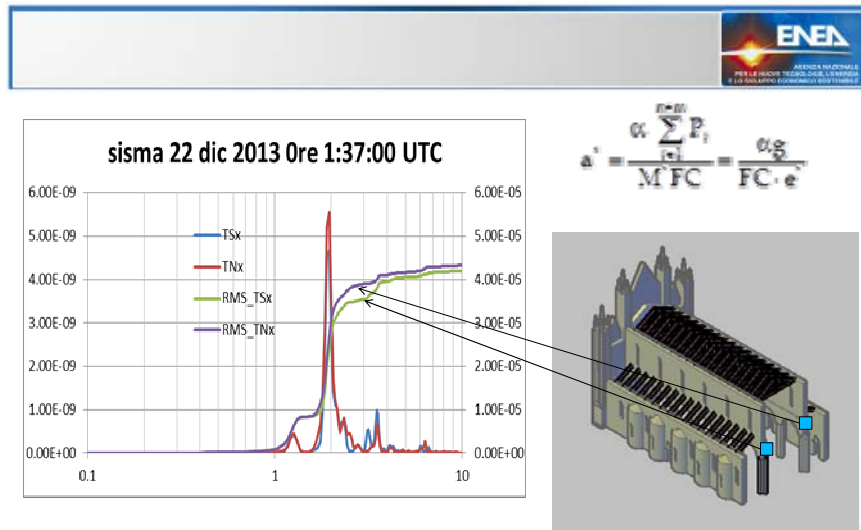


Figure 30. Orvieto Cathedral: Power Spectral Density (PSD) and frequency contribution to the Mean Square Root Acceleration (gRMS) at the transept columns

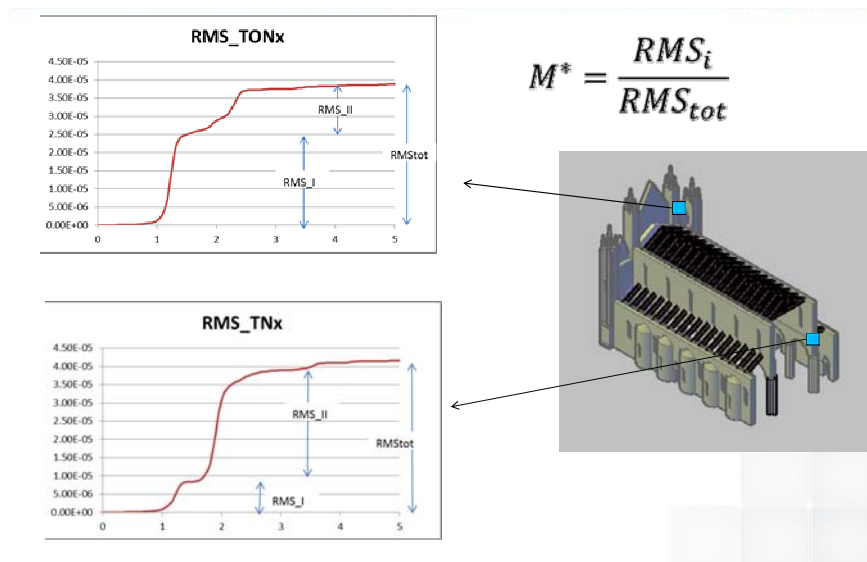


Figure 31. Orvieto Cathedral: frequency contribution to the Mean Square Root Acceleration (gRMS). The gRMS frequency contribution allow to estimate the participating masses to calculate the spectral acceleration activating the collapse kinematics according the LV3 seismic verification.

The analysis of the real and imaginary part of the Cross Spectral Density between different time histories allow to evaluate the critical frequencies related to the (at least) first and second modes of the façade. The first (flextional) mode at 1.27 Hz and the second (torsional) mode at 2.25 Hz have been detected.

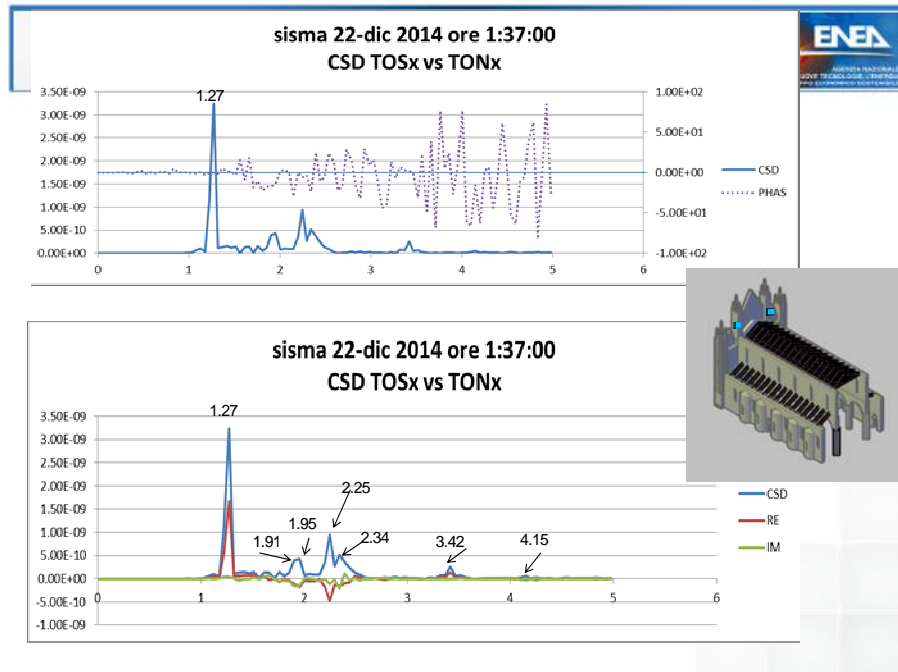


Figure 32. Orvieto Cathedral: Critical frequency identification by mean of the CSD Real and Imaginary analysis of the accelerations measured on the North and South Towers..

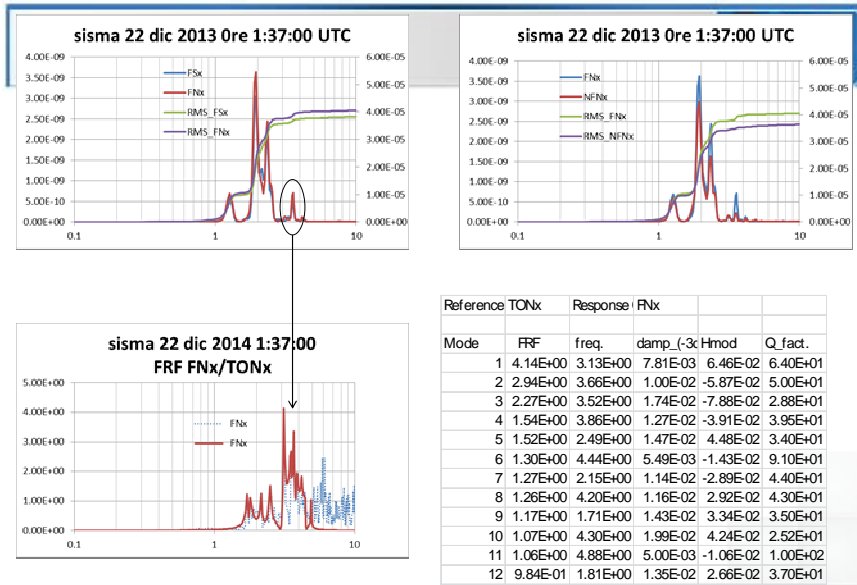


Figure 33. Orvieto Cathedral: Comparison between PSD of North façade and FRF between North Tower (reference) and North façade (Response)

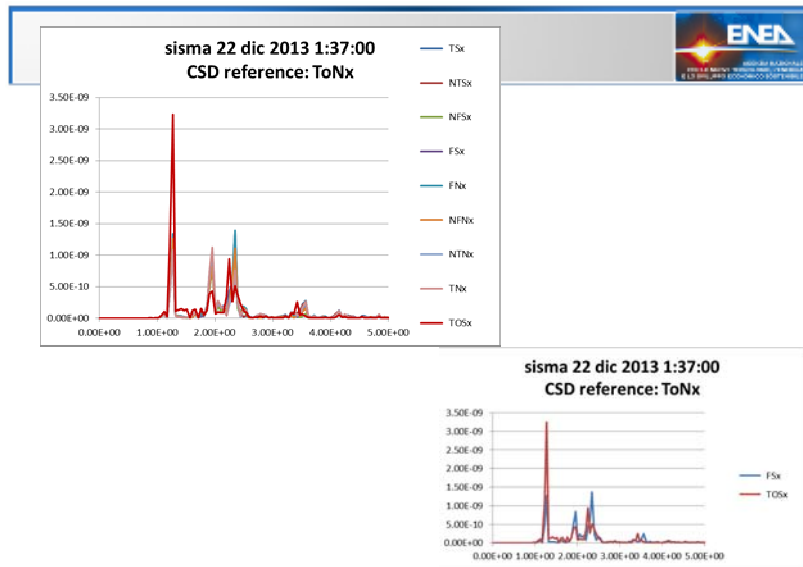


Figure 34. Orvieto Cathedral: CSD between North Tower (reference) and the other measurement points

5. Performance Based Approach

The scope is to verify if the structure fulfill the Limit state performance levels, graduated to the expected seismic input associated to different return periods and probability of occurrence. The structural capacity curve is compared with the seismic demand in terms of response spectra by means of nonlinear static and kinematic analysis. The estimation of the performance level is strongly dependents by the confidence factor (FC) about the knowledge level of the structure. According the **D.P.C.M. 09.02.11**, “Linee Guida per la valutazione e riduzione del rischio sismico del Patrimonio Culturale tutelato con riferimento alle **NTC 2008**” the FC levels defined at this stage are :

- Geometric survey: complete-> FC1=0;
- Identification of the historic and architectonic specificity: completa -> FC2=0;
- Mechanic properties
 - evaluation of the global mechanisms: limited-> FC3 = 0.06
 - evaluation of the local mechanisms -> FC3 = 0.12
- Ground and foundations: limited -> FC4 = 0.06.

In brief, the following FC are evaluated:

- Global mechanisms: Confidence factor FC = 1.12
- Local mechanisms: Confidence factor FC = 1.18

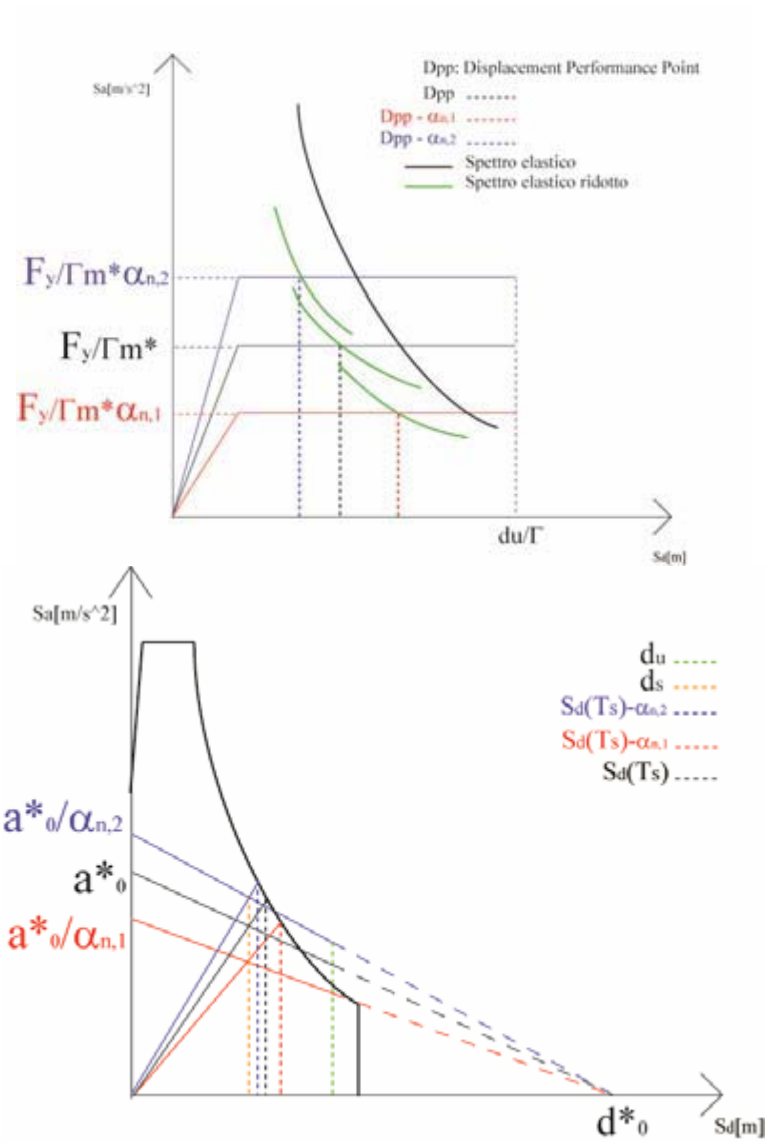


Figure 35. Static and kinematic non-linear analysis.

Scheme of performance based calculation according the D.P.C.M. 09.02.11,

Schema di calcolo per la verifica prestazionale, in accordo D.P.C.M. 09.02.11, "Linee Guida per la valutazione e riduzione del rischio sismico del Patrimonio Culturale Tutelato"



| Verifica Prestazionale del macro elemento N° | Valore | units |
|---|--------|---------------------|
| Meccanismo di collasso N° | | |
| PLV ---> Moltiplicatore di attivazione del cinematismo: a_0 | | [-] |
| Spostamento normalizzato $d^* = d_u \frac{\sum_{i=1}^{n_{mod}} P_i \delta_{x,i}^2}{\delta_{x,i} \sum_{i=1}^{n_{mod}} P_i \delta_{x,i}}$ | | [m] |
| Accelerazione spettrale $a^* = \frac{C_{s,i} \cdot a_{g,i}}{C_{s,i} \cdot C_{s,i}}$ | | [m/s ²] |
| Accelerazione corrispondente allo spostamento d_s | | [m/s ²] |
| Periodo Secante T_s | | [sec] |
| Spettro di spostamento corrispondente a T_s : $S_{de}(T_s)$ | | [m] |
| Verifica $d_u > S_{de}(T_s)$ | | S/No |

Figure 36. Scheme of performance based calculations

6. Orvieto Cathedral: Two Statues positioned on the façade



Figure 37. Orvieto Cathedral: Positioning of the two statue of S. Michel Arcangel and the majesty on the façade



Figure 38. Orvieto Cathedral: The majesty on the main portal

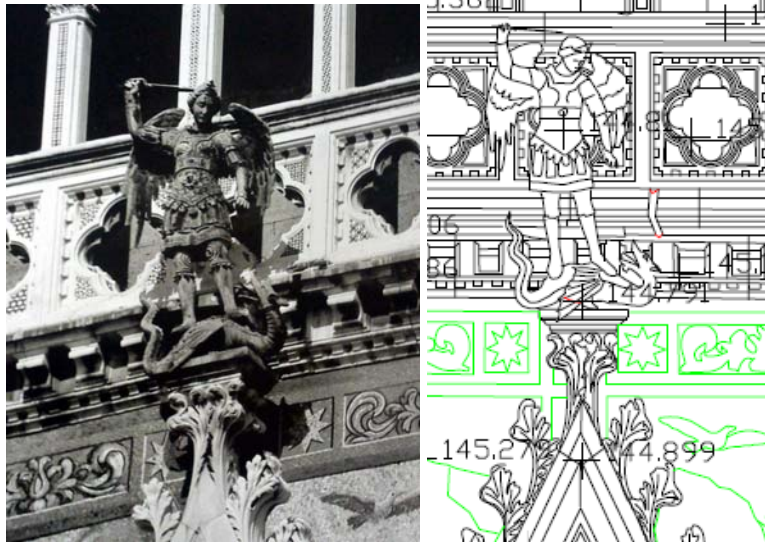


Figure 39. Orvieto Cathedral: S. Michel Arcangel on the left cuspid of the facade

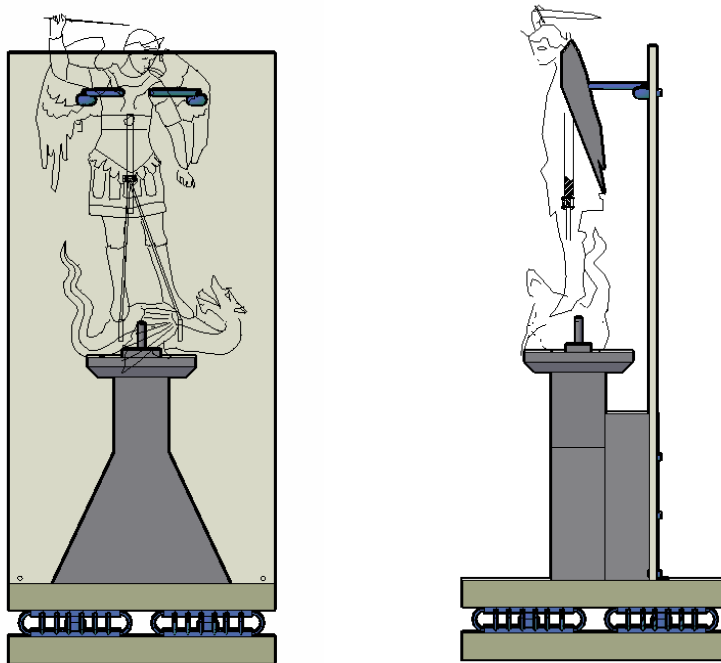


Figure 40. Orvieto Cathedral: The anti seismic basement for the original statue of S. Michel Arcangel in the MODO (Museum of the Opera del Duomodi Orvieto)

7. Conclusions

The multidisciplinary approach of a large spectrum of integrate technologies allows the cracking pattern identification and measurement and the structural dynamic monitoring of the Orvieto Cathedral in order to assess the seismic vulnerability of the entire structure and its structural macro elements. A new approach to estimate the participating masses associated to the macro element kinematics have been defined (see. Figs. 30-31), it is based on the frequency contribution to the Root Mean Square Acceleration, obtained by integrating the Power Spectral Density (PSD) function. This information, when associated to the analysis of the Real and Imaginary part of the Cross Spectral Density function between two acceleration time histories allow to identify the principal (at least first and second) mode shapes.

8. Acknowledgement

The author wishes to thank the “curator” of the museum MODO (Museo Opera del Duomo di Orvieto) Alessandra Cannistrà and Elisabetta Andreani for their support during the complex work on the Majesty and ”San Michele Arcangelo”; The Architect Maurizio Damiani for the active support to the monitoring of the Orvieto Cathedral. Special thanks to Alessandro Colucci and Francesco Di Biagio for the vibration monitoring and data acquisition, Ivan Roselli, Alessandro Giocoli, Salomon Hailemikael and Dario Rinaldis for the seismic monitoring, Marialuisa Mongelli and Angelo Tati for the FEM modelling, Laser Scanning, Sonic tomography, thermography and crack pattern monitoring, Paolo D’Atanasio and Alessandro Zambotti for the RFID technology, Michele Caponero for the FBG monitoring of the cracking pattern, Giorgio Fornetti for the 3 Colour Lidar analysis .

REFERENCES

- De Canio G. (2008). Seismic early warning systems for strategic infrastructures and CUHES. *The 14th World Conference on Earthquake Engineering* October 12-17, 2008, Beijing, China.

- G. Croci, A. Viskovic, A. Herzalla, G. De Canio, M. Erdik, M. Mongelli, I. Roselli, Large masonry models study implementing shaking table tests: Hagia Irene case study. Part II: actions, energy evaluations, dynamic behaviour, 3rd Euro Mediterranean Symposium On Advances in Geomaterial and Structures (AGS'10), 10-12 May, Djerba, Tunisia, 2010.
- De Canio G. (2011). Basi Antisismiche in marmo per i bronzi di Riace. *Archeomatica N°1* **6-10** Dec. 2011
- G. Croci, A. Viskovic, A. Herzalla, M. Erdik M. Akdogan, G. De Canio, L. Antonelli, Seismic assessment by numerical analyses and shaking table tests for complex masonry structures: The Hagia Irene case study, *Advanced Materials Research*, 133-134 (2010) 777-782.
- G. De Canio, P. Andersen, I. Roselli, M. Mongelli, E. Esposito, Displacement Based Approach for a Robust Operational Modal Analysis, 29th IMAC, a Conference on Structural Dynamics, 31 January – 3 February, Jacksonville, Florida, USA, 2011.
- De Canio G., Mongelli M., Roselli I., Lagomarsino S., Rossi M. 2013: Coriolis forces and Rocking To Precession (RTP) free Oscillations of the Obelisco Lateranense. In Proc. ANIDIS2013, 30 Giugno-4 Luglio 2006, Padova, Italy
- De Canio G.: Early Protection Of Strategic Infrastructures And High Vulnerable Statues In Italy. International conference on “Complexity in earthquake dynamics: From nonlinearity to earthquake prediction and seismic stability” Tashkent (UZ) January 25 – 26, 2012.
- De Canio G., Clemente P., Mongelli M., Roselli I., Rinaldis D., Saitta F., Lagomarsino S., Rossi M., 2012, Performance based approach in the assessment of the obelisco Lateranense in Roma, in Proc. of 8th International Conference SAHC (Structural Analysis of Historical Constructions), 15-17 Ottobre 2012, Wrocław, Poland
- De Canio G., 2012, Marble Devices for Base Isolation of the two Bronzes of Riace: a proposal for the Davis of Michelangelo, in Proc. of 15th World Conference on Earthquake Engineering, 24-28 sept 2012, Lisboa, Portugal
- De Canio G.: Early Protection Of Strategic Infrastructures And High Vulnerable Statues In Italy. International conference on “Complexity in earthquake dynamics: From nonlinearity to earthquake prediction and seismic stability” Tashkent (UZ) January 25 – 26, 2012
- De Canio G., Modena C, 2013: Earthquake Protection Of Movable And Semi-Movable Cultural Assets In Their Exposition Sites. In Proc. ANIDIS2013, 30 Giugno-4 Luglio 2013, Padova, Italy
- G. De Canio, M. Mongelli, I. Roselli, 3D Motion Capture Application to Seismic Tests at ENEA Casaccia Research Center: 3DVision System and DySCo Virtual Lab, *WIT Transactions on The Built Environment*, 134 (2013) 803-814. Information on <http://www.afs.enea.it/project/dysco>.

Effects of ambient vibrations on heritage buildings: overview and wireless dynamic monitoring application

Giorgio Monti¹, Fabio Fumagalli², Giuseppe Carlo Marano³,
Giuseppe Quaranta¹, Rossella Rea⁴, Barbara Nazzaro⁴

Abstract

Growing awareness of the negative effects due to ambient vibrations caused by transportation infrastructures in historical centers is attributable to the high vulnerability of heritage buildings, as a consequence of deterioration phenomena and damages that reduced the structural capacity of such valuable constructions over the past centuries. As the mobility demand increases, several cities hosting heritage buildings are subjected to raising traffic loadings, so that construction of new infrastructures is often required. Hence, assessing the effects of short-term vibrations due to construction activities or the consequences of long-term vibrations caused by traffic is very important for the preservation of cultural heritage. An operative approach for evaluating the effects of ambient vibrations based on experimental measurements is a useful tool when a new infrastructure is being built, and can support strategic decisions for the elaboration of transportation plans at the urban level. Therefore, an overview is here presented of existing studies, guidelines and codes that provide pertinent information on this topic. Of special importance is the analysis of existing proposed thresholds, i.e. limit values that, if complied with, damage due to ambient vibrations is not likely to occur. On the basis of such overview, the selection of threshold values for the Flavian Amphitheater is discussed, along with current efforts towards a wireless dynamic monitoring of its dynamic response.

1 Sapienza University of Rome, Italy.

2 Architect, PhD, Italy.

3 Technical University of Bari, Italy.

4 Special Superintendence for the Archaeological Heritage of Rome, Ministry of Heritage, Culture and Tourism, Rome, Italy.

1. Introduction

Ambient vibrations arising from man-made sources, including construction activities, vehicle and rail traffic, may interfere with the surrounding built environment. This is a critical source of concerns for historical centers as specific issues usually concur to increase the global vulnerability [1]. The most relevant one is due to the presence of heritage buildings or buildings protected by special laws because of their importance. Although small amplitude vibrations do not represent, in general, an impellent hazard for the structures, they can increase (over the years) the structural vulnerability in damaged and/or deteriorated elements. Vibrations with a high number of cycles acting on old masonry structures lead to a reduction of the strength due to deterioration of the mortar, thus causing its detachment from the bricks. Additionally, problems attributable to raising mobility demand also combine with existing structural deficiencies in heritage building. For instance, vibrations induced by vehicles and trains travelling become very dangerous when acting on structures that withstood severe dynamic loads (e.g., earthquakes). The excessive roughness of road pavements due to poor maintenance also causes dynamic stress on adjacent buildings. Moreover, the need of high-capacity/high-frequency public transportation systems in modern cities often requires the construction of new infrastructures which, in turn, can induce additional dynamic stress. These problems call for a comprehensive effort aimed at assessing the severity of ambient vibrations as well as their potential effects on heritage buildings. In this perspective, two approaches can be considered. The first one exploits a numerical model of the structure in order to evaluate the effects of ambient vibrations. This approach has the merit of allowing the analysis of different loading scenarios and their uncertainties. However, its effectiveness heavily depends on the hypotheses upon which the numerical simulation is performed. Among the others, a critical task is concerned with the lack of reliable approach and data for modeling the effects of vibrations with a very high number of cycles on old masonry structures. Because of these difficulties, the use of experimental methods is an attractive option. As heritage buildings are concerned, the use of non-destructive experimental techniques must be privileged, and dynamic

monitoring techniques are most popular in this field. Experimental methods can be designed to support the elaboration of numerical models as well as to provide direct information about the potential negative effects of ambient vibrations. A critical issue to be addressed when dynamic monitoring techniques are adopted for assessing the severity of ambient vibrations is the selection of proper threshold values. The problem consists in identifying limit values that, if complied with, damage due to ambient vibrations is not likely to occur. Within this framework, this contribution is intended to provide an overview about studies, guidelines and codes that include pertinent information on the selection of vibration criteria for heritage buildings. The Flavian Amphitheater is considered as case study, and current efforts aimed at installing a wireless sensor network for monitoring its dynamic response are presented.

2. Assessment of the effects due to ambient vibrations on heritage buildings

2.1. Dynamic characterization

Dynamic response characterization can be performed by a variety of displacement, velocity or acceleration sensors. It is the typical practice to use velocity as significant kinematic parameter to assess the effects of vibrations on structures, whereas the use of acceleration is rare. Some velocity-based vibration criteria refer to the components of the velocity vector (PCPV: Peak Component Particle Velocity), whereas others refer to the module of the resultant vector (PPV: Peak Particle Velocity). Typical particle velocity and particle acceleration ranges for traffic-induced vibrations are 0,2 to 50 mm/s and 0,02 to 1 m/s², respectively [2,3]. Different thresholds are usually set for continuous or transient response. For instance, the time parameter $\tau = 1/(2\pi\xi f)$ [s] is introduced in Refs. [2,3], where ξ represents the influence of damping and f is the resonance frequency. Based on this parameter, two cases are defined in Refs. [2,3] (without regard to whether the excitation is deterministic or random). If the forcing function impinges on the structure continuously for more than 5τ , then the vibration is regarded as continuous. Otherwise, the response is re-

garded as transient. This is a simplification, since real loading conditions do not fall easily into a single category. Some vibration criteria also depend on the frequency content. Most building damage from man-made sources occur in the frequency range from 1 Hz to 150 Hz [2,3], and thus some frequency-dependent thresholds are available in this range.

2.2. Identification of threshold values: the European experience

DIN 4150-3 [4] provides guideline values based on velocity measurements to be used in the assessment of the effects due to, both, short-term and long-term vibrations on buildings under preservation orders. Threshold values for short-term vibrations are listed in Table 1.

Table 1. *Vibration criteria for short-term vibrations from DIN 4150-3*

| Frequency range [Hz] | PCPV [mm/s] at the foundation | PCPV [mm/s] at horizontal plane of highest floor |
|----------------------|-------------------------------|--|
| 1-10 | 3 | 8 |
| 10-50 | 3-8 | |
| 50-100 | 8-10 | |

In-between values of the limit PCPV can be computed by linear interpolation. At frequencies above 100 Hz, the threshold value at 100 Hz may be used as minimum value. The PCPV for the vertical component of the floor velocity should be lower than 20 mm/s. When considering long-term vibrations, the velocity in the horizontal plane of highest floor has to be less than 2.5 mm/s. No guideline value is available for the vertical component of long-term vibrations.

The standard SN 640312 a [5] (see Table 2) applies to vibrations due to blasting, construction operations, and vehicle and rail traffic, with frequency content larger than 8 Hz.

Table 2. *Vibration criteria for short-term vibrations from SN 640312*

| Exposure | PPV [mm/s] | | |
|------------|--------------------|-------------------|-------------------|
| | 8 Hz-30 Hz | 30 Hz-60 Hz | 60 Hz-150 Hz |
| Occasional | Between 7.5 and 15 | Between 10 and 20 | Between 15 and 30 |
| Frequent | Between 3 and 6 | Between 4 and 8 | Between 6 and 12 |
| Continuous | Between 1.5 and 3 | Between 2 and 4 | Between 3 and 6 |

Both DIN 4150-3 [4] and SN 640312 a [5] are included within the Italian standard UNI 9916 [6]. On reviewing DIN 4150-3 [4], the Italian standard UNI 9916 [6] suggests an upper threshold value for the vertical component of long-term vibrations equal to 10 mm/s.

An interesting case study deals with the construction of the Vienna underground railways and the adopted measures to protect the St. Steven's Cathedral [7], see Figure 1.

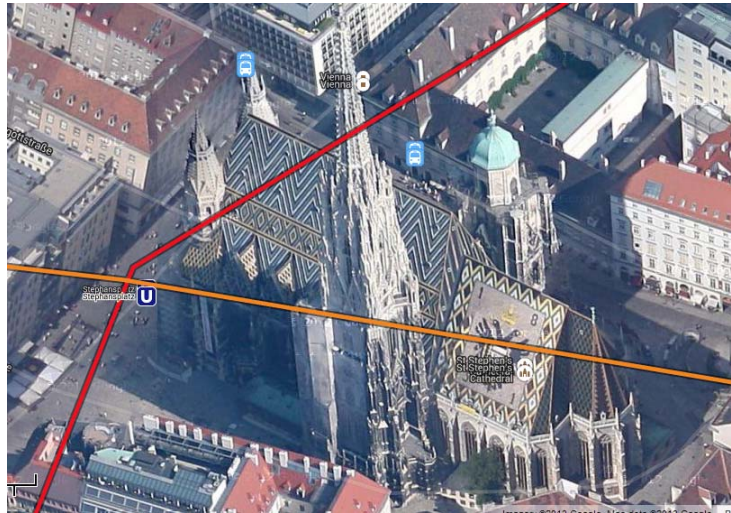


Figure 1. The St. Steven's Cathedral and the Stephansplatz station

The current Romanesque and Gothic form of the cathedral was largely initiated by Duke Rudolf IV on 1359 and stands on the ruins of two earlier churches, the first one consecrated in 1147. The height of the bell tower is about 137 m and there are two 66 m height towers (Pagan Towers) at the main entrance. The station pipes for the “Stephansplatz” station are very close to this famous monument. The underground metro station lies at a depth of about 26 m, a bare 5 m away from the west façade of the St. Steven's Cathedral. In November 1970, the Faculty of Civil Engineering and Architecture of the Vienna Polytechnic Institute was contacted by the City of Vienna to provide an expert appraisal. For construction operations, the upper vibration limit was put at an acceleration equal to 0.20 m/s^2 . For continuous and occasional loading, the identified thresholds were 0.02 m/s^2 and 0.05

m/s^2 , respectively. Observations of these limits proved adequate. It has not clearly indicated, however, if these limits apply to any component of the acceleration or to the module of the resultant vector.

2.3. Identification of threshold values: works from USA and Canada

The Noise, Vibration, and Hazardous Waste Management Office of the California Department of Transportation adopted a guidance manual for the assessment of transportation- and construction-induced vibration [8]. This document contains an overview about vibration criteria, including some guidelines for historical buildings. Some vibration criteria for transient (single-event) and steady-state (continuous) sources when dealing with historical and sensitive buildings were recommended in Ref. [9] (see Table 3). Criteria for continuous vibration are about half the amplitude of criteria for transient sources.

Table 3. *Vibration criteria for historical and sensitive buildings* [9]

| Frequency range [Hz] | Transient vibration PPV [mm/s] | Steady-state vibration PPV [mm/s] |
|----------------------|-----------------------------------|--------------------------------------|
| 1-10 | 6.35 | 3.05 |
| 10-40 | 6.35-12.70 | 3.05-6.35 |
| 40-100 | 12.70 | 6.35 |

The California Department of Transportation also gives the limit PPV value suggested in Ref. [10] for continuous vibration on ancient monuments, which is equal to 2.0 mm/s. The American Association of State Highway and Transportation Officials (AASHTO) defined the maximum vibration levels for preventing damage to structures from intermittent construction or maintenance activities. For historical sites or other critical locations, the identified limiting velocity in Ref. [11] is 2.5 mm/s. An overview about the effects of vibrations on historical buildings is also available from the National Research Council of Canada [12].

2.3. Identification of threshold values: Chinese experience

China and Italy have a comparable number of properties inscribed on the UNESCO World Heritage List [13], and thus they share similar

problems in dealing with the preservation of historical centers. Because of its growing economy, mobility demand in China is raising rapidly and, as a consequence, the construction of new infrastructures may require special care if the interaction with heritage building has to be taken into account. For instance, the effect of vibration on historical buildings due to moving trains in Beijing is addressed in Ref. [14]. Herein, the case study is concerned with the Diameter line (9,156 m long), an important underground line linking the two main railway stations in Beijing, namely the Beijing Railway Station and the Beijing West Railway Station. There are three historical buildings in close proximity to, both, Diameter Line and existing metro Line 2. One heritage structure is the Ming Dynasty City Wall, originally built in 1419, the 17th year of the Yongle period in Ming Dynasty. This key historical and cultural site is a 1.5 km wall under state protection. The second historical construction is the Jingfeng Railway Station Relic, built in 1903 in the last phase of Qing Dynasty; it had been the largest railway station until 1958, and now is a historical building under Beijing city protection. The last historical structure is the Zhengyang Gate and Jianlou Building. It is located at the south end of Tian'anmen square, which is an important carrier of the history and culture of old Beijing city of nearly 600 years, and was officially designated as a "Cultural Relic under Special National Protection". The PPV for the frequency range 10-30 Hz has been considered in Ref. [14] as a sensitive parameter to assess train-induced vibrations and to evaluate the need of special protection measures, and it was calculated by considering two components (one horizontal component and the vertical component). Because of the presence of cracks, the allowable limit for the Ming Dynasty City Wall was taken equal to 1.8 mm/s. For the other two monuments, namely the Jingfeng Railway Station Relic and the Zhengyang Gate, the assumed threshold was equal to 3.0 mm/s, because they were retrofitted recently.

The recent Chinese National Code [15] also sets out allowable velocity limits for historical buildings. A short review of such document appears, therefore, appropriate. Allowable velocity for masonry and stone structures proposed in Ref. [15] are listed in Table 4 and Table 5, respectively. In these tables, V_p is the propagation velocity of the pressure waves. When V_p falls within the indicated range, the corre-

sponding in-between values of the allowable velocity can be calculated by interpolation.

Table 4. Allowable velocity for brick masonry by Chinese National Code

| Level of preservation | Position of controlling points | Direction of controlling points | Allowable velocity for brick masonry [mm/s] | | |
|-----------------------|---|---------------------------------|---|---|------------------|
| | | | $V_p < 1600$ m/s | $1600 \text{ m/s} \leq V_p \leq 2100$ m/s | $V_p > 2100$ m/s |
| National Level | The peak point of load-carrying structure | Horizontal | 0.15 | 0.15-0.20 | 0.20 |
| Provincial Level | The peak point of load-carrying structure | Horizontal | 0.27 | 0.27-0.36 | 0.36 |
| City and County Level | The peak point of load-carrying structure | Horizontal | 0.45 | 0.45-0.60 | 0.60 |

Table 5. Allowable velocity for stone masonry by Chinese National Code

| Level of preservation | Position of controlling points | Direction of controlling points | Allowable velocity for stone masonry [mm/s] | | |
|-----------------------|---|---------------------------------|---|---|------------------|
| | | | $V_p < 2300$ m/s | $2300 \text{ m/s} \leq V_p \leq 2900$ m/s | $V_p > 2900$ m/s |
| National Level | The peak point of load-carrying structure | Horizontal | 0.20 | 0.20-0.25 | 0.25 |
| Provincial Level | The peak point of load-carrying structure | Horizontal | 0.36 | 0.36-0.45 | 0.45 |
| City and County Level | The peak point of load-carrying structure | Horizontal | 0.60 | 0.60-0.75 | 0.75 |

It is interesting to observe that this technical code provides distinct threshold values depending on structural health (which is expressed in terms of V_p) and cultural importance (based on the level of preservation). It is worth noting that allowable velocity for masonry and stone structures proposed in the Chinese National Code [15] were considered when planning a new metro line close to heritage buildings in the historical heart of Beijing [16]. The report in Ref. [16] considers the

planned alignment of metro line 6 and line 8 in Beijing. The Chinese National Code was also considered in Ref. [17] to study the Monument to the martyrs in the autumn of Xinhai Year, a brick-masonry structure with a height of about 30 m built in 1913 in the center of Chengdu City (China). There are fine handwritings and reliefs on the faces and because of the exceptional art design, both structural and architectural damages should be avoided in this monument (the heritage structure is within the list of State Protected Historical Sites). Recently, the Chengdu Subway Line 2 was built close to it, and thus the authors decided to investigate the influence of vibrations caused by this transport infrastructure. The distance between the monument and closest subway station is about 50 m, whereas the embedded depth of the track is about 13 m.

It has been stated in Ref. [17] that fatigue limit is used to identify allowable velocities in the Chinese National Code [15]. Therefore, it can be assumed that vibration criteria in Ref. [15] hold for continuous loading.

3. Wireless dynamic monitoring of cultural heritage

The Flavian Amphitheater (Rome, Italy) - which took the name “Colosseum” from the colossal statue that once stood nearby - is certainly the most famous monuments of the ancient Roman Empire. The effects of, both, long-term and short-term vibrations on the monument deserve special attention, especially in view of the construction of the third underground metro line of the city. In this perspective, a critical task is concerned with the selection of suitable threshold values to assess potential negative effects due to ambient vibrations. DIN 4150-3 [4] is the most popular standard in this field and its use is also covered by the Italian standard UNI 9916 [6]. Therefore, it is a useful reference. Conclusions drawn for protecting the St. Steven’s Cathedral [7] are interesting as well, because they were elaborated for a very similar case study. Finally, the allowable velocities indicated by the recent Chinese National Code [15] are worth of serious consideration. In this case, the highest cultural importance (“National Level”) must be considered. Numerical values of V_p for the Colosseum can be retrieved from recent results reported in Ref. [18], see Table 6.

Table 1. V_p values measured on the Colosseum [18]

| Material | V_p |
|------------|---------------------|
| Travertine | 2600 m/s – 5400 m/s |
| Masonry | 800 m/s – 3600 m/s |
| Tuff | 900 m/s – 2700 m/s |

A wireless sensor network will be installed on the northern wall of the Colosseum for the long-term dynamic monitoring of its dynamic response. The current sensor network consists of 4 accelerometers PCB, series 393B12, with a sensitivity of 10 V/g. Three accelerometers are oriented along the radial direction whereas one accelerometer is oriented along the vertical direction (see Figure 2).

**Figure 2.** Position and orientation of the accelerometers

The sensor network is scalable and spatially reconfigurable. A wireless-based technology has been adopted. Measurements are stored into a web-based repository until the maximum available space is achieved. Subsequently, they are transferred to a local memory space. Power supply is ensured by 9-24 V batteries, and the network is designed to optimize its efficiency and to reduce the energy consumption. As the network is being installed on a heritage building (see Fig-

ure 3), a non-destructive mounting is strictly required. Therefore, each component of the network can be moved without aesthetic damage to the monument.



Figure 3. Installation of the wireless sensor network on the northern wall of the Colosseum

Conclusions

This study reviewed existing criteria to assess the effects of ambient vibrations on heritage buildings. It is useful to highlight that these criteria were identified on the basis of empirical observations, and thus final values (and differences among the proposals) strongly depend on the selected buildings (type and condition, foundation, soil, etc.). Notwithstanding their operative usefulness, the use of such vibration criteria has important limitations, the most important one being the lack a probabilistic definition of the limit state. A more rational use of this approach, therefore, requires new investigations. Finally, this study also presented current efforts towards the installation of a wireless sensor network for the long-term dynamic monitoring of the northern wall of the Colosseum.

Acknowledgments

The wireless sensor network described in this study has been realized in collaboration with SO.TEL. s.r.l. – Società Telecomunicazioni. The support provided by Engineers Andrea Gullotta, Emilio Manolio and Daniela Milone is especially appreciated. The authors also thank

Prof. Yan Xiao and Prof. Bin Xu (Hunan University, China) for the English translation of the Chinese National Code [15]. Any opinions, findings, conclusions, and recommendations expressed in this document are those of the authors and do not necessarily reflect the views of the cited people.

References

[1] Crispino M., D'Apuzzo M.: Measurement and prediction of traffic-induced vibrations in a heritage building, *Journal of Sound and Vibration*, Vol. 246, 2001, pp. 319-335.

[2] ISO 4866, Mechanical vibration and shock - Vibration of buildings - Guidelines for the measurement of vibrations and evaluation of their effects on buildings.

[3] BS 7385-1, Evaluation and measurement for vibration in buildings - Part 1: Guide for measurement of vibrations and evaluation of their effects on buildings.

[4] DIN 4150-3, Structural vibration – Part 3: Effects of vibration on structures.

[5] SN 640312 a, Effet des ébranlements sur les constructions.

[6] UNI 9916, Criteri di misura e valutazione degli effetti delle vibrazioni sugli edifici.

[7] Döller A., Hondl A., Proksch E.: The construction of the Vienna underground railway and measures taken to protect St. Steven's Cathedral, *Technical translation by National Research Council Canada*, Ottawa, 1977.

[8] Transportation- and Construction-Induced Vibration Guidance Manual, 2004, California Department of Transportation.

[9] Konon W., Schuring J. R.: Vibration criteria for historic buildings, *Journal of Construction Engineering and Management*, Vol. 111, 1985, pp. 208-215.

[10] Whiffin A. C., Leonard D. R.: A survey of traffic-induced vibrations, *Report LR419, Department of Environment, Road Research Laboratory*, Crowthorne, Berkshire, England, United Kingdom, 1971.

[11] American Association of State Highway and Transportation Officials, *Standard recommended practice for evaluation of transportation-related earthborne vibrations*, Washington, DC., 1990.

[12] Rainer J. H.: Effect of vibrations on historic buildings: An overview. National Research Council Canada, *Reprinted from the Association for Preservation Technology Bulletin*, Vol. XIV, 1982, pp. 2-10.

[13] UNESCO Official website <http://whc.unesco.org/> (last access: November 23, 2013).

[14] Jia Y. X., Liu W. N., Liu W. F., Zhang H. G.: Study of vibration effects on historic buildings due to moving trains in Beijing, *9th International Symposium on Environmental Geotechnology and Global Sustainable Development*, Hong Kong, 2008, pp.492-499.

[15] GB/T 50452-2008. Technical Specifications for Protection of Historic Buildings Against Man-Made Vibration. China Building Industry Press, Beijing (in Chinese).

[16] Jaquet T., Salcedo V.: Ensuring acceptable vibration levels in listed buildings by means of precise vibration measurements and highly efficient Floating Slab Track, *Proceedings of the AREMA 2012 Annual Conference & Exposition*, Chicago, 2012.

[17] Ma M., Markine V., Liu W., Yuan Y., Zhang F.: Metro train-induced vibrations on historic buildings in Chengdu, China, *Journal of Zhejiang University Science A*, Vol. 12, 2011, pp. 782-793.

[18] Herzalla A., Croci G.: Relazione Tecnica Relazione Conclusiva, *Technical Report CX_3_D_X_N5M_JA_R_1B_002_0*, 2007.

Recordings of the 2009 L'Aquila earthquakes in the Colosseum

A. Caserta¹, F. Marra¹, A. Govoni¹, A. Rovelli¹

Abstract

We show a preliminary study concerning the interaction between the incoming seismic wave-field and the structure of Colosseum during aftershocks of the 6 April 2009 M 6.3 L'Aquila main-shock. By using mainly Arias intensity, we assess how the incoming energy beneath the foundations is conveyed into the monument, through what preferential frequencies such process takes place, how the trapped energy increases the vibration amplitude with floors. Moreover, we also investigate the role played by the near-surface geology in generating differential motions below the monument foundations. In addition we also check, in a preliminary way, the foundation dynamical behaviour under the action of the incoming wave-field.

1. Introduction

Damage episodes caused by earthquakes to the Colosseum through the centuries are well documented since 443 B.C., as an inscription engraved in a stone located at the entrance of the amphitheatre testifies. Damage seems to be concentrated mostly in the southern portion of the amphitheatre, i.e. the Valadier wall (Figure 1), where the near-surface geology shows the presence of small Holocene alluvial valley called *Fosso Labicano* (Funicello *et al.*, 1995; Marra and Rosa, 1995). The coincidence of the damage pattern and the presence of the Holocene alluvial valley suggest that one of the causes of the high level of damage in the Valadier wall side could be the interaction between the seismic wave-field and the near-surface geology. This hypothesis is supported also by studies based on numerical simulations planned and realized to investigate such interaction (Boschi *et al.*, 1995; Moczo *et al.*, 1995).

¹ Istituto Nazionale di Geofisica e Vulcanologia, Roma, Italy.

During the moderate-magnitude aftershocks following the 6 April 2009 M 6.3 L'Aquila main-shock, about 90 km northeast of Rome (Caserta et al., 2013), we installed six portable seismic stations in the Anfiteatro Flavio (Figure 2). All of them were equipped with three-component 5-s velocity transducers, and the horizontal components were oriented along the north–south and east–west directions. Data were sampled at a rate of 1000 Hz, using 24-bit analog-to-digital converters, and time synchronism was provided by a GPS system at each station.

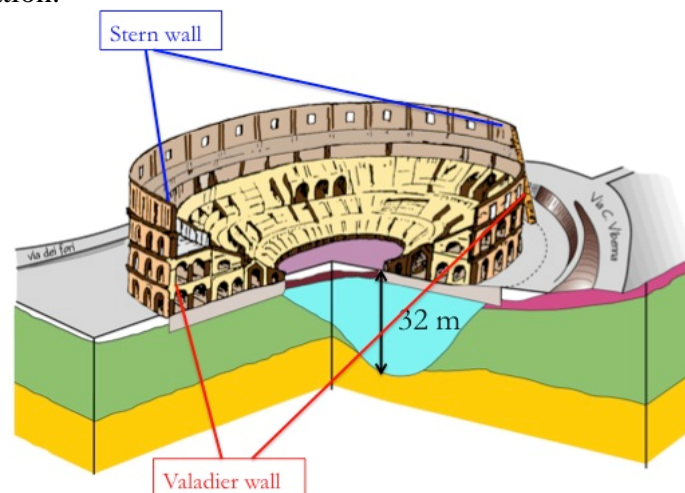


Figure 1. Stereogram of the near-surface geology under the Colosseum. The Valadier wall was reconstructed by Giuseppe Valadier in 1852 under Pio IX P.M. Such reconstruction represents the last step of the restoration process began in 1807 by Pio VII P.M. Redrawn from Funicello et al. (1995).

Such stations provide the first earthquake monument-motion recordings in the long history of the amphitheatre, offering an unprecedented opportunity to calibrate the monument response to central Apennine earthquakes - earthquakes that have been responsible for the largest damage to Rome and to its huge heritage since historical times (Ambrosini et al, 1986; Fäh et al., 1993; Rovelli et al., 1994, 1995; Olsen et al, 2006; Cifelli et al, 2000; Sbarra et al, 2012).

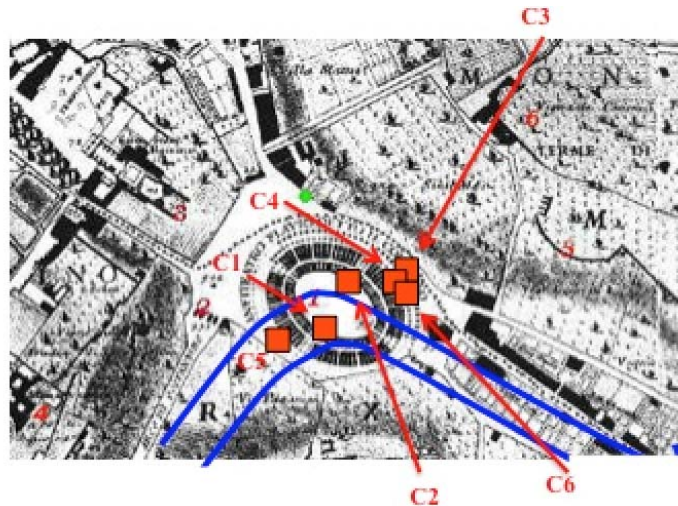


Figure 2: Sketch of the 6 seismic station deployments inside the amphitheatre. C1 and C2 have been installed at the Ipogei on the Fosso Labicano valley and outside it, respectively. C3, C4 and C6 are at the basement, first and second floor, respectively, in the Stern Wall side. C5 has been installed at the first floor on the Valadier wall side. The two blue curves indicate the margins of the Fosso Labicano alluvial valley.

2. Data Analysis

In the present paper we analyze records of stations C1, C2, C3 and C4 (Figure 2) only, the analysis of records from all of the installed stations will be shown in a forthcoming paper.

In order to verify the role played by the Holocene alluvial valley in amplifying the soil shaking, we first analyze the records of the two stations installed at the Ipogei (Figure 3). The Ipogei zone is surrounded by the foundation ring. This latter is an around 14 m thick concrete layer. Therefore, the Ipogei can be considered, as "free field-like" area not affected by foundation, at least at a "first order of approximation". As a consequence, earthquakes recorded by C1 and C2 seismic stations (see Figure 3) can be considered also as input seismic field to the Colosseum structure, including foundation.

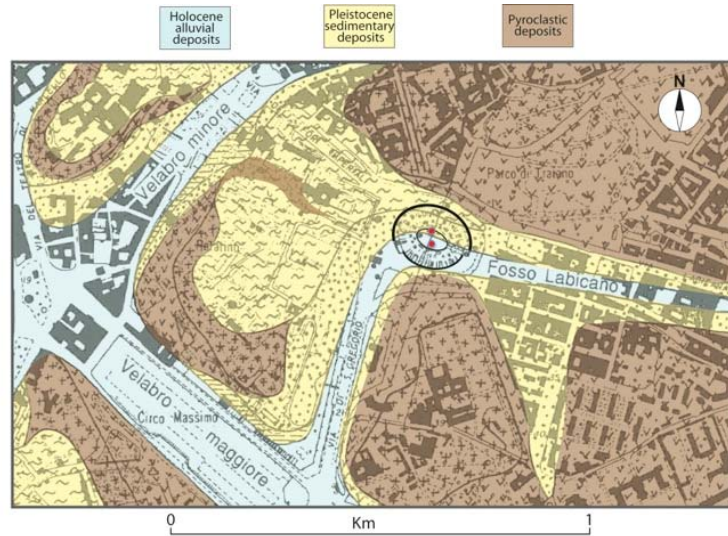


Figure 3: Near-surface geological units of the Colosseum area. The two seismic stations installed at the Ipogei are represented by the two red spots. Seismic stations C1 and C2 are installed outside and inside the Fosso Labicano valley, respectively.

In Figure 4 left panel, the receivers' functions at C1 and C2 obtained for an Mw 4.2 aftershock are plotted. The main peaks are in the frequency range between 1 and 2 Hz in agreement with both theoretical and numerical studies (Fäh et al., 1993; Boschi et al., 1995; Moczo et al., 1995; Rovelli et al., 1994, 1995; Olsen et al., 2006; Bozzano et al., 2008; Caserta et al., 2012).

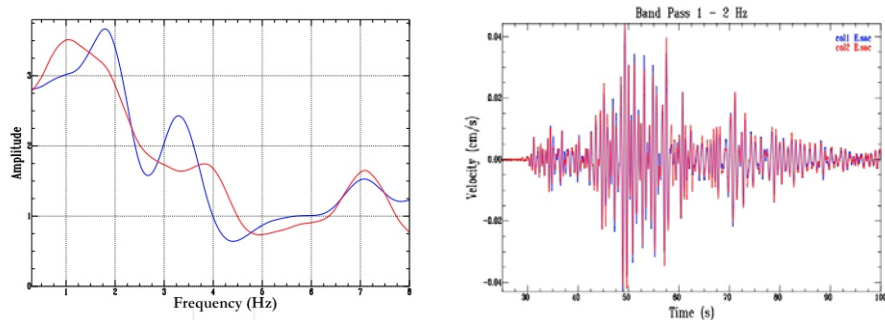


Figure 4: Left panel: receiver functions of the Mw 4.2 aftershock recorded at the two stations installed at the Ipogei. Right panel: Time series of the same aftershock filtered in the frequency band 1-2 Hz.

The evidence of this amplification frequency band was confirmed for the first time by Caserta et al. (2013), who analyzed the 6 April 2009 **M** 6.3 L'Aquila main-shock and its aftershocks.

The difference in spectral amplitude concerning the main peaks seems not enough to identify an actual role played by the Fosso Labicano valley in amplifying the soil shaking. Such feeling is also confirmed by filtered signals showing any amplification one in respect to the other (Figure 4 right panel) even though the Peak Ground Velocity values are in agreement with regression curves according with magnitude and epicentral distance of the considered aftershock (Caserta et al., 2013).

We have also checked (see Figure 5) differences in terms of absorbed energy between C1 and C2 stations by using the Arias intensity defined as (Arias, 1970)

$$I_a = \frac{\pi}{2g} \int_0^\infty a^2(t) dt \quad (1)$$

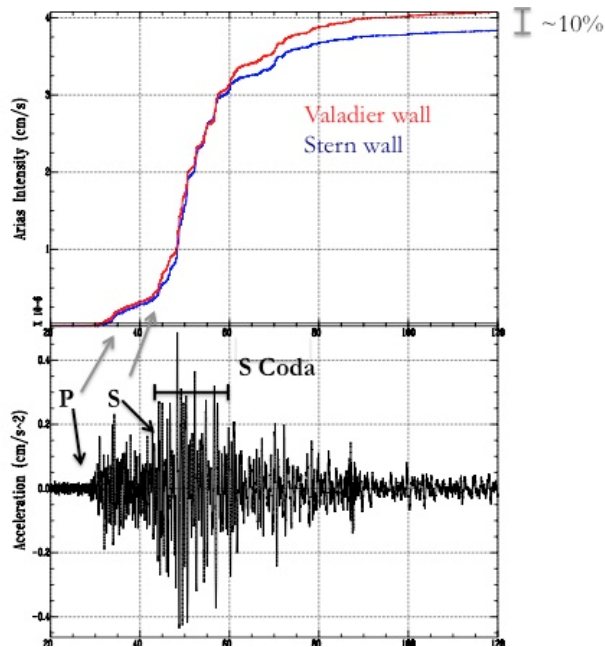


Figure 5. Top panel: Arias intensity according to (1) for C1 and C2 seismic stations. Bottom panel: records of the Mw 4.2 aftershock used in this study.

Where I_a is the Arias intensity in units of length per time, $a(t)$ is the acceleration-time history in units of g, and g is the acceleration of gravity. The result is shown in Figure 5.

An abrupt change in the derivative of I_a takes place around 40s in coincidence with the S phase onset. Such trend persists for the entire S coda, indicating that such phase with its coda is the most energetic part of the whole record.

Adsorbed energy results in 10% more for the station C1, (installed on the Fosso Labicano valley close to Valadier wall), compared to C2 (installed close to Stern Wall outside the valley). This supports the idea that the small sedimentary basin alone can not be considered as responsible for the collapse of the arcades of Valadier wall ring.

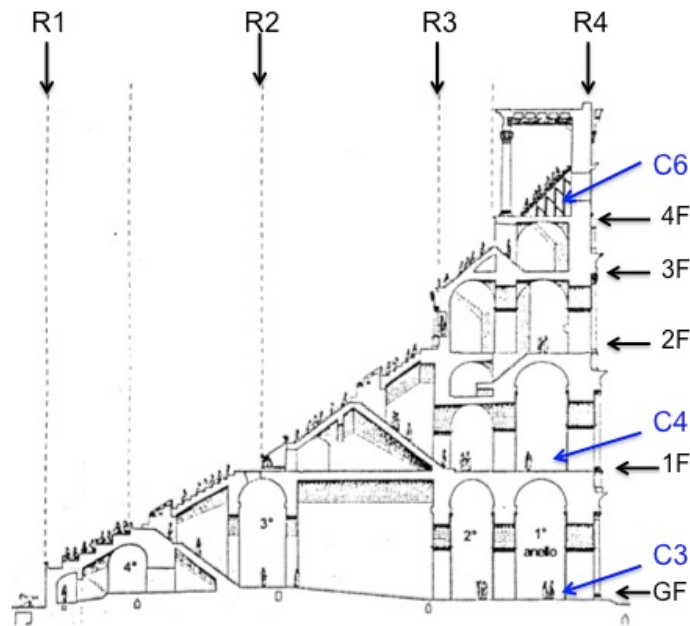


Figure 6: Radial section of the Stern wall from the Stern Buttress point of view. C3, C4 and C6 are the seismic stations. R1, R2, etc., indicate the Colosseum rings. GF stands for ground floor. 1F, 2F, etc. indicate the floors.

Let us analyse now how such energy, that can be considered as input to the Anfiteatro Flavio as already noticed, is absorbed by the structure among its storeys. To do that we include in our analysis other two seismic stations: C3 at the ground floor and C4 at the first floor. They

are aligned on the fourth ring, R4, along a vertical line at the Stern buttress (see Figure 6).

The receiver function at ground floor (Figure 7 left panel) shows the peak in the same frequency range of C1 and C2 but the amplitude is ~20% and 25% less than C2 and C1, respectively. The vibration amplitude in the time domain confirms this conclusion (Figure 7 right panel).

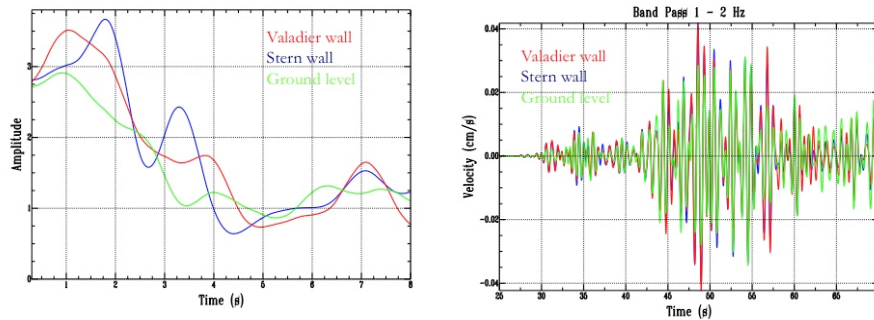


Figure 7. Left panel: comparison among receiver functions of Valadier wall side (station C1), Stern Wall (station C2) and ground floor (station C3). Right panel: comparison in time domain of the same seismic stations.

In terms of absorbed energy the Arias intensity analysis (Figure 8 left panel) says us that C3 absorbs 25% of energy less than C2 (Stern wall side), and 35% less than C1 (Valadier wall side). The only difference between C3 and the other two stations is that this latter is installed on the foundation ring. It seems the role played by foundation is able to absorb around 25% of incoming energy from the Stern wall side and 35% from the Valadier one. Due to the presence of the Fosso Labicano sedimentary valley, the foundation ring is more stressed in its southern part.

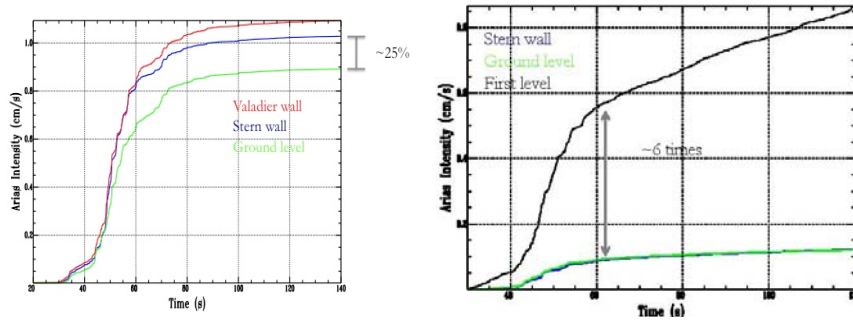


Figure 8: Left panel: comparison among Arias intensity of ground floor (C3), C1 station installed at the Ipogei on the Fosso Labicano sedimentary valley (Valadier wall side) and C2 station installed at the Ipogei outside the valley (Stern wall side). Right panel: comparison between Arias intensity of the first floor and the Ipogei Stern wall side (C2 station) and ground floor (C3 stations).

For the same event, Figure 8 right panel compares the Arias intensity between the first floor and the ground level, with the former being 6 times greater than the latter. It seems that the interaction between the input seismic wave-field and the structure involves the resonant vibration of the Stern wall.

Let us check what are the frequencies involved in such energy transfer process.

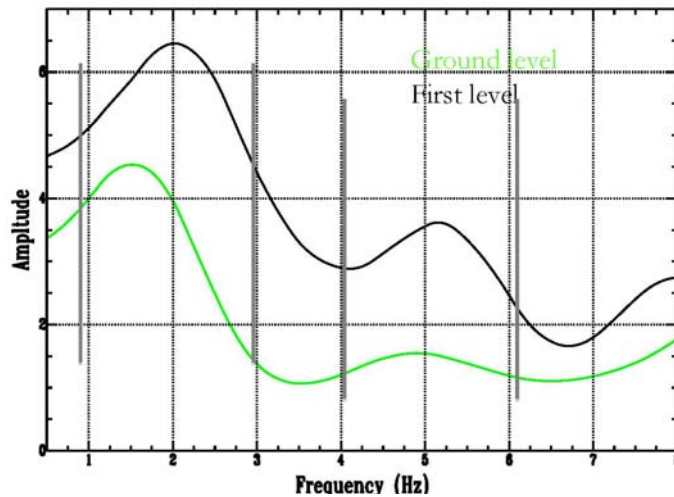


Figure 9. Receiver functions of ground level and first floor. The two frequency band, 1-3 Hz and 4-6 Hz, related to main peaks, are indicated by vertical bars.

The comparison between the receiver functions of the ground floor and the first floor suggests that two frequency bands are interested in the energy transfer process: 1-2 Hz and 4-6 Hz. So, we filtered the record of the same event first in the former frequency band and later in the latter one for the record of the first floor only. Then we compute the Arias intensity for both filtered time series. The result is in Figure 10 indicates that around 50% of the total energy absorbed by the first floor is conveyed through the first frequency band.

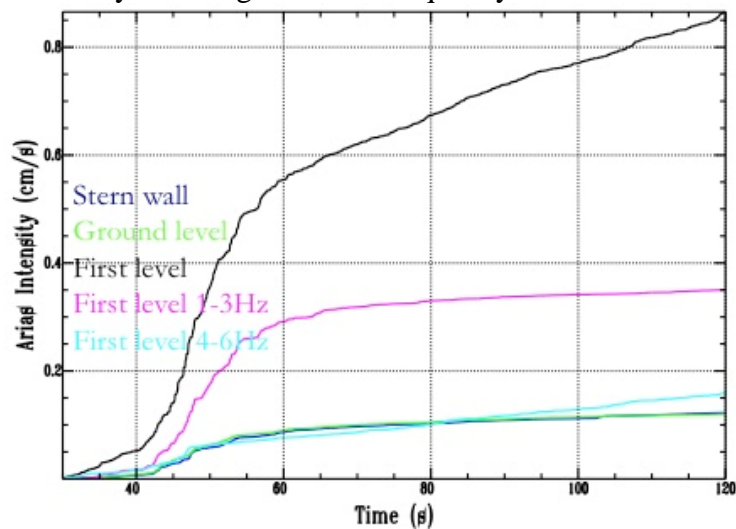


Figure 10. Comparison among different Arias intensities according to the legend.

In contrast, the energy absorbed by the second frequency band is of the same order of magnitude of the absorbed energy at the ground floor.

3. Conclusions

We have shown a preliminary data analysis of the aftershock sequence of the 6 April 2009 M 6.3 L'Aquila main-shock, about 90 km north-east of Rome, aimed at investigating the interaction between the incoming seismic wave-field and the amphitheater. More in detail, we focused the analysis on the role played by both the near-surface geology features and the foundation of the Colosseum, in generating dif-

ferential motion. We have quantified such phenomena in terms of percentage of absorbed energy at different floors of the monument. The preliminary results can be summarized as follows:

1. the presence of Fosso Labicano in the southern part of the Colosseum seems to play a not significant role in amplifying the soil shaking. It determines 10% absorbed energy more than outside the valley;
2. the foundation absorbs 35% and 25% of incoming energy from the Valadier wall side (on the valley) and from the Stern wall side (outside the valley), respectively;
3. the energy at the ground level is transmitted to the first floor mainly through the fundamental resonance frequency.

Item 1 and 2 suggest us thinking of foundation from the Valadier side as more fractured than those on the Stern side. This could be due to two reasons: first, absorbed energy is higher because of the presence of the valley, and second, phenomena linked with subsidence increase the fracture size. This will be the topic of a forthcoming paper.

Acknowledgments

The authors wish to thanks Dr. Piero Meogrossi and Dr. Rossella Rea who are in charge for the Anfiteatro Flavio, for allowing us to install the seismic stations and for supporting us in planning and realizing the whole experiment. Thanks also to Prof. Gianfranco Valente for his help and criticism.

References

[1] Ambrosini S., Castenetto S., Cevolani F., Di Loreto E., Funicello R., Lipari L. and Molin D. (1986). Risposta sismica dell'area urbana di Roma in occasione del terremoto del Fucino del 13-1-1915. *Mem. Soc. Geogr. Ital.* **35**, 445 - 452 (in Italian).

[2] Arias A. (1970). "A Measure of Earthquake Intensity," R.J. Hansen, ed. *Seismic Design for Nuclear Power Plants*, MIT Press, Cambridge, Massachusetts, pp. 438-483.

[3] Boschi E., Caserta A., Conti C., Di Bona M., Funicello R., Magagnini L., Marra F., Martines G., Rovelli A. and Salvi S. (1995). Resonance of subsurface sediments - An unforeseen complication for designers of Roman columns. *Bull. Seismol. Soc. Am.* **85**, 320-324.

[4] Bozzano F., Caserta A., Govoni A., Marra A. and Martino S. (2008). Static and dynamic characterization of alluvial deposits in the Tiber River Valley: New data for assessing potential ground motion in the city of Rome. *J. Geophys. Res.* **113**, B01303, doi: 10.1029/2006JB004873.

[5] Caserta A., Martino S., Bozzano F., Govoni A. and Marra F. (2012). Dynamic properties of low velocity alluvial deposits influencing seismically-induced shear strains: The Grottaperfetta valley test-site (Rome, Italy), *Bull. Earthq. Eng.* doi: 10.1007/s10518-012-9349-8.

[6] Caserta A., Boore D.M., Rovelli A., Govoni A., Marra F., Della Monica G. and Boschi E. (2013). Ground Motions Recorded in Rome during the April 2009 L'Aquila Seismic Sequence: Site Response and Comparison with Ground- Motion Predictions Based on a Global Dataset. *Bull. Seismol. Soc. Am.* **103**, **3**, 1860 - 1874, doi: 10.1785/0120120153.

[7] Cifelli F., Donati S., Funicello R. and Tertulliani A. (2000). High-density macroseismic survey in urban areas. Part 2: Results for the city of Rome, Italy. *Bull. Seismol. Soc. Am.* **90**, 298 - 311.

[8] Fäh D., Iodice C., Suhadolc P. and Panza F. (1993). A new method for the realistic estimation of seismic ground motion in megacities: The case of Rome. *Earthq. Spectra* **9**, 643 - 668.

[9] Funicello R., Lombradi L., Marra F. and Parotto M. (1995). Seismic damage and geological heterogeneity in Rome's Colosseum area: are they related? *Annali di Geofisica* **XXXVIII**, **5-6**, 927 - 937.

[10] Marra F. and Rosa C. (1995). Stratigrafia e assetto geologico dell'area romana, in "La Geologia di Roma - Il Centro Storico". special volume Memorie del Servizio Geologico **50**, 49 - 118. In Italian.

[11] Moczo P., Rovelli A., Labak A. and Malagnini L. (1995). Seismic response of the geological structure underlying the Roman Colosseum and a 2-D resonance of a sedimentary valley. *Annali di Geofisica* **XXXVIII**, 5-6, 939 - 956.

[12] Olsen K.B., Akinci A., Rovelli A., Marra F. and Malagnini L. (2006). 3D ground-motion estimation in Rome, Italy. *Bull. Seismol. Soc. Am.* **96**, 133 - 146.

[13] Rovelli A., Caserta A., Malagnini L. and Marra F. (1994). Assessment of potential strong motions in the city of Rome. *Annali di Geofisica* **XXXVII**, 1745 - 1769.

[14] Rovelli A., Malagnini L., Caserta A. and Marra F. (1995). Using 1-D and 2-D modelling of ground motion for seismic zonation criteria: Results or the city of Rome. *Annali di Geofisica* **XXXVIII**, 591 - 605.

[15] Sbarra P., De Rubeis V., Di Luzio E., Mancini M., Moscatelli M., Stigliano F., Tosi P. and Vallone R. (2012). Macroseismic effects high-light site response in Rome and its geological signature. *Nat. Hazards* **62**, 425 - 443, doi: 10.1007/s11069-12-0085

Evaluation of the Structural Health Status of the Coverings of Villa dei Misteri in Pompeii

Bruno Carpani¹

Abstract

Villa dei Misteri is one of the most visited monuments of the archaeological area of Pompeii. It is sited just outside the ancient city and takes its name from the superb frescoes cycle depicting ritual mysteries. The ancient masonry structures, dating from the 2th century B.C. to the Vesuvian eruption, are protected from weathering by modern roofs built in various materials (reinforced concrete, timber, steel). After the collapse, in the fall of 2012, of a decayed timber beam, the Superintendence decided to carry out, in collaboration with ENEA, a detailed survey of all the covering structures to evaluate its health status and to assess the safety condition of the monument.

This paper illustrates the research methodology developed, which is based on a multidisciplinary approach including historical research, geometrical and structural surveys, damage assessment based on both in situ and laboratory diagnostic tests, UAV (Unmanned Aerial Vehicles) remote sensing to inspect area and coverings not easy to reach in safe, and, as basis for seismic safety assessment, ambient vibration measurement to characterize the dynamic response of the soil and of the most relevant structural components of the Villa. The preliminary results of the first stage of the diagnostic campaign are also presented.

¹ ENEA - Brasimone Research Centre – Camugnano (BO)

1. Introduction

Villa dei Misteri is a suburban Roman villa located just outside the main archaeological area of Pompeii (figures 1-2). Its early structures date to the 2th c. B.C., while significant building phases are attested around 90-70 BC and after the AD 62 earthquake. Discovered in 1909, it is named after the superb painting cycle depicting the sequence of acts of a religious ritual, most likely related to the so-called Dionysiac Mysteries (figures 3-4).

After the systematic excavations of the years 1928-1931 [1], an intense activity of reconstruction was undertaken: in several rooms large parts of masonry walls were rebuilt to give support to new roof structures with the twofold aims of protecting ancient remains and of bringing back the Villa to its former shape. In the course of the period between the 1960s and the 1970s many roof structures, including the *Peristilium* and the *Atrium tuscanicum*, were replaced with heavy reinforced concrete frames [2]. Over the same period, many rooms were covered with flat roofs supported by reinforced concrete and hollow brick elements mixed floors. In recent restoring interventions, timber and steel elements have been preferred, aiming to reduce the loads on ancient masonry.

In the fall of 2012 a timber rafter of the *Peristyle* collapsed. As shown in figures 5-8, the beam end has rotten away due to seepage of rain water through the roof. Although generalized conservative restorations were carried out between 2002 and 2007, this was not sufficient to avoid danger situation for both ancient remains and visitors. In order to assess the monument safety conditions, it was therefore decided to develop a standard procedure whereby these structures will be constantly monitored and regularly subjected to diagnostic examination to check their state of preservation. The present day state of roof structures has required the adoption of a multidisciplinary approach, suitable to other similar monuments, with which both integrity and structural stability can be assessed. In this paper the preliminary results of the first stage of the diagnostic survey are presented.



Figure 1. Aerial view of the domus

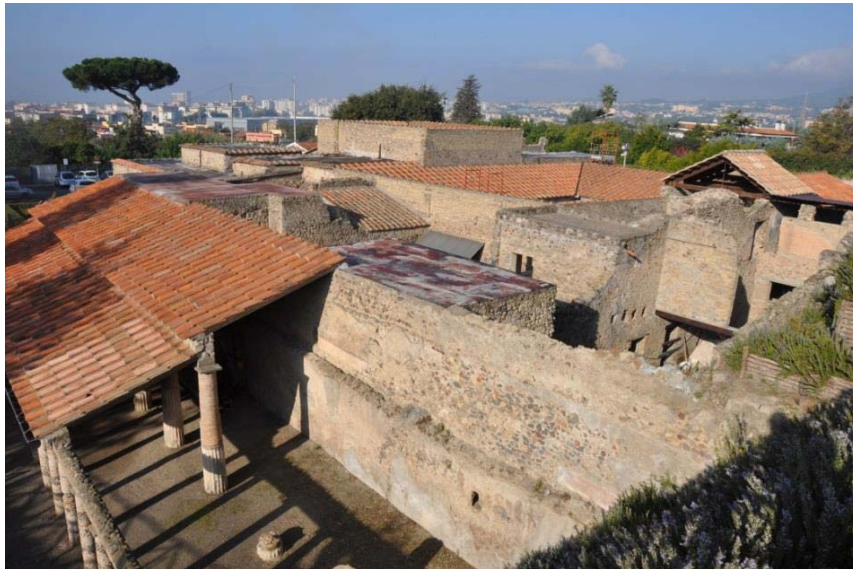


Figure 2. View from the east



Figure 3. The painting cycle depicting scenes from a mysteries rite.



Figure 4. A detail of the cycle



Figure 5. Peristilium: props in place of the collapsed beam



Figure 6. Detail of the rotten end of the collapsed beam



Figures 7-8. Details showing the decay of the collapsed beam

2. Study of the covering structures

2.1 Definition of roof typologies

As a result of the various restoration interventions that have been carried out since the *domus* discovering, the present day state of roofs displays a wide range of structural typologies: simple timber rafters roof (fig. 9) or wooden truss (fig. 10), reinforced concrete frame (fig. 11), flat roofs of precast concrete beams and ceiling bricks (figs. 12-13), reinforced brick-concrete beams (SAP type, figs. 14-15), and steel frame (fig. 16).



Figure 9. Tablinum: rafters roof



Figure 10. Vestibulum: truss roof



Figure 11. Atrium tuscanicum: reinforced concrete frame



Figures 12-13. Great Fresco hall. Views of the flat roof: extrados (right) and intrados (left)

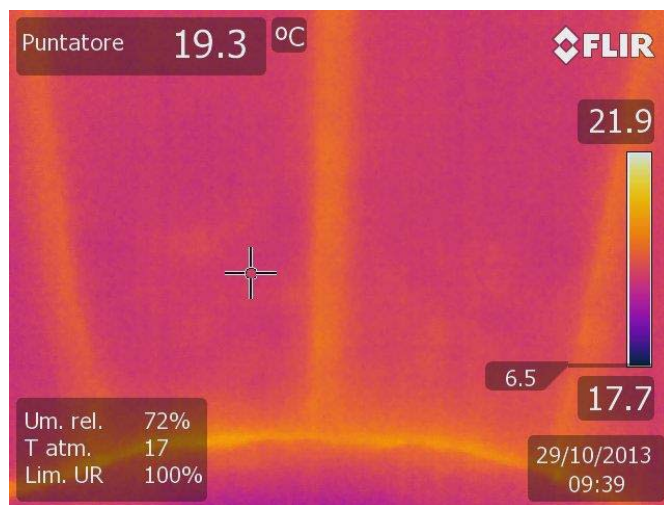


Figures 14-15. Reinforced brick concrete beams



Figure 16. Steel frame roof

The definition of the floors typologies in the different areas of the Villa was mainly based on an in-depth visual examination, performed both inside and outside. Some rooms in which observation alone has not enabled to ascertain the characteristics of the cover (like in presence of vaulted ceilings), have been investigated with the use of a thermal imaging camera, which has allowed to identify the presence of the beams and their framework (figs. 17-18). All data were digitally collected in a specially conceived acquisition form (fig. 19) [3].



Figures 17-18. Thermographic examination of a vaulted room: it can be observed the presence of three beams

The screenshot shows a mobile application interface for data entry. At the top, it displays 'Nessuna SIM', '15:51', and '70%' battery. The main header is 'DATA ENTRY UTSISM - Bologna' with the ENEA logo. The form is divided into several sections:

- PUNTO DI PRELIEVO:** A large photo area labeled 'FOTO 1' showing a construction site.
- EDIFICIO:** Text input field containing 'Villa dei Misteri'.
- N. CAMP.:** Text input field containing '63'.
- LUOGO:** Text input field containing 'Pompei'.
- UBICAZIONE:** Text input field containing 'Peristilio 63 angolo sud-ovest'.
- PROVA:** Radio button selected.
- CAMPIONE:** Radio button unselected.
- saggio:** Text input field.
- OBIETTIVO:** Text input field containing 'Proprieta' trave inclinata in calcestruzzo'.
- GPS - Long. E:** 455892.2
- Lat. N:** 4511555.4
- Proiezione:** UTM Zona 33
- NOTE:** A large text area containing a detailed report: 'indagine con pacometro per localizzare i ferri di armatura da saggio effettuato si rileva: armatura inferiore 6 ferri diametro 14 e stiffe da 10 ogni 22 cm circa. risulta trattamento con passivante, ma ferri particolarmente ossidati risulta uno spessore di circa 2 cm ai lati e sulla parte inferiore di malta tipo emaco la qualita' del calcestruzzo sembra buono (granulometria e consistenza) prelevato campione 2'.
- APPUNTI:** A large empty text area.

At the bottom, there is a footer with 'Operatore: MRG', 'Firma:', 'Data: 29/10/2013 16:41:53', 'Modificato: 09/12/2013 15:51:19', and a page number '27'. A navigation bar at the very bottom includes 'Precedente', 'Successivo', and a record counter 'Record 42 di 64 (ordinato)'.

Figure 19. Data acquisition form on iPad

2.3 Preliminary in-situ tests

In order to better define some technical aspects of the structure, a preliminary diagnostic campaign has been performed, aiming at the definition of the investigation tests necessary for the full characterisation of the coverings.

Particularly, assays were made on reinforced concrete beams (fig. 20), collecting samples later analyzed by means of electron microscopy (SEM; fig. 21), while the identification of the reinforcement bars layout has been carried out using a cover meter (fig. 22).



Figure 20. Assay on a reinforced concrete beam

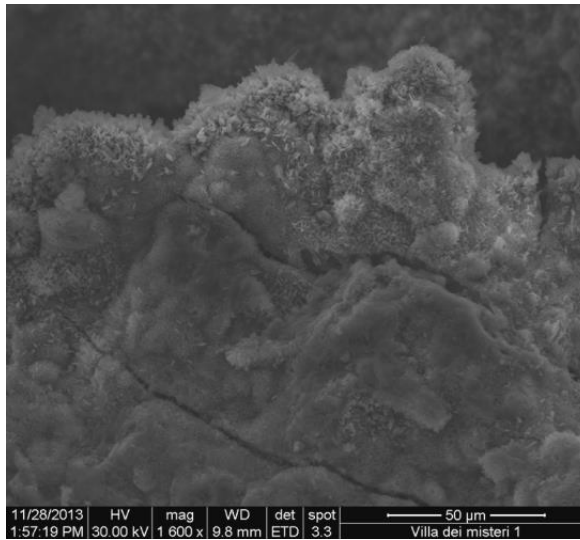


Figure 21. SEM image showing cracks and iron oxide crystals on a reinforcement bar



Figure 22. Detection of reinforcement bars with the use of a cover meter

Sclerometric tests and endoscopic observations have been also performed at the connection between timber elements and masonry, in order to evaluate the conservation state of the beams end (figs. 23-24).



Figure 23. Sclerometric test on a timber element



Figure 22. Endoscopic survey of beam extrados

2.4 Aerial survey: high resolution images acquisition of the roofs by UAV

UAV (Unmanned Aerial Vehicles) remote sensing is a set of techniques for collecting data through the use of sensors mounted on drones operating at low altitude (fig. 23). The proximity sensing is used in all those cases where it is not possible or convenient to use the traditional platforms to collect data from high altitudes or in those contexts in which it can be useful to integrate data from different altitudes of observation. The platform allows to acquire, at low altitude and with high resolution, structural and architectural details of buildings, helping to determine the conservation status, structural damage and collapse danger [4].

In “Villa dei Misteri” the technology has allowed to have an overview of the complex roofs system (fig. 24) and a preliminary assessment of its conservation status. An example of the image processing is shown in Figure 25 in which dark areas are observed on the roof of the *Peristilium*. This particular is very evident in the blue component of the image (the blue spectral band is defined on the water reflection peak), suggesting the presence of a surface layer that retains moisture.



Figure 23. Electric quadricopter used for the aerial survey.



Figure 24. High definition image extracted from video acquired through flights with radio controlled drone.

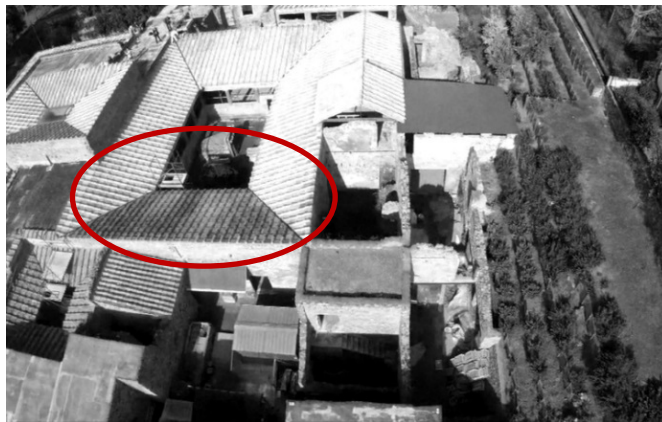


Figure 25. Blue image visualization of the Peristilium roof

3. Ambient vibration analysis techniques for site and structure characterization

Ambient vibration tests were carried out to characterize the dynamic response of the soil and the most relevant structural components of the Villa (fig. 26). For such measurements, as basis for seismic safety assessment, 15 Kinometrics SS-1 seismometers have been deployed in two layouts (fig. 27). In the first one, to characterize the soil, sensors were deployed in the three orthogonal directions at five locations on the ground. The second layout was devoted to obtain information on specific structural elements, such as reinforced concrete beams and roofs, wooden beams, and their relation with the original masonry walls.

At the present time the data analysis is still in progress. Nevertheless, preliminary results seem to show frequency content that could play a critical role in case of earthquake.



Figure 26. Acquisition data station



Figure 27. Sensor layout: the first one in black numbers and the second one in red numbers.

4. Waterproofing weaknesses and structural vulnerability

The aim of the survey was also to suggest a series of interventions that should be undertaken in the short term to preserve both the roofs and the precious decorations present inside the rooms.

Among the suggested interventions, it seems particularly urgent the substitution of degraded waterproof elements like bituminous membranes and covering tiles, and the realization of protections on the top of the perimeter walls to avoid water seepage through the masonries.

Some structural vulnerability have also been detected. In particular, the presence of heavy reinforced concrete frames, in some cases supported by slender unreinforced-masonry elements and lacking of any effective connection to the walls, may be very dangerous in case of seismic events [5] (figs. 28-29).



Figure 28. R.C. beam resting on a slender masonry element



Figure 29. R.C. elements resting on unreinforced masonry without any effective structural connection

5. Final remarks

It has been presented an analysis procedure based on a multidisciplinary approach, with which both integrity and structural stability of the roof structures of Villa dei Misteri can be assessed.

In this first stage of the survey, the main causes of decaying and damage have been identified and preventive measures to reduce risk of damage have been suggested. In particular, some heavy reinforced concrete roof frames are cause for serious concern, especially in the event of earthquakes. Furthermore, preliminary results of ambient vibration analysis show frequency content that may possibly affect the seismic response of the structure.

The described methodology has been developed also with the purpose to qualify a standard analysis procedure applicable to similar roofing typologies, very common in the archaeological site of Pompeii. With that aim, a more detailed diagnostic campaign including two specific sets of in situ tests has been planned. The first one, regarding the RC structures, includes sonic-rebound test (SONREB), core drilling and measurement of the carbonation depth, and compression tests on RC specimens. The second set, focused on timber elements, includes the identification of the wood essence, definition of the class of resistance according to the Italian technical standards (UNI codes), measurement of the moist content, drill resistance tests, and endoscopic observation of timber supports. In the final stage of the study, all the gathered data will be analyzed to assess the safety conditions of the monument, including seismic risk analysis.

Acknowledgement

The activities here described were carried out in the framework of an agreement between the *Soprintendenza Speciale per i Beni Archeologici di Pompei Ercolano e Stabia* and ENEA.

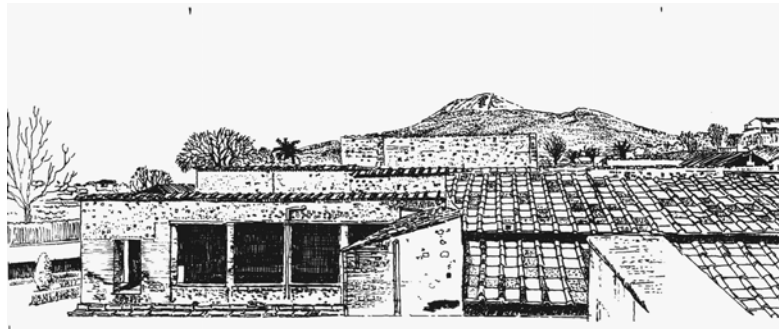
References

- [1] A. Maiuri, *Pompei : i nuovi scavi e la villa dei misteri*, Roma, La Libreria dello Stato, 1937.
- [2] I. Bergamasco, B. Carpani, P. Clemente, V. Papaccio. Seismic preservation of archaeological sites: the case of Pompeii. *8th Int. Conf. on Struct. Analysis of Historical Constr., SAHC* (Wroclaw, 15-17 Oct), Vol. II, 1386-1394. 2012.

[3] S. Bruni, M. Indirli, G. Maino, G. Marghella, A. Marzo, L. Moretti, L. Traverso, L'era post-pc: utilizzo avanzato dei nuovi strumenti digitali, *XI Congresso Nazionale IGIIC Lo Stato dell'Arte – Volume degli atti*, Nardini Ed., 2013.

[4] E. Candigliota, F. Immordino, Historical Heritage Safeguard: Remote Sensing by drones for Knowledge and emergency, *EAI Energia Ambiente ed Innovazione*, 3-4, 78-85, 2013.

[5] I. Bergamasco, V. Papaccio, B. Carpani, P. Clemente, F. Saitta. Seismic preservation of the archeological site of Pompeii: preliminary analyses, *Special EAI: Knowledge, Diagnostics and Preservation of Cultural Heritage, II*, ENEA, Rome, 48-55, 2012.



Dynamic Characteristics of Memorial Columns of Trajan and Marcus Aurelius using Microtremor

Yutaka Nakamura¹, Jun Saita¹ and Tsutomu Sato¹

Abstract

Memorial Columns of Trajan (TC) and Marcus Aurelius (AC) in Rome with a similar structure and size were studied their dynamic characteristics by microtremor measurement. As a result, the fundamental frequencies of horizontal vibration are approximately 1.6 Hz for TC and 1.3 Hz for AC, and caused mainly by bending vibration. These agree with the result of the previous investigation. Predominant frequencies of torsional and longitudinal vibrations are estimated approximately 15.5 Hz and 25.6 Hz, respectively. From these values the propagation velocities of shear wave and longitudinal vibration are estimated as 1900 m/s and 3100 m/s, respectively. Although these values are relatively small, about 65% of typical value, Poisson's ratio is estimated reasonable value about 0.33. On the other hand, the predominant frequencies of the torsional and longitudinal vibrations of AC are approximately 9.1 Hz and 18.8 Hz, respectively, and the velocity of shear wave and longitudinal vibration are estimated considerably low value as 1100 m/s and 2300 m/s, respectively. Longitudinal vibration propagation velocity is more than 50% lower than typical value, and the shear wave velocity is too low to estimate Poisson's ratio. It seems to be caused by low natural frequency of torsional vibration, and it is observed a tightened up vertical long damage on the west side of column body causing low resistance against torsional vibration. The destructive index K_b -value of the columns derived from the fundamental mode of bending vibration is 83 μ /Gal in maximum for upper part of TC and is 212 μ /Gal for top of AC with large variation. Thus, drift angle over 1/120 radian will be caused about 100 Gal of earthquake motion at base ground for TC and lower than 50 Gal of earthquake motion for AC.

¹ System and Data Research, Co., Ltd., Tokyo, Japan

1. Introduction

Memorial Columns of Trajan and Marcus Aurelius (referred as TC and AC hereafter) in Rome had been completed with same structure and size in 113 AD and 193 AD, respectively. Cylindrical surface of each column has spiral relief. Each memorial columns consist of stacked marble blocks hollowing out spiral staircase and each block is approximately 3.6m diameter and 1.52m height in average and has hollowed out 8 steps spiral staircase. Totally 19 blocks including terrace and base of the column are layered for approximately 30m height with two blocks for stature base on terrace. **Figure 1** shows models of staircase and block. Their foundation grounds are hard for TC and relatively soft for AC. AC has been received severe damage of weathering and earthquakes, and massive restoration has been done already in the 16th century. Although TC was made earlier than AC and has



Figure 1. Models of spiral staircase and block

been received the weathering and artificial damages, it still remains almost original form in present.

There have been research works on dynamic characteristics of TC and AC previously, and our research aims to grasp precisely the existing condition and reports the result of the preliminary microtremor measurement for both TC and AC.

2. Microtremor measurement and data analysis

The measurements were done between 10 a.m. to 2 p.m. at 28th March of 2012, TC in the morning and AC in the afternoon. The weather was fine. **Figure 2** shows the distribution of the measuring points for TC and AC, indicating for under the terrace and spiral staircase without accuracy in dimension.

For TC there are five measurement points, TTN, TTE, TTS, TTW and TTC on the terrace, the highest floor. Two couples of measurement points, TTN-TTS and TTE-TTW, were measured simultaneously for detecting rocking and torsional vibration. Also four points on surface ground, TBN, TBE, TBS and TBW were set with contacting the pedestal, and two couples of measurement points, TBN-TBS and TBE-TBW, were measured simultaneously. For measurement of column body, one continuous measuring point TTC, inside of the entrance on east side of the terrace, was set for simultaneous measurement. The spiral staircase of TC turns one rotation by 14 steps. From TTC, four points, TC1 to TC4, were set every 28 steps, and other three points, TC45, TC5 and TC6 were set every 14 steps in the column body, and TC7 five steps under TC6 were set in the pedestal.

For AC, all the measuring points were measured individually. Five points, MTN, MTE, MTS, MTW and MTC on the terrace, under the MTC, six points of MT1 to MT6 were set every 28 steps, and MT7 and MT8 were set 22 steps and 36 steps under the MT6 respectively. The spiral staircase of AC has 14 steps per turn as same as TC. At each point, microtremor of three components EW, NS and UD were measured simultaneously for duration of three minutes with 1/100 seconds sampling.

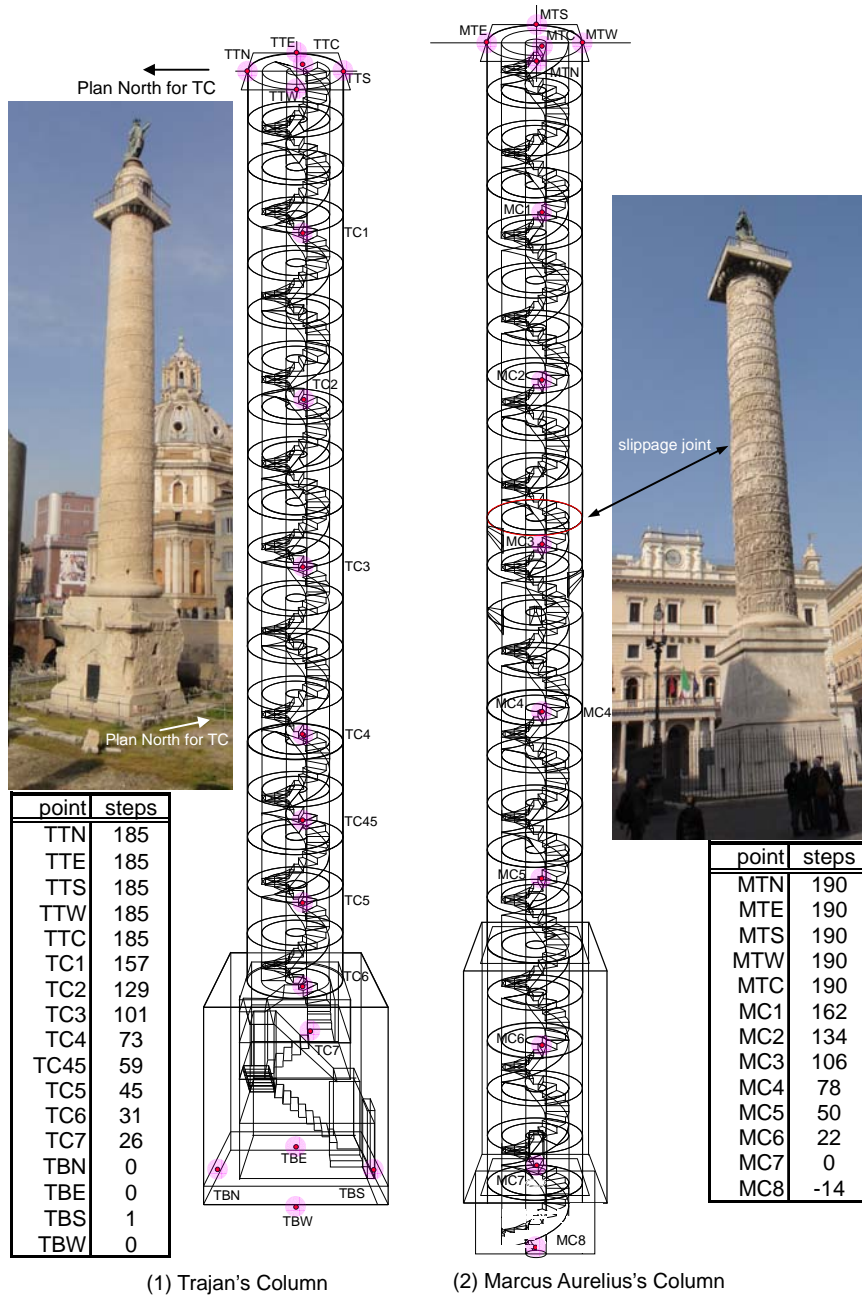


Figure 2. Distribution of the points for microtremor measurements

Frequency analysis has been carried out by Fourier transform for the measured waveform. The response spectra of TC and AC have been estimated using simultaneous and individual measurement, respectively. The analysis used 40.96 seconds (4096 data) length record and the final result was derived from spectra averaged three or four times. Also the spectral ratio of target point against base point or H/V spectral ratio is derived. These results of individual or simultaneous measurement are compared and investigated.

3. Result of analysis

3.1. Column of Trajan

Table 1 shows the results of the analysis of the predominant fre-

Table 1. Results of microtremor measurement of TC

| TC | Simultaneous. | F Hz | maxA | maxKb | |
|--------------|---------------|-------|-------|----------|-----|
| EW | 1st | 1.59 | 18.8 | 83.1 | |
| | 2nd | 8.99 | 7.8 | 5.0 | |
| | 3rd | 19.17 | 6.3 | 1.2 | |
| NS | 1st | 1.59 | 15.5 | 77.2 | |
| | 2nd | 8.99 | 5.2 | 3.4 | |
| | 3rd | 20.29 | 9.3 | 1.0 | |
| Longitudinal | 1st | 25.64 | 7.8 | 0.2 | |
| Torsional | 1st | 15.53 | | | |
| TC | Individual | F Hz | maxA | maxKb | |
| EW | 1st | 1.59 | 188.8 | 2271 | |
| | 2nd | 9.03 | 8.3 | 4.8 | |
| | 3rd | 19.04 | 6.0 | 1.2 | |
| NS | 1st | 1.59 | 98.6 | 1293 | |
| | 2nd | 9.03 | 7.3 | 4.4 | |
| | 3rd | 20.26 | 9.6 | 1.3 | |
| TC | H/V | F Hz | maxA | maxKb/Kg | |
| EW | 1st | 1.51 | 22.0 | 181 | |
| NS | 1st | 1.44 | 11.2 | 111 | |
| Ground: BN | 1st | 5.81 | 1.9 | 0.6 | |
| | BE | 1st | 5.00 | 2.0 | 0.8 |
| | BS | 1st | 5.27 | 2.3 | 1.0 |
| | BW | 1st | 5.00 | 2.3 | 1.0 |

quencies for each component and position. According to this table, comparing simultaneous and individual measurements, they are almost equal for each other on natural frequencies, but there is large difference for first mode shape. On the other hand, from H/V spectral ratio, estimated natural frequencies are little lower but amplification factor is close to the results estimated by simultaneous measurement. The following explains the results of these analyses in detail.

3.1.1. Simultaneous measurements

Figure 3 shows the amplification spectra of the sites along the column elevation against the site TC7, 26 steps from the lowest level in a pedestal as a rigid block, as a result of the simultaneous measurement. It is possible to draw the vibration mode for the entire frequency mode because the phase can be grasped by the simultaneous measurement. Please find an animation to visualize the vibration mode sweeping

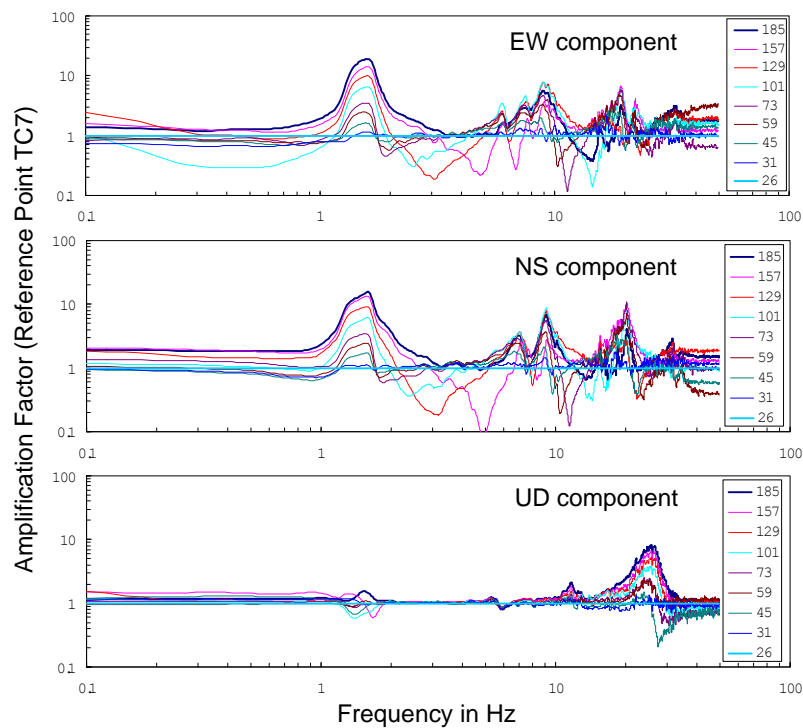


Figure 3. Amplification spectra of TC estimated from simultaneous measurements

frequency in website ([6]).

Figure 4 shows the vibration modes for each peak frequency with considering phase difference. These figures show that the number of peaks of EW component is larger than that of NS component, that the first peak frequency is 1.59Hz for both EW and NS components, and that the shape of the mode diagram is slightly differ from each other.

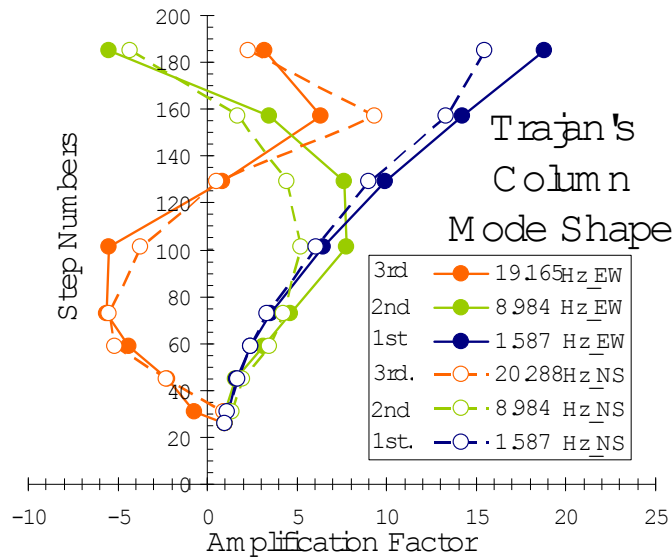


Figure 4. Mode shape of TC estimated from simultaneous measurement

The shape of mode diagram for the first peak frequency is smooth. That of both EW and NS components seems to consist of mostly bending deformation and only that of NS component is recognized overlapped slightly shear deformation.

Second order frequencies with large peak are estimated 8.99 Hz for each direction with the second order mode shape. Natural frequencies of third order are estimated 19.17 Hz for EW and 20.29 Hz for NS with third order mode shape. There are many spectral peaks in response spectra. These peaks might be corresponding to the local damage of column.

For the bending vibration of a uniform cantilever, the natural frequency's ratio between first order mode and second or higher mode is approximately 1: 6.2669...: 17.5449...: In case of shear or torsional

vibration, this ratio becomes 1: 3: 5: According to the result of microtremor measurement, it could be clearly recognized up to the natural frequency of third order mode, and the ratio is approximately 1:5.65:12.06 for EW component and approximately 1:5.65:12.76 for NS component. Consequently the horizontal vibration of TC is estimated consisting of almost bending vibration.

According to the measurements on the terrace, there is torsional vibration at the frequency range between 14 Hz and 19 Hz, and reaching maximum at 15.5 Hz. At other frequency range torsional vibration can not be recognized. At the range between 14 Hz and 19 Hz, the peak and the trough of the vibration modes are interchanged intricately at each measuring points on the column body, and this phenomena may appear the effect of torsional vibration (see an animation on website of SDR, reference [6]). Shear wave velocity of TC is estimated 1900 m/s from the predominant frequency of torsional vibration.

In addition, the vertical vibration of TC predominates at 25.6 Hz, and the vibration mode shape shows the first order. And the propaga-

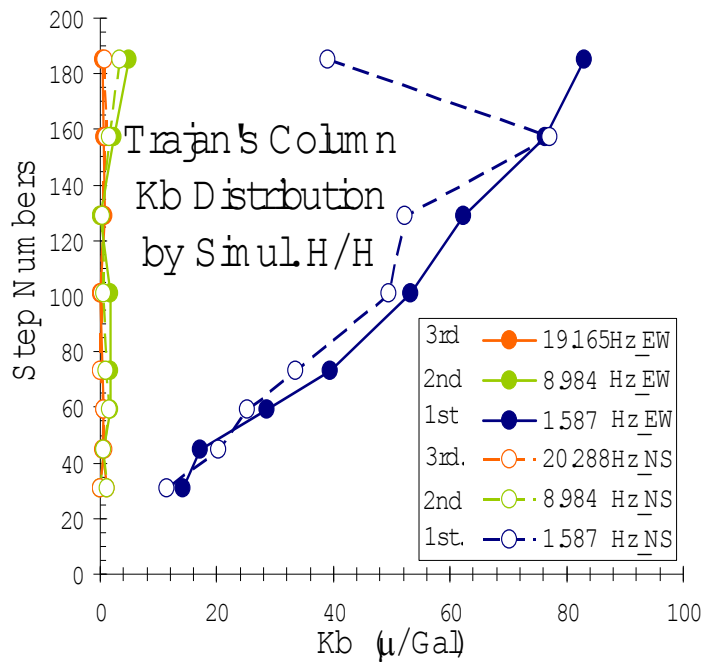


Figure 5. Kb-value of TC estimated from simultaneous measurement

tion velocity of the longitudinal vibration of TC is estimated 3100 m/s, and the Poisson's ratio is estimated 0.33 from the shear wave velocity and it is a reasonable estimation as marble. However, because the estimated velocities of TC are about 65% of the typical value of marble, 4800 m/s for longitudinal vibration or 2900 m/s for shear wave, TC seems to be considerably deteriorated.

Figure 5 shows a destructive index K_b value derived from the estimated amplification mode of horizontal vibration. Please see the detail of K_b value on reference [4] as a name of K_T . According to this figure, the influence of the first order vibration mode is very large, and it is possible to ignore the higher modes. Distribution of K_b values by the first order vibration grows higher toward to the top, and reaches the maximum value of 83 μ /Gal at the top. Strong motion of PGA 100 Gal will cause 1/120 of drift angle at the top of column near terrace. The ability of shear deformation of TC which is made simply by stacking large marble blocks must be considered.

3.1.2. Individual Measurements

(1) Individual spectral ratio

Here the response spectrum ratio against control point is considered in case of using not simultaneous measurement record.

Figure 6 shows estimated mode shape for several orders using spectral ratio against point TC7. According to this, predominant frequencies by third mode are almost equal to the results of simultaneous measurement. On the mode shape, however, the amplification factor becomes larger close to the terrace, although higher mode shape are almost same. Temporal or special stationarity of the column may be disturbed by the activities of other investigation teams on the terrace or inside the column body.

It is expected that the response characteristics can be estimated properly from the spectrum ratio against control point under keeping stationarity in case of not simultaneous measurement. However it is obvious that disturbance of stationarity causes disturbance for the estimation result. Because the column seems to be impacted constitutionally by the shaking to upper part, it is also necessary for response spectrum estimation to reconfirm to take countermeasure as limitation

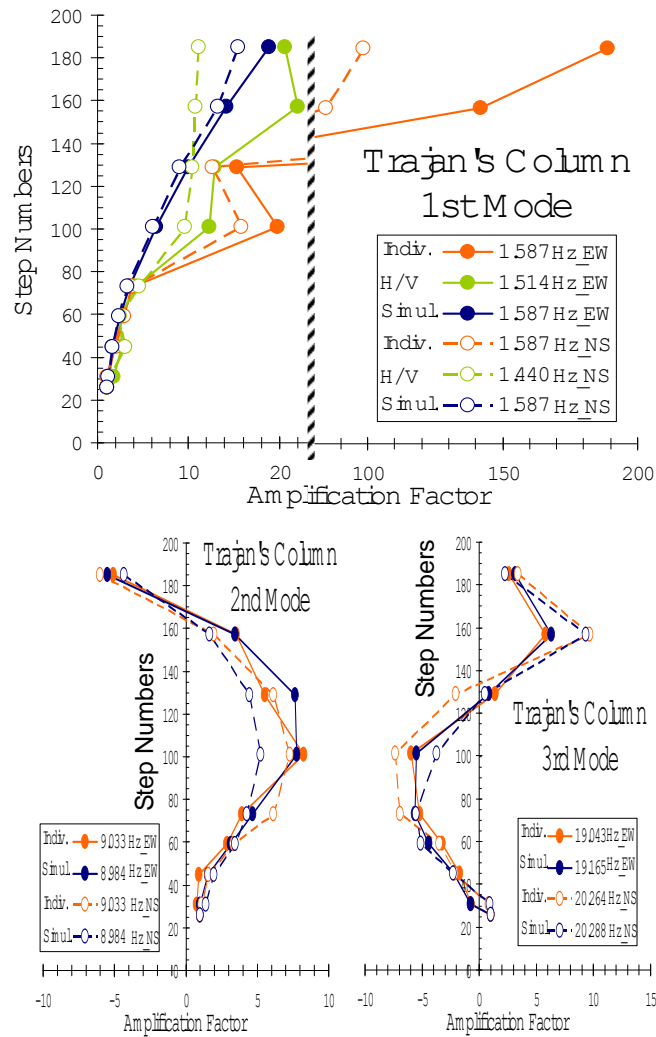


Figure 6. Comparison of the shape of modes of TC between various methods

of other activities during measurement or conducting simultaneous measurement.

(2) H/V and its ratio

Here shows a trial to estimate reasonable response spectrum from individual measurement using H/V spectral ratio. Response of vertical component is rather clear than that of horizontal component at high frequency range. However at lower frequency range, the characteris-

tics of vertical motion on the base ground are similar to that of horizontal motion. This idea uses these characteristics. In case of ground, a peak appears at a frequency corresponding to the predominant frequency of the surface ground, and the peak value gives approximately the amplification factor. Also in case of structures, it is necessary to notice that the H/V spectrum ratio sometimes reflects the motion as rocking vibration.

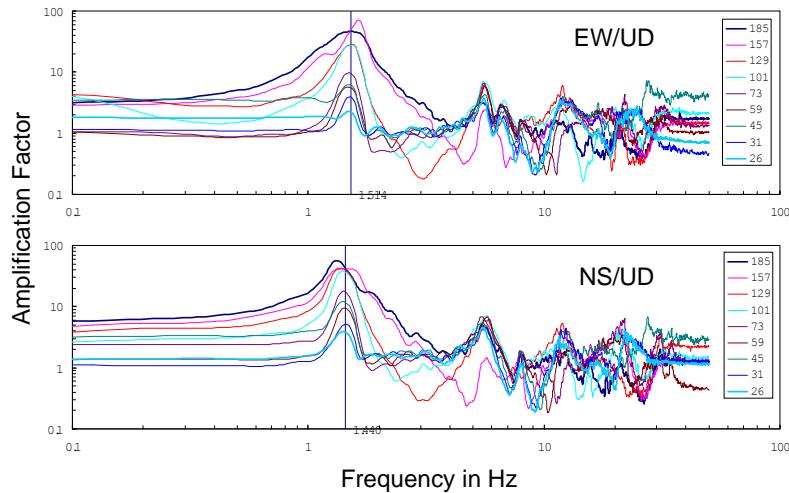


Figure 7. H/V spectral ratio at the sites of TC

Figure 7 shows overlapped H/V of each point at TC. According to this figure, the predominant frequency of 1.5 Hz corresponds to the first order natural frequency of TC. The frequency of 5.59 Hz is recognized at all points, and it can be considered as the natural frequency for surface ground with about twice as amplification factor.

Figure 6 also shows a mode shape corresponding to the principal frequency around 1.5 Hz. According to this figure, the abnormal phenomena of enlargement of amplification factor near the terrace can be avoided, and estimated amplification factors and mode shape are similar to the results of simultaneous measurement mentioned above. In case of individual measurement, it is expected that the amplification factor and mode shape can be estimated roughly by calculating the H/V or the ratio of H/V.

3.2. Column of Marcus Aurelius

On AC each microtremor measurement was conducted individually. **Table 2** shows an analytical result of measurement.

Table 2. Results of microtremor measurements of AC

| AC | Individual | F Hz | maxA | maxKb |
|--------------|------------|-------|-------|----------|
| EW | 1st | 1.29 | 64.0 | 936 |
| | 2nd | 6.59 | 15.2 | 17.9 |
| | 3rd | 15.02 | 12.4 | 2.3 |
| NS | 1st | 1.22 | 53.3 | 957 |
| | 2nd | 6.98 | 19.4 | 15.9 |
| | 3rd | 15.14 | 20.9 | 3.0 |
| Longitudinal | 1st | 18.80 | 57.7 | 1.0 |
| Torsional | 1st | 9.13 | | |
| | 2nd | 25.95 | | |
| AC | H/V | F Hz | maxAF | maxKb/Kg |
| EW | 1st | 1.25 | 18.8 | 212 |
| NS | 1st | 1.22 | 13.9 | 144 |
| Ground:MC7 | 1st | 1.22 | 2.54 | 5.3 |
| CMGW | 1st | 1.37 | 2.76 | 5.6 |

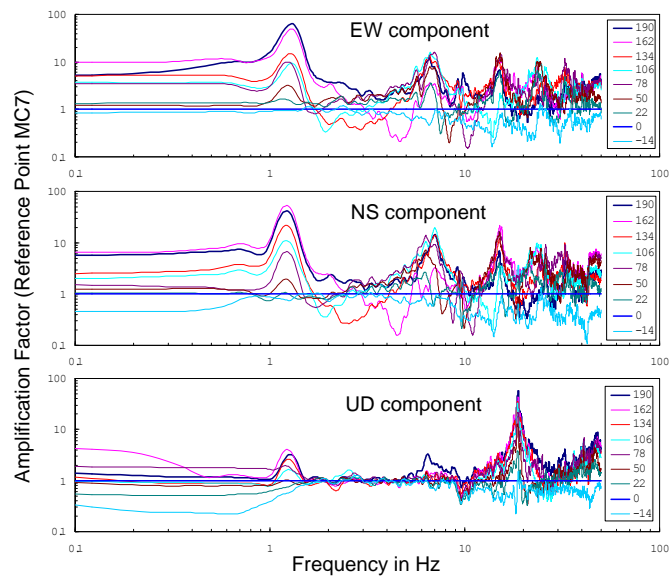


Figure 8. Amplification spectra of AC estimated from individual measurement

(1) Individual spectral ratio

Figure 8 shows the individual spectral ratios of each point to point MC7 corresponding to ground surface level. **Figure 9** shows the mode shapes of first to third order vibrations. According to this figure, large amplification is observed near the terrace for first order mode same as that of TC, and it seems to reflect the activity of people. The influence for higher mode may be smaller than the result of TC. Anyway, it is necessary for grasping the exact response to conduct measurement at another time. The natural frequencies of longitudinal and torsional vibrations are estimated 18.8 Hz and 9.1 Hz, respectively. From this the propagation velocities are estimated 2300 m/s and 1100 m/s, respectively. The estimated velocity of longitudinal vibration is more than 50 % lower than typical value, 4800 m/s. The shear velocity is also estimated too low to calculate the Poisson's ratio. This is caused by the low frequency of torsional vibration. As seen in **Photo 1**, there is trace of restoration for vertical damage clearly appears on west side of AC, and this is considered as a reason why the frequency of torsional vibration is very low.

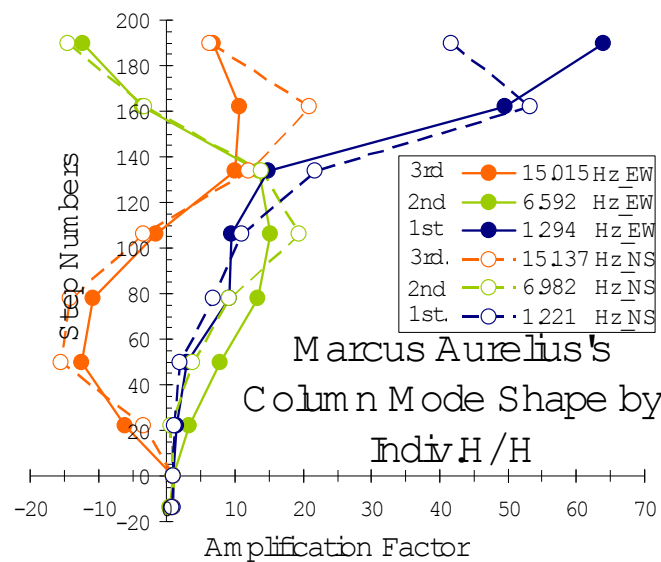


Figure 9. Mode shape of AC estimated by individual measurements



Photo 1. Damage of AC at West Side

(2) *H/V spectral ratio and etc.*

Figure 10 shows overlapped H/V spectral ratio of each measurement point. The first order vibration mode shape is considered to similar to the result of the estimation from the H/V based on the discussion for TC. **Figure 11** shows the mode shapes of first order vibrations.

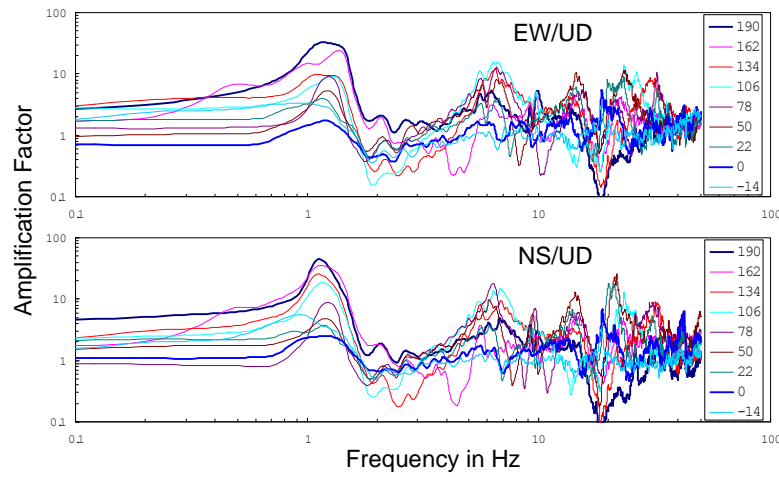


Figure 10. H/V spectral ratio at the sites of AC

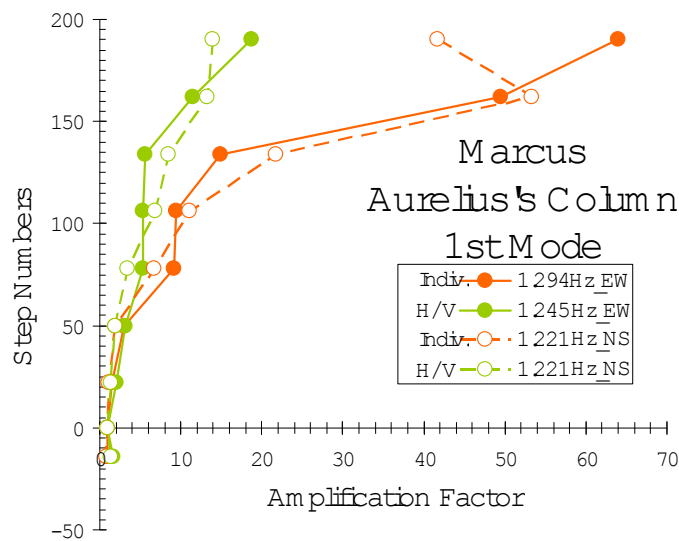


Figure 11. Comparison between first mode shapes of H/V and H/H of AC from individual measurements

The destructive index K_b of AC is calculated from the estimation result of amplification characteristics from H/V ratio, and K_b is compared with the result from the simultaneous measurement of TC. **Figure 12** shows the results of comparison of K_b of TC and AC. K_b

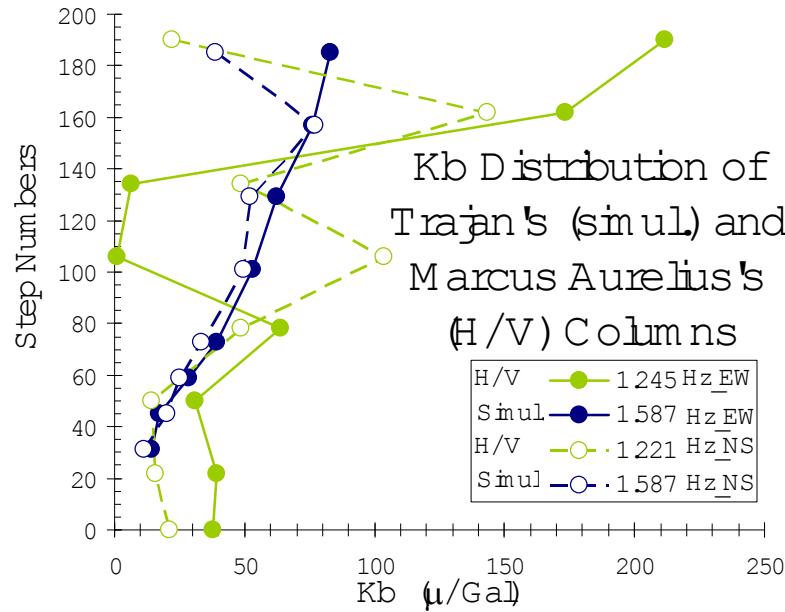


Figure 12. Comparison between estimated Kb-values for TC (blue mark) and AC (green mark)

value of TC grows larger toward to higher point reaching maximum 83 μ /Gal. Kb values of AC shows variation at each point, and the maximum value is 212 μ /Gal near the terrace. In other words, drift angle over 1/120 will occur at TC with over 100Gal of seismic acceleration, and in case of AC the same level of drift angle will occur even under 50Gal. These columns are constructed only stacking the large marble blocks with getting stability only by dead load. It is necessary to consider losing the stability of columns by growing the rocking vibration caused by column-soil interaction.

4. Concluding remarks

This paper describes the results of microtremor measurement for two memorial columns, Trajan's Column and Marcus Aurelius' Column.

Natural frequencies of horizontal vibration are about 1.6 Hz for TC and about 1.3 Hz for AC, and both of them seems to be caused by bending vibration. These are almost similar to previous researches.

The natural frequencies of longitudinal and torsional vibrations of TC are 25.6 Hz and 15.5 Hz, respectively. From this the propagation velocities of the longitudinal vibration and the shear wave are estimated 3100 m/s and 1900 m/s, respectively. These velocities are low value, 65 % of typical value, but the Poisson's ratio is reasonable, 0.33. On the other hand, the natural frequencies of longitudinal and torsional vibration of AC are 18.8 Hz and 9.1 Hz, respectively, and from this the propagation velocities are estimated 2300 m/s and 1100 m/s, and these are very low values. The velocity of longitudinal vibration of AC is extremely low, under 50 % of typical value. And the Poisson's ratio could not be calculated because of too slow shear wave velocity. The natural frequency of torsional vibration of AC is extremely low reflecting the longitudinal damage.

For the estimation of vibration mode, the results of simultaneous and individual measurement were compared. Because the memorial columns vibrate easily, it is confirmed that the result of measurement is easily affected by the human activity inside the column and the affection is difficult to avoid without simultaneous measurement. And also it is confirmed that affection can be avoid with extended usage of H/V spectrum ratio.

According to the results of calculating the destructive index K_b of the columns that are based on the fundamental mode of bending vibration, K_b of TC grows larger toward to the top reaching a maximum of about $83\mu/\text{Gal}$ near the terrace, and that of AC shows variation at each point and the maximum is $212\mu/\text{Gal}$ near the terrace. In other words, drift angle over $1/120$ will occur over 100 Gal of seismic acceleration for TC, and in case of AC the same level of drift angle will occur even under 50Gal. Because both the columns are built with only stacking of marble block, the columns ensure its behavior of the elastic body only with pre-stress caused by its own weight.

Therefore, if the effect of rocking vibration due to the coupling effect between columns and ground becomes larger, it is easy to become unstable. It seems that it will be important to conduct a detailed investigation and determine the limit of the ground motion.

By the additional detailed investigation based on the knowledge obtained by this survey and by the sequential investigation with standardized research method, it is expected that the investigation will

contribute to the reasonable maintenance or restoration plan with grasping the degree or location of damage quantitatively.

This time, simultaneous measurement was conducted only for TC. It is desirable to measure TC and AC again completely for confirmation.

Acknowledgments

The measurement of memorial Columns in Rome was conducted under the supporting of Professor Valente and Associate Professor Tallini of L'Aquila University. We would like to express our thanks for their helps.

References

- [1] Clemente, P. and et al.: La Colonna Antonina in Roma: Valutazione Dgli Esetti Delle Vibrazioni Ambientali, *ASS. I. R. C. CO.*, 1988, pp.207-217.
- [2] Boschi, E. and et al.: Resonance of Subsurface Sediments; an Unforeseen Complication for Designers of Roman Columns, *Short Notes, Bulletin of the Seismological Society of America*, Vol.85, No.1, 1995, pp. 320-324.
- [3] Krstevska, L. and et al.: Experimental Dynamic Testing of Prototype and Model of the Antonina Column in Roma, *11th WCEE*, paper #545, 1996.
- [4] Nakamura, Y. and et al.: Vulnerability Investigation of Roman Colosseum using Microtremor, *12th WCEE*, paper #2660, 2000.
- [5] Clemente, P.: Vibrazioni Indotte Dal Traffico: Un'insidia Per I Monumenti, *ENERGIA, AMBIENTE E INNOVAZIONE*, No.4, 2002.
- [6] Nakamura, Y., Valente, G. And Tallini, M.: Vibration Mode Sweep for Trajan Column, animation on website, <http://www.sdr.co.jp/>, 2012.
- [7] Nakamura, Y., Saita, J. And Sato, T., 2012, Dynamic Characteristics of Memorial Columns of Trajan and Marcus Aurelius using Microtremor, SDR Report No.13, <http://www.sdr.co.jp/>.

The Cochlid Columns in Rome: ambient vibration survey and comparison with previous results

Giovanni Bongiovanni¹, Giacomo Buffarini¹, Paolo Clemente¹,
Cinzia Conti², Francesco Del Monaco⁴, Federica Durante⁴, Antonio
Rovelli³, Fernando Saitta¹, Sandro Serafini¹, Marco Tallini⁴,
Gianfranco Valente⁴

Abstract

The results of ambient vibration surveys of the Cochlid Columns in Rome are shown. The objective of this analysis was the characterization of the dynamic behaviour of the monuments and the comparison with the results obtained with previous similar studies, carried out in the 80s using different instruments and different data analysis methods. The new surveys were performed using two different and independent sets of instruments contemporarily. Data were analysed both in the time and frequency domains. For both the columns the analysis showed the presence of two translational frequencies, quite close one to the other while the previous measurements had pointed out just one resonance, and also higher translational frequencies. A rotational frequency, was also observed. Data analysis pointed out interesting information about the dynamic behaviour of the columns.

1 ENEA C.R. Casaccia, Rome, Italy.

2 SSBA, Rome, Italy.

3 INGV, Rome, Italy.

4 DICEAA-CERFIS, Università dell'Aquila, Italy.

1. Introduction

The Cochlid Columns are both composed by 19 marble blocks carved to obtain a spiral staircase, the so called *cochlea*, connecting the central core to the outer ring. Each block is about 1.5 m tall, for a total height of about 30 m. The external diameter varies from 3.7 to 3.2 m, while the diameter of the internal core varies from 1.0 to 0.5 m.

The Aurelian Column (Figure 1 - left) was erected between 176 and 192 A.D. to celebrate the triumphs of Emperor Marcus Aurelius. It was located in *Piazza Colonna* just in front of *Palazzo Chigi*, that nowadays is seat of the Italian Prime Minister. The structure, height 29.6 m and diameter 3.7 m, is surmounted by a bronze statue of St. Paul and rests on a square pedestal of about 6 m with a height of about 10 m.

The Trajan's Column (Figure 1 - right) was completed in 113 A.D., probably under the supervision of the architect Apollodorus of Damascus. It commemorates Roman emperor Trajan's victories in the Dacian Wars and was located in the Roman Forum, quite close to the Quirinal Hill, where is seat of the Italian Republic President. The column is surmounted by a bronze statue of St. Peter, placed by Pope Sixtus V in 1587, and rests on a square pedestal composed by four rectangular carved blocks for a total of 6.2 m. So the total height is about 40 m.

The extent and the consistency of the underground soil and of the foundations are unknown for both the columns.

In the XVI century the Column of Marcus Aurelius was in very poor static conditions. So Pope Sisto V involved the architect Domenico Fontana to design its restoration (Masiani, 2010). Fontana noticed the presence of sliding and rotation among adjacent blocks (Figure 2) and first questioned if these could be related to any earthquake (Giuffré, 1984). The historical investigation revealed that strong earthquakes, such of January 22nd, 1349, with epicenter in Abruzzo, caused serious damage in Rome and probably also to the column. Fontana designed the restoration of the structure and replaced significant missing portion of marble.

More recently, during cleaning operations of the Trajan's Column between 1980 and 1985, Giuffrè noticed some minor cracks, a couple of which could be attributed to earthquakes (Giuffrè, 1988).



Figure 1. View of the Aurelian (left) and the Trajan's (right) Columns.

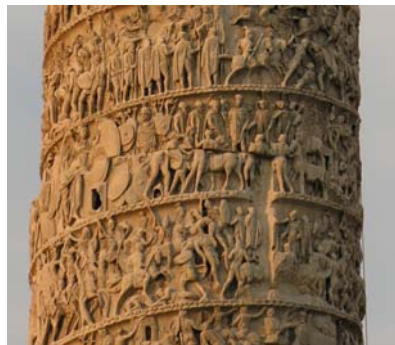


Figure 2. Relative dislocation between two adjacent blocks of the Column of Marcus Aurelius

These are just two examples of the importance of monuments in the study of the historical seismicity of the Italian territory. As a matter of fact, the information about historical events is related to the structural

behaviour of relevant buildings and monuments, and the historical seismicity has been reconstructed thanks to historical documents that reports descriptions about the damages of relevant buildings and monuments. Fortunately several monuments can be still observed and analyzed and so the characteristics of past earthquakes can be estimated.

The analysis and interpretation of the historical documents should also account for all the changes occurred on monuments, due to material degradation, changes in loads, seismic actions, traffic-induced vibrations, presence of other buildings. A suitable study should pass through the complete historical analysis and the structural analysis in the present situation. This can be done only by means of a reliable experimental analysis and an accurate numerical modelling (Bongiovanni, 1990; Buffarini, 2008; Buffarini, 2009) and should also allow the check of its present structural capacity and the definition of a suitable intervention.

It is worth noting that ambient and traffic-induced vibrations, which contribute to the bad health status of structures, could become very dangerous when acting on structures already damaged by earthquakes. In this paper the results of the experimental dynamic analyses carried out on the Aurelian and Trajan's Columns in Rome are shown. They are compared with those obtained in a previous experimental campaign carried out in the 80s.

2. Previous investigations

2.1 Experimental analysis

An experimental study was carried out on several monuments in Rome by ENEA in the 80s in collaboration with the *Soprintendenza Speciale per i Beni Archeologici (SSBA) di Roma* and ISMES. The effects of the traffic induced vibrations were investigated, especially with reference to the vibrations induced by the trains of the underground. Data analyses were performed both in time and frequency domain (Clemente, 1993; Clemente, 1994; Clemente, 1995). Among the monuments also the Aurelian Column (Clemente, 1988) and the Trajan's Column (Clemente, 2002) were studied.

The measurement campaigns were carried out in 1985. Eighteen Teledyne-Geotech seismometers were used, six of them were deployed in vertical direction and twelve in horizontal radial and tangential directions (Figure 3). The signals recorded in analog form on magnetic tape, were then amplified and filtered, and finally sent to an A/D converter and acquired with a sampling step of 0.005 sec. Five series of measurements were performed, lasting 90 minutes each, at different times of the day. The portions of recordings with highest energy content were extracted and analyzed.

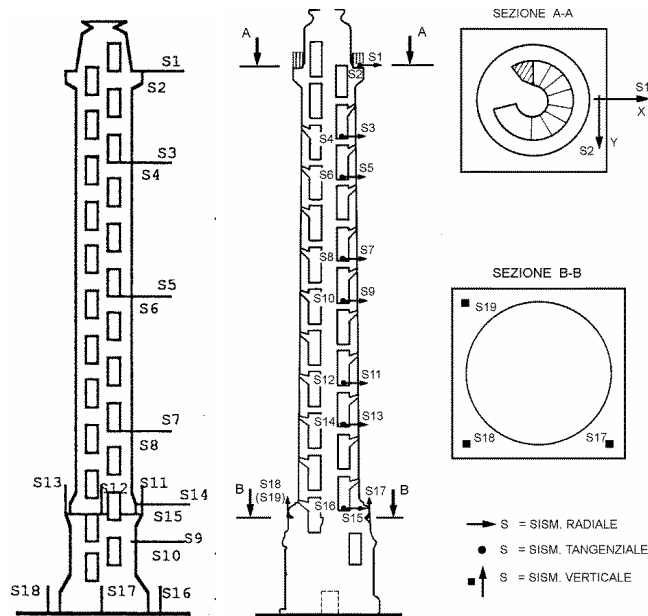


Figure 3. View of the column and sensors deployment.

The results obtained can be synthesized as follows:

- the vibration amplitudes recorded on the Column of Marcus Aurelius were particularly low, with peak values of 0.32 mm/sec along the column, and of 0.15 mm/sec on the pedestal. The spectral analysis pointed out two structural resonances at 1.33 and 6.9 Hz, respectively, associated to modal shapes of the structure (Clemente et al., 1988);

- also the vibration amplitudes of the Trajan's Column were very low, with peak values of 0.10 mm/sec along the column, and of 0.05 mm/sec on the pedestal; the velocity module on the basement was 0.14 mm/sec; the spectral analysis pointed out a resonance frequency at 1.60 Hz, associated to the first modal shape of the structure; other significant peaks were in the range [5.5, 9.0] Hz (Clemente, 2002).

The same fundamental resonant frequencies of the two columns were estimated by Boschi et al. (1995) through ambient vibration measurements performed in the 90s.

2.2 Numerical modeling

The finite element models of the columns were composed of beam elements, with geometrical characteristics equal to those of the stone blocks, and material characterized by a weight density $\rho=27.00 \text{ kN/m}^3$ and a Poisson's ratio $\nu=0.25$. The presence of discontinuities between the blocks, where most of the deformation was located, was simulated in two different ways. In the Aurelian Column model the beam elements had a Young's modulus typical of the marble ($E=60000 \text{ N/mm}^2$), and were joined by means of elements with a very low length with elastic modulus significantly lower than that of the blocks themselves ($E^*=600 \text{ N/mm}^2$). In the Trajan's Column model the Young's modulus of the blocks was chosen in order to optimize the correspondence between the experimental and numerical results ($E=20000 \text{ N/mm}^2$) and no additional elements were considered. In both cases the pedestals were divided into four beam elements. Since the signal analysis did not show the presence of significant soil-structure interaction effects, the column was considered fixed at its base.

The dynamic analysis gave the frequencies reported in Table 1, which were very similar to those obtained experimentally, as well as the modal shapes (Figure 4). The numerical model was used for the response spectrum analysis according to the Italian code for low seismicity areas. The effects of the first three modal shapes were superimposed.

Table 1. Numerical frequencies.

| Mode | Aurelian Column (Hz) | Trajan's Column (Hz) |
|------|-------------------------|-------------------------|
| 1 | 1.33 | 1.7 |
| 2 | 7.8 | 9.0 |

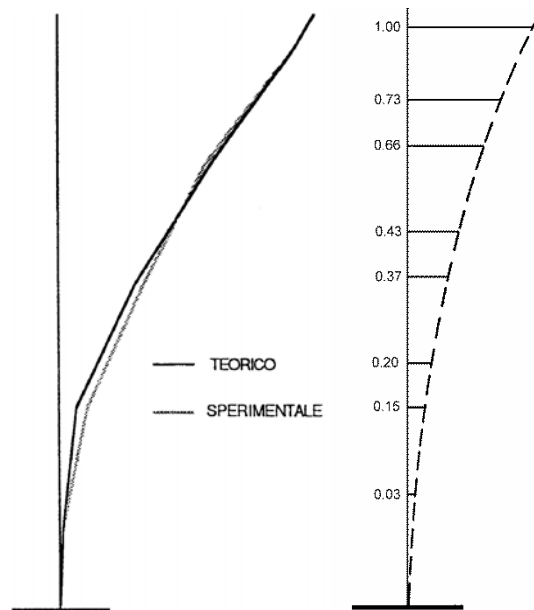


Figure 4. Experimental first modal shapes of the Aurelian (left) and Trajan's (right) Columns.

The assumption of linearity is valid as long as the friction between the blocks is not exceeded and no tensile stresses are present, namely the resultant of the loads is not out of the core of inertia. If the first assumption would be not satisfied slippage would occur resulting in the loss of the geometry of the column; if the second one would be not satisfied tension gap elements should be introduced in the model, corresponding to the discontinuity.

According to the obtained results the ratios between the shear and the normal forces were much lower than the dynamic and the static friction coefficients of the marble. Also normal stresses were quite low, so one can state the stability of the structure, at least with reference to the stresses caused by environmental vibrations and weak

earthquakes. The limitations of the model proved to be inessential, the basic assumptions being always satisfied.

3. New experimental analyses

Another experimental campaign was carried out on the two columns in March 2012. The instrumentation used consisted of two contemporary but independent layouts:

- nine Kinometrics short period (1.0 Hz) seismometers Ranger SS-1 connected to a Kinometrics K2 recorder;
- three stand-alone SARA SL06 recorders with internal triaxial electrodynamic sensor, nominal natural frequency 2 Hz, 24 bit A/D converter, GPS absolute timing, sampling rate set to 100 sample/sec.

The SS-1 seismometers were deployed as follows (Figure 5):

- three sensors, one in the vertical and two in the horizontal directions were at the base of the pedestal, at the lowest level of the staircase;
- three sensors in the horizontal directions were at the base of the column, just above the top of the pedestal;
- three sensors were at the top of the column, all in horizontal directions.

The three SARA recorders were deployed at the base of the pedestal (SD), at the top of the column (ST) and at a middle height (SM), respectively. Each of them had sensors in the three orthogonal directions.

In the Trajan's Column a second configuration was also considered in which sensors were deployed on four levels as shown in Figure 5 (right):

- three sensors, one in the vertical and two in the horizontal directions were at the base of the pedestal, at the lowest level of the staircase;
- two sensors in orthogonal horizontal directions were at the base of the properly said column, just above the top of the pedestal;
- two sensors in orthogonal horizontal directions were at half of the height of the column;

- two sensors in orthogonal horizontal directions were at the top of the column, in horizontal directions.

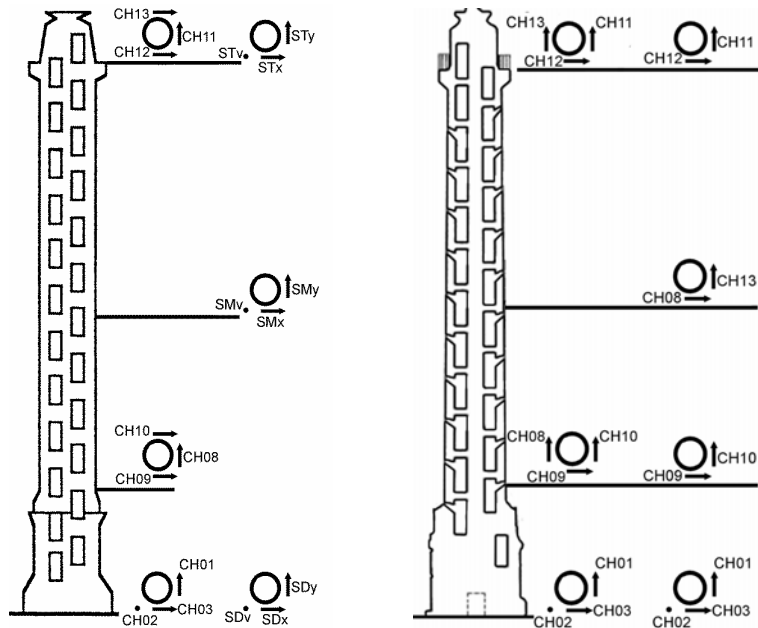


Figure 5. Sensor deployments in the Aurelian (left) and Trajan's (right) Columns

All the tests were analyzed in the frequency domain. The columns showed similar behaviors:

- they both showed two resonance frequencies, equal to 1.24 and 1.30 Hz for the Aurelian Column and to 1.45 and 1.51 Hz for the Trajan's Column (Figure 6); the cross analysis (CSD) confirmed that all these frequencies were structural resonances, associated to modal shapes of the columns;
- other amplifications were around 6.50 Hz and in the range between 9.00 and 10.0 Hz for the Aurelian Column, and between 5.6 and 8.0 Hz and also at 15.6 Hz for the Trajan's Column.

Some differences were also found:

- in the first two modal shapes of the Aurelian Column the displacements at the base of the pedestal and that at the base of the column are 180° out of phase. This behaviour could be related to a significant rotation of the pedestal due to soil deformation,

and to a non effective connection between the pedestal and the column. Furthermore non elastic rotations could interest the column also along its height; this could justify the significant amplification at the top;

- in the vertical direction (CH02) a significant amplification is apparent at around 2.00 Hz in the Aurelian Column, while no significant amplification were in the vertical direction in the Trajan's Column.
- the vertical components at location down, mid and top were examined in the frequency range [1.0, 2.5] Hz. The spectral analysis showed that, at 1.9 Hz, PSDs of recordings in the Aurelian Column was higher at the top (Figure 7) and that the signals were out of phase with a very high value of the coherence function. These effects can be interpreted as due to the hypothesized rocking of the monument. This did not occur in the Trajan's Column.

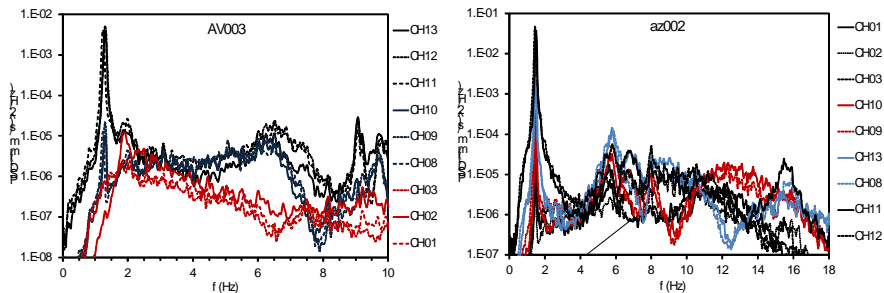


Figure 6. PSDs of the recorded signals on the Aurelian (left) and Trajan's (right) Columns

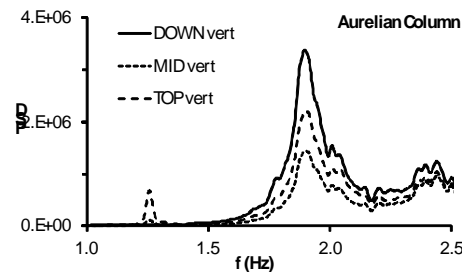


Figure 7. PSDs of vertical recordings on the pedestal (DOWN) and at a middle height (MID) at the top (TOP) of the Aurelian Column

The velocity time history at the top of the column was evaluated for two orthogonal signals and filtered between 1.3 and 1.8 Hz for the Aurelian Column and between 1.0 and 1.5 Hz for the Trajan's Column. Then they were integrated to get the corresponding displacement. The analysis of the particle motion showed that the motion of both the columns consists in an oscillation around an axis varying in time. Figure 8 shows the distribution of the angular position of the particle for angle interval of 5° , pointing out the presence of preferred directions. Furthermore, angle and modulus of the particle motion show a particular periodicity.

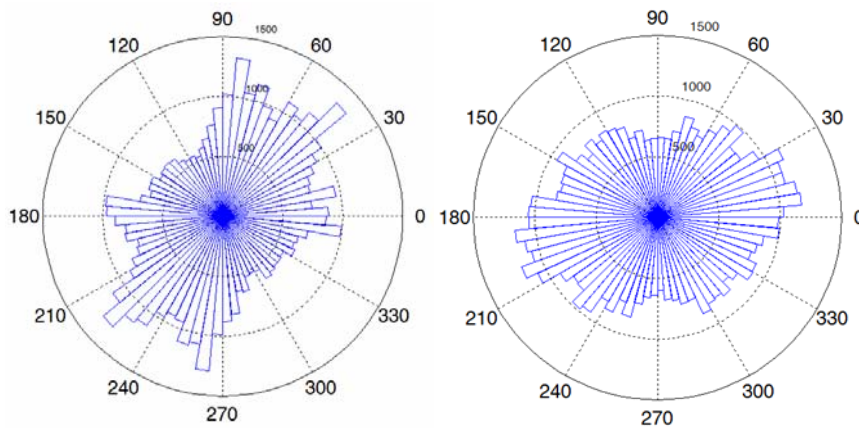


Figure 8. Distribution of the particle motion at the top of the Aurelian (left) and Trajan's (right) Columns

4. Conclusions

The Cochlid Columns in Rome, already objects of dynamic testing in 80s and 90s, have been tested again recently by using modern instrumentation and more sophisticated tools for data analysis. These allowed pointing out a behavior more complex than that inferred during the previous campaigns, which can be summarized as follows:

- two dominating translational frequencies are present, equal to 1.24 and 1.3 Hz in the Aurelian Column, and to 1.45 and 1.51 Hz in the Trajan's Column;

- a translational frequency equal to 2.0 Hz related to vertical motion was found in the Aurelian Column, which could represent an effect of rocking of the basement;
- another translational frequency is at 6.5 Hz in the Aurelian Column, while other translational resonances are between 5.6 and 8.0 Hz for the Trajan's Column;
- a torsional motion, not associated to an elastic modal shape of the top of the structures, at 9.0 Hz in the Aurelian Column, and at 15.8 Hz in the Trajan's Column.

The columns oscillate around an axis, which varies in time. Principal directions for the structure cannot be determined, but preferred directions of the motion are apparent.

The results of this study suggest that the capability of the columns to support future dynamic actions, related to earthquakes, wind, ambient or traffic-induced vibrations, cannot be easily evaluated and deep studies are needed. The lack of knowledge regards:

- the mass distribution, which could not be homogeneous due to the presence of the stair and to historical restorations;
- the mechanical properties of the marble subject to degradation, related to the exposition to weathering, earthquakes and ambient and traffic-induced vibrations;
- the effectiveness of links;
- the geometrical characteristics of the basement and the foundation, as well as the soil mechanical characteristics.

All these aspects are to be investigated in details to define a complete model to interpret the actual behavior of both the columns and to analyze their reliability under medium and strong earthquakes in order to ensure its stability over time.

REFERENCES

- Bongiovanni G., Celebi M., Clemente P., 1990. *The Flaminio Obelisk in Rome: vibrational characteristics as part of preservation efforts*. Int. J. of Earthquake Engineering and Structural Dynamics, 19: 107-118.
- Boschi E., Caserta A., Conti C., Di Bona M., Funicello R., Malagnini L., Marra F., Martines G., Rovelli A. and Salvi S., 1995.

- Resonance of Subsurface Sediments: an Unforeseen Complication for Designers of Roman Columns.* Bull. Seism. Soc. Am., 85: 320-324.
- Buffarini G., Clemente P., Paciello A., Rinaldis D., 2008. *Vibration Analysis of the Lateran Obelisk.* In: 14th World Conference on Earthquake Engineering, Beijing, 12-17 October, S11-055.
- Buffarini G., Clemente P., Paciello A., Rinaldis D., 2009. *The Lateran Obelisk: Experimental analysis and modelling.* In: Protection of Historical Buildings, PROHITECH 09, F.M. Mazzolani (ed.), Rome, 21-24 June, 1: 841-848, London: Taylor & Francis Group.
- Clemente P., 1995. *Traffic-Induced Vibrations on Structures.* In: IABSE Report Extending the Lifespan of Structures, 73(2): 1111-1116.
- Clemente P., 2002. *L'analisi dinamica sperimentale nella salvaguardia dei beni culturali. Alcune esperienze dell'ENEA.* ENEA, Roma.
- Clemente P., 2002. *Vibrazioni indotte dal traffico: un'insidia per i monumenti.* In: Complessità e Sviluppo 2002, 148-156, Roma: ENEA.
- Clemente P., Bongiovanni G., 1993. *Ambient Vibration Effects on the Colosseum.* In: IABSE Report Structural Preservation of the Architectural Heritage, 70: 107-114.
- Clemente P., Bongiovanni G., Marzi C., 1988. *La colonna Antonina in Roma: valutazione degli effetti delle vibrazioni ambientali.* In: Conoscere per intervenire, 3rd ASS.I.R.C.CO. Conf., Catania, 10-12 November, 207-217.
- Clemente P., Rinaldis D., Bongiovanni G., 1994. *Dynamic characterization of the Tempio della Minerva Medica.* In: 10th European Conference on Earthquake Engineering, Vienna, 28 Aug. - 2 Sept., 2: 981-986, Rotterdam: Balkema.
- Giuffrè A., 1984. *Valutazione della vulnerabilità sismica dei monumenti: metodi di verifica e tecniche di intervento. La colonna Antonina. Studi e ricerche sulla sicurezza sismica dei monumenti, Report No. 6.*

- Giuffrè A., Ortolani F., 1988. Le colonne coclidi testimoni dei terremoti di Roma. Studi e ricerche sulla sicurezza sismica dei monumenti. Sapienza Università di Roma, Report No. 7.
- Masiani R., Tocci C., 2010. *Il restauro statico dell'abaco della Colonna di Marco Aurelio Palladio*. Seismic Protection of Structures, 46: 77-88.

Experimental analysis and numerical modeling of the seismic site response at Santa Maria di Collemaggio Basilica in L'Aquila

Sara Amoroso¹, Iolanda Gaudiosi², Giuliano Milana³, Marco Tallini⁴

Abstract

The Basilica of Santa Maria di Collemaggio is an important cultural heritage site, considered as an extraordinary example of Romanic Art in the Abruzzo Region (Italy). Erected in the second half of the XII century, it suffered numerous transformations partly due to the damages incurred as result of several earthquakes. During the April 6, 2009 L'Aquila earthquake ($M_W = 6.3$), the Basilica was strongly damaged and in particular the area of the transept collapsed causing the fall of the dome.

Recently the Eni Company launched the financing project "Ripartire da Collemaggio" for the restoration of this historical building. The project includes a deep geological, geotechnical and geophysical investigations, still ongoing (AA.VV., 2013), that complete the information on L'Aquila subsoil already provided by numerous studies carried on in downtown L'Aquila (MS-AQ Working Group, 2010; Amoroso et al., 2010; Cardarelli e Cercato, 2010; Amoroso et al., 2014; Monaco et al., 2013; Santucci de Magistris et al., 2013; Monaco et al., 2012; Milana et al., 2011).

This paper illustrates the preliminary results of seismic response analyses carried out at Santa Maria di Collemaggio Basilica, by using EERA (Bardet et al., 2000), a monodimensional (1D) code, and QUAD4M (Hudson et al., 1994), a bi-dimensional (2D) software. Both programs are dedicated to model the seismic response of a site also tacking into account for non-linear soil behaviour.

1 Istituto Nazionale di Geofisica e Vulcanologia, L'Aquila, Italy.

2 Istituto Nazionale di Geofisica e Vulcanologia, Cosenza, Italy.

3 Department of Civil, Architectural and Environmental Engineering, University of L'Aquila, L'Aquila, Italy.

4 Istituto Nazionale di Geofisica e Vulcanologia, Rome, Italy.

As a result, 1D and 2D analyses compare simulated vs experimental transfer functions in order to validate the proposed model and to verify the presence of local site effects to be taken into account in the restoration process of Santa Maria di Collemaggio.

1. Introduction

The Basilica of Santa Maria di Collemaggio is an important cultural heritage site, considered as an extraordinary example of Romanic Art in the Abruzzo Region (Italy). Erected in the second half of the XII century, it suffered numerous transformations partly due to the damages incurred as result of several earthquakes. During the April 6, 2009 L'Aquila earthquake ($M_W = 6.3$), the Basilica was strongly damaged and in particular the area of the transept collapsed causing the fall of the dome.

This paper illustrates the preliminary results of seismic response analyses carried out at Santa Maria di Collemaggio Basilica, by using EERA (Bardet et al., 2000), a monodimensional (1D) code, and QUAD4M (Hudson et al., 1994), a bi-dimensional (2D) software. In this respect, Eni is financing the project "Ripartire da Collemaggio" for the restoration of this historical building. The project includes a deep geological, geotechnical and geophysical investigations, still ongoing (AA.VV., 2013), that complete the information on L'Aquila subsoil already provided by numerous studies carried on in downtown L'Aquila (MS-AQ Working Group, 2010; Amoroso et al., 2010; Cardarelli e Cercato, 2010; Amoroso et al., 2014; Monaco et al., 2013; Santucci de Magistris et al., 2013; Monaco et al., 2012; Milana et al., 2011). As a result, 1D and 2D analyses compare simulated vs experimental transfer functions in order to validate the proposed model and to verify the presence of local site effects, that can affect L'Aquila basin seismic response.

2. Geological, geotechnical and geophysical investigations

The area of study was deeply investigated before and after L'Aquila earthquake. In particular, during the past several soundings were carried out for the Botanical Garden part of Santa Maria di Collemaggio Basilica (about fourteen shallow boreholes and a well of 70 m depth), and for the Basilica itself (a couple of verticals), as shown by MS-AQ

Working Group, 2010). In addition the deep boreholes in the historical centre promoted by the University of L'Aquila – Centre for Research and Education in Earthquake Engineering (CERFIS) (Amoroso et al., 2010; Cardarelli e Cercato, 2010), the seismic microzonation study (MS–AQ Working Group, 2010) and the further investigations carried out for the reconstruction of private damaged buildings (Amoroso et al., 2014), together with numerous studies already realized in L'Aquila basin (Monaco et al., 2013; Santucci de Magistris et al., 2013; Monaco et al., 2012; Milana et al., 2011), allowed to develop a detailed geological, geotechnical and geophysical model.

In addition, Eni provided funds for three deep boreholes (80 m, 120 m and 270 m depth) and several shallow ones together with geotechnical and geophysical investigations (seismic dilatometer tests, cyclic laboratory tests, seismic noise measurements, MASW and seismic refraction surveys), still ongoing (AA.VV., 2013), for the Basilica seismic reinforcement and rebuilding project.

3. Geological, geotechnical and geophysical investigations

3.1. Measurements

The Santa Maria di Collemaggio Basilica is located just outside in the south eastern part of the medieval walls of L'Aquila city centre. It is placed in a flat terraced hill whose schematic geological setting consists, from the top to the bottom, of a middle Pleistocene 100 m-thick variably-cemented calcareous breccias (L'Aquila breccias Auct.) which lay onto a 200 m-thick homogeneous lower Pleistocene-upper Pliocene (?) fluvial-lacustrine pelite and sand. In their turn, they are placed onto the deep Meso-Cenozoic carbonate bedrock which its depth decreases toward NE (Amoroso et al., 2010; Del Monaco et al., 2013; MS–AQ Working Group, 2010, 2010; Tallini et al., 2011). L'Aquila breccias thickness decreases from about 100 m in the central sector of L'Aquila city centre (at the Market square) to 0-10 m in the southern slope of L'Aquila hill where they are laterally replaced by sand and pelite and calcareous gravels and breccia layers (Del Monaco et al., 2013).

In the Basilica area, the soundings, carried out by Eni (AA.VV., 2013), improved the fine scale subsoil model. Here, L'Aquila breccias have a thickness of about 44 m and the boundary between them and

the underlying sand and pelite is nearly horizontal. Further a few meters of fine-grained soils (red soils) are locally arranged into or onto them.

3.2. Geotechnical model

The geotechnical model, used for these preliminary numerical analyses, was based on the geological, geotechnical and geophysical investigations already provided by numerous previous studies produced in L'Aquila downtown (MS–AQ Working Group, 2010; Amoroso et al., 2010; Cardarelli e Cercato, 2010; Amoroso et al., 2014; Monaco et al., 2013; Santucci de Magistris et al., 2013; Monaco et al., 2012; Milana et al., 2011). A refined model for the Basilica subsoil will be supplied once all the investigations, supported by Eni, will be available.

The 2D seismic response analyses were performed by considering the geotechnical cross section shown in Fig. 1, while the 1D numerical analyses were focused at the vertical in correspondence to Santa Maria di Collemaggio Basilica.

The seismic microzonation studies (MS–AQ Working Group, 2010) and the deep boreholes (Amoroso et al., 2010) allowed to estimate the thickness and the mechanical and dynamical soil properties of each geotechnical unit *GU*: filling materials “Ri”, alluvial deposits “Al”, debris slope deposits “Dt”, colluvial deposits “Cl”, red soils “LR”, calcareous breccias, divided into three sublayers, “Br1”, “Br2”, “Br3”, fluvial-lacustrine deposits, divided into five sublayers, “L1”, “L2”, “L3”, “L4”, “L5”, and calcareous bedrock “Bedrock”.

Some refinements in the evaluation of the shear wave velocity V_S were performed by considering the results of seismic dilatometer tests (Amoroso et al., 2014; Monaco et al., 2013; Santucci de Magistris et al., 2013; Monaco et al., 2012) and cross-hole test (Cardarelli e Cercato, 2010) and by assuming $V_S \sim 2000$ m/s (Bordoni et al., 2011). In addition, stiffness decay curves G/G_0 and damping ratio curves D , introduced into the numerical analyses, referred to:

- the resonant column/torsional shear test results obtained by Amoroso et al. (2014) into the red soils of the Southern part of L'Aquila city for “LR” and “Cl” units;

- the gravel reference curve used by Tito Sanò into the numerical analyses developed for the seismic microzonation studies (MS–AQ Working Group, 2010) for “Al”, “Dt” and “Ri” units;
- the dense gravel curve evaluated by Modoni and Gazzelloni (2010) for “Br1” and “Br2” units;
- a linear elastic behaviour, assuming a small strain stiffness G_0 and an initial critical damping ratio D_0 equal to $G_0 \sim 3200$ MPa, $D_0 \sim 0.5$ %, for the “Br3”;
- the resonant column/torsional shear test results obtained by C.A.S.E. Project (Monaco et al., 2012) into the fluvial-lacustrine deposits of Roio Piano for “L1”, “L2”, “L3”, “L4” and “L5” units;
- a linear elastic behaviour, assuming a small strain stiffness G_0 and an initial critical damping ratio D_0 equal to $G_0 \sim 9000$ MPa, $D_0 \sim 0.5$ %, for the “Bedrock”.

Tab. 1 summarized the mechanical and dynamical soil parameters of each geotechnical unit GU , by including unit weight γ , Poisson coefficient ν , shear wave velocity V_S , stiffness decay curves G/G_0 and damping ratio D curves.

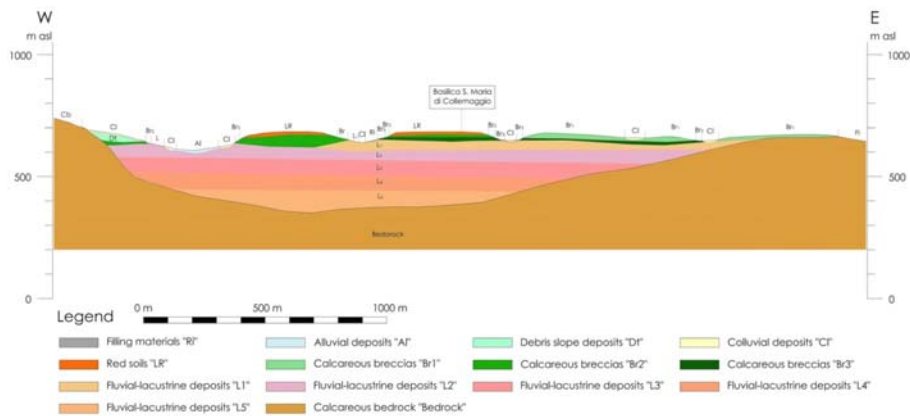


Figure 1. Geotechnical model used for 1D and 2D seismic response analyses (Amoroso et al., 2013),

Table 1. Mechanical and dynamical soil parameters of each geotechnical unit (Amoroso et al., 2013)

| UG | γ (kN/m ³) | ν | V_s (m/s) | G/G_0 and D curves |
|---------|----------------------------------|-------|----------------|---|
| Ri | 17 | 0.2 | 250 | MS-AQ Working Group (2010) |
| Al | 19 | 0.2 | 200 | MS-AQ Working Group (2010) |
| Dt | 19 | 0.2 | 300 | MS-AQ Working Group (2010) |
| Cl | 19 | 0.2 | 350 | Amoroso et al. (2014) |
| LR | 19 | 0.2 | 350 | Amoroso et al. (2014) |
| Br1 | 20 | 0.2 | 600 | Modoni and Gazzelloni (2010) |
| Br2 | 20 | 0.2 | 800 | Modoni and Gazzelloni (2010) |
| Br3 | 21 | 0.2 | 1200 | Linear elastic behavior ($G_0 \sim 9000$ MPa, $D_0 \sim 0.5$ %) |
| L1 | 19 | 0.2 | 550 | Monaco et al. (2012) |
| L2 | 19 | 0.2 | 600 | Monaco et al. (2012) |
| L3 | 19 | 0.2 | 670 | Monaco et al. (2012) |
| L4 | 19 | 0.2 | 740 | Monaco et al. (2012) |
| L5 | 19 | 0.2 | 810 | Monaco et al. (2012) |
| Bedrock | 22 | 0.2 | 2000 | Linear elastic behavior ($G_0 \sim 9000$ MPa, $D_0 \sim 0.5$ %) |

4. 1D and 2D Numerical modeling

Numerical analyses of seismic site response were carried out using the computer codes EERA (Bardet et al. 2000), a monodimensional linear equivalent model, and QUAD4M (Hudson et al. 1994), a bi-dimensional linear equivalent model.

In particular, EERA iterates the analysis in order to follow the variation of normalized shear modulus G/G_0 and damping ratio D with shear strain. It assumes simplified soil deposit conditions such as horizontal soil layers of infinite extent.

Instead, QUAD4M is a dynamic, time domain and equivalent linear two-dimensional computer program. It uses a finite elements procedure approximating the domain with a mesh of finite number of triangular and/or quadrilateral elements interconnected at their common nodes. The code solves the approximated system by using a step-by-step integration in the time domain: the parameters are fixed for the whole duration of the input signal and the computation is repeated with the update of the stiffness and the damping matrices, as happens in the one-dimension code SHAKE (Schnabel et al. 1972; Idriss and Sun 1992). QUAD4M propagates P and/or SV waves with vertical incidence. The artificial reflection of seismic wave should be minimized at the domain boundaries, as well as at the underlying half-space, to

represent the response of an infinite field condition. Lysmer and Kuhlemeyer (1969) introduced base dampers to add damping at each of the nodes at the base of the finite model. Moreover, the software includes a method for the introduction of damping matrices to reduce the damping at highest frequencies, commonly associated with the Rayleigh damping formulation (Lanzo et al., 2003). The latter one establishes two control frequencies that define the frequency interval where the damping can be assumed free from numerical bias. For the 1D and 2D numerical analyses preliminarily five different accelerograms (“DET1”, “DET2”, “DET3”, “NTC08”, “PROB LADE”) selected for the seismic microzonation studies (MS–AQ Working Group, 2010), were used as input ground motions applied on the outcropping bedrock. In short, this paper, illustrates only the results obtained by “DET1” accelerogram together with those achieved by a simple ricker pulse and by using a real accelerogram (“MONTEREALE”). In particular, “DET1” is compatible with the deterministic spectrum obtained from Sabetta and Pugliese (1996) attenuation relation for the moment magnitude M_w – epicentral distance R_{epi} pair ($M_w = 6.7$, $R_{\text{epi}} = 10$ km) established by means of disaggregation analysis. The ricker pulse is characterized by a length of about 0.2 s and a $PGA = 0.261$ g.

It is important to highlight that “DET1” is an artificial accelerogram, not admitted by NTC (2008) and CEN (2003) in order to provide an elastic response spectrum. Their use is allowed in order to provide an elastic response spectrum only in some cases (not for geotechnical works and systems). Anyway, NTC (2008) also specifies the use of accelerograms, obtained via simulations of the source-mechanism and the propagation path, is only possible when the assumed characteristics of the seismogenetic source and the medium propagation are justified.

Nonetheless DET1 was used in this case study mainly to check the reliability of the geotechnical model proposed in linear-equivalent approximation.

At first numerical analyses were run by applying a ricker pulse, as input motion. Due to the characteristic of the input source (impulsive and short in duration), the ricker pulse didn't allow to reach significant strain-compatible values, able to produce important non-linear effects.

On the other side, the use of this pulse do extend the range of frequencies not affected by numerical bias. In fact, in this 2D modeling the first frequency of the soil deposit is 0.4 Hz, while the seismic input is characterized by a predominant period of 0.18 s for “DET1” and 0.06 s for the ricker pulse. In this respect, the solution was approximated with a frequency range of about 0.4-6.2 Hz for “DET1” and 0.4-17 Hz for the ricker pulse. Thus, the ricker pulse has a larger interval (in linear approximation) where it is possible to validate the geological-geotechnical model by means of comparison with experimental data. Moreover, the 2D mesh size was adapted to the velocity model (mesh adaptivity procedure) in order to reduce the computational cost. The minimum element size was assumed equal to 1/6 of the ratio between the lowest value of V_S in the model and the frequency of 10 Hz, chosen as “compromise” frequency between the computational cost and the engineering interest. Consequently the frequency interval, analysed by the ricker pulse for 2D modeling, was reduced to 0.4-10 Hz. The resulting bi-dimensional model considered a geotechnical cross section of 3.7 km of width (Fig. 1), with 98139 triangular elements and 49960 nodes.

Fig. 2 showed the transfer functions, in terms of horizontal component, computed by considering 1D (red curve) and 2D (black curve) linear models with the ricker pulse, as seismic input. Both the numerical analyses detected about 0.7 Hz, as the first fundamental frequency, that is in good agreement with the fundamental frequency of the Standard Spectral Ratio (SSR) at AQ11 station (blue curve), a temporary station installed after the April 6, 2009 within the microzonation activities, that recorded earthquakes from 28 May 2009 to 2 July 2009 (MS–AQ Working Group, 2010; Milana et al., 2011). SSR is evaluated using station AQ12 (Poggio di Roio) as reference site. QUAD4M code showed a slight lower-amplification value at about 0.7 Hz compared to SSR transfer function, while 1D modeling underestimates strongly the amplitude value. The 2D transfer function presented a secondary natural frequency at about 5 Hz and a third one at about 9 Hz, while SSR provides a unique secondary peak centred around 4 Hz.

In addition Fig. 3 depicts the transfer functions computed by considering 1D (cyan line) and 2D (purple line) linear equivalent models ob-

tained using DET1 as the seismic input. The numerical analyses confirm the results previously shown by the ricker pulse.

With regard to the vertical motion NTC (2008), par. 3.2.3.1, states the vertical component of the acceleration can be correlated to the horizontal component of the seismic input. Therefore it could be used a real accelerogram. Montereale site is a reliable site to be adopted as reference site (soil class A, according to NTC 2008). In this respect, MONTEREALE, recorded on the 9th April 2009 (local magnitude $M_L=5.1$ and $PGA=0.1g$) has been used into numerical analyses.

Thus, another 2D numerical analysis has been developed, by exciting the model with a P-SV vertical incident wave. Results in terms of transfer function are shown in Fig. 4. The agreement between SSR and transfer function obtained in linear-equivalent approximation is very satisfying. It is worth underlining that the degree of non-linearity experienced by the soil using MONTEREALE is very slight, due to the low PGA of the accelerogram (the two curves in linear and linear-equivalent approximation have a similar shape).

Fig. 5 illustrated the 2D linear (green curve) and linear-equivalent (red curve) results, in terms of spectral acceleration, by using "DET1" as input motion. Moreover, Fig. 5 shows the 1D elastic response spectrum (purple curve), obtained by multiplying the spectral acceleration, computed by EERA, with the topographic amplification factor S_T , assumed equal to 1.2 (NTC, 2008; CEN, 2003). The graph plots also the input response spectrum (DET1, black curve).

2D results are more cautelative than 1D modelling that shows a lower amplification over a wide period range up to 2 sec.

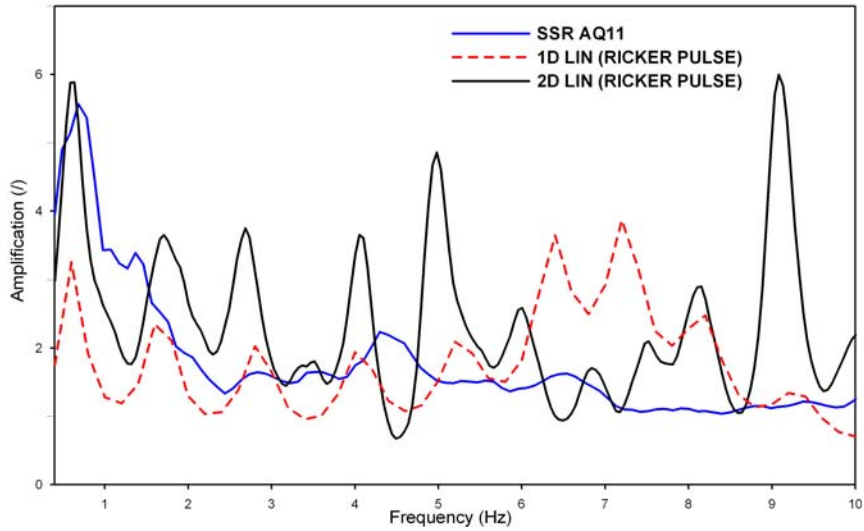


Figure 2. Transfer functions obtained from 1D and 2D numerical modeling compared with SSR at AQ11 station (horizontal component, after Amoroso et al., 2013)

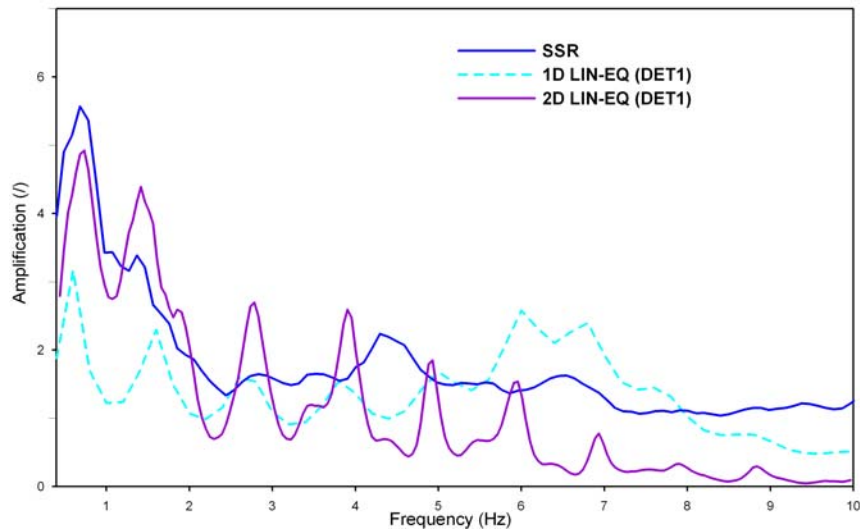


Figure 3. Transfer functions from 2D numerical modeling obtained by using DET1 as input motion in linear approximation, compared with SSR at AQ11 station (horizontal component).

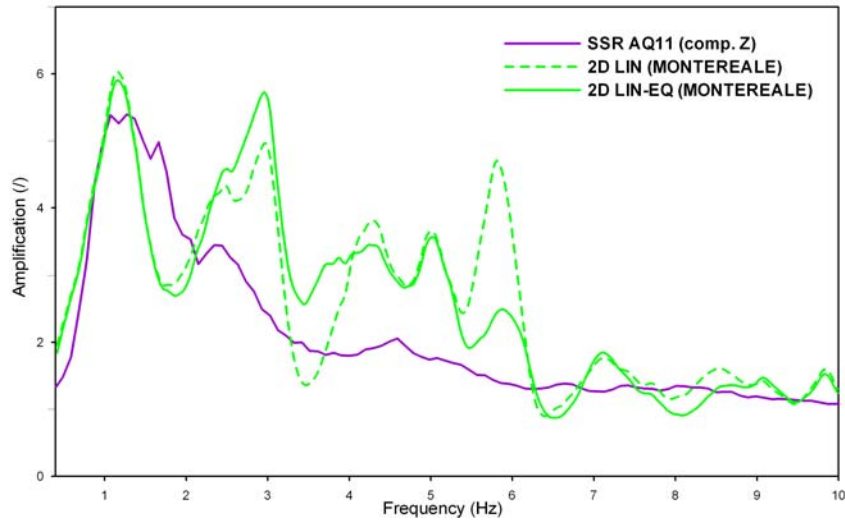


Figure 4. Transfer functions obtained from 2D numerical modeling compared with SSR at AQ11 station (vertical component)

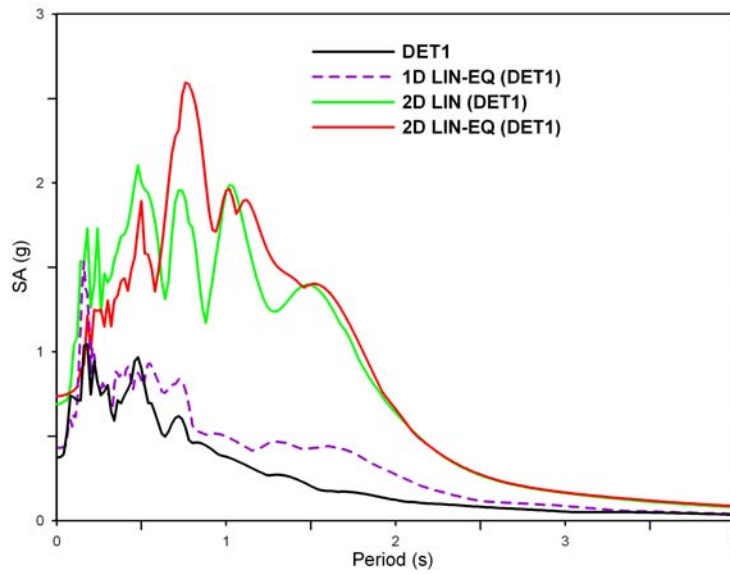


Figure 5. Response spectra obtained from numerical modeling in linear (2D) and linear equivalent (1D and 2D) approximation. For comparison, it is shown the input elastic response spectrum (after Amoroso et al., 2013).

5. Conclusions

The huge amount of geological, geotechnical and geophysical data provided by numerous studies in L'Aquila downtown, allowed to rebuild a preliminary subsoil model for the 1D and 2D seismic response analyses of Santa Maria di Collemaggio Basilica.

Thanks to the availability of strong motion data close to the Basilica, the site was suitable for an accurate seismic modeling. In fact: the consistent data set available for the sequence of 2009 earthquake supplied the rare opportunity to compare numerical and experimental data.

Even though amplification values are not exactly reproduced, QUAD4M results approximated satisfactorily the experimental ones. 2D analysis was able to reproduce, better than 1D code, the SSR at AQ11 station by considering the whole frequency range (0.4-10 Hz). In this respect, the proposed geotechnical model appeared to be reliable, confirming the presence of 2D effects in L'Aquila downtown. Moreover, these results, although preliminary, suggested the same conclusions stated by Bordini et al. (2011): the major amplification effects are in the frequency range of 0.5-1.5 Hz.

Further numerical simulations will be supplied once all the investigations, supported by Eni, will be available in order to provide a more accurate subsoil model and consequently a more refined elastic response spectrum for all the range of period of engineering interest at Santa Maria di Collemaggio Basilica.

References

[1] AA.VV.; 2013: Caratterizzazione geologica, geofisica e geotecnica del sito della basilica di Collemaggio. *Report Consorzio Sperimentazione Edilizia*. University of L'Aquila. <ing.univaq.it/webdisat/cse/cse.html> (In Italian).

[2] Amoroso S., Gaudiosi I., Milana G., Tallini M. (2013). Preliminary results of seismic response analyses at "Santa Maria di Collemaggio" Basilica (L'Aquila, Italy). Proceedings of 32nd Conference Gruppo Nazionale di Geofisica della Terra Solida (GNGTS), 19-21 November 2013, Trieste (Italy), Vol. 2, 172-178.

[3] Amoroso S., Totani F., Totani G., Monaco P.; 2014: Local seismic response in the Southern part of the historic centre of L'Aquila. IAEG XII CONGRESS - TORINO, SEPTEMBER 15-19, 2014 (paper accepted).

[4] Amoroso S., Del Monaco F., Di Eusebio F., Monaco P., Taddei B., Tallini M., Totani F., Totani G.; 2010: Campagna di indagini geologiche, geotecniche e geofisiche per lo studio della risposta sismica locale della città dell'Aquila: la stratigrafia dei sondaggi giugno-agosto 2010. Report CERFIS 1/10. University of L'Aquila. <www.cerfis.it/en/download/cat_view/67-pubblicazioni-cerfis/68-reports.html> (in Italian).

[5] Bardet J.P., Ich I.I., Lin C.H.; 2000: EERA – A computer program for Equivalent-linear site Response Analysis of Layered Soil Deposits. University of Southern California, August 2000.

[6] Bordoni P., Haines J., Milana G., Marcucci S., Cara F., Di Giulio G.; 2011: Seismic response of L'Aquila downtown from comparison between 2D synthetics spectral ratios of SH, P-SV and Rayleigh waves and observations of the 2009 earthquake sequence. Bull. Earthquake Eng., 9, 761–781, DOI 10.1007/s10518-011-9247-5.

[7] Cardarelli E., Cercato M.; 2010: Relazione sulla campagna d'indagine geofisica per lo studio della Risposta Sismica Locale della città dell'Aquila. Prova crosshole sondaggi S3-S4. Rapporto DICEA – Università di Roma La Sapienza per CERFIS – Università dell'Aquila, 13 pp. <www.cerfis.it> (in Italian).

[8] CEN, European Committee for Standardisation; 2003: Eurocode 8: design provisions for earthquake resistance of structures. Part 1.1: general rules, seismic actions and rules for buildings. prEN 1998-1.

[9] De Magistris F.S., D'Onofrio A., Evangelista L., Foti S., Marschini M., Monaco P., Amoroso S., Totani G., Lanzo G., Pagliaroli A., Madiati C., Simoni G., Silvestri F.; 2013: Geotechnical characterization of the Aterno Valley for site response analysis. Rivista Italiana di Geotecnica, Anno XLVIII (in press).

[10] Del Monaco F., Tallini M., De Rose C., Durante F.; 2013: HVNSR survey in historical downtown L'Aquila (central Italy): site resonance properties vs. subsoil model. Engineering Geology, 158, 34-47, DOI 10.1016/j.enggeo.2013.03.008.

[11] Hudson M., Idriss I.M., Beikae M.; 1994: QUAD4M - A computer program to evaluate the seismic response of soil structures using finite element procedures and incorporating a compliant base. University of California, Davis.

[12] Idriss I.M., Sun J.I.; 1992: User's Manual for SHAKE91. Center for Geotechnical Modeling, Department of Civil Engineering, University of California, Davis.

[13] Lanzo G., Pagliaroli A., D'Elia B.; 2003: Numerical study on the frequency-dependent viscous damping in dynamic response analysis of ground. Proc. of Fourth Int. Conf. On Earthquake Resistant Engineering Structures (ERES 2003), Ancona, Italia, 22-24 September.

[14] Lysmer J., Kuhlemeyer R.L.; 1969: Finite Dynamic Model for Infinite Media. Journal of the Engineering Mechanics Division, Proc. of the American Society of Civil Engineers, EM4: 859-877.

[15] Milana G., Azzara R.M., Bergamaschi F., Bertrand E., Bordononi P., Cara F., Cogliano R., Cultrera G., Di Giulio G., Duval A.M., Fodarella A., Marcucci S., Pucillo S., Régnier J., Riccio G.; 2011: The contribution of seismic data in microzonation studies for downtown L'Aquila. Bull. Earthquake Eng. 9, 741-759, DOI 10.1007/s10518-011-9246-6.

[16] Monaco P., Totani G., Amoroso S., Totani F., Marchetti D.; 2013: Site characterization by seismic dilatometer (SDMT) in the city of L'Aquila. Rivista Italiana di Geotecnica, Anno XLVIII, n. 3 (in press).

[17] Monaco P., Totani G., Barla G., Cavallaro A., Costanzo A., D'Onofrio A., Evangelista L., Foti S., Grasso S., Lanzo G., Madiati C., Maraschini M., Marchetti S., Maugeri M., Pagliaroli A., Pallara O., Penna A., Saccenti A., Santucci de Magistris F., Scasserra G., Silvestri F., Simonelli A.L., Simoni G., Tommasi P., Vannucchi G., Verrucci L.; 2012: Geotechnical aspects of the L'Aquila earthquake. In: M.A. Sakr & A. Ansal (eds), Special Topics in Earthquake Geotechnical Engineering, Series Geotechnical, Geological and Earthquake Engineering, 16, 1-66 pp.

[18] MS-AQ Working Group; 2010: Microzonazione sismica per la ricostruzione dell'area aquilana. Regione Abruzzo – Dipartimento della Protezione Civile, L'Aquila, 3 vol. & CD-Rom,

<www.protezionecivile.gov.it/jcms/en/view_pub.wp?contentId=PUB25330> (in Italian).

[19] NTC (2008). D.M. 14/01/2008 - Norme Tecniche per le Costruzioni, pubblicato sulla Gazzetta Ufficiale n. 29 del 4 febbraio 2008. Suppl. Ordinario n. 30. Capitolo 3 Azioni sulle costruzioni (In Italian).

[20] Sabetta F., Pugliese A.; 1996: Estimation of response spectra and simulation of nonstationary earthquake ground motions. Bull. Seismol. Soc. Am., 86, 337-352.

[21] Schnabel P.B., Lysmer J., Seed H.B.; 1972: SHAKE: A Computer Program for Earthquake Response Analysis of Horizontally Layered Sites. Report No. UCB/EERC-72/12. Earthquake Engineering Research Center, University of California, Berkeley, December.

[22] Tallini M., Di Fiore V., Bruno P.P., Castello A., Punzo M., Variale F., Del Monaco F., Tarallo D., Cavuoto G., Pelosi N.; 2011: Sismica a riflessione ad alta risoluzione per il modello del sottosuolo e la stima della pericolosità sismica del centro storico dell'Aquila. Atti del 30° Convegno Nazionale GNGTS - Gruppo Nazionale Geofisica della Terra Solida, Trieste 14-17 novembre 2011 (In Italian).

AUTHOR INDEX

| | |
|------------------------------|----------------------|
| <i>Sara Amoroso</i> | 295 |
| <i>Carlo Baggio</i> | 11 |
| <i>Heinz-Jürgen Beste</i> | 79 |
| <i>Giovanni Bongiovanni</i> | 281 |
| <i>Giacomo Buffarini</i> | 281 |
| <i>Bruno Carpani</i> | 243 |
| <i>Arrigo Caserta</i> | 47, 231 |
| <i>Paolo Clemente</i> | 33, 47, 79, 281 |
| <i>Cinzia Conti</i> | 11, 21, 33, 47, 79 |
| <i>Gerardo De Canio</i> | 183 |
| <i>Francesco Del Monaco</i> | 281 |
| <i>Alessandro De Stefano</i> | 33 |
| <i>Gino D'Ovidio</i> | 47, 79 |
| <i>Federica Durante</i> | 281 |
| <i>Fabio Fumagalli</i> | 217 |
| <i>Iolanda Gaudiosi</i> | 295 |
| <i>Aladino Govoni</i> | 231 |
| <i>Giuseppe Carlo Marano</i> | 217 |
| <i>Fabrizio Marra</i> | 231 |
| <i>Giuliano Milana</i> | 295 |
| <i>Claudio Modena</i> | 111 |
| <i>Giorgio Monti</i> | 217 |
| <i>Yutaka Nakamura</i> | 47, 79, 153, 263 |
| <i>Barbara Nazzaro</i> | 217 |
| <i>Luciana Orlando</i> | 47, 79 |
| <i>Giuseppe Quaranta</i> | 217 |
| <i>Rossella Rea</i> | 47, 217 |
| <i>Antonio Rovelli</i> | 21, 47, 79, 231, 281 |
| <i>Fernando Saitta</i> | 281 |
| <i>Jun Saita</i> | 153, 263 |
| <i>Tsutomu Sato</i> | 153, 263 |
| <i>Sandro Serafini</i> | 281 |
| <i>Mitsuhiro Tachibana</i> | 153 |
| <i>Marco Tallini</i> | 281, 295 |
| <i>Gianfranco Valente</i> | 47, 79, 281 |

DISS_Edition



Carlo Baggio is Associate Professor of Structural Engineering, vice-director at Roma Tre University and vice-president of ARCo. His main research activity concerns non-linear analysis of block masonry and historical structures. He is author of more than 60 papers.



Paolo Clemente, Civil Engineer, Ph.D. in Structural Engineering, post-doctorate at the University Federico II in Naples, joined ENEA in 1985. He is currently Head of Natural Risk Dept. His main fields of interests are: Experimental dynamic analysis of structures and System identification, New anti-seismic technologies, Structural preservation of the cultural heritage, Long-span bridges, Shake table tests, Masonry structures, Seismic input. He has authored about 200 technical papers.



Yutaka Nakamura is President of System and Data Research and former Visiting Professor of Tokyo Institute of Technology (2006-2012). His research activity concerns mainly EEW and vulnerability assessment for structures and ground. His developing systems are the first actual EEW system UrEDAS, Compact UrEDAS, FREQL and AcCo, and his developing techniques are H/V spectral ratio and K-value methods.



Luciana Orlando is Professor of Applied Geophysics and Environmental Geophysics at Sapienza University of Rome. Her current activities include GPR, seismic and electrical tomography devoted to archeology, environmental problems and the diagnosis of archaeological and historical buildings. She is author of over 130 articles.



Antonio Rovelli is Director of Research at INGV, Department of Seismology and Tectonophysics. His interest fields are strong-motion seismology and models of ground shaking. He is author of more than 70 papers on ISI journals.



Gianfranco Valente is Professor of Structural Engineering at L'Aquila University. His research activity concerns mainly non-linear analysis, for geometry and materials, static and dynamic. He is author of more than 100 papers.

ISBN 978-88-940114-1-8



9 788894 011418

ISSN 2612-4009

The soil forever transmits the principal vibrations to Colosseum: 1) at 3.32 a.m. on 6th April 2009, the main shock of L'Aquila earthquake travelled 100 Km, and a seismic sequence was recorded in Rome, on monument and underlying soil; 2) ambient vibrations from trains and cars. The usual model by Structural Engineering cannot receive such dynamic actions, having monument alone with fixed basis. A new reliable multidisciplinary model is proposed, with Colosseum, Constantine arch, foundations, soil, tunnels, trains, and cars.